Institute of Soil Science and Soil Conservation
Chair of Soil Resources
Justus Liebig University Giessen

Trapped, Released, Transformed: How Minerals Shape the Cycling of Organic Matter in Soils

Cumulative dissertation
For the degree of
Doctor rerum naturalium (Dr. rer. nat.)

Submitted to the
Faculty of Agricultural Sciences, Nutritional Sciences,
and Environmental Management

Justus Liebig University Giessen

Submitted by
Alexander Konrad

Giessen, August 2025

With permission of the Faculty of Agricultural Sciences,
Nutritional Sciences, and Environmental Management,
Justus Liebig University Giessen

Examination committee:
1st Reviewer: Prof. Dr. Jan Siemens
2nd Reviewer: Prof. Dr. Ines Mulder
3rd Examiner: Prof. Dr. Andreas Gattinger
3rd Examiner: Prof. Dr. Lutz Breuer

To my family

with deepest gratitude to my parents,

Cornelia Konrad and Walter Schmitz,

my grandfather,

Erich Konrad

and my grandmother, Christl Konrad,

who passed away just days before I submitted this dissertation

you never got to read these pages,

but you shaped the journey that made it possible.

Abstract

Soil organic carbon persistence arises from the intertwined effects of mineral surfaces, microbial activity, and the chemical structure of organic matter, which is further modulated by a soil´s boundary conditions. The ability of minerals to adsorb organic carbon, however, is not sufficient for the persistence of soil organic carbon due to other factors that influence microbial use of organic compounds such as nutrient availability. This dissertation addresses two linked questions: how do minerals govern soil organic matter adsorption and desorption, and how do these organo-mineral interactions feed back on microbial utilization and persistence of mineral-associated organic carbon?

To probe these questions, calorimetry was combined with isotope tracing and mineral long-term field exposure studies. Isothermal titration calorimetry provided the first direct thermodynamic quantification of adsorption of organic acids to mineral surface, showing that salicylic acid and citric acids bind exothermically to goethite. Calorimetry adsorption experiments onto goethite with differing lattice defect densities uncovered intensified exothermic binding and a greater loss of entropy on minerals abundant with defects, highlighting that adsorption thermodynamics can differ even for a single mineral type substantially.

To connect mineral control of organic matter sorption with its microbial fate, uniformly and carboxyl-radiocarbon labeled monomers were adsorbed onto kaolinite, illite and goethite in a set of batch sorption experiments and incubated in loamy and sandy arable topsoil. Despite strong inner-sphere complexation, a substantial share of ligand-bound carboxyl carbon was mineralized. At the molecular scale, microbial carbon use efficiency (CUE) of mineral-adsorbed monomers rose linearly with desorbability (i.e., the ratio of the amount desorbed to the amount sorbed) across all investigated compounds. Notably, CUE values were consistently lower for monomers bound to goethite than to the clay minerals. Taken together, these findings show that mineral surface properties and sorption-desorption dynamics can redirect metabolic allocation between biomass synthesis and respiratory loss.

Recognizing that minerals alter nutrient availability in soil, the dissertations research extended to cover phosphorus dynamics as well. In incubation studies, goethite-amended soil´s strong immobilization of phosphate constrained microbial growth, which channeled metabolism toward higher respiration and lower CUE, while illite did not immobilize phosphorus, resulting in higher CUEs for mineral-adsorbed monomers. Conversely, studying phosphorus transport in forest ecosystems exposed that soil colloids rich in carbon and iron can deliver large quantities of bioavailable phosphorus into sinks mimicking plant roots. This demonstrates that organo-mineral associations can alternate between acting as phosphorus sinks and nutrient shuttles, depending on their saturation state and soil boundary conditions.

Laboratory findings on mineral-associated organic matter cycling were further validated under field conditions investigating minerals buried in temperate grassland and forests for five years. Across all sites, goethite accrued nearly four times more carbon than illite, while the proportion of microbial biomass on mineral-associated organic carbon was higher on illite. Notably, carbon-, nitrogen-, and phosphorus-acquiring enzymes were significantly higher on goethite than illite or the surrounding soil, characteristic of microbial mining under nutrient limitations.

Three overarching insights emerge. First, the amount of carbon stabilized on mineral surfaces is mineral-specific and further depends on molecular functionality and soil properties such as pH and phosphate accessibility, but no sorption-strength threshold dictates bioaccesibility. Second, microbial processing of mineral-associated organic carbon is inseparable from phosphorus cycling, both of which are mediated by mineral type. Third, oxides and clay minerals both contribute to the persistence of organic carbon, but via contrasting mechanisms. Illite´s nutrient-rich surfaces promote rapid turnover with high CUE that channels carbon into new biomass, whereas goethite traps larger amounts in forms less accessible to microbes, leaving the small bioavailable fraction prone to respiration. Together, these findings refine our understanding of how minerals govern organic matter turnover and nutrient availability in soil: their role is soil specific, affected by pH, nutrient availability, and land use.

Table of Contents

Scientific contributions

Peer-reviewed original research papers as first author

Konrad, A., Mulder, I., Diana Hofmann, Stutz, P. K., Lang, F., & Siemens, J. Thermodynamics of sorption of organic acids to iron oxyhydroxides. Under review in the *European Journal of Soil Science*.

Author contributions: **Alexander Konrad**: investigation, method development, validation, writing – original draft, writing – review and editing. **Ines Mulder**: conceptualization, writing – review and editing, funding acquisition, supervision. **Diana Hofmann**: methodology, validation, writing – review and editing. **Friederike Lang**: conceptualization, validation, writing – review and editing, funding acquisition. **Kenton P. Stutz**: conceptualization, validation, writing – review and editing, funding acquisition. **Jan Siemens**: conceptualization, investigation, validation, writing – original draft, writing – review and editing, funding acquisition, supervision.

Konrad, A., Hofmann, D., Siemens, J., Stutz, K. P., Lang, F., & Mulder, I. (2025). Microbial carbon use efficiency of mineral-associated organic matter is related to its desorbability. *Soil Biology and Biochemistry*, *203*, 109740. https://doi.org/10.1016/j.soilbio.2025.109740

Author contributions: Conceptualization: AK, DH, JS, IM, KS, FL; laboratory analysis: AK, DH; data and statistical analysis: AK; writing – original draft preparation: AK, JS, IM; writing – reviewing and editing: all authors; funding acquisition: IM, KS, FL, JS.

Konrad, A., Hofmann, D., Siemens, J., Mulder, I., & Kenton P. Stutz.. Rapid mineralization of mineral-bound carboxyl-carbon of salicylic acid and phenylalanine. Under review in *Soil Biology and Biochemistry.*

Author contributions: Conceptualization: AK, DH, JS, IM, KS, FL; laboratory analysis: AK, DH; data and statistical analysis: AK; writing – original draft preparation: AK, JS, KS; writing – reviewing and editing: all authors; funding acquisition: IM, KS, FL, JS.

Konrad, A., Billiy, B., Regenbogen, P., Bol, R., Lang, F., Klumpp, E., & Siemens, J. (2021). Forest Soil Colloids Enhance Delivery of Phosphorus Into a Diffusive Gradient in Thin Films (DGT) Sink. *Frontiers in Forests and Global Change*, *3*, 577364. https://doi.org/10.3389/ffgc.2020.577364

Author contributions: RB, EK, and JS formulated the hypotheses. AK and JS conceived the experiment. RB, EK, and FL gave feedback regarding the concept and theory in all phases of the study. AK, BB, PR, and JS sampled the soils. AK, BB, and PR carried out the experiments. AK performed statistical analyses and wrote a first draft of the manuscript. All authors discussed the results and contributed to the final manuscript.

Co-authored, peer-reviewed original research papers

Bramble, D. S. E., Ulrich, S., Schöning, I., Mikutta, R., Brandt, L., Poll, C., Kandeler, E., Mikutta, C., Konrad, A., Siemens, J., Yang, Y., Polle, A., Schall, P., Ammer, C., Kaiser, K., Schrumpf, M. (2024). Formation of mineral-associated organic matter in temperate soils is primarily controlled by mineral type and modified by land use and management intensity. *Global Change Biology*, *30*(1), e17024. https://doi.org/10.1111/gcb.17024

Author contributions: **De Shorn E. Bramble:** Conceptualization; data curation; formal analysis; investigation; visualization; writing – original draft. **Susanne Ulrich:** Conceptualization; data curation; formal analysis; investigation; visualization; writing – original draft. **Ingo Schöning:** Conceptualization; methodology; supervision; writing – review and editing. **Robert Mikutta:** Conceptualization; funding acquisition; writing – review and editing. **Luise Brandt:** Visualization; writing – review and editing. **Christian Poll:** Conceptualization; writing – review and editing. **Ellen Kandeler:** Conceptualization; funding acquisition; writing – review and editing. **Christian Mikutta:** Conceptualization; funding acquisition; writing – review and editing. **Alexander Konrad:** Formal analysis; funding acquisition; writing – review and editing. **Jan Siemens:** Funding acquisition; writing – review and editing. **Yang Yang:** Formal analysis; funding acquisition; writing – review and editing. **Andrea Polle:** Funding acquisition; writing – review and editing. **Peter Schall:** Writing – review and editing. **Christian Ammer:** Writing – review and editing. **Klaus Kaiser:** Conceptualization; funding acquisition; supervision; writing – review and editing. **Marion Schrumpf:** Conceptualization; funding acquisition; methodology; supervision; visualization; writing – review and editing.

Brandt, L., Stache, F., Poll, C., Bramble, D. S., Schöning, I., Schrumpf, M., Ulrich, S., Kaiser, K., Mikutta, R., Mikutta, C., Oelmann, Y., Konrad, A., Siemens, J., Kandeler, E. (2023). Mineral type and land-use intensity control composition and functions of microorganisms colonizing pristine minerals in grassland soils. *Soil Biology and Biochemistry*, *182*, 109037. https://doi.org/10.1016/j.soilbio.2023.109037

Author contributions: Conceptualization: MS, IS, EK, CM, RM, KK, JS; laboratory analyses: LB, FS, DSB, SU, AK, CM's lab; data and statistical analysis: LB; writing – original draft preparation: LB, EK, CP; writing – reviewing and editing: all authors; funding acquisition: EK, MS, CM, KK, AK.

Chapter I: Introduction

Soil organic carbon

Soil organic carbon (SOC) represent the C in soil organic matter (SOM). Photosynthetic binding of C is the primary source of SOC, which can be divided into aboveground- and belowground inputs into soil (Schmidt et al., 2011; Sokol et al., 2019). Aboveground inputs include dead plant material like leaves or stems, which in summary is themed plant litter. Dead plant material from roots are an important belowground input as well, but are supplemented by root exudates like sugars and organic acids (Jilling et al., 2021). The magnitude of inputs as well as the ratio between above- and belowground contributions may differ (Sokol et al., 2019). In general, belowground inputs outweighs aboveground inputs in grassland ecosystems and arable soil (Jackson et al., 2017; Swift et al., 1979), with greater variations and approx. 1:1 contributions in forest ecosystems (Crow et al., 2009; Lajtha et al., 2014). Chemical composition of inputs differ between plants and point of entry (Sokol et al., 2019). Therefore the molecular composition of OC entering soil diverge between ecosystems. When OC entered soil, continuous microbial processing and interactions with the soil solid phase remove this site-specific molecular fingerprint with depth (Thieme et al., 2019). Microbes are either using this C source for energy or for biosynthesis (Schimel, 2023), thereby shifting soil OCs molecular fingerprint from plant-derived to microbial derived (Kaiser & Kalbitz, 2012), with microbes catabolic activities as the fundamental driver behind OC losses. Whether these compounds persist depends on protection mechanisms and environmental drivers such as temperature, moisture, and disturbance (Hu et al., 2018; Von Fromm et al., 2025). Losses also occur through leaching (Hussain et al., 2020), erosion (Chappell et al., 2016), and fire (Pellegrini et al., 2022), leaving soil OC stocks in a state of dynamic equilibrium between inputs, transformation, stabilization and outputs.

Why soil organic carbon matters

In recent years, soil OC research has been abundantly linked with climate protection and climate change mitigation (Begill et al., 2023; Bramble et al., 2024; Cotrufo et al., 2015). This is because soil store more organically bound C than atmosphere and vegetation stores C combined (Jobbágy & Jackson, 2000; Todd-Brown et al., 2013). Thus, understanding the impact of climate change and other men-made changes to soil stored OC is of highest significance for humanity: will OC remain bound in soil or will enhanced mineralization increases atmospheric CO_2 concentrations (or, under subhydric conditions, release CH_4), thereby amplifying the greenhouse effect? A more progressive question can also be formulated: can soil-bound OC be increased by management, and, conversely, reduce atmospheric C?

The function of soil OC is not limited to store C. When looking on soil OC from a rather ecological point of view, SOC is intertwined with other elements like nitrogen (N), phosphorus (P), sulfur (S) and others, which as a whole is termed soil organic matter (SOM) (Plante & Parton, 2007). When microbes break down SOM for energy and nutrients, these nutrients are becoming available in a slowly released, plant-available form (Fageria, 2012). Therefore SOM contributes to soil fertility and plant nutrition, while simultaneously playing a pivotal role in the microbial (Hartmann & Six, 2022) and soil food webs (Potapov, 2022). Nutrients might not only be embedded within the molecular structure of SOM, but can be retained by SOM´s charged functional groups (Helling et al., 1964). The capability to retain ionic nutrients from leaching is an important asset for long-term nutrient retention, but also for binding of hazardous heavy metals (Lair et al., 2007) and organic pollutants (Pignatello, 1998), preventing them from entering aquatic ecosystems, groundwater, and the food chain.

Soil physical properties are also affected by SOC. Namely, aggregation of soil particles increases with SOC content (Kong et al., 2005; Ma et al., 2024). Well-aggregated soils are more resistant to compaction and erosion, while simultaneously allow for better root penetration, as well as air and water movement (Hartmann & Six, 2022; Sarker et al., 2022). When the attribute of SOCs high moisture retention capacity is added (Rawls et al., 2003), the exceptional importance of SOC for terrestrial ecosystems in

general and arable land in particular becomes apparent. While the functions of SOC are diverse, there is a simple relationship recognizable: more SOC is better than less SOC.

A short history on soil organic carbon research

In the beginning (1786), F. K. Achard extracted peat with potassium hydroxide, receiving a dark brown solution: the starting point for a century long tradition to characterize soil organic matter using alkaline extraction followed by wet chemical analysis. Following the devastating soil degradation after the great depression in the United States, scientists investigating the turnover of organic carbon (OC) in both, terrestrial, as well as aquatic ecosystems, started working on the concept of molecular recalcitrance. The idea that macromolecular structures in the environment form by the polymerization of small molecules, like phenolic compounds derived from lignin, was popularized by S. A. Waksmans 1936 book “Humus”. These macromolecules were hypothesized to be unavailable by microorganisms, thus leading to a stable fraction of soil organic matter.

In parallel to the concept of recalcitrance, pioneering adsorption studies conducted in the 1960s and early 1970s (i.e. Frissel, 1961.; Meyers & Quinn, 1974; Shiga, 1961) demonstrated that OC derived from plants could bind to clays, providing the first evidence that minerals could retain OC in soil. This work was followed by the landmark contribution of J.M. Oades in the late 1980s, where Oades and his coworkers provided a comprehensive analysis how mineral types such as 1:1 clay minerals, 2:1 clay minerals, as well as iron and aluminum (oxyhydr)oxides interact with OC. This work showed that OC could be protected from rapid microbial degradation by interactions with the soil mineral phase, contributing to the long-term stabilization of OC in soil (Oades, 1989). Oades not only attributed OC longevity in soil to their interplay with minerals, but conceptualized, together with J.M. Tisdall (1982), that soil aggregation can lead to the spatial decoupling of microbial decomposer and OC as substrate.

Later, Six and colleagues (i.e. Six et al., 2000, 2001, 2004) validated this concept by demonstrating that the formation of small aggregates around OC led to the stabilization of this substrate against microbial decomposition.

At the turn of the millennium, scientists working on OC turnover in sediments of aquatic systems discarded the idea of macromolecular recalcitrance (Fig. 1-1). New, non-destructive *in situ* analytical developments (i.e., no alkaline extraction necessary) brought the oceanography research community to the conclusion that there are no recalcitrant macromolecules. Instead, near sediments, OC might be continuously broken down into smaller fragments, while a fraction of OC is stabilized against microbial attack through adsorption to the sediments mineral phase (Fig. 1-1) (Hedges & Keil, 1999).

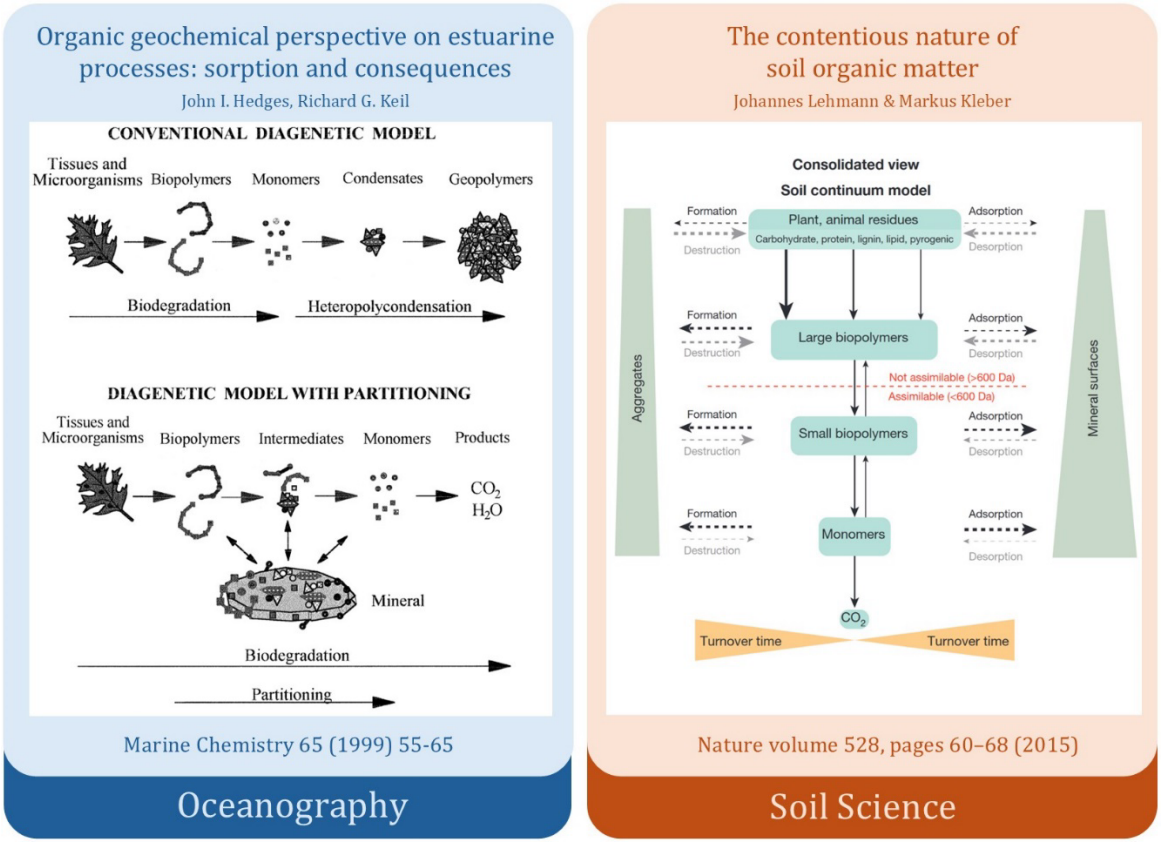

Figure 1-1. Concepts of the fate of organic carbon in aquatic sediments (left, Hedges & Keil, 1999, with permission) and soil (right, Lehmann & Kleber, 2015, with permission).

In soil science, molecular recalcitrance, alongside spatial exclusion through aggregation and sorption to soil minerals, remained a valid concept for OC stabilization.

A decade after the aquatic research community acknowledged the non-existence of recalcitrant macromolecules however, evidence through newly adopted analytical techniques piled up in the field of terrestrial ecosystem research as well (Schmidt et al., 2011).

Soil scientists came to the same conclusion as their maritime colleagues: there might be no recalcitrant macromolecules in soil (Angst et al., 2023; Schmidt et al., 2011). In 2015, Lehmann & Kleber adopted the ideas of Hedges & Keil for soil, by integrating the findings on aggregation for OC stabilization into the already existing model (Fig. 1-1, right side), laying the foundation on the current understanding on soil OC dynamics.

Organo-mineral interactions

The majority of OC in earths biosphere, that means, vegetation (450 Gt) and soils (1700 Gt), but also permafrost (1400 Gt), coastal systems (10 – 45 Gt) and marine sediments (1750 Gt) (Friedlingstein et al., 2022) is situated close to minerals. When OC is transformed and translocated on its biogeochemical journey through the planets ecosystem it will inevitable come in contact with minerals (Kleber et al., 2021). By mass, soil minerals far outweigh OC, which rarely exceeds single-digit percentage (Batjes, 2014; Jobbágy & Jackson, 2000). In soil science, the separation of soil OC into conceptual fractions of mineral-associated OC (MAOC) and particulate OC (POC) indicates that, on a global scale, MAOC turns over much slower than POC (mean turnover time 129 vs. 23 years in the top meter of soil, respectively (but see Zhou et al. 2024)), highlighting the importance of minerals for OC sequestration.

Controlled laboratory experiments and age distribution of OC in the field revealed that the process of adsorption onto mineral surfaces significantly slows the decomposition of SOC (Jones & Edwards, 1998; Mikutta et al., 2007; Saidy et al., 2015; Schrumpf et al., 2013). The extent of stabilization associated to minerals depends on mineral type: 1:1 clays bind only modest amounts of OC, whereas 2:1 clays offer greater sorption capacity, and oxyhydroxides, thanks to their pH-dependent positive surface charge in acidic to neutral soils, exhibit the strongest affinity for organic compounds (Feng et al. 2013; Gao et al. 2018; Georgiou et al. 2022; Saidy et al. 2013).

Moreover, the molecular characteristics of the sorbate play an important role: small, highly functionalized species such as carboxylic acids adsorb more effectively and are retained longer than neutral molecules like sugars and amino acids (Jones & Edwards, 1998; Yeasmin et al., 2014). In general, past research showed that mineralization increases with sorption strength in order of van der Waals forces < polyvalent exchangeable cation bridging < ligand exchange (Mikutta et al., 2007). MAOC does not have to remain adsorbed. Desorption processes which can be followed by microbial uptake (and mineralization) can be facilitated by different mechanisms, with the simplest being a change of equilibrium between soil solution and mineral-adsorbed OC.

Minerals not only retain organic and inorganic molecules (Spohn, 2024; Yeasmin et al., 2014). Microbial communities living on or near mineral surfaces are defined and restricted by mineral-induced nutrient availability and -accessibility, but the research area has barely been explored (Kandeler et al., 2019; Olagoke et al., 2019; Uroz et al., 2015). Microorganisms associated with minerals are of particular interest for global C cycling for two reasons. On the one hand is microbial life a primary reason for loss of OC through mineralization. On the other hand is microbial necromass an important source (Camenzind et al., 2023), with approximately half of all OC in arable soil exhibiting molecular signature of microbial origin (Angst et al., 2021).

Overall, the interplay between minerals, soil OC and microbes is an important control for the turnover of organic matter in soil. Although the stabilization of OC has been linked to adsorption, the subsequent transformation of mineral-adsorbed organic molecules by the soil microbiome and its links to adsorption-desorption kinetics remains unexplored. Likewise, the fate of mineral-bound C atoms directly coordinated to mineral surfaces has yet to be assessed. Despite decades of adsorption experiments, the thermodynamics driving these sorption processes are still unquantified. Finally, the formation of mineral-associated OC and its resident microbiome on pristine minerals under field conditions and influence of land use have yet to be investigated.

Soil minerals

In soil, 1:1- and 2:1 layer phyllosilicate clays and pedogenic (oxyhydr)oxides are the most abundant minerals (Fig. 1-3) (Kirsten et al., 2021). 1:1 clay minerals consists of one silica tetrahedral sheet bonded to one aluminum octahedral sheet in each layer. The most common 1:1 layer clay is kaolinite: its layers are tightly held by hydrogen bonding between tetrahedral oxygens and octahedral hydroxyls (Bergaya & Lagaly, 2013). As a result, kaolinite does not swell with water. This mineral in general shows very little isomorphic substitution (i.e., replacement of Si^{4+} with Al^{3+}, which results in a net negative charge). Cation exchange capacity (CEC) in general is therefore low, with most CEC attributed through edges and OH-surface sites (Ma & Eggleton, 1999). Protonated surface hydroxyl-groups causes positive surface charges under acidic conditions, which can lead to the adsorption of anions. Kaolinite is prevalent in the tropics and subtropics, as they form from mica and feldspars in humid climates under acidic conditions, where bases are extensively leached from soil (Bergaya & Lagaly, 2013).

In 2:1 layer clays, two tetrahedral silica sheets are sandwiching one octahedral aluminum sheet (Bailey, 1991). Isomorphic substitution is more abundant than in 1:1 clays, leading to negative surface charges and high CEC. Cations residing in the interlayer space are balancing these excess charges, with cation (e.g., K^+. Na^+, Ca^{2+}), and whether these cations are exchangeable characterizing different 2:1 layer clay types (Moore & Reynolds, 1997). Substantial isomorphic substitution within the tetrahedral sheets negative charge in illite is satisfied by K^+ cations. Interlayered K^+ is binding layers strongly with fixed basal spacing of 1.0 nm, not allowing for exchange with other cations or the mineral to swell with water (Sposito et al., 1999). Illites are commonly inherited from primary micas in temperate climates and (semi-) arid regions, with neutral pH and the presence of K^+ favoring the stability of illite (Bergaya & Lagaly, 2013). Smectites in contrast have less isomorphic substitution. Here, the negative charge is mostly balanced by exchangeable cations. Basal spacing is not fixed and can swell when wetted.

Because of the exchangeable nature of cations in smectite in comparison to fixed K^+ in illite, the former possess a high CEC of 80 – 120 cmol kg^{-1} (compared to 10 – 40

cmol kg^{-1} for illite) (Odom, 1984). Smectites often develop from basalt, or from weathering illite, when K^+ is removed from the mineral through moderate weathering. Lastly, vermiculite is commonly formed from weathering mica under high precipitation conditions without complete leaching of bases, often in slightly acidic and well-drained soils under forest use. Wetted vermiculite can swell less than smectite, but can exceed even the CEC of the later (Bergaya & Lagaly, 2013).

Al and Fe oxyhydroxides are important secondary minerals, where Al or Fe coordinates with oxygens and hydroxyls to form octahedra (Strauss et al., 1997). Gibbsite, an Al-oxide, precipitates from soil water under humid tropical conditions, representing a weathering stage beyond kaolinite (Herrmann et al., 2007; Wada & Aomine, 1966). Iron oxides form from Fe^{2+} released from primary minerals, which oxidizes and precipitates either as goethite, a yellowish-brown-, or hematite, a red-colored iron oxide (Cornell & Schwertmann, 2003). Formation of either goethite or hematite depends on climate. Cooler and wetter conditions favor the formation of goethite, while warm, dry conditions favor hematite formation (Cornell & Schwertmann, 2003). Presence of organic material and drainage conditions matter as well, with waterlogged periods leading to dissolution of oxides and recrystallisation (Yi et al., 2022). Soil oxides are commonly of low crystallinity and characterized by nanoporous structure with exceedingly high specific surface areas (SSA) (Schwertmann et al., 1985). They occur together with other minerals, where they form coatings. In comparison to permanently negatively charged clay minerals, oxides hydroxyl groups can gain or lose protons, which lead to positively charged surfaces under acidic conditions and negatively charged surfaces under alkaline conditions (Cornell & Schwertmann, 2003).

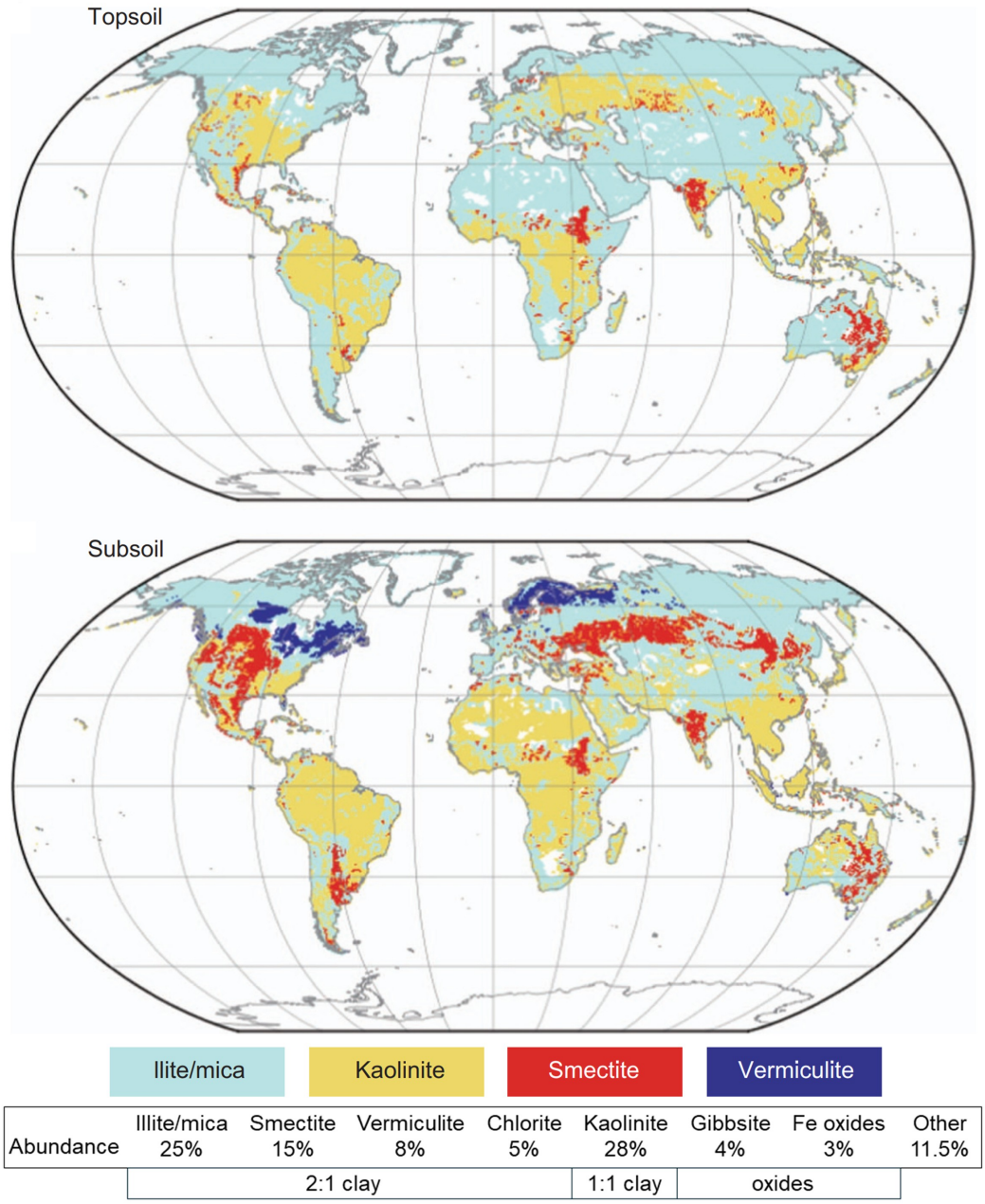

Figure 1-2. Global distribution and abundance of the dominant minerals in top- and subsoil alongside the Earth-wide mean abundance of fine-grained minerals in soil, excluding organic-rich soils and ice-covered regions. Gibbsite, chlorite, quartz and non-crystalline minerals were never the most abundant groups and are therefore not shown within the map (modified from Ito & Wagai, 2017). CC BY 4.0 (https://creativecommons.org/licenses/by/4.0/).

Objectives and Structure of Dissertation

The aims of my dissertation are twofold: to understand the interplay of soil minerals and SOM, and to identify how this relationship affects the microbial cycling of mineral-associated organic matter, especially C in soil. Accordingly, my hypothesis are:

1. A thermodynamic threshold of sorption strength exists, that prevents the microbial processing of sorbed organic compound if exceeded.
2. Due to their covalent binding to mineral surfaces via ligand exchange, sorptive stabilization of C-atoms of carboxylic groups exceeds that of other C-atoms of organic compounds
3. Sorptive stabilization of organic matter against microbial processing increases in the order goethite > kaolinite > illite.

To address hypotheses *2* and *3*, though, minerals loaded with organic molecules must be introduced to soil, and the perturbation nature of doing so must be considered. Namely, the consequences of introducing minerals that can decrease the amount of bioavailable nutrients, especially P, through adsorption to these minerals. Therefore, an additional hypotheses is :

4. Organic compounds and P mutually affect their bio-accessibility due to their co-accumulation on mineral surfaces.

I address these questions in three experimental parts (Fig. 1-4). First, the mechanistic understanding of sorption processes needed to test hypotheses 1-3 will be advanced by method development and quantification of thermodynamics of adsorption of monomers to minerals using isothermal titration calorimetry (Chapter II). Magnitude and characteristics of sorption-desorption processes are further evaluated in miniaturized batch studies. In the second part, the fate of ^{14}C labeled monomers adsorbed to minerals and incubated in arable topsoil, either uniformly ^{14}C labeled to answer hypotheses 2 (Chapter III), or position-specific labeled (carboxyl-^{14}C) to answer hypotheses 3 is investigated (Chapter IV). In the third part, the focus on C cycling is expanded to include P cycling as well. P status in mineral-incubated soil is explored, linking mineral-induced changes in P availability to microbial C use (Chapter III).

Finally, hypotheses 4 is tested by asking whether colloidal, naturally occurring organo-mineral associations can contribute to P availability in soils by quantifying P-fluxes into sinks mimicking plant roots (Chapter V).

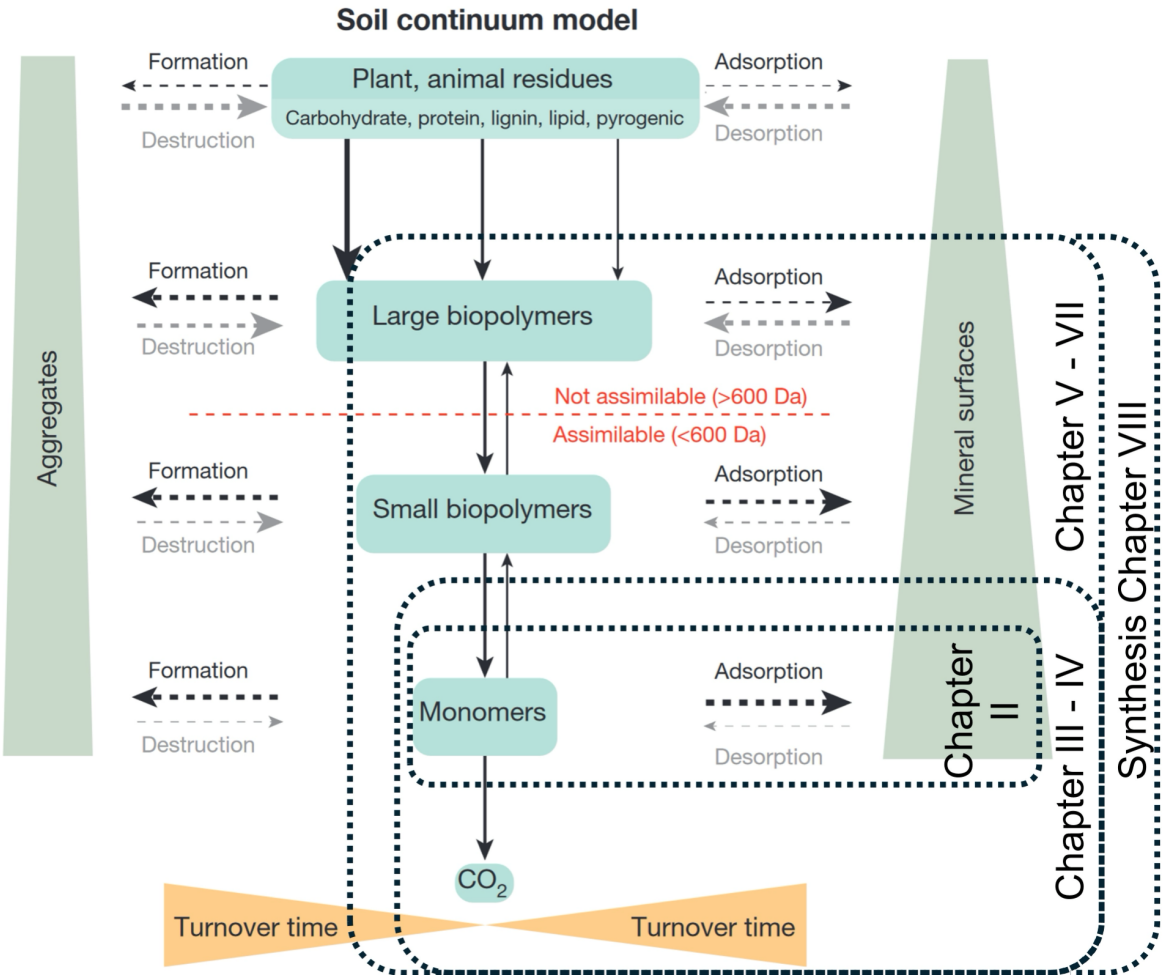

Figure 1-2. Dissertation focus of chapters II-VII, together with the synthesis chapter VIII, situated within the Lehmann & Kleber (2015, with permission) soil-continuum model. Microbial decomposition (solid arrows) breaks down organic residues into large biopolymers, small polymers and monomers, while sorption/desorption and aggregate dynamics (dashed arrows) confer stabilization. Box size and wedge width denote pool size and turnover time.

To reduce the complexity inherent in field-scale studies of mineral-associated organic carbon cycling, the research presented to answer hypotheses 1-4 in chapter II to V were conducted under controlled laboratory conditions. While this approach allows for careful manipulation of variables and helps isolating specific mechanisms, it inevitably neglects the dynamic influences found in natural settings. To address this limitation, I contributed as a co-author to field studies in which pristine minerals were

buried for five years, enabling direct observation of carbon accumulation, microbial colonization, and nutrient availability under *in situ* conditions. The findings from these field-based experiments, presented in Chapters VI and VII, complement the laboratory results by offering insights into the subdecadal processes that govern MAOC accumulation and cycling in real-world environments. From the answers given for within the framework of my dissertation, I synthesize consequences for the cycling of mineral-associated organic matter in light to experimental designs and remaining questions (Chapter VIII).

Chapter II

Thermodynamics of sorption of organic acids to iron oxyhydroxides

***Alexander Konrad*[1]**, *Ines Mulder*[1,4], *Diana Hofmann*[2], *Friederike Lang*[3], *Kenton P. Stutz*[3], *Jan Siemens*[1]

[1]Institute of Soil Science and Soil Conservation, Justus-Liebig University Giessen, Giessen, Germany

[2]Research Centre Jülich, Institute of Bio- and Geosciences, Agrosphere (IBG-3), Jülich, Germany

[3]Faculty of Environment and Natural Resources, Chair of Soil Ecology, University of Freiburg, Freiburg im Breisgau, Germany

[4]Ruhr University Bochum, Institute of Geography, Dept. Soil Sciences and Soil Resources, Bochum, Germany

This is a copyedited version of the manuscript under review in The European Journal of Soil Science.

Graphical abstract

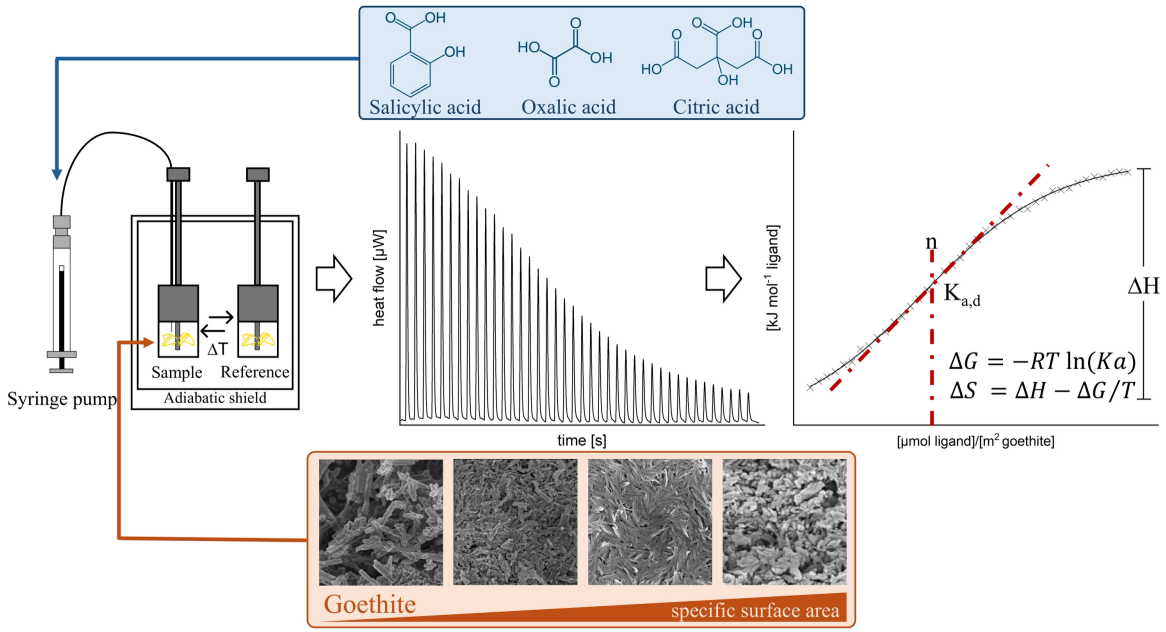

Instrumental setup (left), experiment-generated raw heat signal (middle), and model for isothermal titration calorimetry to decipher the thermodynamics of small organic ligand adsorption to mineral surfaces

Abstract

Adsorption to minerals is a key mechanism in stabilizing organic carbon in soils. We used isothermal titration calorimetry (ITC) to quantify the thermodynamics of binding of citric acid, oxalic acid, and salicylic acid to four goethites with different specific surface areas (SSA, 14 to 120 m^2 g^{-1}). Thermodynamic parameters could be determined for sorption of citric and salicylic acids, while flocculation of particles prevented their quantification for sorption of oxalic acid. For citric acid adsorption, ΔH shifted from -23.5±0.57 to -27.0±0.47 kJ mol^{-1} and ΔS from -8.8±1.54 to -29.9±0.13 J mol^{-1} K^{-1} with increasing SSA and broader (110) diffraction peaks of goethite, thus reducing ΔG from -20.7±0.02 to -18.0±0.03 kJ mol^{-1}. Salicylic acid adsorption was more exothermic (ΔH -40.53±1.93 kJ mol^{-1}) and accompanied by a larger loss of entropy (ΔS = -65.1±1.91 J mol^{-1} K^{-1}), possibly due to chelation of its ortho hydroxyl and carboxyl groups to single iron atoms on the mineral surface. These results demonstrate that ITC can decipher adsorption thermodynamics of organic ligands to mineral surfaces, but ligand-induced flocculation can render the interpretation of results difficult. Crystallite size and lattice defects of adsorbent minerals influence the thermodynamics of sorption by determining the conformation of organic molecules sorbed to goethite surfaces.

Introduction

The fate of organic carbon (OC) in soils is extensively researched as soil represents the largest terrestrial C sink (Georgiou et al., 2022). Sorption to minerals slows down OC mineralization, as demonstrated by age distributions of OC across soil depths and fractions (Saidy et al., 2015; Schrumpf et al., 2013; Spielvogel et al., 2008). Besides clay minerals, iron (oxyhydr-)oxides such as goethite are some of the most common pedogenic minerals (Cornell & Schwertmann, 2003; Guo & Barnard, 2013). Goethite commonly forms needle-shaped crystals and exhibits exceptional sorption capacities for anions or zwitterionic solutes due to the net positive surface charges in acidic and neutral soils (Bramble et al., 2024; Feng et al., 2013; Gao et al., 2018; Georgiou et al., 2022; Saidy et al., 2012). In soils, the introduction of impurities and variable boundary conditions of mineral formation (Schwertmann et al., 1985) cause crystallographic defects, like line defects (dislocation) (Taitel-Goldman et al., 2004), point defects (vacancies) (Madsen et al., 2009), and substitutional defects (Goodman & Lewis, 1981). Generally the number of defects and the specific surface area (SSA) increase with decreasing size of goethite crystallites (Schwertmann et al., 1985; Taitel-Goldman et al., 2004). Defect density of goethite has been shown to play an important role for the adsorption of arsenic moieties of organometallic complexes (Hou et al., 2022), phosphate (Strauss et al., 1997), and OC (Kaiser & Guggenberger, 2003, 2007; C. Mikutta et al., 2004). Despite the relevance of sorption of organic molecules on oxyhydroxide mineral surfaces to the stabilization of OC, their thermodynamics, namely sorption enthalpy (ΔH), Gibbs free energy (ΔG), and entropy (ΔS), have not been quantified to date.

Isothermal titration calorimetry (ITC) is a method able to quantify the thermodynamics of binding-reactions within a single experiment and is regarded as gold standard for studying the thermodynamics of molecular interactions in solution (Bastos et al., 2023). In an ITC experiment, known amounts of sorbate are sequentially titrated into a constantly stirred reaction chamber filled with known amounts of sorbent and the heat released or consumed during the binding reaction is measured (Freire et al., 1990; Wiseman et al., 1989).

While ITC is routinely used to investigate the binding of ligands to macromolecules, the technique has rarely been applied for the study of adsorption of ligands to solid materials (Joshi et al., 2004; Prozeller et al., 2019).

The usage of suspended nanoparticles as sorbent increases the complexity of interactions during the ITC experiment, especially by potential flocculation of particles (Jódar-Reyes et al., 2001). Nonetheless, this technique has been used to study the sorption of orthophosphate onto kaolinite (Penn & Warren, 2009), soil slurries (Penn & Zhang, 2010), gibbsite (Hong et al., 2020), and clay-sized mineral mixtures extracted from soils (Hong et al., 2021) as well as uranium on goethite (Kumar et al., 2022). However, only the studies conducted with gibbsite and clay mineral mixtures obtained ITC data suitable to calculate the desired thermodynamic characteristics (Hong et al., 2020; Hong et al., 2021).

The aim of this study was to explore the potential and limitations of ITC to elucidate the thermodynamics of sorption of small organic acids to goethite. Oxalic acid, citric acid, and salicylic acid were chosen as organic model ligands because of their ubiquity in soil and strong binding affinities to goethite (Jones & Edwards, 1998; Yeasmin et al., 2014). Four goethite minerals of different crystallinity, specific surface area (SSA), and density of surface defects were investigated. Sorption was studied at a slightly acidic pH of 5.5. We hypothesized, that 1) sorption of oxalic- and citric acid yield similar changes in enthalpy ΔH and Gibb´s free energy ΔG at pH 5.5 as both ligands contain two deprotonated carboxyl groups at that pH, and 2) ΔH and ΔG of ligand adsorption to minerals increase with increasing surface area and increasing number of defects of minerals.

Material and Methods

All chemicals were purchased from Sigma Aldrich (Darmstadt, Germany), with purities >99%. Ultra-pure water was sourced from a Purelab Flex 2 Water Purification System (Veolia Water Solutions and Technologies, Buchinghamshire, United Kingdom).

Goethite synthesis and characterization

Commercially available goethite BAYFERROX 920Z (LANXESS Deutschland GmbH, Cologne, Germany) and three self-synthesized goethite minerals were used for this study. Two iron hydroxides were synthesized using 10 M NaOH titrated into a constantly stirred, freshly prepared 0.5 M $FeCl_3$ solution up to pH 12 (Dultz et al., 2019). To create hydroxides with different specific surface areas, the suspensions were stored for 68 days at 4 °C and 8 °C, respectively, before adjustment to pH 6 with 0.2 M HCl. The third goethite was synthesized by aeration of an $NaHCO_3$-buffered 0.05 M $FeCl_2$ solution with compressed air injected through perforated polyethylene tubes (Goodman & Lewis, 1981; Fischer et al., 1998). Mineral suspensions were filled into Spectra/Por 2 dialysis membranes with a molecular weight cut-off of 12-14 kDa and dialyzed against deionized water until the conductivity of the suspensions dropped below 5 µS cm^{-1}. All suspensions were afterwards freeze-dried and ground using a mortar and pestle.

Mineral purity was confirmed via x-ray powder diffraction using an Empyrean 3 X-ray diffractometer (Malvern-PANanalytical B.V, Worcestershire, Great Britain) equipped with a copper source. Specific surface areas, pore volume, and pore size distribution of mesopores were investigated via nitrogen sorption at 77 K after drying for 18 h at 65 °C using a Quantachrome Quadrasorb evo (Anton Paar Germany GmbH, Ostfildern-Scharnhausen, Germany). The morphology of goethite was studied with a scanning electron microscope (SEM) GeminiSEM 560 (Carl Zeiss Microscopy Deutschland GmbH, Oberkochen, Germany) after mounting on sample holders with carbon tabs.

Isothermal titration calorimetry

Experimental setups for all investigated mineral phases and organic acid combinations followed the same general procedure: Heat production or consumption during adsorption of carboxylic acids as ligands on mineral surfaces were measured with a dynamically calibrated thermal activity monitor 3 (TAM 3, TA Instruments Inc., Newcastle, Delaware, USA) equipped with a 4 mL nano calorimeter. The reference ampoule of the calorimeter was filled with suspensions of the same mineral and exchanged weekly to avoid sedimentation. The calorimeter was dynamically calibrated after each suspension change to account for potential differences in suspension heat capacity. Mineral suspensions and ligand solutions of varying concentrations in 0.01 M KCl background electrolyte were adjusted to pH 5.5 ± 0.01 with HCl and KOH to mitigate the heat signal of the acid-base neutralization during titration. Sorbate solutions were filtered through <220 nm polyether sulfone syringe filters in a sterile environment. The calorimeter syringe system was rinsed several times, first with 0.1 M HCl to remove potential goethite, followed ethanol to reduce the risk of microbial processing of the organic sorbates. Sorbents and sterile-filtered sorbates were degassed under vacuum for 30 minutes, followed by 5 minutes in an ultrasonic bath at room temperature. The titration unit was assembled under sterile conditions afterwards. The system was equilibrated prior to titration to reach thermal stability (standard deviation < 50 nW, slope < 50 nW h^{-1}).

After temperature equilibration, experiments during method development consisted of 20 to 40 titrations at 25 °C with volumes from 0.5 to 3 µL, dosing-speeds of 0.1 - 1µL s^{-1} and titration intervals between 8 - 30 minutes into mineral suspensions ranging from 5 g L^{-1} and 40 g L^{-1}. Potential organic acid-induced mineral dissolution during titration experiments was investigated by analyzing dissolved iron in the suspensions after ITC experiments. To this end, suspensions were centrifuged at 17.000 x g for 60 min and the supernatant analyzed using inductively coupled plasma optical emission spectroscopy (ICP-OES) (Agilent 720, Agilent Technologies Inc., Santa Clara, USA).

Subsequently, blank measurements were performed by repeating ITC experiments with 0.01 M KCl solutions (likewise adjusted to pH 5.5) instead of mineral suspensions to subtract the heat of dilution from ligand titration into the mineral suspensions.

Data analysis

Experimental raw data (e.g., time evolved, timing of the consecutive injections, heat flow) were exported from the calorimeter using TAM Assistant 3.0 (TA Instruments Inc., Newcastle, Delaware, USA). Baseline correction was performed with Origin Pro 2024b (OriginLab Corporation, Northampton, MA, USA), using the integrated asymmetric least square smoothing function(Eilers & Boelens, 2005). Baseline-corrected data were subsequently exported to NanoAnalyze 4.0.2 (TA Instruments Inc., Newcastle, Delaware, USA), integrated for heat flows, and corrected for blank titrations.

The adsorption thermodynamics was modeled using the independent, one-site binding model integrated into the NanoAnalyze software based on the Wiseman isotherm (Wiseman et al., 1989). The Wiseman isotherm was developed and is typically used for analyzing the binding of ligands to biological macromolecules. This model assumes that (1) all binding sites are considered identical with the same affinity for the ligand, (2) the binding of a ligand to one site does not affect the binding at another site, and (3) that the number of binding sites for ligands per macromolecule equals 1. Application of this isotherm to the binding of ligands to a mineral surface requires a careful consideration of dimensions of the variables that are used as input for the modeling of the binding reaction. The one-site binding model typically used to describe ligand-macromolecule interactions expresses the concentrations of ligands, macromolecular sorbent and ligand-macromolecular complexes in the dimension [mol L^{-1}]. For describing the binding of ligands to mineral surfaces, a former study therefore determined the number of reactive binding sites on the surface of their gibbsite minerals in separate potentiometric titration experiments(Hong et al., 2020) to derive the concentration of gibbsite binding sites in [mol L^{-1}] for the interpretation of their ITC experiments. In order to derive all sorption and thermodynamic parameters in a single ITC experiment, we decided to use instead the surface of the minerals as direct input and thus express the concentration of the sorbent as [m^2 L^{-1}].

This adjustment will not affect the value of ΔH that is determined in the titration experiment, since ΔH is derived directly from changes of the measured heat flow. Similarly, this uncommon dimension of the sorbent concentration will not affect the estimation of the association constant K_a from the titration experiment, because K_a is considered in the Wiseman equation via the parameter *r*, in which K_a is combined with total mineral surface concentration, so that the units of K_a and sorbent concentration cancel out (Wiseman et al., 1989, p. 1). The parameter *r* and hence K_a are derived from the slope of the sigmoidal binding curve at its inflection point. However, when applying the Wiseman model for the interpreting the titration experiments with the dimension [m^2 L^{-1}] for the sorbent concentration, we have to consider that the dimension of the x-axis of the binding curve in our case is not dimensionless, but in the unit [mol m^{-2}]. If the assumption of one binding site per unit of sorbent is met, then the inflection point of the sigmoidal binding curve is exactly at a ratio of 1 on the x-axis, which describes the binding stoichiometry *n*. Hence, when plotting the x-axis of the binding curve in the dimension [mol ligand m^{-2} mineral surface area], the parameter *n* directly indicates the number of sorption sites per m^2 surface area of the mineral. To test the feasibility of our approach, we repeated the estimation of thermodynamic parameters and K_a after transforming the sorbent concentration from the unit [m^2 L^{-1}] into [mol binding sites L^{-1}] by multiplying the parameter *n* retrieved from the one site binding model with the surface area concentration [m^2 L^{-1}] in our suspension. Using this value as input for *M* (now in mol binding sites L^{-1} mineral suspension) yielded a parameter *n* of 1 (Supporting Information Fig. S2-1). The estimated thermodynamic parameters of adsorption, including K_a remained unchanged, confirming the applicability of our approach.

The Gibbs free energy of adsorption ΔG and the entropy change ΔS of the sorption reaction can be derived from general thermodynamic relationships. The Gibbs free energy of adsorption ΔG [J mol^{-1}] is related to the equilibrium association constant K_a (eq. 1):

$$\Delta G = -RT \ln (K_a), \qquad \text{(eq. 1)}$$

where R is the gas constant [J K^{-1} mol^{-1}] and T the temperature [°K]. Adsorption ΔG can be separated into enthalpic (ΔH [J mol^{-1}]), as well as entropic (ΔS [J mol^{-1} K^{-1}]) contributions via equation (eq. 2):

$$\Delta G = \Delta H - T\Delta S \quad \text{(eq. 2)}$$

Successful ITC experiments were repeated in triplicates, with the thermodynamics of each experimental replicate modelled separately. Inverse variance-weighted means were computed from values x_i with standard errors σ_i for modelled thermodynamic parameters with standard errors, e.g. ΔH and n (eq. 3):

$$\bar{x} = \frac{\sum_{i=1}^{n} \frac{x_i}{\sigma_i^2}}{\sum_{i=1}^{n} \frac{1}{\sigma_i^2}}. \quad \text{(eq. 3)}$$

The standard errors of the weighted means $\sigma_{\bar{x}}$ are given by (eq. 4):

$$\sigma_{\bar{x}} = \sqrt{\frac{1}{\sum_i^n \frac{1}{\sigma_i^2}}}. \quad \text{(eq. 4)}$$

Means of modelled parameters without standard errors, e.g. ΔG, ΔS and K_a were calculated as arithmetic means.

Results and Discussion

Characteristics of minerals

The SSA of minerals ranged from 13.75 m^2g^{-1} for commercial BAYFERROX goethite to 119.56 m^2g^{-1} for goethite synthesized using compressed air (Fig. 2-1). For convenience, we refer to these minerals as Goe-14 (13.75 m^2 g^{-1}), Goe-93 (92.55 m^2 g^{-1}), Goe-112 (111.89 m^2 g^{-1}) and Goe-120 (119.56 m^2 g^{-1}). Scanning electron microscope (SEM) images showed comparably large elongated rhombic shapes with clear crystal faces for Goe-14, clear needle-like shapes for Goe-93 and Goe-112, and finer grain structures for Goe-120 (Fig. 2-1). Powder X-ray diffraction (XRD) spectra confirmed that all minerals were pure goethite, with XRD peaks broadening with increasing SSA (Fig. 2-1). The full width at half maximum (FWHM) of each 110 peak ($FWHM_{110}$) after

baseline correction increased with increasing SSA, thus indicating a decreasing crystallinity with increasing SSA (Supporting Information S2 & Tab. 1).

This relationship corresponded with the crystal morphology observed with SEM, as reported earlier (Echigo et al., 2012).

Fig. 2-1. Scanning electron microscopy recordings of synthesized goethite with specific surface areas from 13.75 $m^2 g^{-1}$ (top left), up to 119.56 $m^2 g^{-1}$ (bottom left), with powder X-ray diffractograms and pore size distribution of the four goethite samples (right).

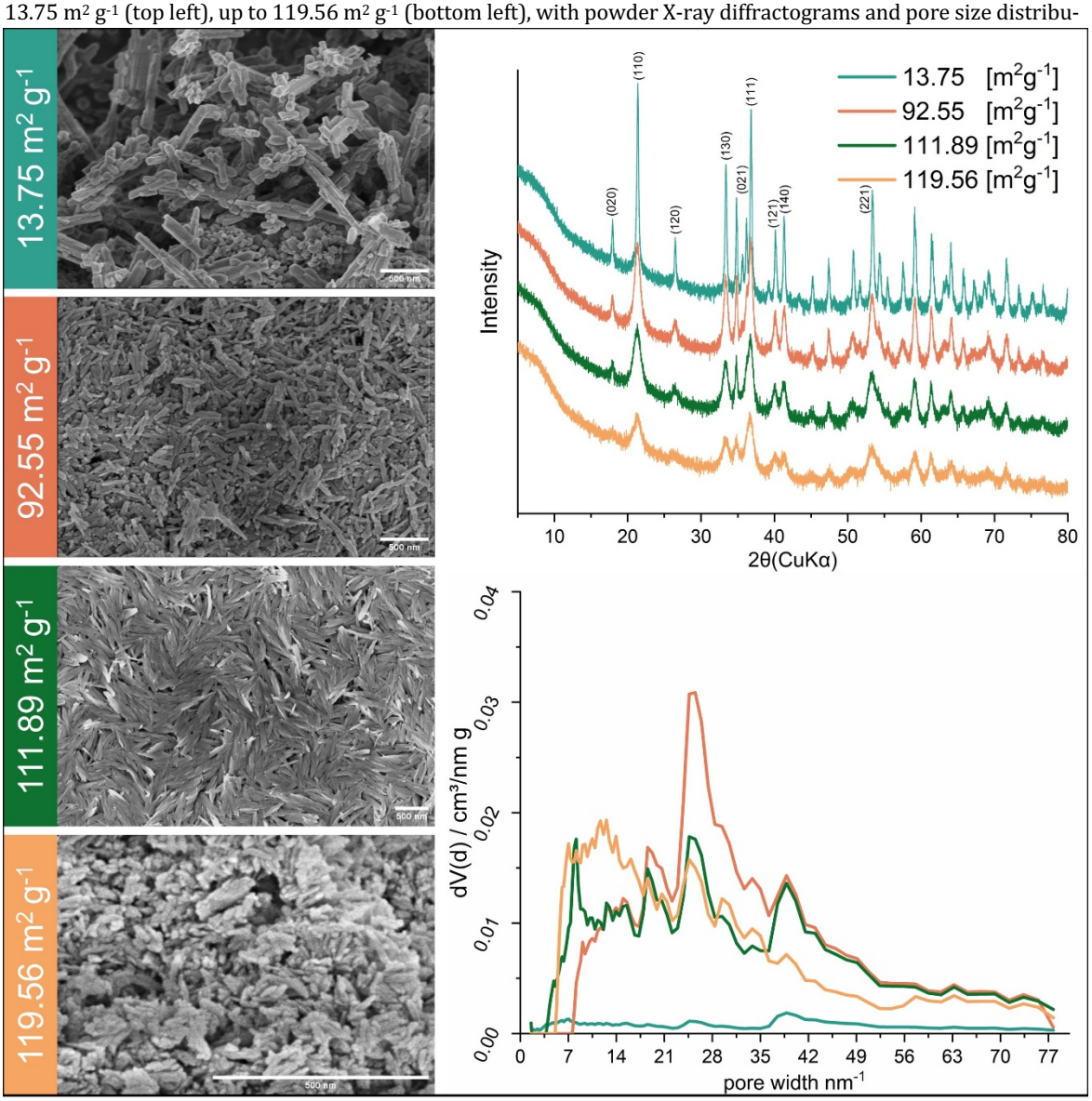

Preliminary experiments to avoid flocculation and dispersion

Ligand-induced flocculation and dispersion emerged as the main challenge in obtaining usable data during our ITC experiments. We identified four distinct patterns of flocculation (Fig. 2-2). We could not achieve a stable suspension with the most crystalline goethite Goe-14. Within minutes of starting the agitator, colloids flocculated and settled at the bottom of the measuring ampoule (Fig. 2-2a). Despite this sedimentation, the ITC experiment with citric acid and flocculated goethite revealed small exothermic heat spikes followed by endothermic spikes with amplitudes smaller than 1 µW. Since no dissolved iron was found in the suspension after the experiment, we exclude dissolution of goethite by citric acid as a reason for the heat production and consumption. Thus, we conclude that only flocculation and dispersion dominated the heat flow in this experiment.

A second flocculation phenomenon occurred when the sorbate injection rate exceeded 0.1 µL s^{-1}. Above this dosage speed, sorbates did not mix properly with the suspension during the initial titrations. Instead, noisy and time-delayed exothermic signals were generated (Fig. 2-2b).

The third flocculation phenomenon was observed when oxalic acid was injected into any goethite suspension. Oxalate caused flocculation and immobilization of colloids around the injection cannula (Fig. 2-2c), which induced partial sedimentation and a clear supernatant at the end of the sorption experiment even while the agitator was still running. Since no dissolved iron was found in the suspension, bridging of goethite particles by monodentate binding of oxalic acid molecules to different mineral surfaces was most likely the driver of flocculation. Indeed, FTIR measurements showed that goethite-adsorbed oxalic acid formed monodentate structures with the ligand's two carboxylic acid functional groups being bound to different hydroxyl groups on

minerals surfaces (Yeasmin et al., 2014). Therefore, the contribution of flocculation and ligand-exchange to heat flow cannot be disentangled.

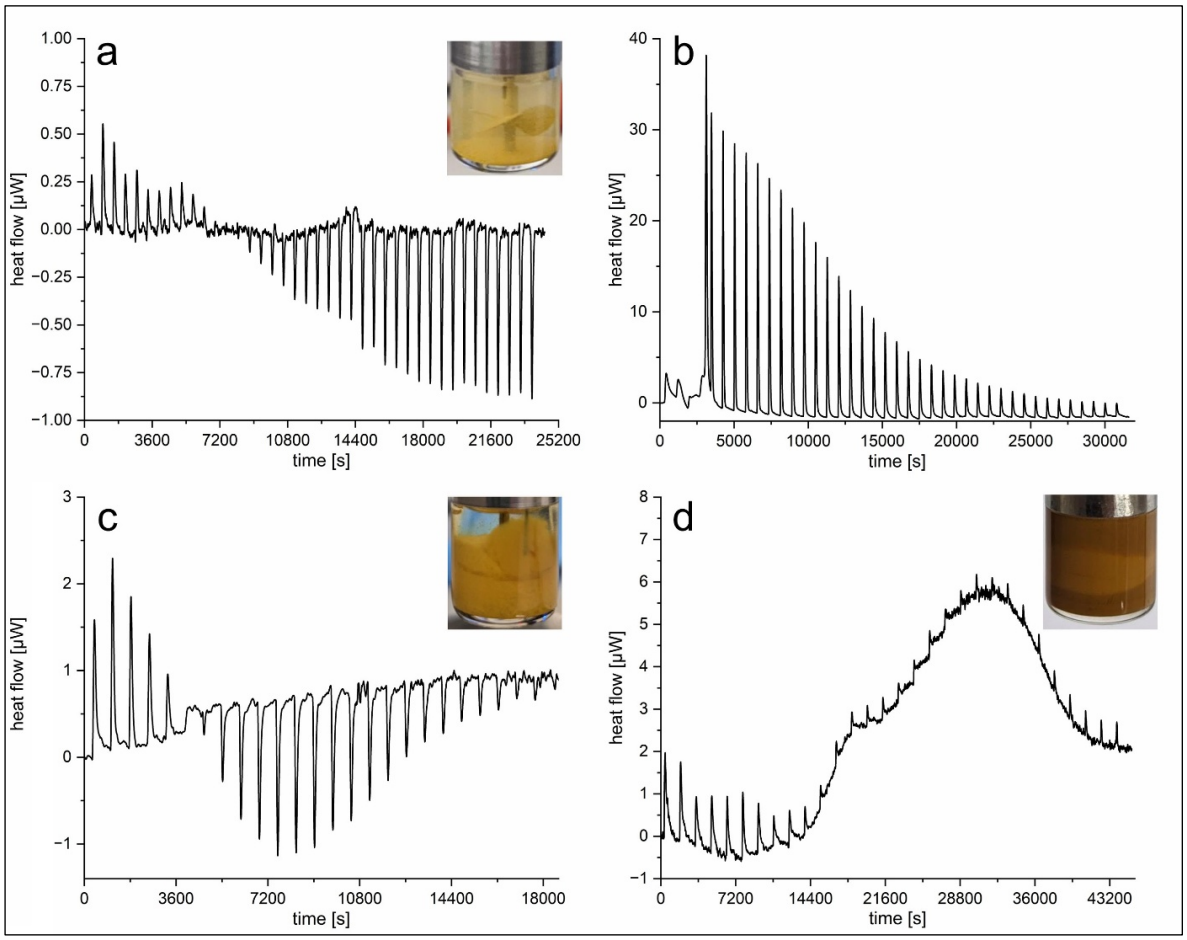

Fig. 2-2. Flocculation observed during method development in isothermal titration calorimetry experiments with no baseline correction applied. (a) Goe-14 with citric acid showed flocculation and sedimentation, accompanied by low exothermic heat signals, followed by low endothermic heat flow spikes. (b) High dosage speeds of citric acid into Goe-112 lead to noisy heat spikes during the initial injections of sorbate solution of the experiment. (c) Thermograms of oxalic acid adsorption to Goe-93 with exothermic signals followed by endothermic signals and flocculation of the mineral phase. (d) Salicylic acid adsorption to Goe-112 with strong baseline shifts and two-toned suspension after the experiment.

Lastly, sequential titration of salicylic acid to Goe-93 and Goe-112 led to reproducible baseline shifts (Fig. 2-2d). After disassembling the reaction ampoule, we observed that the suspension surrounding the agitator changed color (Fig. 2-2d). The calorimeter's agitator operates at constant power, but a change in the suspension's viscosity during titration would have caused friction-induced heat to enter the calorimeter shifting the baseline, with observations of high viscosity in flocculated aqueous

goethite suspensions and water-like viscosity in dispersed suspensions support this theory (Blakey & James, 2003). While software can correct these baseline shifts, the two-toned suspension observed after the experiment raises concerns about adequate mixing of minerals and sorbates, and therefore the validity of the obtained thermodynamic parameters.

We tried to prevent flocculation phenomena by enhancing the intermixing of the suspension through agitator modifications. The shaft of the standard agitator, the 18 carat golden propeller, was shortened to fit two stacked agitators within the suspension of the measurement ampoule. In other experimental trials, 3D-printed helical polypropylene agitators were placed into reference and measurement ampoule and tested (Supporting Information Fig. S2-3). Both approaches, however, failed to produce stable baselines. Thus, all successful ITC experiments to retrieve thermodynamics of adsorption were performed with one 18 carat gold agitator set to a maximum of 110 rpm allowing best possible mixing. Additionally, a low dosage speed of the injections (0.05 µL s^{-1}) was chosen to avoid localized high concentrations of free ligands within the suspension as encountered in Fig. 2-2b.

Adsorption thermodynamics of citric and salicylic acid on goethite

All successful experiments showed that salicylic acid and citric acid adsorption to goethite at pH 5.5 resulted from enthalpy-driven processes that were accompanied by a loss of entropy (ΔH, ΔS < 0; Tab. 2-1). The stoichiometry parameter *n* and therefore sorption capacity derived from the ITC experiment was 1.7–2.8 μmol m^{-2} for citric acid adsorbed to goethite with SSA from 93 – 120 m^2 g^{-1} (Tab. 2-1).

Table 2-1. Thermodynamics of adsorption of citric acid to goethite of specific surface areas (SSA) of 92.55 to 119.56 m^2 g^{-1} and salicylic acid to goethite of SSA of 119.56 m^2 g^{-1}.

		Citric acid		Salicylic acid
SSA [m^2 g^{-1}]	92.55	111.89	119.56	119.56
$FWHM_{110}$ [2θ]	0.799	1.013	1.128	1.128
K_a [mol^{-1}]	4348±37	2703±47	1449±28	6667±41
n [μmol m^{-2}]	1.71±0.05	2.79±0.05	2.77±0.03	0.20±0.03
ΔH [kJ mol^{-1}]	-23.5±0.57	-24.0±0.65	-27.0±0.47	-40.53±1.93
ΔG [kJ mol^{-1}]	-20.7±0.02	-19.6±0.03	-18.0±0.03	-21.7±0.1
ΔS [J mol^{-1} K^{-1}]	-8.8±1.54	-15.0±0.42	-29.9±0.13	-65.1±1.91
-TΔS [kJ mol^{-1}]	2.6±0.63	4.1±0.40	8.9±0.04	19.4±0.57

This is in close agreement with previous work on orthophosphate (not citric acid) adsorption of 2–3 μmol m^{-2} to a variety of goethite samples (Strauss et al., 1997). Hence, the comparison supports the validity of our ITC results for sorption capacities. Additionally, citric acid experiments conducted with Goe-93, Goe-112, and Goe-120 (Fig. 2-3) demonstrated that the sorption capacity on a μmol m^{-2} basis of Goe-120 was 162% of the sorption capacity of Goe-93 (Tab. 2-1, stoichiometry parameter *n*) although its SSA equaled only 121% of the Goe-93 SSA. This disproportionally large increase in sorption capacity with increasing SSA points to the relevance of the abundance of defects within the crystal lattices for adsorption of citrate. Vice versa, the disproportionally large decrease in sorption capacity with decreasing SSA might also indicate that not all pore surfaces of increasingly larger mineral particles that are measured by N_2 adsorption are accessible for dissolved citric acid in the short time

interval of the ITC experiment. This would lead to an increased time delay between injection of sorbate and adsorption to unoccupied binding sites. As a consequence, heat from diffusion-delayed adsorption may be either detected as part of the baseline drift and subtracted, or attributed to a later titration event.

ΔH of citrate sorption to goethite ranged from 23.5 kJ mol^{-1} to 27.0 kJ mol^{-1} (Tab. 2-1), which is similar to the ΔH value of -24.4 kJ mol^{-1} for the sorption of ortho-P (2 mM solution) to gibbsite at pH 4.2 (Hong et al., 2020). The similarity of reaction enthalpies is likely due to the fact that adsorption of both, citrate and ortho-P to both goethite and gibbsite is dominated by ligand exchanges with hydroxyl surface groups of the minerals.

The ΔG values we derived for the sorption of citrate to the three goethites (-18.04 to -19.0 kJ mol^{-1}) was slightly smaller than the value of -25.7 kJ mol^{-1} reported for the sorption of ortho-P to gibbsite (Hong et al., 2020).

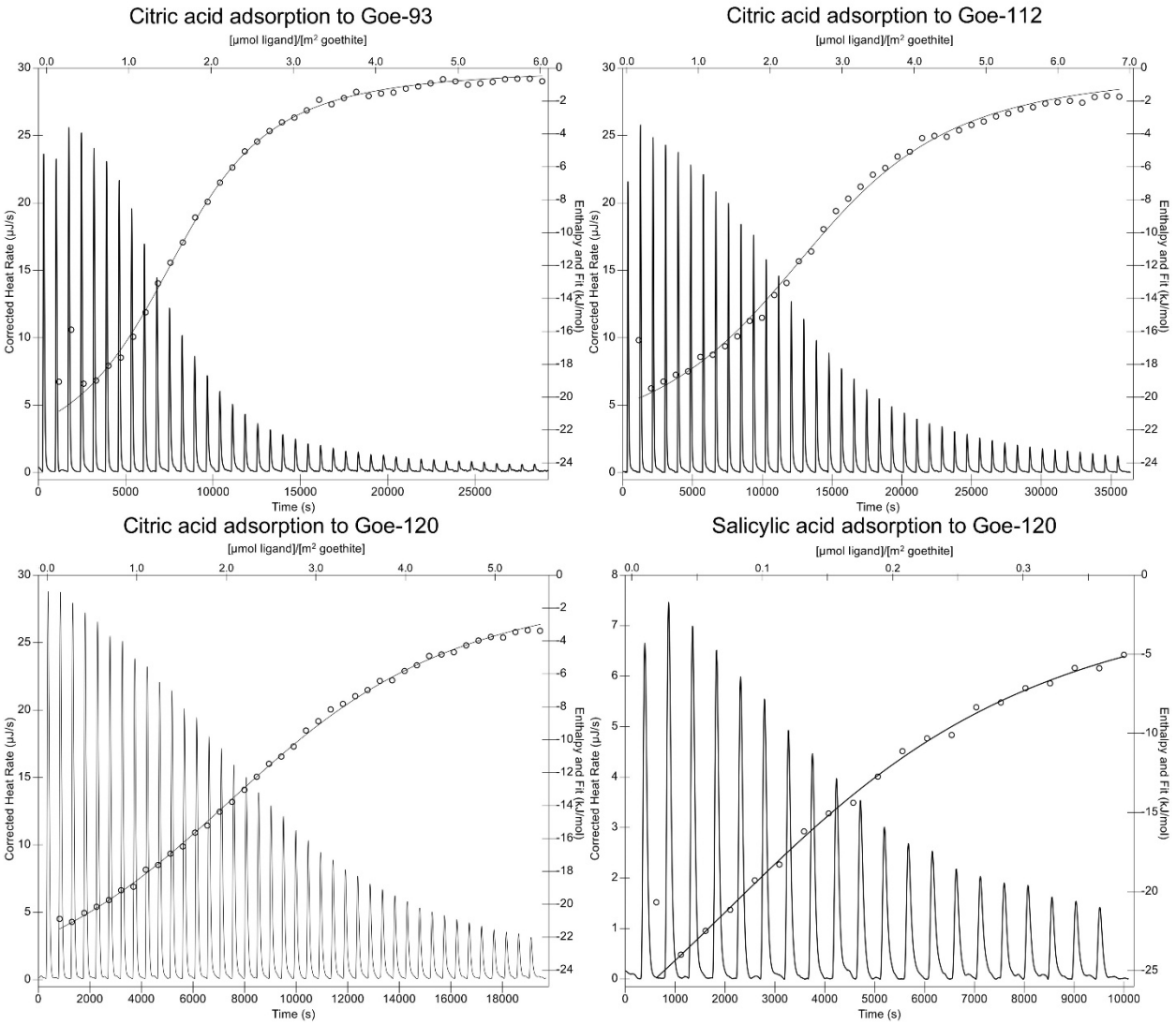

Fig. 2-3. Thermograms and fitted independent binding models from titration experiments with citric acid and goethite minerals with specific surface areas (SSA) of 92.55 (Goe-93), 111.89 (Goe-112), and 119.56 m^{2}g^{-1} (Goe-120), as well as salicylic acid adsorption onto goethite with SSA of 119.56 m^{2}g^{-1}after blank correction.

Both ΔH of sorption and system ΔS became more negative with increasing goethite SSA and FWHM of the 110 diffraction peak (Tab. 2-1). This trend can be explained by the number of available binding sites for citric acid on goethite that vary regarding crystallite size and the abundance of defects within the crystal lattices. More binding sites enable more adsorption of molecules from aqueous solutions to mineral surfaces that lead to a loss of entropy from free diffusion in solution to a more ordered state

on surfaces. Hydroxyl release by the ligand-exchange reaction and diffusion in solution would counteract a part of the system's loss of entropy. In addition, carboxyl-group oxygen atoms can bind to lattice Fe in different coordination modes. These include monodentate surface complexes, bidentate chelation to a single Fe center, and monodentate bridging between two Fe atoms. Each binding mode imposes a distinct degree of conformational freedom on the sorbed ligands: Monodentate-bound acids retain greater rotational and torsional flexibility, which leads to a smaller entropy loss compared to more constrained bidentate chelation or monodentate bridging. The increased entropy loss and lower ΔG of citrate sorption to goethite with SSA (Goe-120 > Goe-112 > Goe-93) thus indicates that higher SSA and $FWHM_{110}$ are related to more lattice defects (Hou et al., 2022) that induce more bidentate chelation and monodentate bridging.

In comparison to citric acid, the adsorption thermodynamics of salicylic acid to goethite could only be determined for Goe-120 (Fig. 2-3, Tab. 2-1). Surprisingly, adsorption of salicylic acid was more exothermic than that of citric acid. This cannot be explained by ligand-binding of the one carboxyl-group of salicylate to Fe on mineral surfaces. Instead, the hydroxyl group in ortho-position to the carboxyl group likely facilitated bidentate chelation with surface Fe atoms, thus leading to stronger covalent interactions and more negative ΔH. Zeltner et al. as well as Yost et al. assumed a chelate structure forming between goethite and salicylic acid after investigation of FTIR spectra (Davis & Hayes, 1987; Yost et al., 1990). Further studies of the adsorption of polyvinylalcohol to goethite(Kavanagh et al., 1976) and alcohols to hematite via chemisorption of hydroxygroups (Yun et al., 2018) support this theory. The formation of a chelate structure of salicylate with its rigid aromatic ring and possible intramolecular hydrogen bonding with the hydroxyl groups of the goethite surface would also explain the much larger loss of entropy compared to adsorption of citric acid (Tab. 2-1). Citric acid has a flexible aliphatic backbone, and thus when one or more carboxyl-groups are coordinated to surface-Fe atoms, the molecule retains rotational and torsional freedom to a higher degree compared to salicylate.

Potentials and limitations of isothermal titration calorimetry for determining the thermodynamics of organo-mineral interactions

ITC is able to detect virtually any molecular interaction by measuring the production or consumption of heat, a universal feature of the processes. However, this universality also poses a challenge to determine the thermodynamics of single processes, as heat signals from unrelated processes can interfere and complicate the measurement and deconvolution of interaction-specific heat signals (Bastos et al., 2023). Not only flocculation, which has been described within this study and in literature (Jódar-Reyes et al., 2001), but also organic acid-induced mineral dissolution and re-crystallization (Reichard et al., 2007; Y. Zhang et al., 1985) may lead to changes in thermograms that are not related to adsorption processes. Possible interfering processes require careful optimization and specific adjustment of experimental conditions as indicated by flocculation in our pre- and main experiments. ITC thus is not suitable as a high-throughput method for investigating large numbers of molecule-mineral combinations. Yet it is suitable to determine thermodynamic parameters for sorption processes with high binding affinities such as phosphate to soil colloids (Hong et al., 2020; Hong et al., 2021) and carboxyl acids to goethite in this study.

Originally, models to infer thermodynamics of binding interactions from ITC data were developed for macromolecule interactions with ligands (e.g. Claveria-Gimeno et al., 2017), not binding interactions of ligands with colloidal systems. The general assumption of simple one-site binding models (including Wiseman et al. 1989 and this study), that all binding sites have the same binding affinity therefore would be violated when goethite crystallites possess binding sites of different reactivity (Kaiser & Guggenberger, 2003, 2007; C. Mikutta et al., 2004). The application of these models to ITC measurements of soil ligand exchanges nonetheless provides the mean sorption thermodynamics of a given molecule to a mineral phase.

To conclude, our study demonstrates that ΔH, ΔS, and ΔG of sorption of low molecular weight organic acids to goethite, together with the sorption capacity for the given molecule can be determined by ITC. Moreover, variations in specific surface area and

related abundance of defects of the mineral lattice as well as sorbate configuration determine ΔG of adsorption not only via shifts in ΔH, but also via modulations of ΔS.

Conclusion

By quantifying the thermodynamics of adsorption of citric acid and salicylic acid to goethite, we show that higher SSA and lattice defects strengthen binding and constrain ligand conformation. Although ITC is sensitive to flocculation, its direct heat measurements provide unique mechanistic insight into the binding of organic ligands to minerals. These insights can improve prediction of soil organic carbon persistence and information on soil carbon cycling. Future work should broaden the ligand- and mineral suite, examine pH effects, and develop instrumentation to mitigate flocculation.

Author Contributions

Alexander Konrad: investigation, method development, validation, writing – original draft, writing – review and editing. **Ines Mulder**: conceptualization, writing – review and editing, funding acquisition, supervision. **Diana Hofmann**: methodology, validation, writing – review and editing. **Friederike Lang**: conceptualization, validation, writing – review and editing, funding acquisition. **Kenton P. Stutz**: conceptualization, validation, writing – review and editing, funding acquisition. **Jan Siemens**: conceptualization, investigation, validation, writing – original draft, writing – review and editing, funding acquisition, supervision.

Acknowledgements

This work was funded by the German Research Foundation (DFG, grant no. 465123895). Experimental data were obtained within the DFG Priority Program 2322 “Systems ecology of soils – Energy Discharge Modulated by Microbiome and Boundary Conditions (SoilSystems)”. We thank the staff of the core projects, the Priority Program office and the BExIS team for their work in maintaining the project infrastructure, and the Priority Program Scientific Committee for their role in setting up the project. We gratefully honor the memory of Gerhard Brümmer, to whom we owe the

Goe-120. We thank Kai Jansen for preparing and providing the goethite with the SSA of 93 $m^2 g^{-1}$. We would like to thank Martin Kaupenjohann for his idea and foresight to employ isothermal titration calorimetry to obtain the thermodynamics of adsorption processes on soil minerals and for the possibility of using the calorimeter. Furthermore we express our gratitude to Anne Wagner, Maike Mai and Jaane Krüger for their invaluable help in setting up the calorimeter, as well as Ralf Sack, precision mechanics workshop JLU Giessen, for helping out with fixing calorimeter shafts and agitators when these delicate parts could not handle soil science.

Chapter III

Microbial carbon use efficiency of mineral-associated organic matter is related to its desorbability

Alexander Konrad[1], Diana Hofmann[2], Jan Siemens[1], Kenton P. Stutz[3], Friederike Lang[3], Ines Mulder[1,4]

[1]Institute of Soil Science and Soil Conservation, iFZ Research Center for Biosystems, Land Use and Nutrition, Justus Liebig University Giessen, Heinrich Buff Ring 26-32, 35390 Giessen, Germany

[2]Institute of Bio- and Geosciences, Agrosphere (IBG-3), Forschungszentrum Jülich, Wilhelm-Johnen-Str., 52425 Jülich, Germany

[3]Chair of Soil Ecology, Institute of Forest Sciences, University of Freiburg, Bertoldstraße 17, 79098 Freiburg, Germany

[4]Institute of Geography, Soil Sciences and Soil Resources, Ruhr University Bochum, Universitätsstr. 150, 44801 Bochum

This is a copyedited version, peer reviewed version of the following article: Microbial carbon use efficiency of mineral-associated organic matter is related to its desorbability. Konrad, A., Hofmann, D., Siemens, J., Stutz, K. P., Lang, F., & Mulder, I. (2025). *Soil Biology and Biochemistry*, *203*, 109740. https://doi.org/10.1016/j.soilbio.2025.109740

Abstract

Interactions between organic substances, minerals, and microorganisms are crucial for organic carbon (OC) stabilization in soil. We hypothesized that thresholds of sorption strength (described by the sorption coefficient of the Freundlich isotherms) and desorbability (i.e., the ratio of the amount desorbed to the amount sorbed) of organic monomers control the extent of their microbial processing.

Freundlich sorption isotherms and desorbability of uniformly ^{14}C-labeled glucose, acetylglucosamine, phenylalanine, salicylic acid, and citric acid onto goethite, kaolinite, and illite were studied in batch experiments. Monomers adsorbed to minerals were mixed with loamy and sandy arable topsoil and incubated at 25°C. Mineralization of mineral-adsorbed monomers was observed over three weeks, after which the assimilation into microbial biomass, and the ^{14}C remaining in soil were quantified. Subsequently, the mineralization of incubated soils was observed for additional three weeks after glucose priming.

The adsorption of carboxylic acids onto minerals exceeded that of (amino) sugars and phenylalanine, with the overall highest amounts both adsorbed and retained after desorption with water for goethite. Assimilation of monomer ^{14}C into microbial biomass and the microbial carbon use efficiency (CUE) of mineral-adsorbed monomers in both soils increased linearly with the monomer desorbability from mineral phases. Furthermore, the CUEs of monomers adsorbed to goethite were lower than those of the same monomers adsorbed to clay minerals. In terms of total amount of carbon retained in the soil, carboxylic acids adsorbed on goethite showed highest values, emphasizing the significance of oxides for the stabilization of OC within soils. Priming of incubated soil with non-labeled glucose caused an additional mineralization of monomer-C, with the priming effect decreasing from goethite to clay minerals.

We conclude that sorption strength and desorbability shape microbial utilization of mineral-bound organic compounds, but no universal thresholds determine bio-accessibility of sorbed organic compounds.

Introduction

Soils represent the largest terrestrial carbon (C) reservoir. Sequestration of organic C (OC) in soils plays a significant role in global C cycling, though the contribution of regulating factors remain uncertain (Georgiou et al., 2022). In the past decade, theories that emphasize the relevance of recalcitrance of biomolecules for OC sequestration have been superseded by concepts that stress the occlusion of OC in soil aggregates and sorption of OC to mineral surfaces (e.g. Lehmann & Kleber, 2015). These concepts also include the pathways by which OC enters the soil (Sokol et al., 2019) with subsequent microbial processing of diverse plant litter for stabilizing OC (Cotrufo et al., 2013, Lehmann et al., 2020).

Sorption to minerals slows down the mineralization of OC as demonstrated in laboratory experiments (Jones & Edwards, 1998; Kalbitz et al., 2005; R. Mikutta et al., 2007; Saidy et al., 2015) and the age distributions of OC across soil depths and fractions (Kleber et al., 2005; Schrumpf et al., 2013; Spielvogel et al., 2008). The capacity of minerals to bind OC as mineral-associated OC (MAOC) differs between 1:1 clay minerals with low sorption capacity, 2:1 clay minerals with high sorption capacity, and iron oxyhydroxides (Fe oxides) with exceptional sorption capacity due to their net positive surface charges in acidic and neutral soils (Feng et al., 2013; Gao et al., 2018; Georgiou et al., 2022; Saidy et al., 2013). The sorbate matters as well: smaller and more functionalized compounds such as deprotonated carboxylic acids adsorb more strongly and are more efficiently preserved in soils than sugars and neutral amino acids (D. L. Jones & Edwards, 1998; Yeasmin et al., 2014).

Aside sorption, biotic factors play a pivotal role in soil C cycling. Approximately half of all OC in arable soil exhibits molecular signatures of microbial origin (Angst et al., 2021). Models predicting soil OC cycling attempt to account for this by integrating microbial carbon use efficiency (CUE) which is defined as the ratio of OC remaining in the microbial biomass to the OC consumed (Sulman et al., 2014; G. Wang et al., 2013). In soil, CUE of the same molecule can exhibit considerable variation (Brown & Jones, 2024) due to microorganisms optimizing their fitness (Schimel, 2023). Minerals can affect CUE since they act as both microbial habitats as well as sinks for OC and nutrients

like phosphorus (P)-containing organic and inorganic compounds (Kandeler et al., 2019; Spohn, 2024; Uroz et al., 2015).

Organic C translocated in the soil solution or released by roots into the rhizosphere—a zone of high microbial activity (Berendsen et al., 2012)—can enhance mineralization of mineral-associated organic carbon (MAOC) through a process known as "priming" (Jilling et al., 2021). Sugars, like glucose, among the most abundant root exudates, play a key role in fueling the soil microbiome (Gunina & Kuzyakov, 2015; Hütsch et al., 2002). The glucose-induced priming effect on sorbed small organic molecules with different functional groups has been minimally investigated so far.

Regardless of priming effects, microbial processing of sorbed compounds would necessarily depend on desorbability (e.g., the ratio of the amount desorbed to the amount sorbed). However, the interaction between sorption strength (approximated by the sorption coefficient from Freundlich isotherms), desorbability, and microbial processing has yet to be quantified. We hypothesize that (1) the sorption strength and desorbability of monomers control microbial processing, with thresholds of sorption strength and desorbability determining the quantity of microbial processing, (2) in addition to the biochemical processes involved in metabolism, adsorption and release of monomers from mineral surfaces, as well as soil properties, affect microbial CUE, and (3) the addition of glucose increases the mineralization of adsorbed monomers due to priming, and the priming-induced mineralization increases with the strength of sorption and thus retention of OC.

These hypotheses were tested in sorption-desorption experiments with uniformly ^{14}C-labeled monomers and kaolinite (1:1 clay mineral), illite (2:1 clay mineral), and goethite (Fe-(oxyhydr)oxide), combined with incubation experiments of mineral-monomer associations in two arable topsoils with differing clay content. Kaolinite, illite, and goethite were selected as they represent distinct mineral classes with unique sorption characteristics. Kaolinite has limited cation exchange capacity but exposes hydroxyl groups, influencing adsorption through hydrogen bonding. Illite, with a higher cation exchange capacity, supports various interactions (Sposito, 2020), while goethite's high surface charge and hydroxyl groups allow for strong ligand exchange (Cornell & Schwertmann, 2003). Glucose (sugar), acetylglucosamine (amino sugar),

phenylalanine (amino acid), and carboxylic acids (salicylic and citric acid) were chosen as model compounds of organic monomers due to their ubiquity in soils and range of functional groups relevant to microbial processing (Kleber et al., 2021). Sugars tend to interact through weak adsorption, amino acids through polar and hydrophobic interactions, and carboxylic acids through ligand bonding (Jones & Edwards, 1998; Yeasmin et al., 2014). To assess microbial P limitation from mineral additions, particularly goethite, phosphate levels in the soil solution were measured after three weeks of incubation. Additionally, the incubation experiment for glucose adsorbed to goethite in the clayey soil was repeated after pre-saturating the goethite with phosphate to test whether alleviating potential P limitations would increase microbial carbon use efficiency for glucose. Soils were further treated with non-labeled glucose after incubating for three weeks and mineralization of monomer-C was quantified for additional three weeks to assess whether mineral-adsorbed monomers were susceptible to priming. Together, these combinations of minerals and monomers allowed us to explore a broad range of sorption behaviors and their effects on microbial processing, offering insights into how mineral composition influences the stability and bioavailability of mineral-adsorbed OC in soils.

Materials and methods

Materials and chemical reagents

Non-labeled chemicals with purities > 99% were procured from Sigma-Aldrich (Darmstadt, Germany). Polyethylensulfone syringe filters with pore sizes of < 220 nm and < 450 nm were sourced from VWR International GmbH (Darmstadt, Germany). Uniformly ^{14}C labeled D-glucose, N-acetyl-D-glucosamine, L-phenylalanine, salicylic acid, and citric acid were procured from American Radiolabeled Chemicals (St. Louis, Missouri, USA). Ultra-pure water (18.2 MΩ, < 2 ppb TOC) was obtained from a Purelab Flex 2 Water Purification System (Veolia Water Solutions and Technologies, Buckinghamshire, Unted Kingdom).

Preparation of model minerals

Two phyllosilicates, kaolinite (Quarzwerke GmbH, Frechen, Germany) and illite (Inter-ILI. Engineering Co. Ltd., Kosd, Hungary), as well as a self-synthesized goethite, were selected as sorbents. The clay minerals were freed from carbonates, iron oxides, and OC in accordance with the methodology outlined by Tributh and Lagaly (1986). Subsequently, the pH was adjusted to 10 using sodium carbonate, and the clay size fraction < 2 µm was separated by sedimentation based on Stokes' law. The samples were transferred into cellulose acetate tubing (Spectra/Por 2 RC Tubing, with a molecular weight cut-off of 12-14 kDa, Spectrum Laboratories, Inc., Rancho Dominguez, California, USA) and placed in buckets filled with deionized water for dialysis to remove salts. The deionized water was replaced frequently until the electrical conductivity of the suspension reached values below 10 µS cm^{-1}. Goethite was synthesized according to the methodology described by Dultz et al. (2019). In brief, 10 M NaOH was added at a flow rate of 1 ml min^{-1} to a constantly stirred 0.5 M $FeCl_3$ solution, up to a pH of 12. Subsequently, the suspension was stored at 4°C for 68 days, after which the pH was adjusted to pH 6 with 0.1 M HCl. The suspension was then dialyzed and freeze-dried analogously to the procedure for the clay minerals. Purified clay minerals and self-synthesized goethite were ground with a mortar and pestle and characterized by powder X-ray diffraction analysis (Empyrean, Malvern PANalytical B.V., Malvern, United Kingdom) to ascertain their purity (Supplementary material S1).

Specific surface areas (SSA) were measured by N_2 adsorption using the Brunauer-Emmett-Teller method on a Quantachrome Quadrasorb evo (3P Instruments GmbH & Co. KG, Odelzhausen, Germany), showing SSA of 92.5, 17.2 and 43.7 $m^2 g^{-1}$ for goethite, kaolinite and illite, respectively. Scanning electron microscopy images of the minerals were obtained using a GeminiSEM 560 (Carl Zeiss Microscopy Deutschland GmbH, Oberkochen, Germany) (Supplementary material S1).

Measurement of radioactivity

Quantification of ^{14}C was conducted for both the sorption-desorption batch study and the soil incubation experiments (a graphical overview on the experimental setup can be found in the Supplementary material S2). The radioactivity was measured using a daily calibrated TriCarb 3300 (PerkinElmer, Inc., Shelton, Connecticut, USA) liquid scintillation counter (LSC). All liquid samples (sodium hydroxide solutions as CO_2 sinks, soil extracts) were mixed with 10 mL of Ultima Gold XR scintillation cocktail (PerkinElmer, Inc., Shelton, Connecticut, USA) and vigorously shaken prior to scintillation counting. Solid samples (e.g. minerals and soils) were incinerated using a Hidex OX 600 oxidizer (Hidex Oy, Turku, Finland) using Oxysolve C-400 scintillation cocktail (Zinsser Analytic, Frankfurt, Germany) for subsequent LSC measurements. The oxidizer results were corrected for ^{14}C recovery rates. It has been recently reported that $^{14}CO_2$, trapped in NaOH, will degas from the lye-cocktail mixture over time, depending on CO_2 saturation, used scintillation cocktail and the time evolved before measurement (Boos et al., 2022, 2023). We accounted for this phenomenon by repeated measurements of same CO_2-samples and corrected the mineralization data with the resulting calibration curve (Supplementary material S3).

Sorption isotherms and desorbability

Sodium azide solutions were used at 0.01 M as background electrolyte for suspensions and solutions to prevent microbial action (Cabrol et al., 2017). Minerals were suspended at concentrations of 40.80 g L^{-1}, 40.13 g L^{-1} and 9.28 g L^{-1} for kaolinite, illite and goethite, respectively. The pH of the suspensions was adjusted to 5.5 using NaOH and HCl. Solutions of ^{14}C-labeled monomers (4000 Bq mL^{-1}) were prepared at concentrations of 0.02, 0.1, 0.2, 0.5, 1.0 and 2.0 mM, set to pH 5.5 and filtered through < 0.22 µm polyether sulfone filters for sterilization. Batch sorption studies were

conducted in triplicates in 1.5 mL polypropylene tubes (Sarstedt AG &Co., Nümbrecht, Germany) by mixing 0.5 mL of mineral suspension with 0.5 mL of monomer solution for all concentrations. Thus, monomer concentrations inside the tubes ranged between 0.01 and 1.0 mM and were corrected for mineral volume displacing solution. Tubes containing 0.5 mL 0.01 M NaN_3 and 0.5 mL ^{14}C-labelled monomer solution were prepared for the second lowest and second highest monomer concentration to check for adsorption on surface of the tubes and microbial processing of monomer in accordance to OECD guideline 106 (OECD, 2000). Tubes were shaken for 16 hours at 1,500 rpm at 25°C (neoMix, neoLab Migge GmbH, Heidelberg, Germany) in the dark, centrifuged for 10 minutes at 17,000 g so that 920 µL of the supernatant could be retrieved for scintillation counting.

Reversibility of monomer adsorption for each model compound was determined at second lowest and second highest concentration using a two-step desorption procedure. Minerals from the batch sorption study were resuspended in 920 µL of fresh 0.01 M NaN_3 and shaken for 1 hour at 1,500 rpm in the dark, followed by centrifugation and removal of 920 µL of supernatant, analogous to the procedure of the sorption study. The desorption step was repeated with pH 5.5 adjusted NaH_2PO_4 at a concentration of 0.1 M as competing anion for 1 hour. Minerals used for the desorption experiments were resuspended in NaN_3 and oxidized to check activity balance. At highest concentrations, analogous sorption experiments with non-labelled solutions were performed and supernatant checked for cations using optical emission spectroscopy with inductively coupled plasma (ICP-OES) (Agilent 720 ICP-OES ES, Agilent Technologies Inc., Santa Clara, USA) to exclude mineral dissolution in the presence of organic molecules.

Incubation

Minerals were sterilized by γ-irradiation of 10 kGy with a ^{60}Co source (Dalkmann et al., 2014), subsequently suspended in a sterile-filtered 0.01 M NaCl solution and set to pH 5.5. Sterile mineral suspensions and sterile-filtered ^{14}C-monomer solutions at pH 5.5 were added at concentrations matching those of the second lowest concentration of the sorption study into 50 mL PP centrifuge tubes and shaken end-over-end for 16 h at 25°C. This concentration was chosen in order to avoid a saturation of sorption sites while loading the minerals with monomers (which would be a concern at higher

concentrations), as well as the antimicrobial effects of salicylic and citric acids (Fang et al., 2020; Khan et al., 2020). The resulting suspensions were then centrifuged at 4.000 g for 2 h, the complete supernatant discarded. The mineral pellet was centrifuged again, and excess solution removed. The minerals were freeze-dried and ground, aliquots of the minerals were combusted. Farmyard manure-fertilized, air-dried arable topsoils sieved at < 2 mm from 2-20 cm soil depth were collected from two long-term field experiments in Germany as disturbed soil samples and used for incubation experiments according to OECD test no. 307 (OECD, 2002). Dikopshof soil is a moderately aggregated Haplic Luvisol, while the Thyrow soil is a weakly aggregated Haplic Retisol (Tab. 3-1). A complete description including microbial and mineralogical data is available in the publication by Lorenz et al. (2024).

Table 3-1. Total organic carbon (TOC), total nitrogen (TN), TOC/TN ratio (C/N), total soil phosphorus (P), oxalate-extractable iron (Fe_O), dithionite-extractable iron (Fe_d), and basal respiration of the arable topsoils Dikopshof and Thyrow.

Site	Soil group	TOC [%]	TN [%]	C/N	P [mg kg^{-1}]	Fe_o [g kg^{-1}]	Fe_d [g kg^{-1}]	pH ($CaCl_2$)	Soil Texture (WRB)	Basal respiration [µg CO_2 h^{-1} g^{-1} dw]
Dikopshof, Universität Bonn, Germany	Haplic Cambisol	1,10	0,14	7,90	7,60	2,55	10,95	6,00	SiL	0,62
Thyrow, Humboldt-Universität Berlin, Germany	Haplic Retisol	0,69	0,08	8,70	6,10	0,39	2,27	5,20	LS	0,49

The soils were pre-incubated at 60% water holding capacity for 10 days at 25°C in the dark. The amount of mineral with adsorbed monomers added to the soils was chosen in a way that the soil mineral composition was changed as little as possible, while providing sufficient ^{14}C for detection. For each treatment (soil x mineral x monomer), 56 g of pre-incubated soil and 240 mg of ^{14}C-loaded, freeze-dried goethite, or 300 mg of ^{14}C-loaded clay mineral were carefully admixed with a spatula for 10 minutes. Duran flasks with a volume of 250 mL (SCHOTT AG, Mainz, Germany) were modified by the addition of a bent wire fixed to the cap of the flask, which held a standard 20 mL PP LSC vial filled with 1 mL of 1 M NaOH. Each mineral-admixed, pre-incubated soil (equal to 14 grams of air-dry soil) was filled in triplicate into the modified glass flasks, resulting in a 1-centimeter-thick soil layer at the bottom of the flasks. To quantify exactly the added radioactivity and check for initial mineralization until airtight sealing of the incubation vessels after 20 minutes of mineral addition, three aliquots of 0.5 grams each were taken out of each flask, ethanol was added in excess, the soil was dried, and ^{14}C

activity was measured. The flasks were incubated at 25°C in a circulating air incubation cabinet in the dark. Sodium hydroxide in the alkali traps was replaced frequently and $^{14}CO_2$ measured. To counteract the loss of water during sample collection and the hydrophilic nature of NaOH, strips of humid paper tissues of 3x7 cm were added hanging into the incubation flasks.

Water-extractable ^{14}C, microbial biomass ^{14}C, and bulk soil ^{14}C were determined after three weeks of incubation using three aliquots of 0.5 g of incubated soil from each replicate. The water content of the aliquots utilized for the bulk soil ^{14}C measurements was analyzed using a HB43-S halogen moisture analyzer (Mettler Toledo Inc., Columbus, USA), which demonstrated comparable water contents to those observed at the outset of the experiment, with a mean of 60 ± 4% WHC. The remaining aliquots were extracted using a chloroform fumigation extraction (CFE), as described by Vance et al. (1987) and modified by Murage and Voroney (2007) in 15 mL centrifuge tubes. Briefly, one aliquot from each incubation replicate was fumigated with chloroform for 16 hours, afterwards extracted with 2.5 mL of 2 M KCl for 90 minutes shaking end-over-end. The remaining non-fumigated aliquot was directly, analogously extracted. All tubes were subsequently centrifuged, and the supernatant filtered. The ^{14}C content of the extracts was measured, with the difference between fumigated and non-fumigated extracts yielding microbial biomass ^{14}C. The non-fumigated extracts were used as a proxy for water-extractable organic ^{14}C ($WEO^{14}C$). Microbial CUE was calculated as the percentage of ^{14}C assimilated into microbial biomass to ^{14}C microbially processed (^{14}C assimilated + ^{14}C mineralized). Furthermore, the phosphate concentrations in non-fumigated extracts were quantified photometrically (Genesys 150, ThermoFisher Scientific Inc., Waltham, Massachusetts, USA) as phosphomolybdate complexes with malachite green at 660 nm (Van Veldhoven & Mannaerts, 1987).

After three weeks of incubation, non-labeled glucose solutions (similar to 0.1% of the soil organic carbon content) were added and admixed carefully with a spatula to the remaining mineral-amended incubation flask replicates (Blagodatskaya et al., 2009), resulting in a 5- to 10-fold higher OC input into the soil compared to the average daily root exudation (Kuzyakov & Domanski, 2000). The incubation period was extended for further three weeks, during which time the evolution of $^{14}CO_2$ was more frequently measured. At the experimental endpoint, the pH values of all soil-mineral-monomer

mixtures were determined in 0.01 M $CaCl_2$ (soil:solution ratio of 1:5). Because high activities in $^{14}CO_2$ samples at the experimental endpoint of 21 days showed continuous mineralization of goethite-bound citric acid in both soils, the incubation of this treatment was prolonged up to 84 days. CFE was performed after 21 and 84 days yielding identical results for CUE. Glucose solutions were added afterwards, and mineralization measured as described above.

Phosphate-amended glucose-goethite experiment and oxalate-extractable ^{14}C fraction

Iron-hydroxides are known to strongly bind large quantities of phosphate-P. To test the impact of potential microbial P limitation in goethite-amended incubation experiments, glucose-adsorbed goethite was loaded with phosphate-P and subsequently used for an analogous incubation study. Therefore, 40 mg of freeze-dried, glucose-loaded goethite was resuspended in 1 mL of sterile-filtered 0.1 M NaH_2PO_4 adjusted to pH 5.5. The suspension was shaken for 60 minutes, centrifuged, the supernatant decanted, and the minerals lyophilized. Following the determination of phosphate-P and ^{14}C in the supernatant, the phosphate-saturated, glucose-loaded goethite was added to the pre-incubated Dikopshof soil in the same goethite topsoil ratio as in the main incubation experiment. The amended soil was incubated for three weeks, and $^{14}CO_2$, microbial biomass, WEO^{14}C, and soil ^{14}C were measured in triplicate as described above. Extraction residues from CFE of fumigated and non-fumigated samples were sequentially extracted using acidic oxalate for 4 h in the dark (Schwertmann, 1964), their activity measured afterwards in the extracts.

Data analysis

Sorption isotherms, cumulative $^{14}CO_2$ evolved over time and mass balances after three weeks of incubation were plotted using Origin Pro 2023b (OriginLab Corporation, Northhampton, Massachusetts, USA). Sorption data was fitted using the Freundlich isotherm (eq. 1) (Freundlich, 1907):

$$q = K_F C^N \qquad \text{(eq. 1)}$$

where q is the number of monomer molecules sorbed (nmol m^{-2} SSA), C is the equilibrium concentration (µmol L^{-1}) and the Freundlich affinity coefficient K_F (describing

monomer affinity to mineral surface in nmol m^{-2}/(µmol $ml^{-1})^{1/N}$), as well as *N* (curvature of the sorption isotherm) as the Freundlich exponent/linearity index. The two-step-desorption experimental data were used to quantify desorbability of OC separately for each desorption step.

The cumulative $^{14}CO_2$ evolution during the initial incubation over three weeks was fitted using a double pseudo-first order kinetic (eq. 2):

$$^{14}C\ mineralized\ (\%) = qe1 \times (1 - e^{-k1 \times t}) + qe2 \times (1 - e^{-k2 \times t}) \quad \text{(eq. 2)}$$

with the sum of *qe1* and *qe2* describing the fraction of added ^{14}C added being mineralized at t = ∞, *k1* and *k2* as the kinetic rate constants of mineralization and *t* as the time evolved since the start of the incubation in days. Mineralization after glucose priming was corrected for by the amount of soil removed after three weeks for chloroform-fumigation-extraction and $^{14}CO_2$ evolved was fitted using the double pseudo-first order kinetic, with qe3 and qe4 describing ^{14}C mineralized at *t* = ∞ (eq. 3), as well as *k3* and *k4* as the kinetic rate constants. If the fitted function showed *k3* values above 100 (indicating direct mineralization of the respective fraction), a new model was calculated without kinetic rate constant *k3* (also eq. 3):

$$^{14}C\ mineralized\ after\ priming\ (\%) = qe3 \times (1 - e^{-k3 \times t}) + qe4 \times (1 - e^{-k4 \times t}) \quad \text{(eq.3)}$$

The additional fraction of ^{14}C mineralized after glucose priming was quantified as the difference between the fitted regression models of incubation and priming at t = ∞ (eq. 4):

$$Priming\ effect\ (\%) = qe3 + qe4 - qe1 - qe2 \quad \text{(eq. 4)}$$

Correlations between sorption and incubation data were analyzed using R Statistical Software (version 4.2, R Core Team, 2022). Boxplots and regression plots were plotted using the ggplot2 package (Wickham, 2016). Histograms and Q-Q plots were used to check data to be normally distributed. Pairwise comparisons were performed using the Wilcoxon-Mann-Whitney-Test (Mann & Whitney, 1947; Wilcoxon, 1945). False discovery rates of pairwise comparisons were controlled using the Bonferroni-Holm method (Holm, 1979).

Results

Sorption and desorption

Non-linear Freundlich isotherms describe the sorption of carboxylic acids to all minerals. In comparison, linear isotherms describe the sorption behavior of phenylalanine and acetylglucosamine (Fig. 3-1, Supplementary material S4). In general, the quantity of monomers adsorbed per SSA decreased in the following order: goethite > kaolinite > illite (Fig. 3-1).

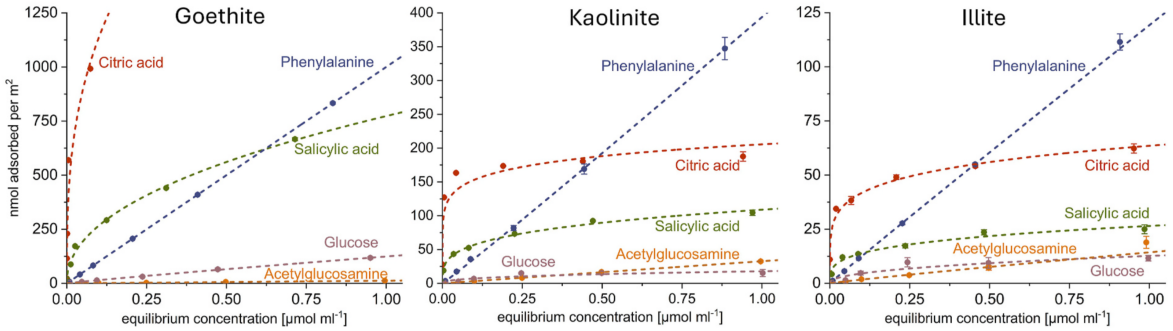

Figure 3-1. Freundlich isotherms of adsorption of monomers to goethite (left), kaolinite (middle) and illite (right).

After desorption in 0.01 M NaN_3 at the second lowest monomer concentration (c=0.05 µmol ml^{-1}), retained ^{14}C exhibited the same pattern (goethite > kaolinite > illite). The exception was acetylglucosamine, which decreased in the order goethite > illite > kaolinite (Tab. 3-2).

Table 3-2. Adsorbed monomers [nmol m^{-2}] after 18 h at monomer additions at 0.05 µmol ml^{-1} and 0.5 µmol ml^{-1}. Additionally, the percentage of monomers retained after desorption for 1 h in 0.01 M NaN_3, as well as after the sequential desorption with 0.1 M phosphate are given.

Monomers	Initially sorbed [nmoles m^{-2}]			% retained after desorption using 0.01M NaN_3			% retained after desorption using 0.1M PO_4^{3-}		
	Goethite	Kaolinite	Illite	Goethite	Kaolinite	Illite	Goethite	Kaolinite	Illite
Glucose	7.18±0.16	2.75±0.14	1.41±0.02	94.06±2.33	73.42±6.87	58.14±8.15	54.12±1.24	n.d.	4.20±0.64
	64.81±5.72	15.25±2.24	8.51±1.30	94.28±6.14	68.29±0.84	77.13±15.24	54.98±7.27	6.58±3.23	n.d.
Acetylglucosamine	0.55±0.03	1.66±0.11	0.81±0.05	n.d.	45.02±6.32	n.d.	n.d.	8.00±5.65	n.d.
	6.25±0.65	16.71±0.79	7.14±1.09	n.d.	4.44±0.00	n.d.	n.d.	n.d.	n.d.
Phenylalanine	20.64±0.76	17.40±0.35	5.59±0.18	92.61±4.43	87.72±0.19	87.44±1.48	16.54±2.25	3.16±1.61	4.35±1.26
	211.26±4.58	169.05±7.45	54.93±0.64	89.91±1.52	90.67±4.72	87.01±0.40	15.95±0.49	4.37±1.28	3.56±1.10
Salicylic acid	87.67±0.1	43.42±0.18	12.05±0.09	88.63±0.21	80.66±1.15	70.08±1.93	23.97±0.3	42.16±0.68	54.46±3.58
	440.45±0.49	92.44±0.71	23.55±1.19	72.22±1.08	79.59±1.69	77.8±13.09	25.76±1.76	34.32±1.46	38.87±5.91
Citric acid	114.98±0.01	127.17±0.54	34.44±0.14	99.87±0.01	96.76±0.22	89.67±0.73	29.13±1.36	2.15±0.19	20.73±4.2
	1134.4±10.54	180.50±0.84	54.09±0.57	93.47±0.39	98.38±0.48	79±1.87	10.57±1.31	10.17±0.84	17.09±3.21

Mineralization

The initial mineralization observed in the first 20-minutes after homogenization of pre-incubated soil with monomer-loaded minerals exhibited comparable patterns for both soils without discernible trends for specific minerals or monomers (Fig. 3-2, Supplementary material S5). The highest initial mineralization (20% of monomer ^{14}C added) was observed for acetylglucosamine adsorbed to goethite in both soils. In contrast, only 0.5–5.1% of ^{14}C was mineralized within acetylglucosamine-clay mineral mesocosms.

Throughout the three weeks of incubation, mineralization fitted well to double pseudo first order kinetics ($R^2 > 0.9$, Supplementary material S6). The highest rates and cumulative mineralization (Fig. 3-2) were found for citric acid adsorbed to kaolinite and illite in both soils.

In comparison, citric acid adsorbed on goethite in the Thyrow soil showed the lowest fraction of ^{14}C mineralization (22%). The same treatment for the Dikopshof soil yielded a higher mineralized fraction indicating the relevance of the soil for mineralization (59%). In general, the mineralization of substrate bound

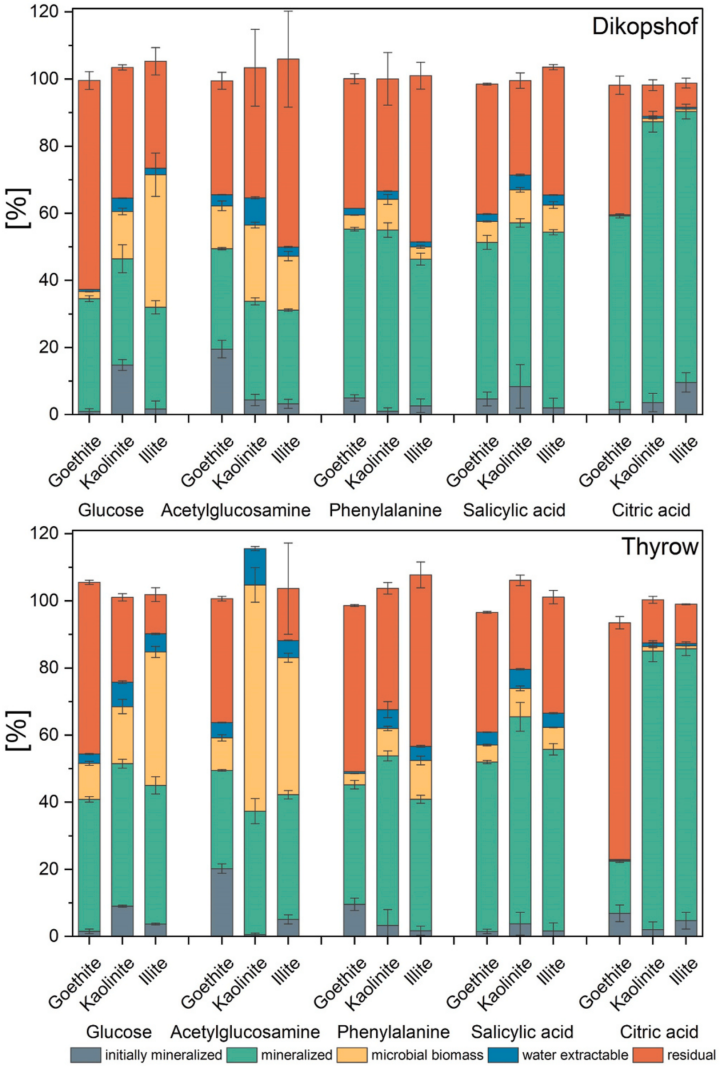

Figure 3-2. Fate of monomer-C added adsorbed to goethite, kaolinite or illite incubated in Dikopshof (top) or Thyrow (bottom) soil with different monomers after three weeks of incubation in percent of 14C added, with error bars (n = 3).

to goethite was smaller than the one observed for clay mineral-bound substrate.

Exceptions were acetylglucosamine, which exhibited high initial mineralization. The same common findings held true for ^{14}C previously bound to goethite assimilated into biomass for both soils (Fig. 3-3a, Supplementary material S5), except for phenylalanine in Dikopshof soil where biomass-^{14}C was higher for goethite than for illite (Fig. 3-2).

Assimilation and carbon use efficiency

Sugars were assimilated to a higher degree in Thyrow soil compared to Dikopshof soil, which contrasted with the results for carboxylic- and amino acid-amended soil. The extremes were exceedingly low amounts of assimilated goethite-sorbed glucose in Dikopshof soil and substantial amounts of assimilated kaolinite-bound acetylglucosamine in Thyrow soil. In fact, up to 100% of the monomer ^{14}C was microbially metabolized in kaolinite-acetylglucosamine incubation experiments with Thyrow soil, while only 52% from the same monomer-mineral combination was microbially processed in Dikopshof soil (Fig. 3-2).

No such pronounced differences between soils were observed for carboxylic and amino acid-loaded minerals. The assimilation of citric acid into microbial biomass was generally small (Fig. 3-2, 3-3a).

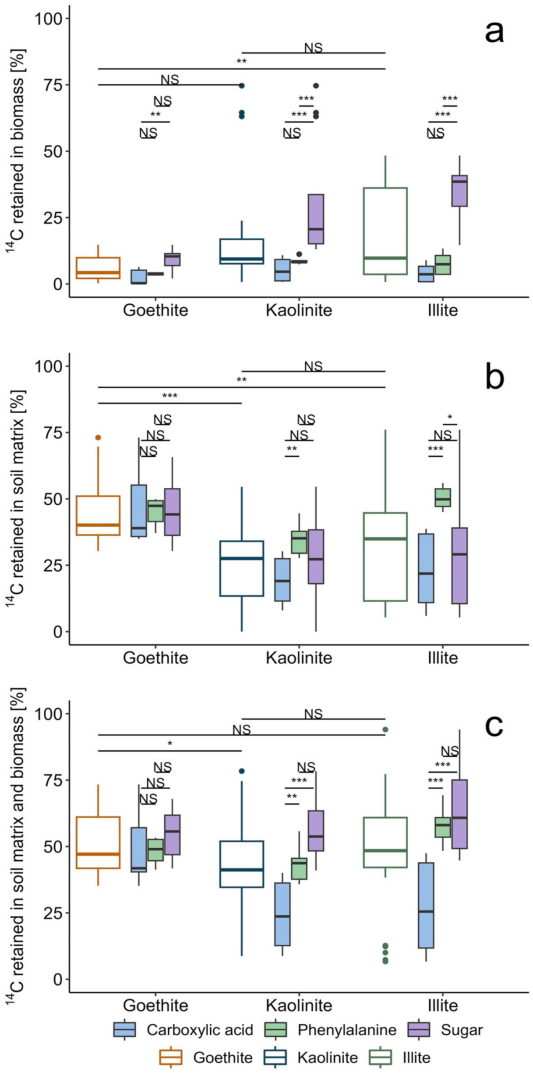

Figure 3. Fate of goethite-, kaolinite- and illite-adsorbed monomers after three weeks of incubation in Dikopshof and Thyrow soil based on the percentage adsorbed at the start of the experiment, assimilated into microbial biomass (a), retained sorbed onto mineral surfaces or within the soil matrix, i.e. residual fraction (b), and retained within the soil either by assimilation into biomass or by retention within the soil matrix (c). Monomers were grouped into sugars (glucose, acetylglucosamine; n = 12 per mineral), phenylalanine (n = 6 per mineral) and carboxylic acids (salicylic acid, citric acid; n = 12 per mineral). Bonferroni-Holme adjusted pairwise comparisons using Wilcoxon Mann Whitney tests display significant differences in [%] of monomers retained in biomass, soil matrix or within biomass and soil matrix between goethite and clay mineral amended soil, and differences between sugar (glucose, acetylglucosamine), phenylalanine and carboxylic acids (salicylic acid, citric acid) adsorbed to each mineral. Significance levels: *p ≤ 0.05, **p ≤ 0.01, ***p ≤ 0.001; and NS not significant (p > 0.05).

Phenylalanine and salicylic acid, on the other hand, demonstrated only slightly different amounts of assimilation in microbial biomass in both soils.

From a mineral perspective, the percentage of ^{14}C retained within the microbial biomass was greater for clay minerals than goethite regardless of soil (Fig. 3-3a). This difference was greatest for glucose and acetylglucosamine, while carboxylic acids were only marginally assimilated when adsorbed to any mineral. In contrast, ^{14}C retained in soil which was not accounted for by microbial biomass or WEOC was significantly higher for goethite than clay minerals. Similar percentages of organic acids and sugars were retained by goethite (Fig. 3-3b). Combining retention by assimilation into biomass and sorption to the soil matrix, clays and oxides showed comparable proportions of added ^{14}C retained (Fig. 3-3c). In absolute terms, however, goethite retained much more carboxylic acid ^{14}C than either kaolinite or illite (Fig. 3-4).

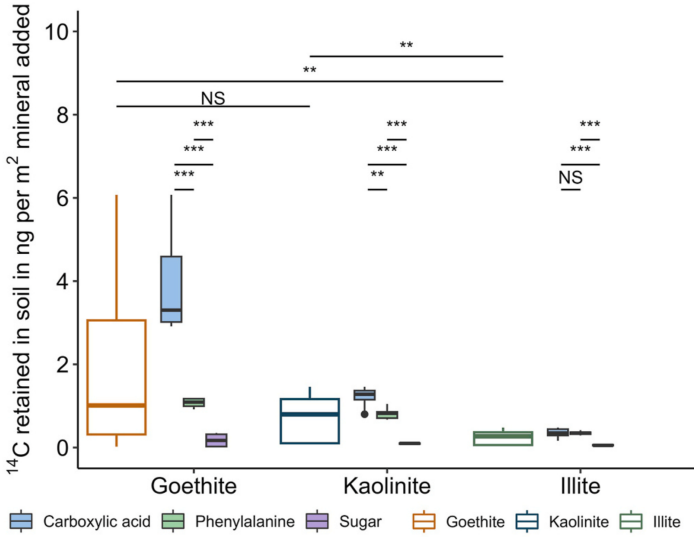

Figure 3-4. Nanogram ^{14}C retained per m^2 specific mineral surface area after three weeks of incubation by assimilation into microbial biomass or within soil matrix. Bonferroni-Holme adjusted pairwise comparisons using Wilcoxon Mann Whitney tests display significant differences in ng C m- 2 mineral retained be tween goethite and clay mineral amended soil, and differences between sugar (glucose, acetylglucosamine), phenylalanine and carboxylic acids (salicylic acid, citric acid) adsorbed to each mineral. Significance levels: **p ≤ 0.01, ***p ≤ 0.001; and NS not significant (p > 0.05).

The CUEs of mineral-adsorbed monomers exhibited a trend like that of assimilation. Goethite exhibited lower CUE values compared to clay minerals: 0.5-23.0% for goethite vs. 0.9-66.4% for illite and kaolinite (Fig. 3-5, Supplementary material Tab. S3-1). Among sugars, glucose bound to goethite in Dikopshof soil had the lowest CUE of 6.5%.

Soil again mattered: monomers in Thyrow soil were processes with a higher CUE values than those in Dikopshof (Fig. 3-5, Supplementary material Tab. S3-1).

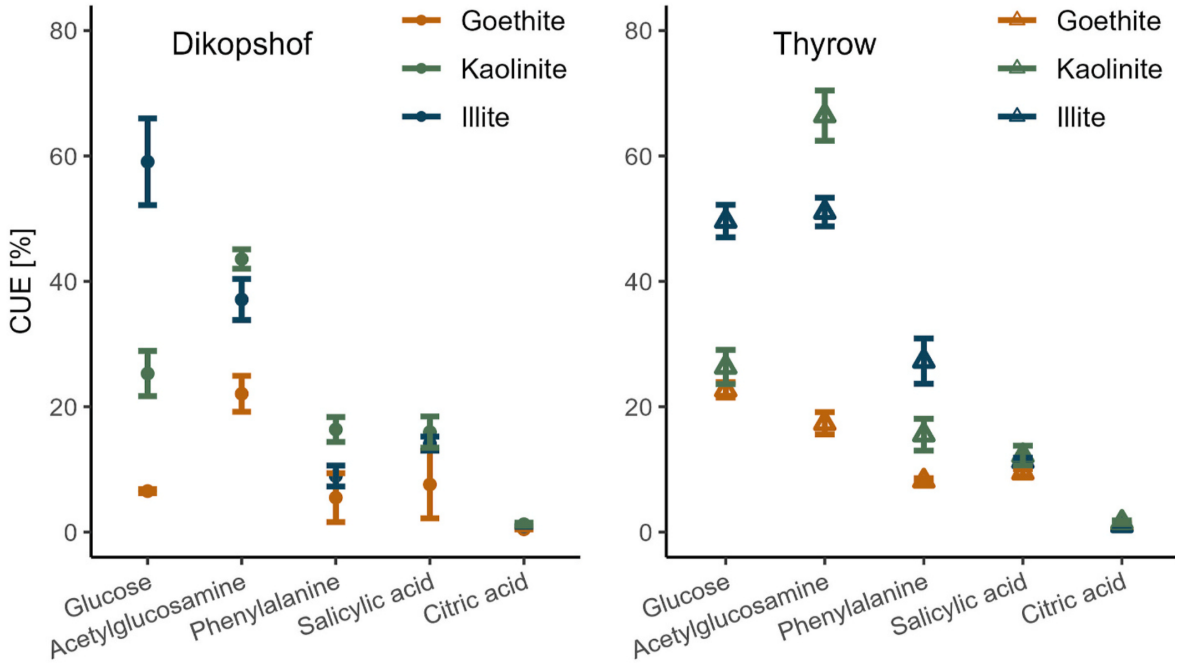

Figure 3-5. Microbial carbon use efficiencies of monomers adsorbed to minerals incubated in either Dikopshof (left), or Thyrow (right) soil after three weeks of incubation.

Phosphorus deficiencies and mineral retention of fumigated microbial residues

After three weeks of incubation, goethite-amended soils showed significantly lower PO_4-P concentrations than soils admixed with clay minerals for both soils likely due to P sorption to the added goethite (Fig. 3-6). Overall, sandy Thyrow soil extracts yielded on average 4 to 5 times higher phosphate-P concentrations than Dikopshof soil extracts because of smaller contents of P-sorbing (hydr)oxides (Tab. 3-1).

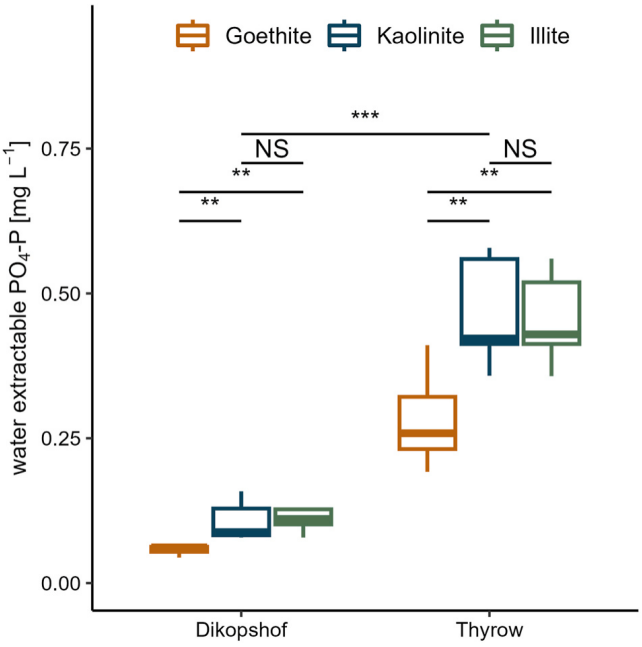

Figure 3-6. Phosphate concentrations after three weeks of incubation in 2 M KCl soil extracts (w/v ratio 1:5) grouped by minerals and soil. Bonferroni-Holme adjusted pairwise comparisons using Wilcoxon Mann-Whitney tests display significant differences in phosphate concentrations between goethite and clay mineral amended soil, and overall differences between Dikopshof and Thyrow soil. Significance levels: **p ≤ 0.01, ***p ≤ 0.001; and NS not significant (p > 0.05). One incubated sample per mineral x monomer x soil treatment was analyzed, thus each box consists of 21 replicates.

Microbial processing of goethite-adsorbed glucose in Dikopshof soil increased when goethite was loaded with phosphate prior admixture with soil. The effect was such that mineralization and assimilation of goethite-adsorbed glucose into biomass reached the same levels as that of glucose bound to P-free goethite in Thyrow soil (Tab. 3-3).

In principle, microbial OC might have been sorbed to minerals after cellular dissolution with chloroform gas preventing extraction with KCl. To check for retention of microbial OC after the KCl extraction, chloroform fumigated and non-fumigated soil with goethite-bound glucose were sequentially extracted with 2 M KCl and acidic oxalate at pH 3 for 4 h in the dark (Schwertmann, 1964). Sequential extractions yielded comparable results for fumigated and non-fumigated soil (Supplementary material Fig. S3-4). Consequently, retention of microbial assimilated ^{14}C on goethite surfaces after fumigation and extraction with KCl was excluded.

Table 3-3. Fate of uniformly ^{14}C labeled glucose adsorbed to either goethite or phosphate-loaded goethite after three weeks of incubation in either Dikopshof or Thyrow soil.

Soil	Mineral	initial mineralization [%]	mineralized [%]	biomass [%]	WEOC [%]	residual [%]	microbial processed [%]	CUE [%]	mass balance [%]
Dikopshof	Goethite	1.0 ± 0.8	30.5 ± 0.5	2.1 ± 0.1	0.6 ± 0.0	62.3 ± 2.7	32.7 ± 0.5	6.5 ± 0.3	95.5 ± 2.2
Dikopshof	PO_4^{3-} loaded goethite	0.0 ± 0.0	35.6 ± 0.0	11.1 ± 0.1	1.7 ± 0.0	50 ± 1.6	46.6 ± 0.1	23.7 ± 0.2	98.3 ± 1.8
Thyrow	Goethite	1.6 ± 0.7	36.6 ± 0.7	10.8 ± 0.6	2.8 ± 0.1	51.1 ± 0.7	47.4 ± 0.5	22.7 ± 1.2	101.3 ± 0.7

Linking sorption-desorption behavior and microbial processing

No unified relationship was found between sorption coefficients K_F and microbial processing of sorbed OC (Supplementary material Fig. S3-5). Monomers mattered: High sorption coefficients of organic acids resulted in similar CUEs and ^{14}C assimilation in both soils, while lower K_F values of sugars led to divergent assimilation and CUEs between soils (Supplementary material Fig. S3-5). No relationship was found also between desorbability and mineralization of monomers in both soils (Fig. 3-7a). However, the fraction of mineral-associated organic compounds that could be desorbed with 0.01 M NaN_3 after sorption was linearly related with the fraction of microbially assimilated ^{14}C and the CUE for both soils (Fig. 3-7b, d). The same was observed for total microbial processing of ^{14}C (mineralized + assimilated^{14}C) in Thyrow soil, but not for Dikopshof soil (Fig. 3-7c).

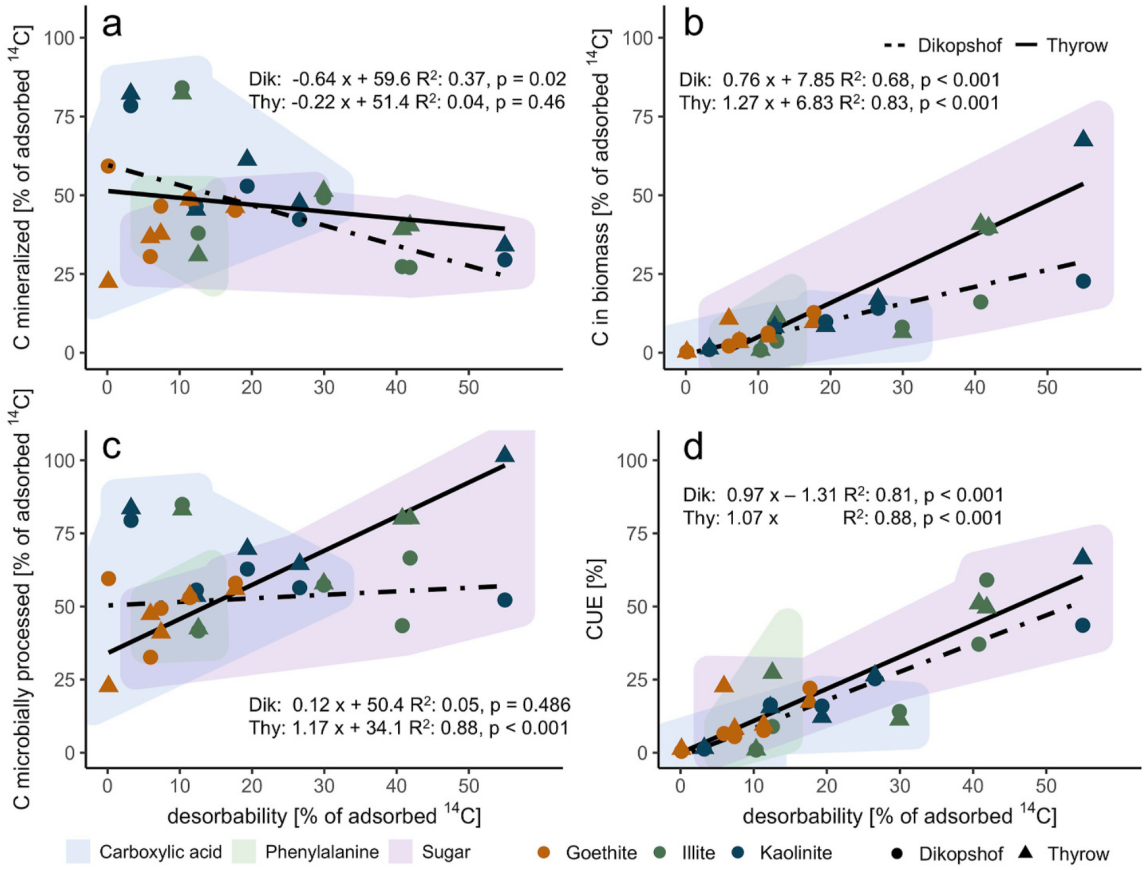

Figure 3-7. Correlation between the mean values for ^{14}C desorbed from minerals after shaking with 0.01 M NaN_3 in batch sorption studies (mean STD: 2.87 %, Table 3-2) and mineral-adsorbed ^{14}C mineralized after three weeks of incubation (a), assimilated into biomass (b), microbially metabolized (c) and microbial carbon use efficiency (d) in Dikopshof (Dik) and Thyrow (Thy) soil (mean STD: 1.99 %, Supplementary Information Tab. S3-3). Monomers were grouped as carboxylic acids (salicylic acid, citric acid), phenylalanine (as the only amino acid) and sugars (glucose, acetylglucosamine).

Glucose-induced mineralization

The addition of glucose to mineral-amended soils after three weeks of incubation increased the percentage of mineral-associated monomer ^{14}C that could be mineralized in almost all mesocosms; the exception was illite-bound phenylalanine in Dikopshof soil. The additional ^{14}C mineralization was significantly larger for goethite treatments compared to kaolinite (Fig.3-8a). Only for Thyrow soil, additional $^{14}CO_2$ released due to glucose additions increased with increasing ^{14}C retained in the soil matrix after the first three weeks of incubation primarily in goethite-amended soils (Fig. 3-8b, c). No changes of soil pH were observed during the incubation experiment (Dikopshof: pH 6.04 ± 0.03, Thyrow: pH 5.04 ± 0.02).

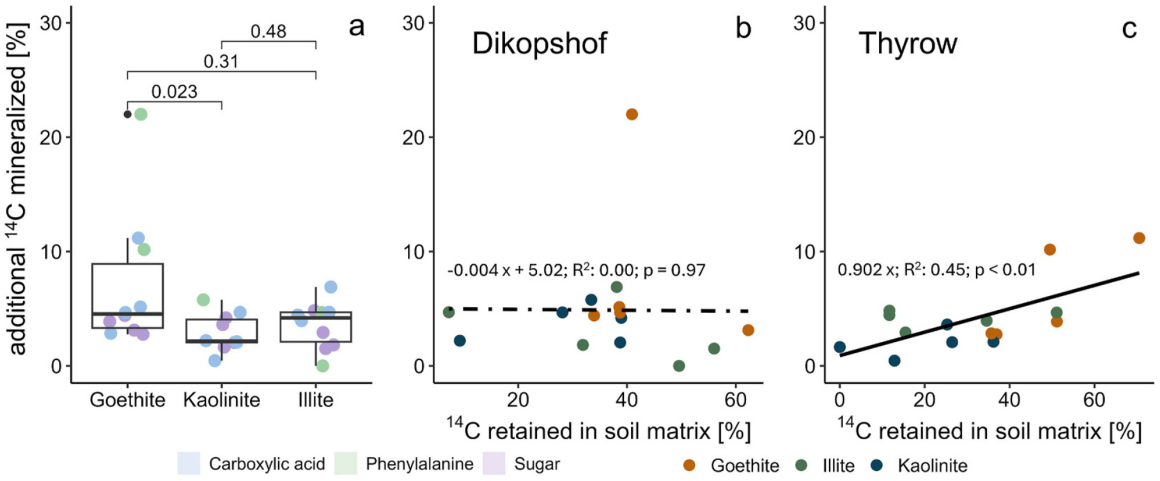

Figure 3-3. Effect of glucose-induced priming on the mineralization of mineral adsorbed monomer 14C. Monomer 14C adsorbed to goethite was mineralized to a significantly larger extend than ^{14}C adsorbed to kaolinite after priming (a). While no correlation was found between the percentage of monomer-C retained in soils after three weeks of incubation and the additional mineralization after glucose addition in Dikopshof soil (b), the fraction of $^{14}CO2$ released due to priming increased with the fraction of 14C retained in the soil matrix for the Thyrow soil (c).

Discussion

Sorptive control of microbial processing of mineral associated monomers

The superior ability of goethite, and Fe-(hydr)oxides in general, over clay minerals to sorb and retain dissolved OC, and preserve mineral-associated organic carbon (MAOC) has been demonstrated in both laboratory (Saidy et al., 2013; Yeasmin et al., 2014) and field studies (Bramble et al., 2024). Our batch sorption study yielded similar results (Fig. 3-1), with goethite sorbing more of all monomers than kaolinite and illite on a per surface area basis, with the exception of acetylglucosamine. These findings align with Yeasmin et al. (2014), who observed similar sorption capacity for glucose on goethite under batch conditions with ^{14}C-labeled monomers in 0.01 M NaN_3, though at an equilibrium pH rather than at a fixed pH 5.5. However, retention of OC after desorption in our study differed slightly; Yeasmin et al. (2014) observed higher retention of citric acid on goethite and kaolinite and greater binding of citric acid and phenylalanine on illite.

Sorption strength and desorbability alone explained neither initial mineralization in the first 20 minutes nor total mineralization after three weeks. For instance, more than 40% of total mineralization of goethite-bound acetylglucosamine occurred in the first 20 minutes. These levels are in line with mineralization rates of up to 1.1% per minute for glucose added to soil found in the literature (Gunina & Kuzyakov, 2015). Rinsing ^{14}C-loaded minerals with water after sorption could have reduced the introduction of non-adsorbed and thus easily mineralizable OC into soil. Instead, we only decanted supernatants, and minerals were not rinsed to avoid desorption. For monomers with marginal sorption to minerals—glucose and acetylglucosamine (Fig. 3-1)—a majority of ^{14}C remained within the supernatant, which would increase the potential for error during decantation. This could explain the high initial mineralization observed in some mesocosms, like glucose bound to kaolinite or acetylglucosamine bound to goethite.

Conversely, this would not apply to goethite-adsorbed citric acid and (to some extent) salicylic acid as high mineralization was observed despite < 0.1% of added OC being recovered from the supernatant. Rapid initial mineralization of monomers with higher sorption coefficients may be driven by OC sorbed to more accessible binding sites such as external surfaces with shorter diffusion distances to microorganisms, which is likely due to adsorption of monomers below observable saturation points.

Edge-bound monomers could also have been more easily removed by exchange with dissolved organic matter and nutrients in the soil solution. This effect might be stronger for monomers bound via ligand-exchange reactions (e.g., monomers containing carboxyl-groups) as shown by phosphate-induced desorption (Tab. 3-2). Comparatively more phosphate in Thyrow soil extracts than in those of Dikopshof soil (Fig. 3-6) thus would be a reason for rapid mineralization of goethite-bound citric acid observed in the former. Furthermore, hydrophobic OC can displace sorbed hydrophilic OC—i.e., all monomers in the experiment—from mineral phases (Kaiser & Zech, 1997). Competitive sorption therefore can be a plausible cause for rapid mineralization for all monomers used in this study, not just organic acids. Subsequent microbial processing would have been fueled by OC adsorbed within mineral pores and is therefore rate-limited by diffusion of new sorbates as well as desorption of monomers (Pignatello & Xing, 1996).

Results for citric acid adsorbed to goethite suggest that ligand exchange can be effective at reducing mineralization and overall microbial processing. Most of the citric acid sorbed to goethite at pH 5.5 was mineralized in Dikopshof soil (pH > 5.5), while only 29% was mineralized in Thyrow soil (pH < 5.5). Introduction into Dikopshof soil brought goethite closer to its point of zero charge (PZC). As the pH approaches the PZC, goethite surfaces became less positively charged (Filius et al., 2000), reducing electrostatic attraction between (partly, pH < pKa3) deprotonated citric acid and mineral surface, potentially causing additional monomers to desorb. Adding goethite to Thyrow soil on the other hand brought the mineral further away from its PZC, increasing electrostatic attraction of the sorbate. This might also explain the relationship found in Thyrow, but not Dikopshof soil for desorbability determined at pH 5.5 and the overall amount of microbially processed monomer-C (Fig. 3-7c). Interestingly, differences between the magnitude of microbial processing of goethite-adsorbed monomers incubated in both soils decreased with increasing desorbability for carboxyl-group–containing monomers as well as glucose and aceylglucosamine. In fact, pH-dependent differences in the amount of microbially processed monomers between soils found for organic acids is reversed for glucose (Thyrow > Dikopshof) as more OC would be adsorbed through hydrogen bonding at higher pH (Olsson et al., 2011). Clay minerals, in contrast, were characterized by overall higher desorbability and microbial processing when compared to goethite. However, microbial processing increased together with

desorbability only in sandy Thyrow soil. In clay-rich, aggregated Dikopshof soil, high desorbability might have been counteracted by re-adsorption of desorbed monomers onto native clay minerals or pedogenic oxides, or diffusion into aggregates away from decomposer (Lehmann & Kleber, 2015).

Biological processing of mineral-associated monomers

Our results indicate that OC assimilated into biomass relative to microbially processed OC — that is CUE — is linearly related to the fraction of mineral adsorbed monomers extractable with 0.01 M NaN_3 and thus the reversibility of sorption (Fig. 3-7d), instead of sorption strength. Two control levels of CUE are at work as Schimel (2023) has pointed out. First, biochemical pathways and substrate chemistry limit the percentage of substrate-C that can be assimilated. Second, environmental and physiological conditions force the microbiome to regulate its biochemistry to optimize fitness. The first is exhibited by the low biochemically possible CUE of carboxylic acids, which are not easily desorbed from iron oxides and clay minerals via ligand-exchange (Jones & Edwards, 1998; Yeasmin et al., 2014) but are also readily metabolized for gaining energy Citric acid, for example, is central to energy-yielding metabolism and specifically the tricarboxylic acid cycle. Hence the low CUE of carboxylic acids was rather related to their biochemical processing than to their low desorbability. In line with the low CUE in our incubation experiment, the CUE of citric acid in a topsoil from an Eutric Cambisol grassland was 24±4 % (Brown & Jones, 2024). This also applies to salicylic acid which has an average CUE in arable soils below 20% (Jones et al., 2018).

However, the CUE of goethite-adsorbed glucose in Dikopshof soil was as low as 7%, despite typical CUEs of glucose in soil around 40% (Schimel, 2023) and highest values around 75% (Sugai and Schimel, 1993). In general, CUE for goethite-sorbed monomers were lower than those for monomers adsorbed to clay minerals. These findings suggest that environmental and physiological conditions restricted the microbial processing of monomers sorbed to goethite. Goethite efficiently binds phosphate (Antelo et al., 2005; Geelhoed et al., 1998) and organic P (Amadou et al., 2022). Therefore, microbial communities in goethite-amended mesocosms might have encountered P limitations (Fig. 3-6). Such P limitation was confirmed for the Dikopshof soil since CUE, assimilation and mineralization of goethite-bound glucose increased to levels comparable to

Thyrow soil after loading goethite with P (Tab. 3-3). Minerals incorporated into soil therefore remain micro-habitats of microbial activity responding to altered nutrient availability. Similar findings were observed in a field study with mineral bags buried in topsoil of grasslands in southern Germany (Brandt et al., 2023). In that study, retrieved goethite with adsorbed organic matter had lower phospholipid fatty acid (PLFA) to OC ratios and higher enzyme activities in C-, N-, and P-cycling than illite, thus suggesting goethite induced C, N and P deficiencies while illite-bound OM and nutrients desorbed more readily and were more accessible for the microbiome (Brandt et al., 2023).

In our study, sugars bound to clay minerals desorbed more easily and were assimilated to a greater extent. The efficient assimilation of sugars into microbial biomass is promoted by their biochemical processing. Hence the linear relationship between desorbability and CUE was also caused by the combination of efficient biochemical assimilation and desorption of sugars.

CUE also depends on cellular maintenance and thus can be modified by stress (Schimel, 2023). The physical effect of clay minerals and iron (hydr-)oxides on resident microorganisms can induce cellular stress, with greater stress typically in the latter than the former. For instance, the needle-like structures of goethite have been demonstrated to penetrate the peptidoglycan layers of bacteria and outer cell membrane (Glasauer et al., 2001). A strain of *Escherichia coli* also showed reduced growth and protective biofilm formation when in contact with goethite while contact with kaolinite and montmorillonite, in contrast, promoted growth (Cai et al., 2018). Thus, in our study, clay mineral-influenced microhabitats would have been conducive to microbial growth whereas goethite would have been hostile.

Our results also show that additional MAOC can be mineralized after glucose application (Fig. 3-8, Supplementary material Fig. S3-4, Tab. S3-3). Priming is the most likely explanation: Glucose provides an energy-rich substrate that can increase exo-enzyme production and more mineralization of MAOC. Our findings of additional MAOC mineralization after glucose addition are consistent with other studies (Jilling et al., 2021; H. Li et al., 2021). Specifically, in Thyrow soil (Fig. 8c), goethite-adsorbed organic acids were strongly retained in incubations without glucose, but became available for microbial processing to a larger extent after glucose application.

In Dikopshof, by comparison, a lack of glucose-enhanced mineralization was most likely due to desorption of ligand-bound monomers caused by the soil's pH before glucose was added. This desorption caused an effective mineralization of goethite sorbed monomers so that only very little of them was available for priming-induced mineralization after the first three-week incubation. Either way, organic acids retained by the soil mineral phase may be more prone to release and mineralization upon glucose-induced priming. However, the extent of additional MAOC mineralization after glucose addition was small compared to the fraction of monomer C originally retained.

Implications for C cycling in soil

It is prudent to consider the experimental context when applying our results to arable soils in field settings. Our study traced the fate of mineral-associated monomers for only three weeks, during which monomers adsorbed to clay minerals were assimilated more efficiently into microbial biomass than those on goethite (Fig. 3-3a, Fig. 3-5). However, the long-term retention of ensuing microbial necromass, potentially through spatial exclusion (Balesdent et al., 2000; Rasmussen et al., 2005) or re-adsorption to minerals (Angst et al., 2018; Cotrufo et al., 2013), cannot be assessed within this timeframe. Nonetheless, microbial necromass could significantly contribute to soil OC formation, especially in arable soils, depending on microbial death pathways (Camenzind et al., 2023). Additionally, this study isolated individual minerals, while in natural soils, clay minerals and pedogenic iron oxides often co-occur. Field observations (Bramble et al., 2024; Brandt et al., 2023) support similar differences between iron (hydr-)oxides and illite, albeit also with isolated minerals. Our observation that goethite sorbs and retains organic compounds more efficiently than illite (Fig. 3-3c, Fig. 3-4) may vary in soils where these minerals are intermixed. However, studies in arable soils of the humid tropics, with varying contents of kaolinite, gibbsite, and goethite, reveal that soils with a high oxide-to-clay mineral ratio exhibit reduced microbial respiration and greater retention of MAOC over extended incubation (Kirsten et al., 2021). Thus, the observed behavior of carboxylic acids likely highlights key differences between oxides and clay minerals and underscores their distinct roles in C cycling within soil systems.

Conclusions

Assimilation of organic monomers associated with minerals into microbial biomass and the resulting CUE increase linearly with desorbability. Monomers initially adsorbed to clay minerals were retained in the soil primarily through stabilization within the microbial biomass. In contrast, a majority of monomer-C adsorbed to goethite remained sorbed to the soil matrix. However, part of this C can be desorbed and microbially cycled with comparatively low CUE. Our results highlighted the quantitative importance of small organic acid sorption to soils for overall C sequestration, substantiating the relevance of future research of this process. Although the findings of our laboratory experiments are in line with field observations, factors like nutrient availability at mineral surfaces, fluctuating temperatures and wet-dry cycles may influence the retention of mineral-associated organic matter in the environment.

Author Contributions

Conceptualization: AK, DH, JS, IM, KS, FL; laboratory analysis: AK, DH; data and statistical analysis: AK; writing – original draft preparation: AK, JS, IM; writing – reviewing and editing: all authors; funding acquisition: IM, KS, FL, JS.

Declaration of competing interests

The authors declare that they have no known competing financial interests of personal relationships that could have appeared to influence the work reported in this paper.

Acknowledgements

This work was funded by the German Research Foundation (DFG, grant no. SI 1106/17-1 and grant no. 465123895). We thank Marcel Lorenz for his coordination of the DFG priority program SPP 2322 – SoilSystems: Systems ecology of soils – energy discharge modulated by microbiome and boundary conditions. We would also like to thank Prof. Dr. Elena Evguenieva-Hackenberg and Andreas Jäger for their management of the radioactive control area at the Justus-Liebig-University Giessen. We would like to extend our gratitude to Andrea Ecker, Simon Horn, and Stefan Köppchen for their invaluable assistance in the radioactive control area at Forschungszentrum Jülich when we were running out of time and hands. We thank Klaus Kaiser, University of Halle, for his feedback and inspiring discussions.

Chapter IV

Rapid mineralization of mineral-bound carboxyl-carbon of salicylic acid and phenylalanine

Alexander Konrad[1], *Diana Hofmann*[2], *Jan Siemens*[1], *Friederike Lang*[3], *Ines Mulder*[1,4], *Kenton P. Stutz*[3]

[1]Institute of Soil Science and Soil Conservation, iFZ Research Center for Biosystems, Land Use and Nutrition, Justus Liebig University Giessen, Heinrich Buff Ring 26-32, 35390 Giessen, Germany

[2]Institute of Bio- and Geosciences, Agrosphere (IBG-3), Forschungszentrum Jülich, Wilhelm-Johnen-Str., 52425 Jülich, Germany

[3]Chair of Soil Ecology, Institute of Forest Sciences, University of Freiburg, Bertoldstraße 17, 79098 Freiburg, Germany

[4]Institute of Geography, Soil Sciences and Soil Resources, Ruhr University Bochum, Universitätsstr. 150, 44801 Bochum

This is a copyedited version of the manuscript under review in *Soil Biology and Biochemistry.* 10.2139/ssrn.5218595

Abstract

Ligand-bound carboxylic acids are considered a stabilized fraction of mineral-adsorbed carbon in soil. Carboxyl-^{14}C labeled phenylalanine or salicylic acid were adsorbed onto goethite, kaolinite, or illite, and subsequently incubated in both loamy and sandy arable topsoil for three weeks. Contrary to our expectations, more mineral-adsorbed carboxyl-C was mineralized than remaining C in salicylic acid and phenylalanine irrespective of mineral type or soil due to competitive desorption followed by preferential mineralization. Factors that control the desorbability of organic molecules are more important for their stabilization in the soil than the bond strength.

Short communication

In a recent experiment (Konrad et al., 2025), we found that microbial mineralization and assimilation of carbon (C) from mineral-adsorbed salicylic acid and L-phenylalanine increased with desorbability from goethite, kaolinite and illite. Desorbability is the amount desorbed indexed to the amount adsorbed for a given extractant (0.01 M NaN_3 in Konrad et al., 2025). This concurs with past research that protection of organic matter against mineralization increases with sorption strength—e.g., van-der-Waals forces < polyvalent exchangeable cation bridging < ligand exchange (R. Mikutta et al., 2007)—only when desorbability is inversely related to sorption strength. Furthermore, the question remains whether desorbability regulates the microbial processing of the entire molecule or only the adsorbed C atoms. If the latter, covalently bonded C atoms in carboxyl groups ought to be retained in soil to a greater extent than other moieties such as substituted phenyl, or aliphatic structures.

We tested this proposition by incubating carboxyl-^{14}C–labeled salicylic acid and L-phenylalanine adsorbed to goethite, kaolinite or illite parallel to the uniform-^{14}C label incubation experiment in Konrad et al. (2025). Sorption was performed in 0.01 M NaCl at pH 5.5 and the sorbed compounds were incubated in the same arable topsoils from Dikopshof and Thyrow. Dikopshof is a loamy, aggregated Luvisol (pH 6.0), while Thyrow is a sandy Haplic Retisol (pH 5.2). Both soils were fertilized with farmyard manure (see Lorenz et al., 2024 for further details). At pH 5.5, both monomers can perform ligand exchange reactions via their carboxyl group.

Minerals were identical to Konrad et al. (2025). Carboxyl-^{14}C labeled monomers came from American Radiolabeled Chemicals (St. Louis, Missouri, USA). In agreement with the earlier experiment, sorption of phenylalanine- and salicylic acid-carboxyl-^{14}C decreased from goethite > kaolinite > illite. Sorbed amounts of salicylic acid carboxyl-^{14}C equaled 87.7 nmol m^{-2} for goethite, 43.4 nmol m^{-2} for kaolinite and 12.1 nmol m^{-2} for illite. Those of phenylalanine carboxyl-^{14}C were 20.6 nmol m^{-2} for goethite, 17.4 m^{-2} for kaolinite, and 5.6 nmol m^{-2} for illite.

Soils were pre-incubated for 10 days at 25 °C and 60% water-holding capacity in the dark, subsequently mixed with either 240 mg of ^{14}C-loaded goethite or 300 mg of ^{14}C-

loaded kaolinite or illite in 56 g of soil, and separated into three aliquots into 250 mL Schott flasks containing a scintillation vial with 1 mL 1 M NaOH to capture $^{14}CO_2$. Before being closed airtight 20 minutes after the addition of minerals, triplicate aliquots of mineral-amended soil were taken, treated with ethanol to prevent further microbial processing, and combusted to quantify initial mineralization of ^{14}C. For three weeks, mineralization was calculated from the total accumulation of $^{14}CO_2$ in NaOH via liquid scintillation counting (TriCarb 3300, PerkinElmer Inc., Shelton, Connecticut USA) with the same double pseudo-first-order kinetic equation in Konrad et al. (2025, Eq. 2). At the end of the three weeks, microbially-assimilated and water-extractable carboxyl-^{14}C were extracted in triplicate in 2 M KCl with and without chloroform-fumigation, respectively (Murage & Voroney, 2007; Vance et al., 1987). Residual carboxyl-^{14}C in the soil matrix was determined by combustion of soil in triplicate using a Hidex OX 600 oxidizer (Hidex Oy, Turku, Finland) and subtracting the ^{14}C activity in fumigated and water extracts. Mineralization over time and mass balances were plotted using Origin Pro 2024b (OriginLab Corporation, Northampton, Massachusetts, USA). Microbial carbon use efficiency (CUE) equaled the amount of ^{14}C in microbial biomass relative to microbially processed ^{14}C. The differences in the fates of the carboxyl-^{14}C- and uniform-^{14}C-labeled monomers (Konrad et al., 2025) were analyzed for significance using Welch's t-test (Welch, 1947) in R (R Core Team, 2022).

The majority of carboxyl-C in both substrates was mineralized in both soils (Fig. 4-1). For all substrate-mineral-soil combinations, mineralization rates for carboxyl-C were higher than uniform-^{14}C labels in Konrad et al. (2025) (+7 – 33 percentage points) and retention on minerals was generally lower (-24 – +2; Table 4-1).

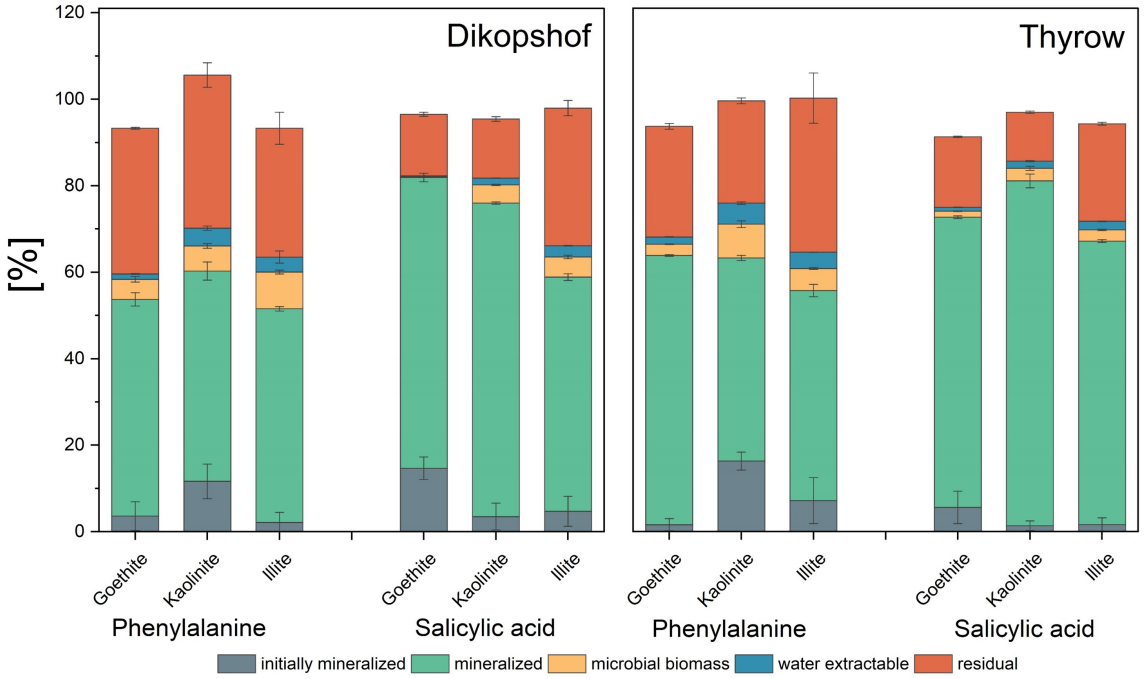

Figure 4-1. Fate of carboxyl-^{14}C traced after three weeks of incubation in loamy Dikopshof (left) and sandy Thyrow soil (right) into microbial biomass, water extractable ^{14}C, ^{14}C retained in soil matrix (residual) and ^{14}C mineralized.

The rate and extent of microbial processing of carboxyl-C was similar in both soils (Fig. 4-2a-d), with initial mineralization often being too rapid for accurate fits even with double pseudo first-order kinetics. Carboxyl-C from salicylic acid was generally retained less and always mineralized more than from phenylalanine (Table 4-1).

Three main observations can be made in comparison to Konrad et al. (2025): i) More mineral-bound carboxyl-C was microbially processed compared to C in other functional groups (Table 4-1), ii) differences in the magnitude of carboxyl-C cycling between the two soils were smaller than the effects of monomer (phenylalanine vs. salicylic acid) and mineral type (Figs. 4-1 & 4-2); and iii) microbial CUE of carboxy-^{14}C correlated with desorbability by substrate (salicylic acid: $y = 0.19x$, R^2 = 0.88; phenylalanine: $y = 0.85x$, R^2 = 0.95) (Supplementary material Fig. S4-1), but not by soil type (Dikopshof: R^2 = 0.6; Thyrow: R^2 = 0.53). That most carboxyl-C was mineralized within the first days of incubation indicates that, the majority of mineral adsorbed carboxyl-C, including ligand-exchanges, is quickly mineralized either when still adsorbed to mineral surfaces or after desorption (Figs. 4-1 & 4-2). The substantial loss of carboxyl-C compared to C in other functional groups suggests that mineralization occurs after desorption.

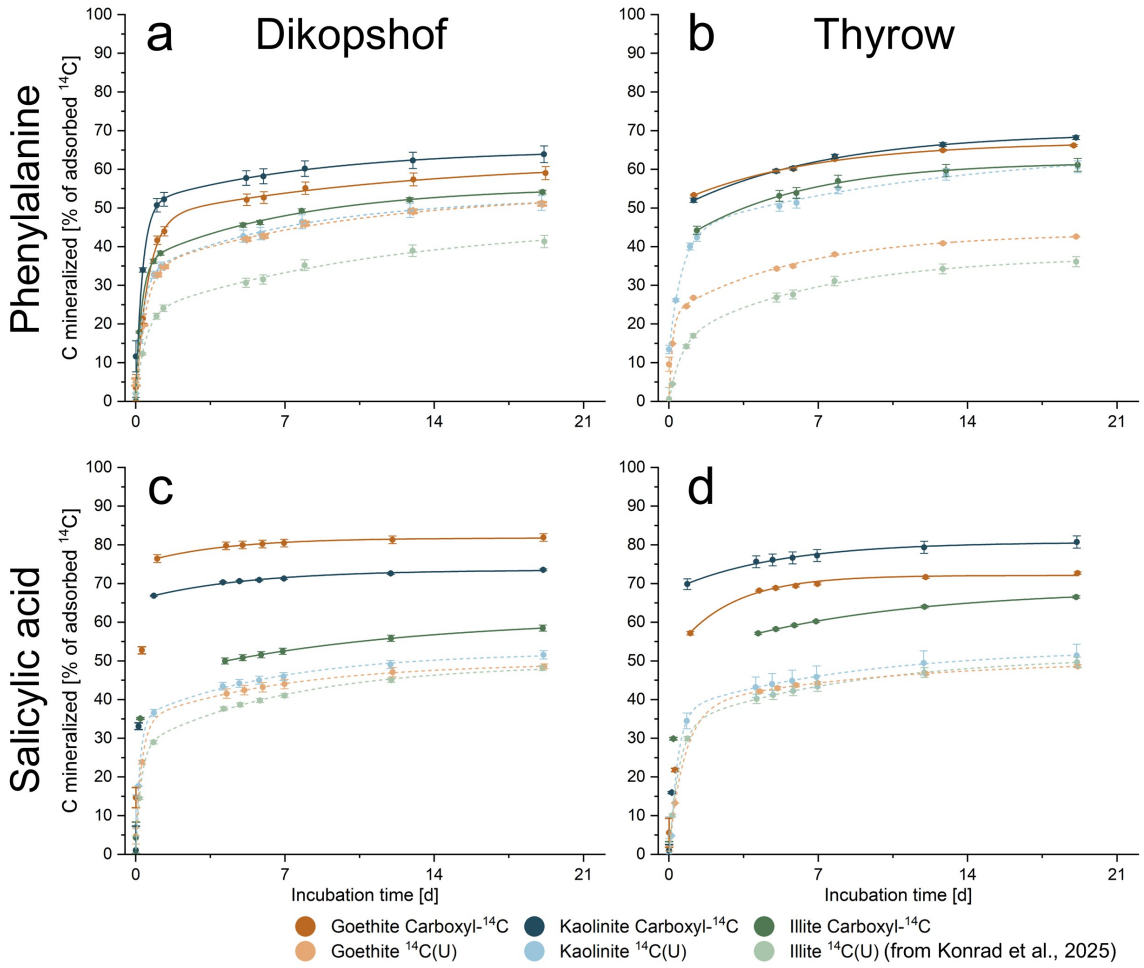

Figure 4-2. Cumulative mineralization of ^{14}C labeled carboxyl groups of phenylalanine (panel a, b) or salicylic acid (panel c, d) adsorbed to either goethite, kaolinite or illite incubated in loamy Dikopshof (panel a, c) or sandy Thyrow (panel b, d) topsoil in comparison to uniformly labeled phenylalanine and salicylic acid from Konrad et al. (2025).

Table 4-1. Fate of carboxyl-^{14}C (1-^{14}C) in salicylic acid and phenylalanine adsorbed to goethite, kaolinite, or illite after three weeks of incubation in loamy Dikopshof (Dik) or sandy Thyrow (Thy) topsoil, and its difference to the fate of uniformly labeled phenylalanine and salicylic acid (Δ^{14}C(U) in Konrad et al. (2025). 1-^{14}C values are percentage of C mineralized, assimilated into biomass, extractable by water (WEOC), and retained as residues on minerals. Δ^{14}C(U) values represent the absolute difference in percent (i.e., percentage points) between 1-^{14}C and ^{14}C(U) values. Significant differences between 1-^{14}C and ^{14}C(U) are indicated (* $p < 0.1$, ** $p < 0.05$, *** $p< 0.01$).

			mineralized [%]			biomass [%]			WEOC [%]			residual [%]			recovery [%]	microbially processed [%]		CUE [%]		
			1-^{14}C	Δ^{14}C(U)		1-^{14}C	Δ^{14}C(U)		1-^{14}C	Δ^{14}C(U)		1-^{14}C	Δ^{14}C(U)		1-^{14}C	1-^{14}C	Δ^{14}C(U)		1-^{14}C	Δ^{14}C(U)	
Dik	Salicylic acid	Goethite	81.9 ± 2.1	+33.0	***	0.2 ± 0	-6.0	*	0.2 ± 0	-2.0	**	14.2 ± 0.5	-24.5	***	96.5 ± 1.8	82.1 ± 2.1	+29.1	***	0.3 ± 0	-11.1	*
	Salicylic acid	Kaolinite	76 ± 2.9	+23.1	*	4.2 ± 0.2	-5.7	**	1.6 ± 0.1	-2.8	**	13.7 ± 0.5	-14.4	**	95.5 ± 2.3	80.2 ± 2.8	+17.4	*	5.2 ± 0.3	-10.7	*
	Salicylic acid	Illite	58.9 ± 3.1	+9.7	*	4.7 ± 0.4	-3.4	*	2.6 ± 0.1	-0.4	*	31.8 ± 1.8	-6.3	*	98 ± 1.1	63.5 ± 2.7	+6.2		7.4 ± 0.9	-6.8	**
Thy	Salicylic acid	Goethite	72.7 ± 3.7	+24.1	**	1.4 ± 0.1	-3.7	**	0.9 ± 0	-2.9	***	16.3 ± 0.2	-19.4	***	91.3 ± 3.5	74.1 ± 3.7	+20.4	*	1.9 ± 0.2	-7.6	**
	Salicylic acid	Kaolinite	81.1 ± 0.8	+19.9	*	2.9 ± 0.5	-5.5	**	1.6 ± 0.1	-4.1	***	11.3 ± 0.3	-15.2	**	97 ± 1.1	84 ± 1.2	+14.3		3.5 ± 0.5	-8.8	**
	Salicylic acid	Illite	67.2 ± 1.7	+15.9	*	2.6 ± 0.2	-3.9	***	2 ± 0.1	-2.2	**	22.5 ± 0.3	-12.1	*	94.3 ± 2	69.7 ± 1.7	+11.9	*	3.7 ± 0.2	-7.6	***
Dik	Phenylalanine	Goethite	53.7 ± 1.8	+7.2	*	4.6 ± 0.6	+0.4		1.3 ± 0.1	+0.0	*	33.7 ± 0.2	-7.2		93.3 ± 2.5	58.4 ± 2.3	+9.1	*	7.9 ± 0.8	-0.3	
	Phenylalanine	Kaolinite	60.3 ± 6.1	+13.8		5.8 ± 0.5	-3.3		4.1 ± 0.5	+1.6	*	35.4 ± 2.8	+2.0		105.6 ± 2.3	66.1 ± 5.6	+10.5		8.9 ± 1.5	-7.4	*
	Phenylalanine	Illite	51.5 ± 2.7	+13.5	*	8.5 ± 0.4	+4.8	***	3.5 ± 1.4	+2.1		29.8 ± 3.7	-19.8	**	93.3 ± 8.1	60 ± 3.2	+18.4	**	14.1 ± 0.	5.2	*
Thy	Phenylalanine	Goethite	63.8 ± 1.5	+26.1	***	2.6 ± 0.1	-0.7	***	1.7 ± 0	+1.1	***	25.6 ± 0.7	-23.9	***	93.7 ± 0.8	66.4 ± 1.4	+25.4	***	3.9 ± 0.2	-4.2	**
	Phenylalanine	Kaolinite	63.3 ± 2.2	+17.9	*	7.8 ± 0.8	-0.4		4.9 ± 0.3	-0.7		23.7 ± 0.7	-12.5	**	99.6 ± 1.8	71.1 ± 1.5	+17.5	*	11.0 ± 1.	-4.5	
	Phenylalanine	Illite	55.7 ± 6.7	+15.8	*	5.1 ± 0.2	-6.5	*	3.8 ± 0	-0.4		35.6 ± 5.8	-15.5	*	100.2 ± 1.7	60.8 ± 6.5	+18.3		8.5 ± 1.3	-18.8	*

Desorption happens when changes in solution composition cause other solutes to diffuse towards mineral surfaces, some of those solutes to replace inner-sphere complexes within hours via competitive desorption (i.e. displacement of an adsorbed ligand by a different ligand, like dissolved organic matter or ortho-phosphate; Kaiser & Zech, 1997), and displaced monomers to diffuse away from mineral surfaces. Microbial processing occurs simultaneously with these competitive adsorption-desorption processes and thus are rate-limited by diffusion from minerals to decomposers (Moyano et al., 2018; Pignatello & Xing, 1996).

The comparably low retention of carboxyl-C via mineral-binding also highlights the role of other associations such as electrostatic interactions, H-bonding and hydrophobic exclusion in determining the balance between adsorption, desorption, and microbial processing. For instance, chelation is the preferred adsorption process for salicylic acid to goethite via its de-protonated carboxyl and ortho-hydroxy groups at the mineral loading used in this experiment (87.7 vs. conservative max. 50–95 nmol m^{-2} reported in Yost et al., 1990). But salicylic acid is easily displaced by DOM and other poly- and di-carboxylic acids (Gu et al., 1996, 1994). In contrast, both the de-protonated carboxyl group and protonated amino group in zwitterionic phenylalanine can adsorb via electrostatic interactions (Yeasmin et al., 2014) as well as self-assemble with hydrophobic phenyl edges (Mossou et al., 2014). When displaced by dissolved organic matter, even more phenylalanine can adsorb to mineral surfaces due to more negative surface charges in soil compared to added minerals (Gao et al., 2018).

When accessible, carboxyl-C is often the first C mineralized due to decarboxylation, which has already been described for alanine added to soil either as solution (Dippold & Kuzyakov, 2013) or mineral-bound (Dippold et al., 2014). The remaining monomer-C undergoes other biochemical pathways, sometimes in combination with carboxyl-C as evidenced by the greater assimilation and higher CUE of phenylalanine carboxyl-C—a proteinogenic amino acid—into microbial biomass than for salicylic acid carboxyl-C (Table 1). After desorption as whole molecules and preferential mineralization of carboxyl-C, partitioning and van-der-Waals interactions between siloxane surfaces and aromatic rings can occur, resulting in re-adsorption and reduced bioavailability of C-atoms other than carboxyl-C (Keiluweit & Kleber, 2009). However, since the incubation

was only three weeks, the long-term retention of both mineral-bound and microbially assimilated C can only be speculated.

In both instances, the propensity to dissociate—that is, desorbability—is determined by factors beyond sorption strength. The addition of substrate-coated minerals to soil leads to changes in boundary conditions, new interactions and thus altered desorbability of adsorbates. Mineral characteristics likely matter more than soil cation exchange capacity, texture, pH and nutrient availability as indicated by similar patterns between the two soils. Yet it should be noted that both soils are agricultural topsoils with a narrow pH range and regular farmyard manure additions with shared litter composition (Simon et al., 2025), and thus the potential role of soil and entire ecosystems in determining desorbability and thus C mineralization may be larger than observed (Stutz, 2023).

Our results demonstrate that even ligand binding to mineral surfaces does not necessarily protect the C involved in coordination with the mineral surface from microbial processing. Competitive desorption followed by partial mineralization best explains how inner-sphere associations of carboxyl groups can be overcome and mineralized while other functional groups persist. Mineralogy seems to matter more than other soil properties, but any factor that alters the tendency for mineral-bound compounds to desorb—e.g., increasing pH, or increased concentrations of oxyanions in solution could lead to mineralization at the expense of sequestration.

Author Contributions

Conceptualization: AK, DH, JS, IM, KS, FL; laboratory analysis: AK, DH; data and statistical analysis: AK; writing – original draft preparation: AK, JS, KS; writing – reviewing and editing: all authors; funding acquisition: IM, KS, FL, JS.

Declaration of competing interests

The authors declare that they have no known competing financial interests of personal relationships that could have appeared to influence the work reported in this paper.

Acknowledgements

This work was funded by the German Research Foundation (DFG, grant no. SI 1106/17-1 and grant no. 465123895). We thank Marcel Lorenz for his coordination of the DFG priority program SPP 2322 – SoilSystems: Systems ecology of soils – energy discharge modulated by microbiome and boundary conditions. We would also like to thank Prof. Dr. Elena Evguenieva-Hackenberg and Andreas Jäger for their management of the radioactive control area at the Justus-Liebig-University Giessen. We would like to extend our gratitude to Andrea Ecker, Simon Horn, and Stefan Köppchen for their invaluable assistance in the radioactive control area at Forschungszentrum Jülich when we were running out of time and hands. We thank Klaus Kaiser, University of Halle, for his feedback and inspiring discussions.

Chapter V

Forest Soil Colloids Enhance Delivery of Phosphorus Into a Diffusive Gradients in Thin Films (DGT) Sink

***Alexander Konrad*[1]**, *Benjamin Billiy*[1], *Philipp Regenbogen*[1], *Roland Bol*[2], *Friederike Lang*[3], *Erwin Klumpp*[2] *and Jan Siemens*[1]

[1]Institute of Soil Science and Soil Conservation, iFZ Research Center for Biosystems, Land Use and Nutrition, Justus Liebig University Giessen, Heinrich Buff Ring 26-32, 35390 Giessen, Germany

[2]Institute of Bio- and Geosciences, Agrosphere (IBG-3), Forschungszentrum Jülich, Wilhelm-Johnen-Str., 52425 Jülich, Germany

[3]Chair of Soil Ecology, Institute of Forest Sciences, University of Freiburg, Bertoldstraße 17, 79098 Freiburg, Germany

This is a copyedited, peer reviewed version of the following article: Forest Soil Colloids Enhance Delivery of Phosphorus Into a Diffusive Gradient in Thin Films (DGT) Sink. Konrad, A., Billiy, B., Regenbogen, P., Bol, R., Lang, F., Klumpp, E., & Siemens, J. (2021). *Frontiers in Forests and Global Change*, *3*, 577364. https://doi.org/10.3389/ffgc.2020.577364

Abstract

Phosphorus (P) is preferentially bound to colloids in soil. On the one hand, colloids may facilitate soil P leaching leading to a decrease of plant available P, but on the other hand they can carry P to plant roots, thus supporting the P uptake of plants. We tested the magnitude and the kinetics of P delivery by colloids into a P sink mimicking plant roots using the Diffusive Gradients in Thin-Films (DGT) technique. Colloids were extracted with water from three forest soils differing in parent material using a method based on dispersion and sedimentation. Freeze-dried colloids, the respective bulk soil, and the colloid-free extraction residue were sterilized and mixed with quartz sand and silt to an equal P basis. The mixtures were wetted and the diffusive fluxes of P into the DGTs were measured under sterile, water unsaturated conditions. The colloids extracted from a P-poor sandy podzolic soil were highly enriched in iron and organic matter compared to the bulk soil and delivered more P at a higher rate into the sink compared to bulk soil and the colloid-free soil extraction residue. However, colloidal P delivery into the sink was smaller than P release and transport from the bulk soil developed on dolomite rock, and with no difference for a soil with intermediate phosphorus-stocks developed from gneiss. Our results provide evidence that both the mobility of colloids and their P binding strength control their contribution to the plant available P-pool of soils. Overall, our findings highlight the relevance of colloids for P delivery to plant roots.

Introduction

Intact forest ecosystems are of extraordinary relevance for biodiversity, the functioning of biogeochemical cycles, landscape water balance and human health (Watson et al., 2018). Phosphorus (P) is an essential element for all living organisms (Elser et al., 2007) and a major limiting factor for the productivity of forest ecosystems, as well as an important driver for soil and ecosystem development (Lang et al., 2017). Recent studies indicate that forests may lose their ability to recycle P due to climate change and enhanced global nitrogen (N) input (Jonard et al., 2015). Understanding the functioning of forest ecosystems and their nutrient cycles is therefore of utmost importance for their protection and sustainable use.

Natural soil colloids (diameter <1,000 nm) embody the smallest particulate phase in soils. Colloids bind larger amounts of P through their high specific surface area compared to other soil components (de Jonge et al., 2004). These particles are formed through weathering, the formation of secondary minerals and the incomplete degradation of organic material (e.g., Missong et al., 2016). Due to their small size, colloids are subject to Brownian motion so that they diffuse through the soil solution, whereby smaller particles are more strongly influenced by the Brownian motion and diffuse faster than large colloids (e.g., Molnar et al., 2019).

The importance of colloids for P-binding and -transport in agricultural soils, which receive P-containing fertilizers, has been recognized for quite some time (e.g., de Jonge et al., 2004; Haygarth et al., 1997; Heathwaite et al., 2005; Ilg et al., 2005; Jacobsen et al., 1997; Jiang et al., 2015; Li et al., 2020). More recently, the importance of colloids for P-binding and –transport was also shown for unfertilized forest soils (Gottselig et al., 2017a,b, 2020; Missong et al., 2018a,b; Wang et al., 2020). These studies revealed that the P-content of colloids of acidic forest soils was up to 16 times larger than the P-contents of the corresponding bulk soils (Missong et al., 2018b). They also showed that up to 91% of the P leached from forest topsoils was not truly dissolved, but bound to colloids (Missong et al., 2018a). Determined by field flow fractionation, these colloids could be subdivided into three size classes of particles smaller than 25 nm rich in organic carbon (C), particles between 25 and 240 nm composed mainly of organic C, iron

(Fe), silicon (Si), and aluminum (Al), and finally particles between 240 and 500 nm with an important contribution of phyllosilicates (Missong et al., 2018a). In calcareous forest soils, calcium (Ca) was the primary metallic element in water-dispersible colloids (WDC) (Wang et al., 2020).

The availability of P bound to colloids for plant uptake is crucial for evaluating the relevance of particle-facilitated Pleaching and redistribution for P-cycling in ecosystems. If the P bound to colloids would be well-accessible for plants, then transport of P from intensely rooted topsoils into deep subsoils or out of the ecosystem together with colloids would have severe consequences for the P supply to the vegetation and the stability of ecosystems. Montalvo et al. (2015a) demonstrated that colloids from a volcanic soil (Andosol) could also act as P-carriers supporting the diffusional transport of P to plant roots and the subsequent P-uptake of plants in hydroponic systems, while no such effect was observed for particles derived from a strongly weathered tropical soil (Oxisol). Based on their finding that ortho-P and hexamethaphosphate bound to Fe-oxide colloids were well-accessible for spinach grown in nutrient solution, Bollyn et al. (2017) emphasized the potential role of pedogenic Fe-oxides for the P-availability in soils and the possibility of using synthetic Fe-oxides as nanofertilizer facilitating P transport to roots. Therefore, an important question is whether colloids from more widely distributed soils of temperate climate zones, like Cambisols, could also support the diffusional P transport to roots and whether this process does also occur in porous media under water-unsaturated moisture conditions. Unsaturated porous media provide many opportunities for attachment of colloids to water-solid interfaces and water-air interfaces or their entrapment in thin water films (Flury & Aramrak, 2017; Kretzschmar et al., 1999). Hence, the enhancement of diffusional colloidal P transport to roots or similar P sinks might be less relevant in water-unsaturated porous media, like most terrestrial soils, than in hydroponic systems. Indeed, Bollyn et al. (2019) observed no additional fertilizer effect of P bound to Fe-oxide nanoparticles compared to soluble KH_2PO_4 when added to strongly weathered tropical soils. They argued that the much smaller diffusion coefficient of colloids compared to orthophosphate in combination with its lower bioavailability were responsible for this lacking additional fertilizer effect in relation to ortho-phosphate. Nevertheless, the experiments of Bollyn et

al. (2019) demonstrated that P bound to Fe-oxides increased plant growth and P uptake relative to a zero P control, indicating that it can be used by plants at least partly.

We examined the delivery of P bound to natural soil colloids from forest soils to artificial P sinks in comparison to P-delivery from colloid-free soil and bulk soil. To this end, we extracted colloids from three forest soils differing in parent material and soil P stock with water. For each of the three soils, the colloids, the colloid-free extraction residue and the respective bulk soil were mixed with quartz silt and sand and P-delivery into artificial P-sinks was quantified at a moisture content equal to 90% waterholding capacity using the Diffusive Gradients in Thin-Films technique (DGT) (H. Zhang et al., 1998). DGT is based on the continuous depletion of P in the soil solution around the sampler. Reduced P concentrations are then compensated by desorption of P from the soil solid phase. DGT therefore measures the P fraction that can be released into soil water and transported to a sink after soil solution depletion, thus simulating the diffusive uptake of P by plant roots (Kruse et al., 2015). For soils in which P uptake by plants is limited by diffusion, DGT is a good predictor of plant-available P (Degryse et al., 2009), since DGT mainly extracts plant-available P as shown by ^{33}P isotope dilution studies (Mason et al., 2013; L. Six et al., 2012). Considering that the mobility of WDC by diffusion and the lability of colloid-bound P are important drivers for their role in ecosystems, the DGT technique provides valuable insights into the behavior of WDC at the root-soil interface. We hypothesized that: (1) colloids deliver more P at a faster rate into the P-sink than bulk soil and colloid-free residual soil, and that (2) soil properties control the magnitude and the kinetics of colloid-facilitated P-delivery into a nutrient sink according to their impact on colloid mobility, the partitioning of P between WDC and non-dispersible soil material and the P binding strength of colloids. Thus, soil properties control the potential relevance of colloids for plant nutrition.

Materials and methods

Forest Sites

Disturbed soil samples from A-horizons and the O/A-transition horizon were collected from three mature beech forest sites in Germany in a sampling campaign in summer 2017. All sites were similar with regard to their forest stand characteristics (tree species composition and stand age), while they differed in the source material of soil formation (Table 5-1) and therefore in their soil P-stock and -availability (Lang et al., 2016, 2017; Prietzel et al., 2016). The soil sampled at the Mitterfels site (MIT) developed on paragneiss and had the highest P content (Tables 5-1, 5-2), followed by the sample from the calcareous site Mangfall (MAN) located in the dolomite alps the with a slightly smaller P content, while the sample from the sandy podzolic soil of the site Lüss (LUE) had a much smaller P content (Tables 5-1, 5-2). For further information regarding the sites visit https://ecosystem-nutrition.uni-freiburg.de/.

Table -1. Characteristics of the study sites Mangfall (MAN), Mitterfels (MIT) and Lüss (LUE) *(Lang et al., 2017; Prietzel et al., 2016)*.

Location (WGS84)	N: 47.608364° E: 11.817519°	N: 48.976008° E: 12.879879°	N: 52.838967° E: 10.267250°
Soil type (WRB, 2015)	Rendzic Leptosol (Rendzina)	Hyperdystric chromic folic cambisol (Humic, Loamic, Nechic)	Hyperdystric folic cambisol (Arenic, Loamic, Nechic, Protospodic)
Parent material	Dolostone (Triassic)	Paragneiss	Sandy till
Humus form (*ad-hoc*-AG Boden 2005)	Mull	Moder	Mor-like moder
Altitude (m a.s.l.)	1,130	1,023	115
Mean annual precipitation (mm)	2,110	1,299	779
pH (measured in H_2O)	7	3.8	3.5
P_{resin} A horizon (mg kg^{-1})	56	70	11

Extraction and Preparation of Water-Dispersible Colloids

Water-dispersible colloids (WDC) were extracted from topsoil samples from the MAN, MIT and LUE sites following an extraction routine based on suspension in water with subsequent sedimentation and centrifugation steps developed by Missong et al. (2016) and Séquaris & Lewandowski (2003). The centrifugation times for the separation of colloids were determined according to Hathaway (1956) to separate the WDC fraction <700 nm. First 0.2 L demineralized water was added to 100 g sample material and shaken on an overhead shaker for 6 h. Subsequently 0.6 L demineralized water was added, the suspension was left to settle for 20 min and the supernatant was pipetted

off. The supernatant was centrifuged at 4,000 g for 4 min and the supernatant was removed by pipette.

Table 5-2. Elemental composition of P-sources of the study sites Mangfall (MAN), Mitterfels (MIT), and Lüss (LUE) after microwave-assisted extraction and ICP-OES and TOC/TN measurements in [g kg^{-1}], including C:N and C:P ratios.

Site	Fraction	Elemental composition [g kg^{-1}]						C:N ratio	C:P ratio
		Al	Ca	Fe	*P*	C	*N*		
MAN	Bulk soil	38.59	71.61	20.84	0.97	199.40	9.30	21:1	151:1
	Residual soil	36.79	73.92	19.93	0.97	172.80	7.40	23:1	191:1
	WDC	76.08	26.02	36.84	1.57	111.80	10.20	11:1	39:1
MIT	Bulk soil	34.00	0.87	29.22	1.17	178.50	8.60	21:1	115:1
	Residual soil	32.48	0.89	28.14	1.04	253.20	13.50	19:1	215:1
	WDC	49.72	0.85	60.65	3.26	305.60	39.30	8:1	48:1
LUE	Bulk soil	5.84	0.41	3.92	0.14	58.60	2.30	52:1	119:1
	Residual soil	5.17	0.41	3.44	0.13	164.40	6.50	52:1	1,107:1
	WDC	43.96	0.98	49.14	1.91	244.80	16.30	15:1	77:1

The supernatant after centrifugation was centrifuged again at 14,000 g for 90 min and the supernatant discarded, thus we potentially lost the smallest WDC. The amount of P bound to WDC lost with the supernatants was quantified through separation from dissolved P using dialysis tubes (SpectrumTM Labs Spectra/PorTM 7, Repligen Corporation, Rancho Dominguez, USA) with subsequent colorimetric measurements (Van Veldhoven & Mannaerts, 1987). The sedimented portion after this process step formed the WDC P-source, while the sedimented soil components after shaking and sedimentation, as well as the sedimented soil components after centrifugation at 4,000 g formed the colloid-free residual soil fraction. The WDC suspensions obtained by extraction were shock-frozen in 45 mL PE bottles using liquid nitrogen. The caps of the PE bottles were then removed and replaced with fine-pored filters (GE WhatmanTM SG81, GE Healthcare Bio-Sciences, Marlborough, USA) for freeze-drying (Christ Beta 1–8 LSCplus, Martin Christ Gefriertrocknungsanlagen GmbH, Osterode am Harz, Germany). The dried WDC powders were subsequently transferred into 1 L PE bottles and homogenized for 6 h using an overhead shaker.

Bulk soil and residual soil (residue of the WDC-extraction) were dried in a drying cabinet at 40 °C. After drying, bulk soil, residual soil and WDC were sterilized with a ^{60}Co source as described by (Dalkmann et al., 2014) to prevent microbial cycling of P. Total C and -N contents of the P-sources were measured using an vario MAX cube (Elementar Analysensysteme GmbH, Langenselbold, Germany). Aliquots (0.5 g) of the three

different P-source materials were digested using 5 mL 69% HNO_3, 3 mL 30% H_2O_2 (both ROTIPURAN©R Supra, Carl Roth GmbH + Co. KG, Karlsruhe, Germany) and 5 mL H2O by microwave-assisted extraction (Öztan & Düring, 2012) and the P-contents were determined by inductively coupled plasma optical emission spectrometry (ICP-OES) (Agilent 720 ICP-OES ES, Agilent Technologies Inc., Santa Clara, USA) as specified in DIN ISO 22036:2009-06 at the element-specific wavelength of 213.618 nm. Particle size distributions of WDC were obtained by Nanoparticle Tracking Analysis (NTA). Three replicates of WDC suspension from every site were analyzed using the laser unit NanoSight LM 14 (Malvern Panalytical Ltd., Malvern, United Kingdom) combined with the microscope NanoSight LM 10 (Malvern Panalytical Ltd., Malvern, United Kingdom). Images were evaluated by the NTA 3.0 software (Malvern Panalytical Ltd., Malvern, United Kingdom) (Supplementary Material Tab. S5-1).

Test System

A mixture of 60 mass-% quartz sand and 40 mass-% quartz silt (20.5 g in total, Gebrüder Dorfner GmbH & Co., Hirschau, Germany) were filled into 60 mL screw-cap beakers made of polycarbonate (Thermo Fisher Scientific, Waltham, Massachusetts, USA). The particle size composition of the quartz mixture determined according to DIN 19683/2 was 1.0% medium sand, 60.4% fine sand, 20.0% coarse silt, 12.3% medium silt, 4.1% fine silt, and 2.2% clay. After autoclaving, the beakers were opened in a sterile environment and the equivalent of 1 mg P of a P-source [bulk soil, residual soil or WDC of the sites MAN, MIT, and LUE, as well as an ortho-phosphate solution (Certipur©R , Merck KGaA, Darmstadt, Germany) as a positive control] was filled into a screw-cap beaker. The screw-cap beakers were closed again and mixed for 6 h on an overhead shaker (Heidolph REAX 2, Heidolph Instruments GmbH & CO. KG, Schwabach, Germany). The screw-cap beakers were then opened again in a sterile environment and autoclaved water was added with an air cushion pipette until 90% of the water holding capacity was reached. The water holding capacity of the porous media including the individual soil fractions was determined in preliminary tests according to Alef & Nannipieri (1995, p.106). The screw cap beakers were then closed for 24 h. During this time, an equilibrium of P between the added water and the soil solid phase was established. The screw-cap beakers were opened again in the sterile environment and one

DGT [LSLP-NP Loaded DGT device for P and metals (B) in soil, DGT Research, Quernmore, Great Britain] was inserted in each beaker and gently pressed into the substrate. The screw cap beakers were closed and the DGTs were removed after 24, 48, 72, 120, and 168 h, with three DGTs per treatment removed after 48 h. The ambient temperature during the experiment was kept constant at 22 ± 0.3 °C.

The semi-permeable filter membranes were rinsed with demineralized water afterwards to stop the mass transport into the device. The DGTs were opened at the groove of the housing and the diffusion layers together with the semipermeable membrane, as well as the ferrihydrite gels were transferred to 2 mL Safelock tubes (Eppendorf AG, Hamburg, Germany) and stored at 4 °C until further analysis. The ferrihydrite gels were than eluted with 0.25 M H_2SO_4 as described by Zhang et al. (1998). The P-concentrations of the eluates were determined using the method of Van Veldhoven and Mannaerts (1987) after formation of phosphomolybdate complexes with malachite green and measured at 630 nm by a UV/Vis photometer (T80 Spectrophotometer, PG Instruments Ltd., Lutterworth, Great Britain) (Supplementary Material Tab. S5-2). Additionally the diffusion layers of the disassembled DGTs after 168 h exposure time to the P-sources were rinsed with water and Al, Ca, Fe, and P concentrations in the gels were determined using ICP-OES after microwave-assisted digestion similar to the P-sources, using 5 mL 69% HNO_3, 3 mL 30% H_2O_2, and 5 mL H_2O for each gel. Due to the harsh extractant used and the high temperatures, the resulting concentrations can be interpreted as total elemental concentrations.

Statistical Analysis

The statistical evaluation of the measurements after 48 h was performed with R (version 3.5.1, The R Foundation for Statistical Computing, Vienna, Austria) and RStudio (version 1.1.456, RStudio Inc., Boston, USA). The software packages used included lme4 (v. 1.1.21), lsmeans (v. 2.30.0) multcomp (v. 1.4.10), and multcompView (v. 0.1.7). The cumulated amount of P in the sinks delivered from the bulk soil, residual soil, or WDC of the sites after 48 h were investigated by pairwise comparisons using the t-test statistics after testing of homogeneity of variances (Bartlett, 1937). The mean values of the pairwise comparisons were adjusted using the false discovery rate (FDR) (Benjamini & Hochberg, 1995).

The kinetics of P accumulation in the DGTs after 24, 48, 72, 120, and 168 h were calculated and evaluated with SigmaPlot Version 12.0 (Systat Software GmbH, Erkrath, Germany). The transport of P from the P-source into the sink of the DGT device is controlled by two kinetic processes, the desorption of P from the solid phase (WDC, bulk soil or residual soil) into the aqueous phase and the diffusion of dissolved P (and colloidal P) through the aqueous phase into the DGT. Both kinetic processes result in a decreasing amount of P delivered to the DGTs per unit time with increasing duration of the experiment. We therefore decided to describe the delivery of P into the DGTs by means of an empirical first order law of velocity model that lumps the desorption rate constant and the diffusion rate constant into one effective parameter (Atkins & de Paula, 2013, p. 840):

$$A_t = A_0 \times (1 - e^{-pt})$$

With A_0 as the total amount of P delivered into the P-sinks up to t = ∞ [µg], p as the release and transport rate of P [h^{-1}] and t as the time of measurement [h]. We assume that the number of five points of time of our experiments would not have allowed the estimation of desorption rate constants and diffusion rate constants independently.

Results

Elemental Composition of Soils and Their Fractions

The largest Al- and Ca-concentrations were found for MAN soil (Table 5-2), while MIT soil showed the largest Fe-concentrations. The WDC of all three sites were enriched in the elements Al, Fe, and P compared to the bulk soil and the residual soil (WDC > bulk soil > residual soil). Most striking is the much stronger enrichment of Fe (WDC/bulk soil ratio of 13:1) and P (WDC/bulk soil ratio of 14:1) in the WDC of the sandy site LUE compared to the MAN soil (Fe ratio of 1.8:1, P ratio of 1.6:1) and MIT soil (Fe ratio of 2.1:1, P ratio of 2.8:1). Moreover, WDC had smaller C:N and C:P ratios than bulk soil and residual soil. While C was enriched in the WDC fraction of MIT and LUE in comparison to the bulk soil, a depletion of C was found for MAN. Analysis of the supernatants after centrifugation at 14,000 g revealed that 3.3% (LUE), 2.9% (MIT), and 0.6% (MAN) of WDC bound P got discarded during WDC extraction.

WDC Size Distribution

The mean size of the WDC particles was similar for the three sites with an average of 195 nm for MAN (median 188 nm), 188 nm for MIT (median 180 nm), and 195 nm for LUE (median 173 nm). However, the size distribution of particles differed between sites (Figure 5-1). The WDC size distribution was characterized by three main peaks, one around 50 nm particle size, one around 100–150 nm particle size and one around 200– 250 nm particle size. The share of the largest size fraction of the particles decreased in the order MAN > MIT > LUE. The WDC of LUE contained the largest concentration of the medium-sized colloidal particles.

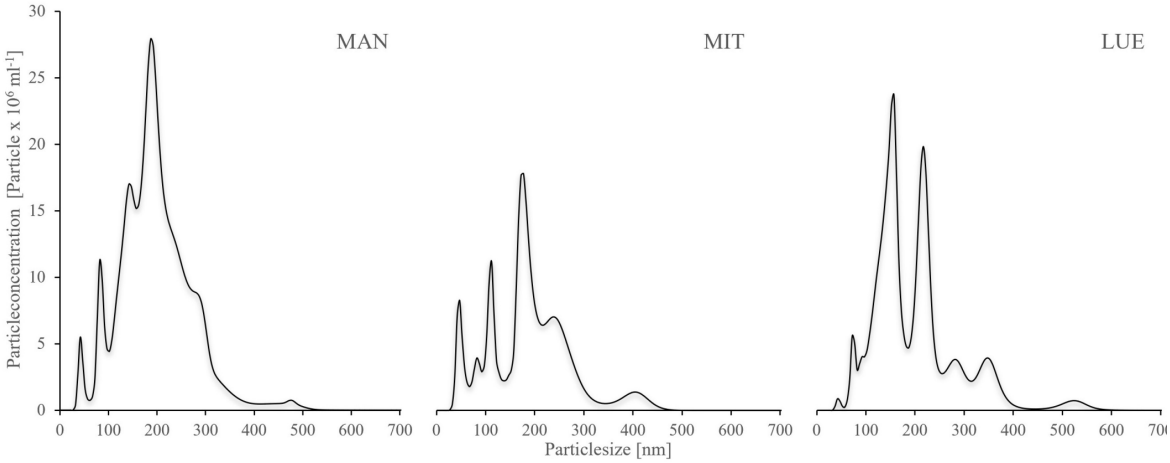

Figure 5-1. Size distribution of the WDC extracted from the topsoils of the sites Mangfall (MAN), Mitterfels (MIT), and Lüss (LUE), determined using Nanoparticle Tracking Analysis (NTA). NTA is capable of measuring natural colloids >50 nm, thus smaller particles were not detected. Size distribution showed three main peaks across all three sites, one around 50 nm, one between 100–150 nm and one around 200–250 nm. Most larger particles were found at MAN, followed by MIT and LUE.

Delivery of P Into the DGTs

The largest amounts of P were found in the DGTs in contact with the ortho-phosphate—solution of the positive control (24 h: 37.3 µg; 48 h: 51.2 µg, 47.7 µg, 44.6 µg; 72 h: 40.18 µg; 120 h: 60.1 µg; and 168 h: 63.0 µg). The regression models of the P-supply into the DGTs and the statistical evaluation of the DGT measurements after 48 h revealed differences in the supply of P from the bulk soils, WDC and residual soils of the different sites into the DGTs (MAN < MIT < LUE) (Figure 5-2 and Table 5-3). Furthermore, the order of the rates of P–release and –transport from the three P-sources into the DGTs varied between sites. While P-release and –transport increased in the order WDC < residual soil < bulk soil for MAN, the order was residual soil < bulk soil = WDC for MIT, and residual soil < bulk soil < WDC for LUE. Multiple pairwise comparisons of the cumulated P quantities in the DGTs after 48 h between the P sources showed no significant differences ($p < 0.05$) at the MAN site. However, significant differences between residual soil on the one hand and bulk soil and WDC on the other hand at the MIT site, and significantly different rates of P-release and -transport between all fractions at the LUE site (Table 3) were observed. The WDC of the P-rich, calcareous MAN site supplied the smallest P quantities in the experiment both over 48 h and the entire (168 h) measurement period. In contrast, the largest P quantities from P sources derived from soil were delivered by the WDC of the LUE site, which after 48 h supplied on average 74 times the quantity of P as the WDC of the MAN site (Table 5-3).

Table 2. Mean values and standard deviations of P delivered into the DGTs within 48 h by different P-sources (n=3).

Site	Soil fraction	Mean [µg]	*SD*	Group
MAN	Bulk soil	0.227	0.071	a
	Residual soil	0.147	0.029	a
	WDC	0.108	0.012	a
MIT	Bulk soil	0.603	0.026	a
	Residual soil	0.368	0.013	b
	WDC	0.603	0.086	a
LUE	Bulk soil	5.661	0.561	a
	Residual soil	2.291	0.287	b
	WDC	7.961	0.246	c

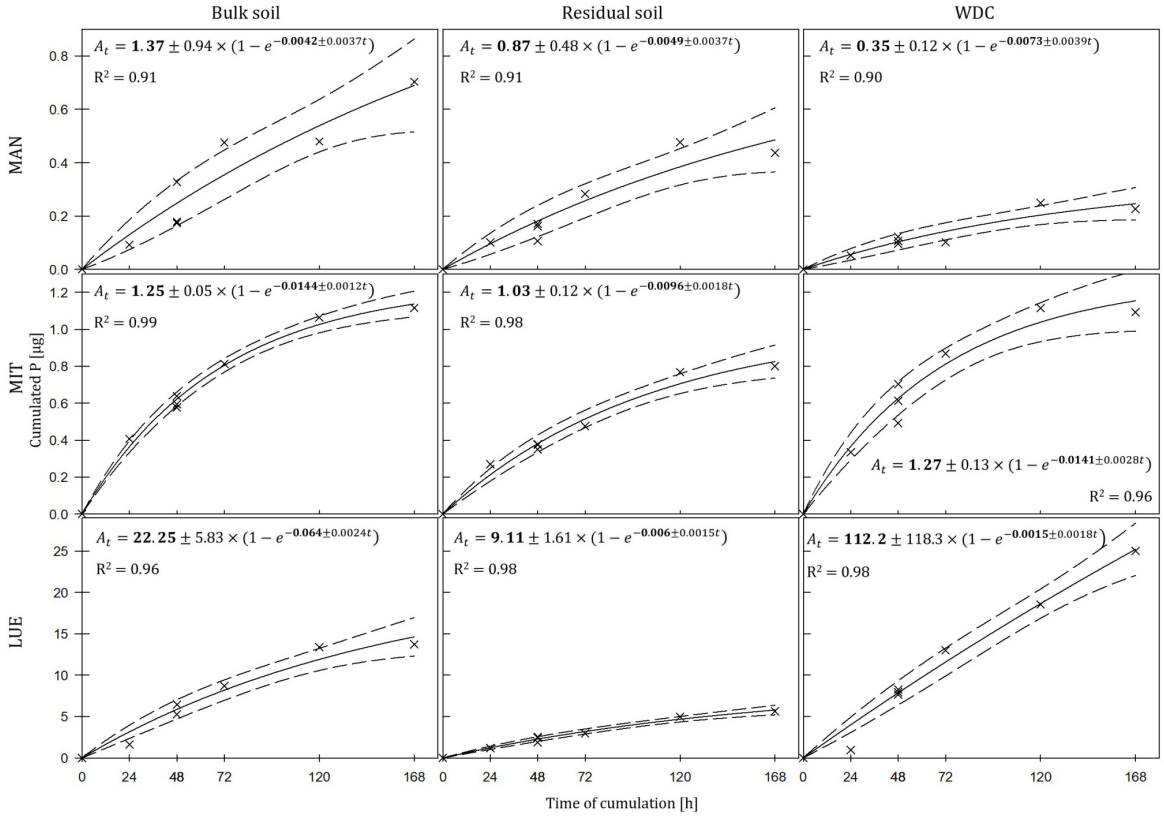

Figure 5-2. Kinetics of P-delivery by bulk soil, residual soil, and WDC of the sites Mangfall (MAN), Mitterfels (MIT), and Lüss (LUE). P quantities cumulated in DGTs after 24, 48, 72, 120, and 168 h are displayed with crosshairs, the regression models with lines and the corresponding 95% confidence intervals with dashed lines. Note the different scaling of y-axes for the three sites. The estimated parameters are shown in bold ± their standard error.

In addition to the highest cumulated P quantities, the regression model for the Prelease and –transport from the WDC of the LUE site into the DGTs indicated no decrease in the P-replenishment rate over the experimental time span of 168 h (Figure 5-2). Furthermore, when disassembling the DGTs in contact with the WDC of the LUE site a dark brown suspension between diffusion gel and filter membrane and a coloration of the diffusion gel (Figure 5-3), as well as a dark brown coloration of the nutrient sinks themselves (Figure 5-4) were recognized.

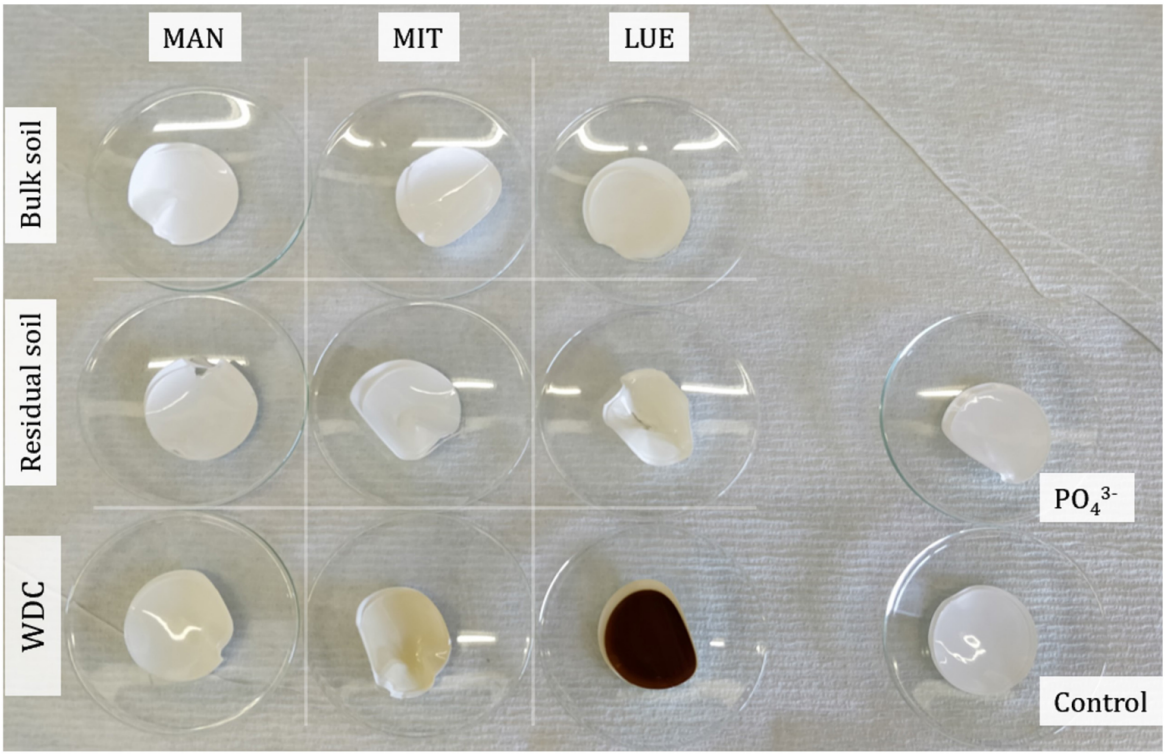

Figure 5-3. Diffusion gels and filter membranes of the disassembled DGTs after 168 h accumulation time of all P-sources and sites. The diffusion gel of the WDC from the site Lüss (LUE) showed a strong coloration due to the diffusion of WDC into the gel.

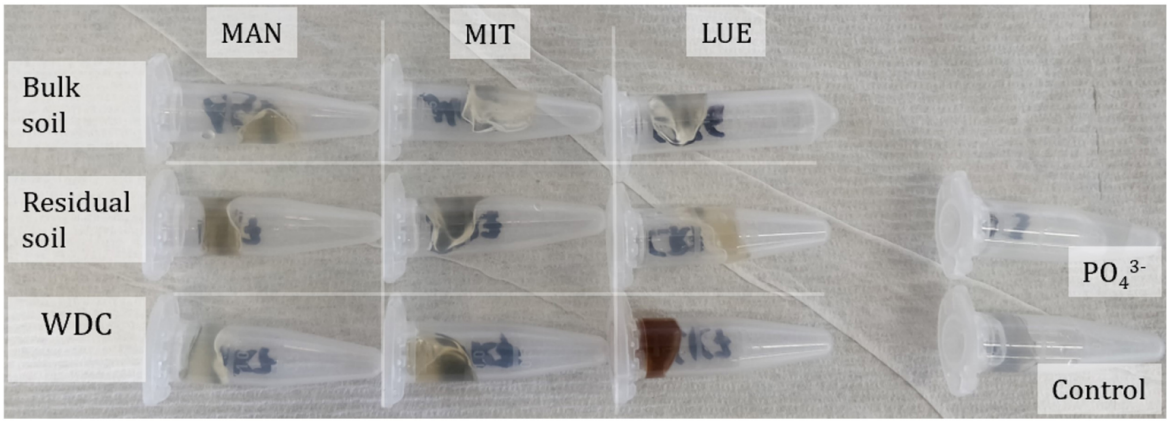

Figure 5-4. Ferrihydrite gel nutrient sinks of the disassembled DGTs after 168 h accumulation time of all soil fractions and sites following their extraction with sulfuric acid. The nutrient sink of WDC of the site Lüss (LUE) showed a strong coloration due to the diffusion of WDC into the sink.

These colorations also occurred to a small extent in the gel layers and nutrient sinks that were in contact with the WDC fraction of the MIT site, while they were absent in gel layers and nutrient sinks that were in contact with the WDC fraction of the MAN site. The elemental analyzes of the diffusion layers after 168 h exposure time to the P-sources by ICP-OES after microwave-assisted extraction revealed that gels used for bulk soil and the colloid-free soil residuals from the calcareous site MAN contained the largest amount of Ca in the experimental setup, while no Ca was traceable in the gels in contact with WDC from this site (Table 5-4). Furthermore, Al and Fe were absent in the diffusion layer in contact with WDCs extracted from MAN. In contrast, the highest amounts of Al and Fe were detected in the colored gel of the WDC from the LUE site, while the WDCs from the Fe-rich MIT site contained in comparison only marginal amounts of Fe in the gel.

Table 5-3. Elemental composition of diffusion layer gels after 168 h in contact with the P-sources of the sites Mangfall (MAN), Mitterfels (MIT), and Lüss.

Site	Fraction	Elemental composition [mg gel^{-1}]			
		Al	Ca	Fe	*P*
MAN	Bulk soil	<LOD	0.031	0.003	0.006
	Residual soil	<LOD	0.029	<LOD	0.004
	WDC	<LOD	<LOD	<LOD	<LOD
MIT	Bulk soil	0.002	<LOD	0.006	0.004
	Residual soil	0.004	0.010	0.009	0.004
	WDC	<LOD	0.006	0.004	0.004
LUE	Bulk soil	<LOD	<LOD	<LOD	<LOD
	Residual soil	0.002	0.007	0.009	0.006
	WDC	0.018	0.016	0.058	0.007
Matrix blank	1	0.001	0.012	0.002	0.004
	2	<LOD	0.011	0.001	0.004
	3	<LOD	0.007	0.001	0.004

Water-dispersible colloids (WDC) from MAN and MIT showed no increased concentrations for aluminum (Al), calcium (Ca), iron (Fe), and phosphorus (P) compared to blank gels, while WDC from LUE were enriched in these elements, indicating the diffusion of compounds derived from WDC into the DGTs at this site. <LOD indicates elemental concentrations below detection limit.

Discussion

P-Release From the Solid Phase of the Different Soils and Soil Fractions

The delivery of P to the DGTs by different P-sources reflected the speciation, binding, and solubility of P in the soils. Prietzel et al. (2016)demonstrated with X-ray absorption near-edge structure spectroscopy (XANES) that in the Ah horizon of the calcareous MAN site, P is present mainly in organic form (either bound to Ca, most likely as precipitate of Ca and inositol hexakisphosphate or as unsorbed organic P), as well as in inorganic form bound to Al-(hydr)oxides. These P-forms show low solubility (precipitates) or desorbability [Al-(hydr)oxides] at the given pH-value of 7.0, resulting in marginal amounts of P transported into the sinks compared to MIT and LUE. The sandy soil of the LUE site features a low sorption capacity for inorganic P (Lang et al., 2017). In line with this limited P sorption capacity, a large fraction of water-soluble P of most likely microbial origin was detected for the Ae horizon at LUE (Lang et al., 2017). Both, the limited P sorption capacity of the soil material and the large fraction of water-soluble P likely promoted the delivery of P by the LUE bulk soil in the DGTs.

Delivery of P Bound to WDC Into the DGTs

Water-dispersible colloids from the P-poor LUE site delivered significantly more P into the DGTs than the bulk soil or the colloid-free residual P-source. The almost linear increase in cumulated P over time from the LUE WDC indicated the immediate compensation of the depleted P concentration in the pore water surrounding the DGTs. This phenomenon was not observed for any other soil fraction at the other sites. Noteworthy, the amount of P cumulated over the measurement period of 168 h in the DGTs in contact with the LUE WDC exceeded the P-capacity of the DGTs of 6.7 µg (Zhang et al., 1998). Although P can be sorbed to the ferrihydrite P-sink above this P-capacity, the ferrihydrite binding sites were already loaded to such extent that P-species were likely not immediately removed from the gel surrounding the ferrihydrite so that the rate of P-accumulation in the DGTs should have decreased over time (Davison & Zhang, 2012). Considering the distinctly increased Fe and P content in the WDC fraction compared to the bulk soil at the site LUE, the measured P flux into the DGT, as well as the coloration of diffusion gel and nutrient sink inside the DGTs (Figures 5-3, 5-4), the intensive P

delivery by LUE WDC could have been caused by mobile OM-Al(Fe)-P complexes (Gerke, 2010) dissolved organically-bound P (e.g., phosphate esters) and mobile OM-Al- and Fe-containing WDC (Jiang et al., 2017). This assumption is supported by the analysis of the diffusion gels using ICP-OES, showing the diffusion of Al, Ca, and Fe into the samplers. Because the gels were rinsed thoroughly before digestion, we assume that most measured complexes, molecules, and WDC have diffused into the gels and were not just attached to its surface. Since the diffusion layer and the nutrient sink use the same type of gel, P-containing compounds that diffused into the diffusion layer may have also diffused into the nutrient sink over time. It must be stated that the use

of the colorimetric method might exclude a part of organic P transported into the DGT. The digestion of the gels with 0.25 M H_2SO_4 and the malachite green method however likely released most P bound to DOM (Baldwin, 1998), OM-Al/Fe complexes (Gerke, 2010), and colloids (Stainton, 1980) through hydrolysis and quantified it in addition to ortho-phosphate. Nevertheless, we likely underestimated the total amount of P translocated into the sinks.

The potential of the DGT technique to measure the transport of colloids into a nutrient sink depends on whether these compounds can diffuse through the filter membrane and the diffusive gel layer during the time of the experiment (Davison & Zhang, 2012). The polyethersulfone filter membrane used in the DGTs has a pore width of 450 nm and should be permeable for most WDC in our experiment. While (H. Zhang & Davison, 1999) stated the average pore size of polyacrylamide gels cross-linked with agarose derivative used for diffusive gel layers with radii >5 nm, van der Veeken et al. (2008) demonstrated the diffusion of latex particles with radii up to 129 nm into these gels. However, diffusion coefficients (Dc) strongly decrease with increasing spherical diameter of the particle according to the Stokes Einstein equation. As a result, WDC particles or large molecules diffuse much slower than ions like ortho-phosphate. For example, Dc in water is 9.5 10-11 m^2 s^{-1} for a spherical particle of 5 nm, 5.95 10-12 m^2 s^{-1} for 80 nm, and 2.4 10-12 m^2 s^{-1} for 200 nm diameter (T = 295.15 K).

We used particle Dc to estimate the distance they could travel due to Brownian motion based on their “mean squared displacement.” The square root of this estimate indicated that very small particles of 5 nm diameter could have moved 10 mm on average

during the 168 h of the experiment, much more than the thickness of the diffusion layer of 0.8 mm. Further calculations, now assuming an equal mix of 5, 80, and 200 nm sized colloids and a density of 2 g cm^{-3} for all particles estimate colloid concentrations to be in the order of 1.7–5.1 10-8 mol l^{-1}. These concentrations could have been large enough to cause a potential diffusion of all added 5 nm colloids and even 21% of the added 80 nm diameter colloids across the diffusion layer into the DGT sink during the 168 h of our experiment (Supplementary Material S5-4). Hence, it appeared possible that the diffusion of mobile colloids was an important reason for the fast and constant delivery of P into the DGTs in contact with the LUE WDC.

Unfortunately the used particle tracking analysis is not able to quantify natural colloids <50 nm properly due to technical restrains (Gallego-Urrea et al., 2011). Therefore, a larger portion of particles smaller than 50 nm might have been present in the WDC of LUE than indicated by the NTA data of Figure 5-1. Overall, the results for the LUE site supported our hypothesis that colloids supply P more efficiently into a P sink than bulk soil or colloid-free residual soil.

Montalvo et al. (2015a,b)demonstrated that colloids and nanoparticles carry P to root surfaces, thereby contributing to the P supply and uptake of plants in hydroponic systems and under water-saturated soil conditions. However, especially in most agricultural soils except Hydragic Anthrosols (WRB, 2015, “paddy rice soils”), water-saturated conditions occur rarely and if, then only for very limited periods of time. Under more common unsaturated conditions the mobility of colloids and nanoparticles in porous media like soils is strongly reduced by interception of particles at water-air interfaces or in thin water films (e.g. Flury & Aramrak, 2017; Kretzschmar et al., 1999). The results of our experiment for the LUE site indicated that colloids can likely carry P to a sink also under water-unsaturated conditions.

Soil pH, WDC Composition, and P-Speciation as Drivers for WDC Mobility and P-Delivery

While the WDC from LUE delivered P at a quick rate, the results for MAN and MIT did not show increased P supply into the DGTs compared to the bulk soil. This suggested that soil properties, as well as the WDC properties controlled their mobility and the binding strength of WDC-P. Since the lowest P quantities were delivered by WDC from the calcareous site MAN and neither coloration of the DGT diffusive gels were visible nor Al, Ca, or Fe were detectable after digestion by ICP-OES, we assumed that the extracted MAN WDC lack OM-Fe-/Al-P complexes and small P-bearing colloids that contributed to the P-flux into the sinks at LUE. Wang et al. (2020) showed that in the Oh and Ah horizons of the MAN site, P was mainly bound to WDC >240 nm rich in Al and Si, which were likely formed from phyllosilicates (Missong et al., 2018a). These larger WDC were not able to diffuse into the sinks of the DGTs due to their size. Two reasons, high Ca^{2+} concentrations and a circumneutral pH value of the soil might limited the mobility of the small WDC from MAN and the P-release into the dissolved phase from these particles. Large concentrations of Ca^{2+} released from the MAN soil derived from dolomite rock might have promoted the flocculation of these clay mineral particles in the porous media. Flocculated WDC would not diffuse in the soil solution or with a much lower rate than single particles because of their larger hydrodynamic radius and mass (Banchio et al., 1999). Furthermore, flocculated WDC may have been retained in the pore space, which in turn may have changed the permeability of the porous medium (Molnar et al., 2019). Moreover, the pH value of 7.0 of the MAN bulk soil was closer to the point of zero charge of many soil components compared to the pH values of the acidic forest soils in MIT and LUE, which may have led to aggregation of the MAN WDC. Aggregation has been demonstrated for example for titanium nanoparticles in porous media at pH values close to the point of zero charge of the nanoparticles (Dunphy Guzman et al., 2006). Contrary to MAN, the WDC from the acidic forest soils of MIT and LUE were likely better dispersed at pH values much lower than the particles point of zero charge. The strong binding of (dissolved) organic matter to Fe- and Al-(hydr)oxides at low pH values (Kaiser et al., 1997) can promote the mobilization of particles (Cheng & Saiers, 2015; Kretzschmar et al., 1995; Philippe & Schaumann,

2014), thus enhancing also the mobility of P bound to these particles. The (weak) podzolic features of the LUE soil would support the theory of diffusion of OM-Fe/Al-P complexes into the DGTs. Missong et al. (2018b) found indications of a translocation of WDC-bound P from the topsoil to the Bsv horizon of the LUE soil. Similarly, Wood et al. (1984), Turner et al. (2012), Celi et al. (2013), and Wu et al. (2014) reported translocation of P during podzolization. However, according to Lang et al. (2017) podzolization was not promoting P transport to greater soil depths at the LUE site. Although comparable amounts of Al and Fe were added with the WDC from the MIT soil as with WDC from the LUE soil to the quartz sand and silt mixture, 10 times less Fe was found in the diffusion layer of the DGT in contact with MIT colloids, and no Al was detectable. The larger Fe contents of the MIT WDC potentially reflected a stronger cementation of individual colloids, which might have reduced their mobility.

Conclusions

Our study demonstrates the enhanced delivery of P by colloids compared to bulk soil and colloid-free soil extraction residue into DGTs in a porous medium under unsaturated conditions. This underpins the relevance of natural colloids for the supply of soil P to plants. Therefore, leaching of these colloids from intensely rooted topsoils to deep subsoils with few roots, or the export of these particles with surface runoff or interflow can decrease the plant availability of P in terrestrial ecosystems. The magnitude and kinetics of colloid-facilitated P delivery likely depend on the mobility of colloids and the strength of the binding of P to the colloids. Building up on previous work on this issue we could confirm that the mobilization of P by and from mobile colloids plays a crucial role for DGT extraction of P.

Author contributions

RB, EK, and JS formulated the hypotheses. AK and JS conceived the experiment. RB, EK, and FL gave feedback regarding the concept and theory in all phases of the study. AK, BB, PR, and JS sampled the soils. AK, BB, and PR carried out the experiments. AK performed statistical analyses and wrote a first draft of the manuscript. All authors discussed the results and contributed to the final manuscript.

Funding

This study was funded in the framework of the Priority Program SPP 1685 Ecosystem Nutrition-Forest Strategies for Limited Phosphorus Resource of the Deutsche Forschungsgemeinschaft (DFG SI 1106/8-1, 2).

Acknowledgements

Thanks to Astrid Jäger, Diedrich Steffens, and Caroline Löw for their comments that helped to improve the experimental design. We also thank Elke Müller, Elke Schneidenwind, and Ann-Kathrin Nimführ for their technical assistance in the laboratory, as well as Jan Wolff for the provision of resin-P data for the topsoil at the Mangfall (MAN) site. We gratefully acknowledge the help of Daniel F. Kaiser, Sebastian Loeppmann,

Marius Schmitt, and Jaane Krüger during the sampling of soils. Without the help of Daniel F. Kaiser and Linda Vogt we never would have been able to extract many kilograms of soil for the isolation of colloids. Big thanks to Jaane Krüger also for organizing and administrating our collaboration.

Chapter VI

Formation of mineral-associated organic matter in temperate soils is primarily controlled by mineral type and modified by land use and management intensity

De Shorn E. Bramble[1,2], Susanne Ulrich[3], Ingo Schöning[1], Robert Mikutta[3], Luise Brandt[4], Christian Poll[4], Ellen Kandeler[4], Christian Mikutta[5], **Alexander Konrad[6]**, Jan Siemens[6], Yang Yang[7], Andrea Polle[7], Peter Schall[8], Christian Ammer[8], Klaus Kaiser[3], Marion Schrumpf[1]

[1]Max-Planck-Institute for Biogeochemistry, Jena, Germany

[2]Department of Hydrogeology, Institute for Geosciences, Friedrich Schiller University [3]Soil Science and Soil Protection, Martin Luther University Halle-Wittenberg, Halle (Saale), Germany

[4]Department of Soil Biology, Institute of Soil Science and Land Evaluation, University of Hohenheim, Stuttgart, Germany

[5]Soil Mineralogy, Institute of Mineralogy, Gottfried Wilhelm Leibnitz University Hannover, Hannover, Germany

[6]Institute of Soil Science and Soil Conservation, iFZ Research Center for BioSystems, Land Use and Nutrition, Justus Liebig University Giessen, Giessen, Germany

[7]Department of Forest Botany and Tree Physiology, Georg August University Göttingen, Göttingen, Germany

[8]Department of Silvicultur and Forest Ecology of the Temperate Zones, Georg August University Göttingen, Göttingen, Germany

This is a copy-edited, peer reviewed version of the following article: Formation of mineral-associated organic matter in temperate soils is primarily controlled by mineral type and modified by land use and management intensity. Bramble, D. S. E., Ulrich, S., Schöning, I., Mikutta, R., Brandt, L., Poll, C., et al. (2024). *Global Change Biology*, *30*(1), e17024. https://doi.org/10.1111/gcb.17024

Abstract

Formation of mineral-associated organic matter (MAOM) supports the accumulation and stabilization of carbon (C) in soil, and thus, is a key factor in the global C cycle. Little is known about the interplay of mineral type, land use and management intensity in MAOM formation, especially on subdecadal time scales. We exposed mineral containers with goethite or illite, the most abundant iron oxide and phyllosilicate clay in temperate soils, for 5 years in topsoils of 150 forest and 150 grassland sites in three regions across Germany. Results show that irrespective of land use and management intensity, more C accumulated on goethite than illite (on average 0.23 ± 0.10 and 0.06 ± 0.03 mg m^{-2} mineral surface respectively). Carbon accumulation across regions was consistently higher in coniferous forests than in deciduous forests and grasslands. Structural equation models further showed that thinning and harvesting reduced MAOM formation in forests. Formation of MAOM in grasslands was not affected by grazing. Fertilization had opposite effects on MAOM formation, with the positive effect being mediated by enhanced plant productivity and the negative effect by reduced plant species richness. This highlights the caveat of applying fertilizers as a strategy to increase soil C stocks in temperate grasslands. Overall, we demonstrate that the rate and amount of MAOM formation in soil is primarily driven by mineral type, and can be modulated by land use and management intensity even on subdecadal time scales. Our results suggest that temperate soils dominated by oxides have a higher capacity to accumulate and store C than those dominated by phyllosilicate clays, even under circumneutral pH conditions. Therefore, adopting land use and management practices that increase C inputs into oxide-rich soils that are under their capacity to store C may offer great potential to enhance near-term soil C sequestration.

Introduction

Soils play a pivotal role in the global carbon (C) cycle as they are the largest terrestrial C pool (Georgiou et al., 2022; Paustian et al., 2016). The sorption of dissolved organic matter (DOM) onto mineral surfaces facilitates long-term stabilization of organic carbon (OC) in soils, with mineral-associated organic matter (MAOM) contributing to as much as 90% to total soil organic matter (OM) (R. Mikutta et al., 2019; Sokol et al., 2022). Given the importance of mineral-organic associations, there is pressing need to understand the factors controlling MAOM formation in order to predict the mitigation potential of soils and their response to global change.

The availability of reactive mineral surfaces for OM sorption is a decisive factor for the formation of MAOM (Creamer et al., 2019; Kaiser & Guggenberger, 2003; Kögel-Knabner et al., 2008; Lehmann & Kleber, 2015; Neurath et al., 2021; Sokol et al., 2022). Soil minerals are, however, not equally efficient in sorbing OM (Creamer et al., 2019; R. Mikutta et al., 2007; Neurath et al., 2021). Laboratory experiments demonstrated that iron (Fe) (oxyhydr)oxides (hereafter termed 'oxides') sorb more OM than phyllosilicate clay minerals (hereafter termed 'clays') (Gao et al., 2018; Han et al., 2021; Saidy et al., 2013; Tombácz et al., 2004). The higher sorption capacity of oxides is attributed to their net positive surface charge under acidic and neutral conditions and their often larger specific surface area (SSA) (Gao et al., 2018; Kaiser & Guggenberger, 2003; Saidy et al., 2013). The capability of oxides to bind OM more strongly might also play a role (Gao et al., 2018; Saidy et al., 2013). Still, it remains untested whether oxides are capable of sorbing more OM than clays under field conditions. Since oxides and clays both occur in the same particle size fraction and tend to associate with each other (Khomo et al., 2017; Kirsten et al., 2021), straightforward differentiation of their individual contributions to soil OC storage is difficult. In addition, MAOM might not only form from interaction of DOM with minerals, but also stem from residues of microorganisms that colonize the minerals (Angst et al., 2021; Cotrufo et al., 2013), with the colonization patterns varying between different mineral types (Brandt et al., 2023; Dong et al., 2022; Uroz et al., 2015). Field incubation of pristine minerals (Kandeler et al., 2019; Liebmann et al., 2022; Vieira et al., 2020) offers the opportunity to directly determine the

contributions of oxides and clays to MAOM formation, but such an approach has not yet been applied along a gradient in land use and soil management intensity.

Land use, which is well known to shape the characteristics of the OM inputs (Bolan et al., 2011), is assumed to control the amount of MAOM formation. Temperate forest and grassland ecosystems account for about 20% of global soil OC stocks (IPCC, 2001). Therefore, understanding the controls on MAOM formation in these ecosystems has major implications for C budgeting upon global climate change. The importance of the quantity and quality of OM inputs for MAOM formation has been demonstrated in a number of laboratory experiments (Córdova et al., 2018; Cotrufo et al., 2022; Gao et al., 2018; Han et al., 2021; Kaiser & Guggenberger, 2000). Primary productivity and abundance of potentially strongly sorbing biopolymers, such as lignin derivates (Sokol et al., 2019), are generally higher in forests than grasslands (Bolan et al., 2011; Krause et al., 2022). However, this does not necessarily translate into higher MAOM-C stocks under forest vegetation (Herold et al., 2014). Indeed, studying land use effects on MAOM over short time scales remains a challenge because of the relatively slow turnover of OM in this pool (Herold et al., 2014; Schöning et al., 2013). The presence of large amounts of MAOM from previous land use could make it even more difficult to detect MAOM-C changes driven by current land use. Furthermore, the assessment of land use effects on MAOM-C stocks across a large spatial scale might be confounded by the heterogeneity in soil mineralogical characteristics and their different effects on MAOM formation (Herold et al., 2014; Keller et al., 2022). To our knowledge, no attempt has yet been made to disentangle the effect of mineral type and land use on the efficiency of MAOM formation under field conditions. Hence, there are still open questions about the efficiency of MAOM formation under different land uses, and the relative importance of land use and mineral type for MAOM formation.

In forests, intensive thinning and harvesting can alter soil OC stocks by reducing litter inputs (Mayer et al., 2020). In a 50-year litter removal experiment, Lajtha et al. (2014) observed an overall 51% decrease in the content of MAOM. In non-experimental forests, thinning and harvesting effects on OC stocks were usually only detectable in the organic layer (Grüneberg et al., 2013; Mayer et al., 2020; Mosier et al., 2019 and references therein). Therefore, it is not yet clear whether the magnitude of MAOM formation

is affected by these forest management practices. The selection of coniferous over deciduous tree species typically leads to wider soil C:N ratios and lower soil pH (Cools et al., 2014). This increase in soil acidity and C:N ratio decreases microbial C use efficiency, resulting in greater DOM production relative to microbial assimilation and OM oxidation (Cools et al., 2014; Córdova et al., 2018), and thus, potentially more MAOM formation. While OC stocks in the organic layer are typically higher in coniferous than deciduous forest, this trend is not consistent in mineral soil (Mayer et al., 2020, and references therein; Waring et al., 2022). This might be in part explained by the confounding effect of soil characteristics (e.g. texture and fertility) since these two forest types are typically established on contrasting soils (Lugato et al., 2021; Mayer et al., 2020).

In grasslands, fertilization and grazing are important management practices affecting soil OC stocks (Conant et al., 2017). While there are numerous studies on the influence of these practices on total soil OM (Conant et al., 2017; Mayer et al., 2020), their effects on MAOM formation are understudied. Moreover, the results of the few studies that exist are not always intuitive and consistent. For example, while fertilization increased plant biomass, it did not affect MAOM-C stocks (Keller et al., 2022). Fertilization is also assumed to enhance microbial bio- and necromass production and, consequently, MAOM formation (Cotrufo et al., 2013; Poeplau et al., 2018, 2019). However, fertilizer-induced increase in microbial activity can lead to faster turnover of MAOM (Bradford et al., 2008; Stoner et al., 2021). Fertilization also reduces plant diversity (Apostolakis et al., 2022; Klaus et al., 2018), which might result in loss of MAOM since plant diversity has been found to be positively linked to soil OC storage (Anacker et al., 2021; Chen et al., 2018; Cong et al., 2014; Lange et al., 2015; Prommer et al., 2020). The higher soil OC stocks in the species-rich grasslands were mainly ascribed to the positive link between plant diversity and plant productivity. In fertilized grasslands, fertilization is likely to be a more decisive driver of plant productivity than plant diversity (Socher et al., 2012). To this end, the relationship between plant diversity and soil OC storage, and the consequences for MAOM formation needs to be investigated specifically for different fertilization levels. Grazing can increase soil OC contents (Franzluebbers & Stuedemann, 2009) but can also have no effect (Piñeiro et al., 2010) or cause significant reductions in soil OC (Paz-Kagan et al., 2016; Wright et al., 2004), depending on the intensity of

grazing and interactions with vegetation, soil properties and precipitation (Eze et al., 2018; Piñeiro et al., 2010). Yet, studies that consider these interactions are rare. As the effects of grazing and fertilization are seldom assessed in combination, their relative importance for MAOM formation across a large spatial scale is still not known.

The main objective of this study was to quantify the efficiency of MAOM formation for goethite and illite, the most abundant iron oxide and clay in temperate soils (Cornell & Schwertmann, 2003; Ito & Wagai, 2017; Journet et al., 2014), when placed in the same soil environment. To quantify effects of different land use types and management intensities as well, we exposed containers filled with pristine minerals for 5 years to ambient conditions at 5 cm depth in the mineral soil of 150 forest and 150 grassland sites across three regions in Germany. By exposing pristine minerals over a 5-year period, we were able to study the formation of MAOM as a consequence of current land use regimes. Our setup enables the first-time assessment of the relative importance of mineral type, site conditions (soil and climatic factors), land use (forest vs. grassland) and management practices (thinning and harvesting, and tree species selection in forests; fertilization and grazing in grasslands) on the formation of MAOM. We hypothesized that the amount of MAOM formed (i) depends on mineral type, being higher for goethite than illite, (ii) is higher in forests, especially in coniferous forests than in grasslands and (iii) is controlled by management intensity in both, forests and grasslands.

Materials and methods

Study region and management

The study was conducted in the *Biodiversity Exploratories* (BE), which is a large-scale and long-term research platform established in 2006 for studying the effects of forest and grassland management on biodiversity and ecosystem processes (Fischer et al., 2010). The BE comprise a set of standardized field plots located in three regions of Germany: the Schwäbische Alb, Hainich-Dün and Schorfheide Chorin. The study regions are defined by distinct climatic, geological and soil conditions (Table 6-1), thereby enabling the assessment of the influence of these factors on ecosystem processes. Each study region includes 50 forest plots and 50 grassland plots, resulting in a total of 300 study sites across regions and land uses.

Each forest plot covers an area of 100 m × 100 m within the larger forest (Fischer et al., 2010). The forests are dominated by European beech (*Fagus sylvatica*), oak (*Quercus robur* and *Quercus petraea*), Norway spruce (*Picea abies*) or Scots pine (*Pinus sylvestris*), and consist of either unmanaged (for at least 60 years), even-aged or uneven-aged stands (Schall et al., 2018). We categorized each plot as coniferous or deciduous forest based on the dominant tree species to assess the effect of these two tree functional types on MAOM formation. As an additional measure of the effect of forest management, we used the silvicultural management intensity index (SMI) developed by Schall and Ammer (2013). The SMI is the additive effect of two components: the risk of stand loss (SMIr) and the stand density (SMId). The SMIr reflects the effects of tree species identity and stand age on the probability of stand loss and is calculated as the probability of a stand to be lost before reaching the age of 180 years (i.e. a reference age for an old growth forest). The SMIr is highest for Norway spruce, followed by Scots pine, oak and European beech and decreases nonlinearly with stand age. Since there is a greater risk of coniferous than deciduous forest stands to break down, SMIr is strongly positively correlated with per cent conifer share (Supporting Information Fig. S6-1). The SMId quantifies the difference between the actual stand stocking (i.e. the actual basal area of a stand at a specific site) and the carrying capacity of that site (i.e. the maximum natural basal area), thus reflecting the forest developmental stage (i.e. lower stocking in young stands) and the intensity of thinning and harvesting. The grassland plots are 50 m × 50 m in size and include meadows that are fertilized and mown; pastures that are fertilized, mown and grazed; and pastures that are grazed but not mown or fertilized (Fischer et al., 2010).

We calculated the intensity of fertilization (kg N ha^{-1} $year^{-1}$) and grazing (livestock units days ha^{-1} $year^{-1}$) according to Blüthgen et al. (2012), using the calculation tool of Ostrowski et al. (2020) implemented in the Biodiversity Exploratories Information System (BExIS). As plots that are fertilized are also commonly mown, we excluded mowing from our analyses to avoid issues with collinearity.

Table 6-1. Overview on climatic conditions, soil and land use management in the three study regions Schwäbische Alb, Hainich-Dün and Schorfheide-Chorin (mean values across the plots with standard deviation). conif. plots in coniferous forest, n = 37; decid. plots in deciduous forest, n = 112; Fe_d and Al_d, dithionite-extractable Fe and Al; Feo and Alo, oxalate-extractable Fe and Al; grass, grassland plots; MAP, mean annual precipitation in the years 2016–2020; MAT, mean annual air temperature in the years 2016–2020; min. grass, Schorfheide-Chorin grassland plots with mineral soil, n = 22; org. grass, Schorfheide-Chorin grassland plots with organic soil, i.e., Histosols and Gleysols, n = 27; SMId, density component of the silvicultural management index (Schall & Ammer, 2013), which reflects the thinning and harvesting intensity; SMIr, risk component of the silvicultural management index, which reflects conifer share; WEOC, water-extractable OC. For SMId, SMIr, fertilization, grazing, aboveground biomass and plant species richness an average over the years 2016–2020 was taken. For the litter C input and litter C:N ratio, an average of the years 2015–2019 was taken. For more information on the measurement of the variables see Supporting Information.

	Study region		
Parameter	Schwäbische Alb	Hainich-Dün	Schorfheide-Chorin
Elevation (m a.s.l.)	460–860	258–500	3–140
MAT (°C)	8.2 ± 0.7	9.2 ± 0.7	9.7 ± 0.6
MAP (mm)	902 ± 49	485 ± 48	581 ± 29
Typical soils	Leptosols, Cambisols	Cambisols, Stagnosols, Luvisols	Histo-, Gley- and Luvisols in grasslands; Cambi-, Areno- and Podsols in forests
Clay (g kg $^{-1}$)	53.6 ± 13.3 (grass)	42.3 ± 13.0 (grass)	12.9 ± 4.5 (org. grass)
			21.2 ± 9.6 (min. grass)
	49.3 ± 9.6 (conif.)	29.6 ± 9.6 (conif.)	5.4 ± 1.9 (conif.)
	50.6 ± 12.8 (decid.)	37.1 ± 14.4 (decid.)	3.4 ± 1.1 (decid.)
Sand (g kg $^{-1}$)	5.7 ± 4.5 (grass)	5.8 ± 2.3 (grass)	65.0 ± 10.7 (org. grass)
			28.6 ± 13.5 (min. grass)
	3.4 ± 1.3 (conif.)	5.4 ± 1.3 (conif.)	90.0 ± 4.6 (conif.)
	6.8 ± 4.9 (decid.)	5.8 ± 1.7 (decid.)	84.8 ± 6.1 (decid.)
Soil OC (g kg $^{-1}$)	71.0 ± 17.1 (grass)	47.2 ± 12.5 (grass)	188.4 ± 107.9 (org. grass)
			27.1 ± 6.2 (min. grass)
	67.4 ± 25.9 (conif.)	37.4 ± 9.6 (conif.)	28.3 ± 12.2 (conif.)
	67.7 ± 25.2 (decid.)	42.2 ± 16.9 (decid.)	29.9 ± 17.0 (decid.)
Soil C:N ratio	10.6 ± 1.3 (grass.)	10.1 ± 0.45(grass)	10.7 ± 1.4(org. grass)
			10.6 ± 0.6 (min. grass)
	14.1 ± 1.9 (conif.)	13.8 ± 2.0 (conif.)	20.6 ± 2.2 (conif.)
	13.2 ± 1.2 (decid.)	13.3 ± 1.8 (decid.)	17.3 ± 1.8 (decid.)
Soil pH	6.3 ± 0.6 (grass)	6.9 ± 0.5 (grass)	7.0 ± 0.8 (org. grass)
			5.9 ± 0.7 (min. grass)
	5.0 ± 1.0 (conif.)	6.0 ± 0.8 (conif.)	3.5 ± 0.1 (conif.)
	5.7 ± 0.7 (decid.)	4.9 ± 0.8 (decid.)	3.6 ± 0.1 (decid.)
Root biomass (g cm $^{-3}$)	259.9 ± 119.4 (grass)	275.4 ± 94.2 (grass)	348.0 ± 196.2 (org. grass)
			502.9 ± 211.7 (min. grass)
	113.3 ± 80.6 (conif.)	104.3 ± 19.0 (conif.)	50.6 ± 25.5 (conif.)
	106.6 ± 57.2 (decid.)	124.6 ± 62.5 (decid.)	68.1 ± 25.9 (decid.)
WEOC (mg kg $^{-1}$)	72.1 ± 23.0 (grass)	73.5 ± 28.3 (grass.)	112.5 ± 37.0 (org. grass)
			58.9 ± 21.2 (min. grass)
	186.6 ± 67.5 (conif.)	96.9 ± 21.6 (conif.)	106.0 ± 47.0 (conif.)
	180.3 ± 75.9 (decid.)	109.4 ± 47.3 (decid.)	91.6 ± 33.5 (decid.)
Fe_o (g kg $^{-1}$)	3.0 ± 1.4 (grass)	2.1 ± 0.6 (grass)	10.1 ± 7.1 (org. grass)
			1.4 ± 0.4 (min. grass)
	2.9 ± 0.9 (conif.)	2.8 ± 0.7 (conif.)	1.2 ± 0.3 (conif.)
	2.6 ± 1.0 (decid.)	3.1 ± 0.7 (decid.)	1.2 ± 0.3 (decid.)
Al_o (g kg $^{-1}$)	0.6 ± 0.7 (grass)	0.4 ± 0.2 (grass)	0.02 ± 0.04 (org. grass)
			0.3 ± 0.2 (min. grass)
	0.4 ± 0.3 (conif.)	0.3 ± 0.1 (conif.)	0.6 ± 0.2 (conif.)
	0.6 ± 0.4 (decid.)	0.2 ± 0.1 (decid.)	0.5 ± 0.1 (decid.)

Table 6-1. (Continued).

Parameter	Study region		
	Schwäbische Alb	Hainich-Dün	Schorfheide-Chorin
Fe_d (g kg $^{-1}$)	23.4 ± 5.4 (grass)	14.0 ± 2.6 (grass)	24.1 ± 14.7 (org. grass)
			4.7 ± 1.6 (min. grass)
	23.9 ± 9.7 (conif.)	14.7 ± 0.9 (conif.)	2.5 ± 0.8 (conif.)
	25.8 ± 5.9 (decid.)	11.5 ± 3.9 (decid.)	2.5 ± 0.8 (decid.)
Al_d (g kg $^{-1}$)	69 ± 3.4 (grass)	5.3 ± 1.9 (grass)	0.7 ± 0.4 (org. grass)
			0.8 ± 0.3 (min. grass)
	10.8 ± 6.0 (conif.)	6.8 ± 1.7 (conif.)	0.8 ± 0.3 (conif.)
	10.0 ± 3.7 (decid.)	3.9 ± 1.5 (decid.)	0.6 ± 0.2 (decid.)
Forest parameters			
Dominant forest type	(Mixed) beech forests, spruce forests	European (mixed) beech forests	Pine—durmast oak forests, (mixed) beech forests
SMId	0.27 ± 0.10 (conif.)	0.12 ± 0.03 (conif.)	0.30 ± 0.14 (conif.)
	0.37 ± 0.16 (decid.)	0.27 ± 0.21 (decid.)	0.31 ± 0.19 (decid.)
SMIr	0.77 ± 0.02 (conif.)	0.65 ± 0.09 (conif.)	0.22 ± 0.06 (conif.)
	0.09 ± 0.10 (decid.)	0.03 ± 0.03 (decid.)	0.06 ± 0.03 (decid.)
Litter C input (g m^2)	227.0 ± 38.7 (conif.)	201.4 ± 21.4 (conif.)	247.3 ± 53.7 (conif.)
	257.7 ± 44.8 (decid.)	264.2 ± 44.1 (decid.)	257.5 ± 46.3 (decid.)
Litter C:N ratio	47.9 ± 2.9 (conif.)	46.5 ± 4.3 (conif.)	63.8 ± 2.9 (conif.)
	40.2 ± 4.8 (decid.)	41.8 ± 4.6 (decid.)	43.0 ± 5.1 (decid.)
C stock of organic layer (kg m $^{-2}$)	1.33 ± 0.42 (conif.)	0.66 ± 0.32 (conif.)	2.92 ± 1.16 (conif.)
	0.84 ± 0.39 (decid.)	0.59 ± 0.16 (decid.)	1.01 ± 0.45 (decid.)
Grassland parameters			
Grazing (livestock units days ha $^{-1}$ year $^{-1}$)	76.9 ± 105.7	112.4 ± 199.3	120.5 ± 149.9 (org. grass)
			244.9 ± 219.2 (min. grass)
Fertilization (kg N ha $^{-1}$ year $^{-1}$)	55.6 ± 74.1	42.9 ± 52.3	2.2 ± 4.1 (org. grass)
			11.1 ± 22.1 (min. grass)
Aboveground biomass (g m $^{-2}$)	142.7 ± 72.9	123.6 ± 62.6	208.8 ± 70.7 (org. grass)
			257.8 ± 78.3 (min. grass)
Species richness (count of plant species per 16 m^2)	32.6 ± 8.4	37.2 ± 11.8	19.6 ± 3.0 (org. grass)
			30.2 ± 3.2 (min. grass)

Experimental design

A total of 3648 mineral containers were installed at all 300 sites between November 2015 and January 2016. The mineral containers had a surface area of 35 cm^2 and consisted of a plastic ring that framed a 50-µm mesh which served to prevent root ingrowth and mineral losses but allowed for water passage and microbial colonization (Figure 6-1a; Brandt et al., 2023). Given the container design, translocation of OM into the containers can result from: (i) transport of DOM from soil OM decomposition or root exudates via the soil solution, (ii) transport of small (<50 µm) particulate material and microbes by percolating soil water and (iii) ingrowth of fungi followed by transport of OM and bacteria via fungal hyphae (see Frey et al. (2003), See et al. (2022)). The containers were filled with either a mixture of 12 g of synthetic goethite (Bayferrox® 920 Z, CAS-No. 51274-00-1, Lanxess AG, Cologne, Germany) and 12 g of

washed and annealed sea sand (VWR, CAS-No. 14808-60-7; >63 µm) or 12 g of natural illite (Inter-ILI. Engineering Co. Ltd., Kosd, Hungary) and 33 g of sea sand. Selected chemical, physical and mineralogical properties of the minerals and sea sand can be found in Table 6-2. Information on their DOM sorption capacity is presented in Supporting Information Fig. S6-3. The addition of the sand to the containers ensured that drainage was not impeded. More sand was mixed with illite to standardize the volume of sample material in the containers.

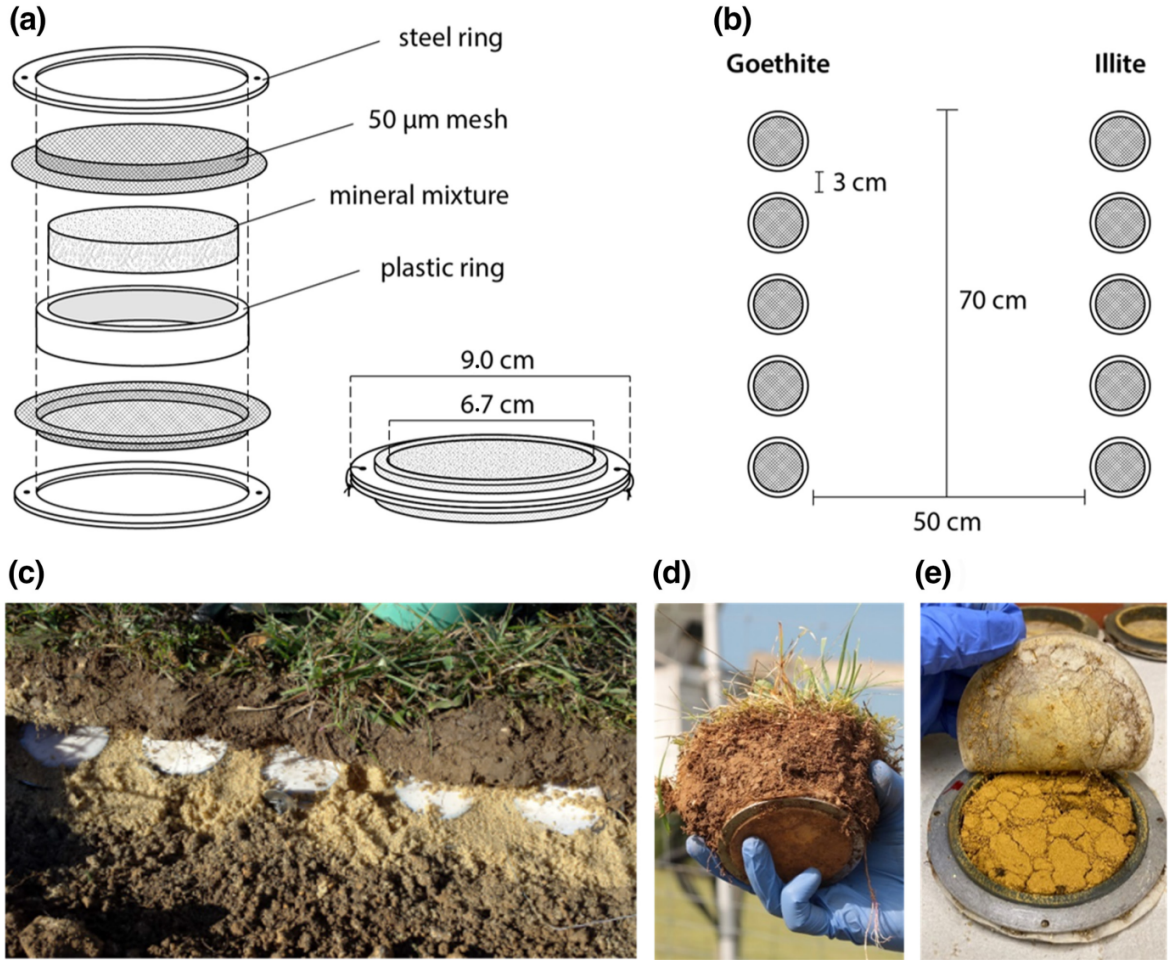

Figure 6-1. (a) Setup and dimensions of a mineral container; (b) schematic top view of the mineral container placement in 5 cm soil depth; (c) photo of a row of minerals container on a sand bed during installation in 2015; (d) photo of sampling a mineral container and the surrounding soil; (e) photo of an opened mineral container (reprinted from Brandt et al., 2023 with the permission from Elsevier).

Five replicates of mineral containers containing either goethite or illite were placed at 5 cm soil depth in a horizontal slit in the soil. The two types of mineral containers were positioned directly opposite to each other at a distance of 50 cm (Figure 6-1b). We filled

the space created in the soil by placing sand above and below the mineral containers (Figure 6-1c) to prevent holes and to standardize the physical conditions under which the containers were exposed.

Table 6-2. Selected properties of pristine minerals goethite, illite and sea sand: (a) Reaction (pH in $CaCl_2$ solution); oxalate- and dithionite- citrate-bicarbonate (DCB)-extractable Al, Fe and Mn (Al_o, Fe_o, Mn_o and Al_d, Fed, Mn_d respectively), no oxalate-soluble Si and Mn detectable; specific surface area (SSA); point of zero charge (PZC); (b) Element concentration (C:N analyser; X-ray fluorescence spectrometry), since no inorganic carbon was detectable, C represents organic C; (c) Cation exchange capacity (CEC) and exchangeable cations; n.a., not analysed; n.d., not detectable. Details on the methods can be found in the Supporting Information.

Sample	pH ($CaCl_2$)	Al_o g kg^{-1}	Fe_o g kg^{-1}	Al_d g kg^{-1}	Fe_d g kg^{-1}	Mn_d g kg^{-1}	SSA (N_2-BET) m^2 g^{-1}	PZC
(a)								
Goethite	7.3	0.17	1.82	1.36	614.52	0.28	20.4	7.8
Illite	7.0	0.26	0.12	n.d.	0.25	n.d.	40.7	n.a.
Sea sand	6.7	n.d.	n.d.	n.d.	n.d.	n.d.	1.1	n.a.

Sample	C g kg^{-1}	N g kg^{-1}	C:N	Fe g kg^{-1}	Mn g kg^{-1}	Al g kg^{-1}	Si g kg^{-1}	K g kg^{-1}	Mg g kg^{-1}	Ca g kg^{-1}	P g kg^{-1}
(b)											
Goethite	0.40	0.19	2.1	613.49	0.46	2.15	0.24	1.00	0.28	0.36	0.12
Illite	0.42	0.38	1.1	4.07	0.07	149.33	265.58	70.24	7.50	2.31	0.21
Sea sand	0.10	0.04	2.5	n.d.	0.02	5.02	460.59	1.24	0.56	0.29	0.03

Sample	CEC (pH 7) mmol$_c$ kg^{-1}	Al^{3+} mmol$_c$ kg^{-1}	Fe^{3+} mmol$_c$ kg^{-1}	Ca^{2+} mmol$_c$ kg^{-1}	Mg^{2+} mmol$_c$ kg^{-1}	K^+ mmol$_c$ kg^{-1}	Na^+ mmol$_c$ kg^{-1}	NH_4^+ mmol$_c$ kg^{-1}	Ca, Mg, K, Na saturation of CEC (pH 7) %
(c)									
Goethite	n.a.	n.a.	n.a.	n.a.	n.a.	n.a.	n.a.	n.a.	n.a.
Illite	165.5	<0.01	3.7	110.4	33.2	14.5	2.6	0.03	>97
Sea sand	4.8	n.d.	n.d.	3.5	0.4	0.5	0.4	n.d.	100

Collection, preparation and analysis of mineral and soil samples

Three of the five replicated mineral containers of each type were extracted from the field in August 2020 after ca. 5 years of exposure to natural soil conditions. The soil overlying the mineral containers was also taken and a composite sample was created for each mineral type (Figure 6-1d). All samples were transported to the laboratory in coolers. The mineral containers were opened (Figure 6-1e) and, if necessary, visible fine roots and hyphae were removed with a tweezer. We also weighed the contents of the mineral cylinders to account for potential losses during the 5-year field exposure. We did not observe any difference in the dry mass of the minerals in the containers during the experimental period. This suggests that there were no significant losses.

Nevertheless, as we aimed at determining elemental concentrations and not stocks or fluxes, potential small losses of minerals are not relevant to the objectives our study. The mineral replicates were combined, thoroughly homogenized, freeze-dried and finely ground. Soil samples were air-dried, sieved to <4 mm, and a portion was ground for elemental analysis. The moisture content of the air-dried soil samples was determined by drying a 2-g aliquot at 105°C for 24 h. Total C (TC) and total nitrogen (TN) concentration of the field-exposed mineral and soil samples were determined by dry combustion at 1100°C using a varioMAX Cube elemental analyser (Analysensysteme GmbH, Langenselbold, Germany). The inorganic C (IC) concentration of the soils was determined with the same analyser after removal of OC by heating the samples to 450°C for 16 h. The OC concentration was calculated as the difference between TC and IC. As we anticipated very low IC concentrations in the mineral samples, they were analysed for IC by suspending 200 mg of sample material in 50 mL 2 M HCl at 50°C and subsequent detection of released CO_2 (soliTIC module interfaced to the varioMAX Cube elemental analyser). Since IC concentrations on the minerals were negligible, TC equates OC. Given the twofold difference in SSA of goethite (20.4 $m^2 g^{-1}$) and illite (40.7 $m^2 g^{-1}$), we express the amount of accumulated OC per m^2 of pristine mineral. Note, although the mineral containers contained different ratios of sand to pristine mineral, the very low SSA and negligible OM sorption capacity of quartz implies that the accumulated OC can be solely ascribed to the contained reactive minerals (Table 6-2; Supporting Information Fig. S6-2).

Additional soil and plant properties

For examining the influence of land use and management intensity on the MAOM-C accumulation, further soil and plant variables (soil texture, soil pH, OC stock of the soil organic layer, litter C and C:N ratio, water-extractable OC (WEOC), aboveground plant biomass and plant species richness) were used. For information on sampling and measurement of these variables see the Supporting Information.

Data analysis

All data were analysed using R (version 4.2.0, R Core Team, 2022). Student's t-test was used to test the effect of mineral type on MAOM-C accumulation. We used histograms

and Q–Q plots to check that the data were normally distributed. We did the same before performing an analysis of variance (ANOVA). Levene's test was used to verify that the assumption of homogenous variances was not violated. For each mineral type, we assessed the effect of vegetation type separately for each study region using one-way ANOVA and Tukey's honest significant difference tests. The same statistical analyses were used to assess the effect of study region on MAOM-C accumulation in beech forests separately for goethite and illite. The relationship between MAOM-C accumulation and the OC concentration in the overlying soil material in mineral soils and organic grassland soils were assessed by linear regression analysis. To explore management effects in forests and grasslands on the MAOM-C accumulation, individual piecewise structural equation models (SEMs; Lefcheck, 2016) were constructed for each mineral. The SEMs were developed from the conceptual models presented in Figure 6-2.

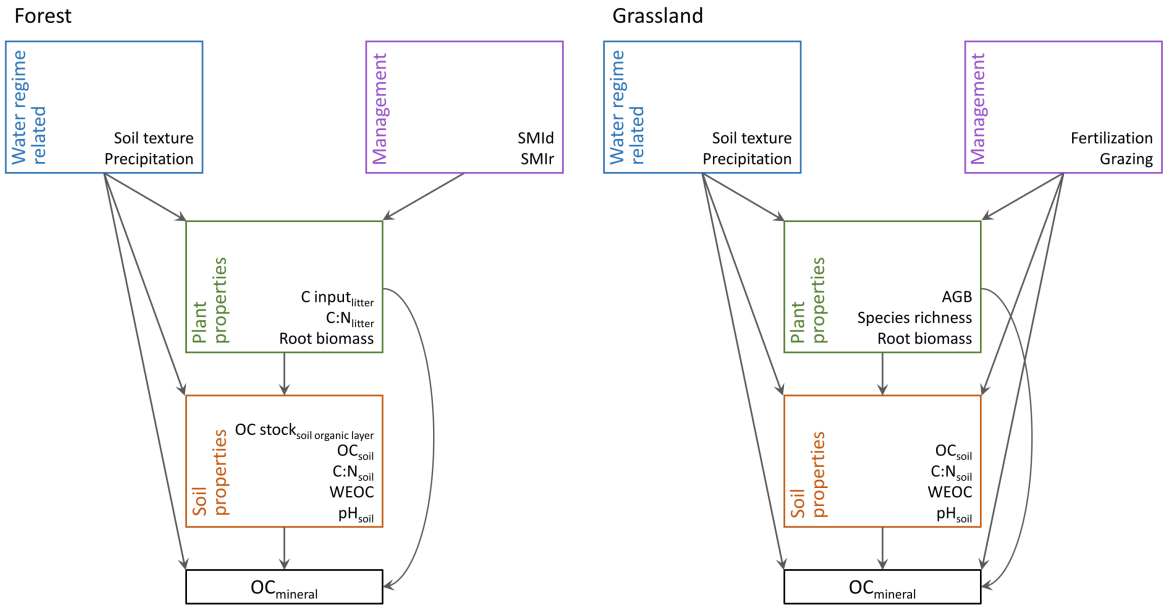

Figure 6-2. Conceptual models for forests and grasslands with all the variables and paths tested in the structural equation models. C:N litter, C:N ratio of litter fall; C:N soil, C:N ratio of the mineral soil; OC input litter, mass of C in litter fall; OC mineral, OC concentration in goethite or illite mineral containers; OC soil, OC concentration in the mineral soil; OC stocks soil organic layer, OC stocks in the soil organic layer; SMId, Density component of the silvicultural management index, which reflects the thinning and harvesting intensity; SMIr, Risk component of the silvicultural management index, which reflects per cent conifer cover; WEOC, water-extractable OC. With the exception of the OC concentration in the overlying soil (in forests and grasslands) and grazing intensity, variables that were not linked to MAOM-C accumulation on pristine minerals were removed from the models. We decided not to remove the OC concentration in the overlying soil to visually highlight the relative importance of soil OM quantity (OC concentration) and quality (C:N ratio) on the MAOM-C accumulation on minerals. MAOM, mineral-associated organic matter; OC, organic carbon.

Besides the management variables, the conceptual models contained water regime-related variables that might have an effect on MAOM formation by influencing DOM fluxes. Plant and soil properties were incorporated as mediating variables that might link the management variables to MAOM formation. The SEMs were performed with the piecewiseSEM 2.1 R package (Lefcheck, 2016). In all SEMs, study region was included as random factor. This allowed us to determine how much of the explained variance in MAOM-C accumulation was due to fixed (management, water regime, plant and soil properties) and random effects (study region). The variance explained solely by the fixed factors in our models is denoted as the $R^2_{marginal}$ (R^2_m), while that explained both by the fixed and random effects is denoted as the $R^2_{conditional}$ (R^2_c). PiecewiseSEM uses tests for directed separation to evaluate the relevance of missing paths (i.e. not based on priori hypothesis) in the model. Only when we could ascribe them to cause and effect relations, these additional effects were included as paths in the models. Otherwise, they were considered as covariances. We applied log transformation to all explanatory variables that were not normally distributed (SMIr, C:N litter, OC stocksoil organic layer and C:N soil in forests, and fertilization and grazing intensity in grasslands). Models with p values ≥.05 were considered valid. The overall fit of these models was assessed with Fisher's C statistic and Akaike information criterion (AIC). Variables (except for management indices, and OC concentration and C:N ratio of the overlying soil) and paths that were not significant ($p > .1$) for either mineral were excluded from the final models.

Results

Effect of mineral type on MAOM accumulation

After 5 years of field exposure, the amount of OC that accumulated per gram of pristine mineral was almost two times higher for goethite than illite (4.71 ± 4.85 and 2.45 ± 1.26 mg g^{-1} respectively). These concentrations correspond to 10% and 86% of the sorption capacity of goethite and illite as determined in sorption experiments with DOM from the Oa horizon of a spruce forest (see Supporting Information Fig. S6-2). If OC concentration is expressed per unit SSA of pristine mineral, it was four times higher on goethite than illite (Figure 6-3). The higher accumulation on goethite was consistent across study regions and vegetation types (Figure 6-4).

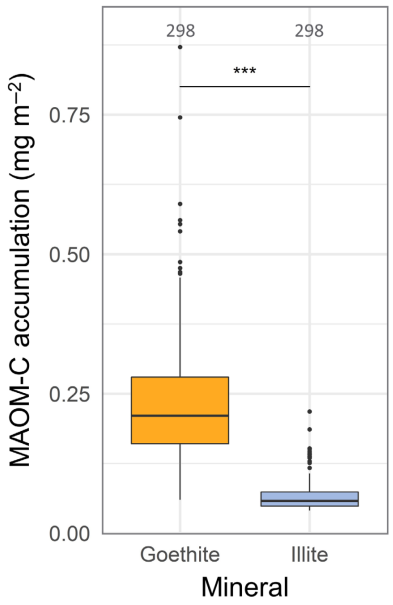

Figure 6-3. Accumulation of MAOM-C on two different pristine minerals (goethite and illite) buried for 5 years at 5 cm depth in the topsoil of forests and grasslands in three regions across Germany. The organic C content is expressed per m2 of pristine mineral. The horizontal line represents the median. Outliers are represented by black dots outside the whisker of the plot. ***Significant difference at p ≤ .001 between the two minerals. The number of replicates per box are at the top of the plots. MAOM, mineral-associated organic matter.

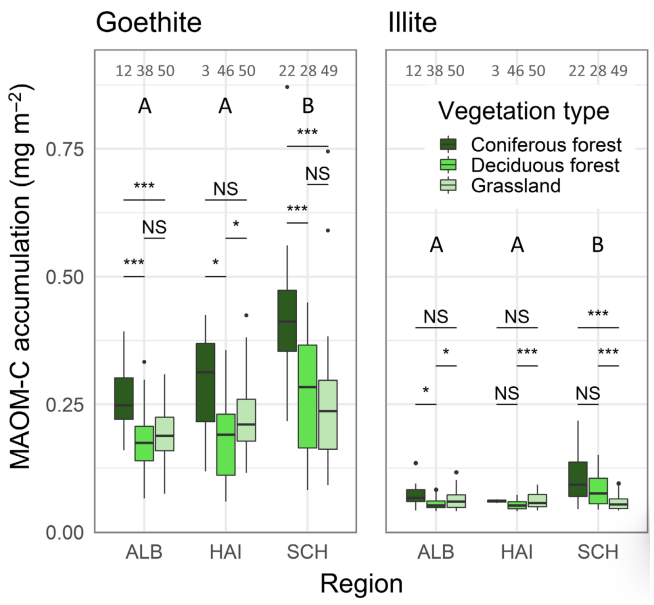

Figure 6-4. Effect of vegetation type on MAOM-C accumulation on pristine minerals (goethite and illite) buried for 5 years at 5 cm depth in the topsoil of forests and grasslands in three regions across Germany. The organic C content is expressed per m2 of pristine mineral (goethite and illite). Data for each mineral are further separated by study region: Schwäbische Alb (ALB), Hainich-Dün (HAI) and Schorfheide-Chorin (SCH). The horizontal line represents the median. Outliers are represented by black dots outside the whisker of the plot. Significance levels: *p ≤ .05; ***p ≤ .001; and NS not significant (p > .05). The number of replicates per box are at the top of the plot. Different uppercase letters indicate a significant (p ≤ .05) difference between study regions. MAOM, mineral-associated organic matter.

Land use and study region effect on MAOM accumulation

On average across study regions, similar amounts of OC accumulated in forests and grasslands for both goethite (0.24 ± 0.02 and 0.22 ± 0.01 mg m^{-2}) and illite (0.06 ± 0.00 and 0.06 ± 0.00 mg m^{-2}). However, when differentiating between coniferous and deciduous forests, MAOM-C accumulation was generally higher under coniferous forests compared to other vegetation types (Figure 6-4). This effect was most pronounced in the Schorfheide-Chorin region, especially for goethite. Interestingly, MAOM-C accumulation was sometimes higher under grasslands than deciduous forests. In general, more OC accumulated on minerals buried in Schorfheide-Chorin than the other two study regions. This was even the case when only beech forests—the only tree species that was present in all three study regions—was considered (Supporting Information Fig. S6-5).

Influence of management practices, plant and soil properties on MAOM accumulation

Forests

The SEMs showed that SMId, which reflects the thinning and harvesting intensity, had a net negative effect on MAOM-C accumulation for both goethite (standardized coefficient (β) = -.014) and illite (β = -.010). The effect was mediated by litter C input and OC stocks in the soil organic layers (Figure 6-5). The SMIr, which reflects the stand composition and is strongly linked to conifer share (Supporting Information S1), had a net positive effect on MAOM-C accumulation (β = .25 and .07 for goethite and illite respectively). A strong positive effect of the SMIr was mediated by the C:N ratio of the litter and the OC stocks in the soil organic layer. A smaller negative effect was again mediated by litter C input and OC stocks in the soil organic layer. For goethite, there was an additional positive direct effect of the SMIr on MAOM-C accumulation. Surprisingly, MAOM-C accumulation was not linked to the OC concentration of the overlying mineral soil (OC_{soil}; Figure 6-5). The pH and the concentration of WEOC in the overlying soil were also not relevant for MAOM formation (data not shown). Forty-two and 41% of the variation in MAOM-C accumulation on goethite and illite, respectively, was explained by the fixed factors (management, plant and soil properties) in the forest SEMs.

The consideration of study region as random factor did not increase the explained variance (R^2_C = .44 and .41 for goethite and illite respectively).

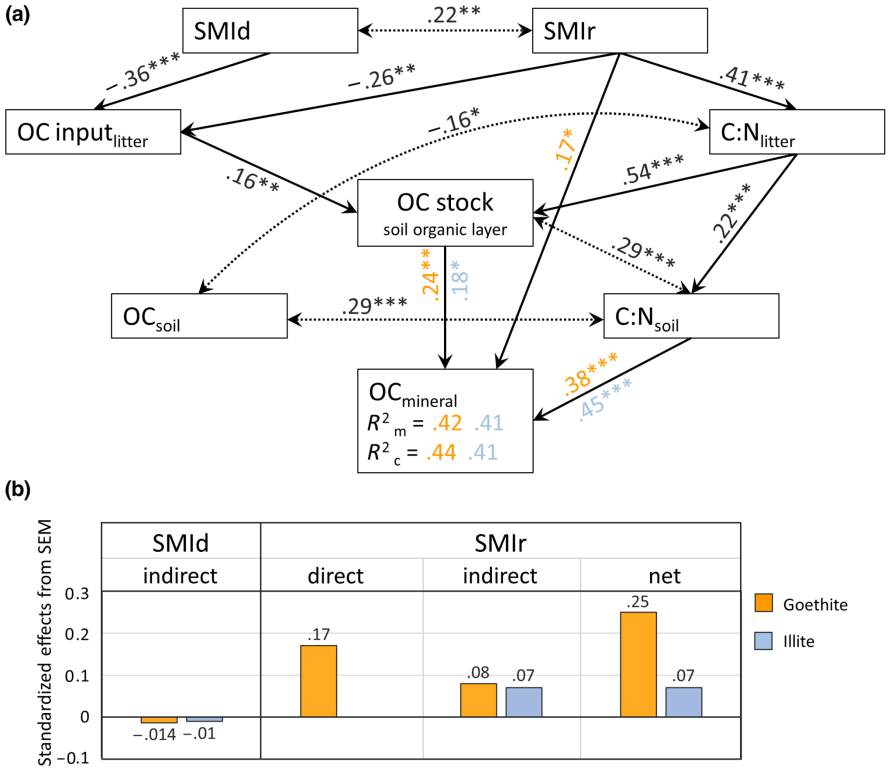

Figure 6-5. Piecewise structural equation model representing the direct and mediated effects of management on MAOM-C accumulation on pristine minerals (goethite and illite) buried for 5 years at 5 cm depth in the topsoil of forests across three regions in Germany (a) and the standardized effects of the management (b). $C:N_{litter}$, C:N ratio of litter fall; $C:N_{soil}$, C:N ratio of the soil; OC input litter, mass of C in litter fall; OC mineral, OC content in goethite or illite in mineral containers; OC_{soil}, OC concentration in the soil; OC stocks soil organic layer, OC stocks in the soil organic layer; SMId, density component of the silvicultural management index, which reflects the thinning and harvesting intensity; SMIr, risk component of the silvicultural management index, which reflects per cent conifer cover. Single-headed arrows indicate causal relationships (paths) while doubled-headed arrows indicate covariances. Values on top of the arrows are standardized coefficients (β) with significance levels: NS, not significant (p > .1); m.05 > p < .1; *p ≤ .05; **p ≤ .01; ***p ≤ .001. Standardized coefficients in black are relevant for both minerals while those in orange and blue are relevant for goethite and illite respectively. Study region was denoted as a random factor in the model. Two coefficients of determination are given for the response variable—marginal (R^2_m) and conditional R^2 (R^2_c), that is, without and with considering the effect of the random factor respectively. Model parameters: goethite (Fisher's C = 22.14; AIC = 70.14; p value = .333; n = 143; df = 20) and illite (Fisher's C = 25.00; AIC = 73.00; p value = .201; n = 143; df = 20). AIC, Akaike information criterion; MAOM, mineral-associated organic matter; C:N, carbon to nitrogen ratio; OC, organic carbon; SEM, structural equation model.

Grasslands

Fertilization positively (β = .14 and .22 for goethite and illite respectively) and negatively (β = -.16 and -.12 for goethite and illite, respectively) affected MAOM-C accumulation by increasing aboveground plant biomass and decreasing plant species richness respectively (Figure 6-6).

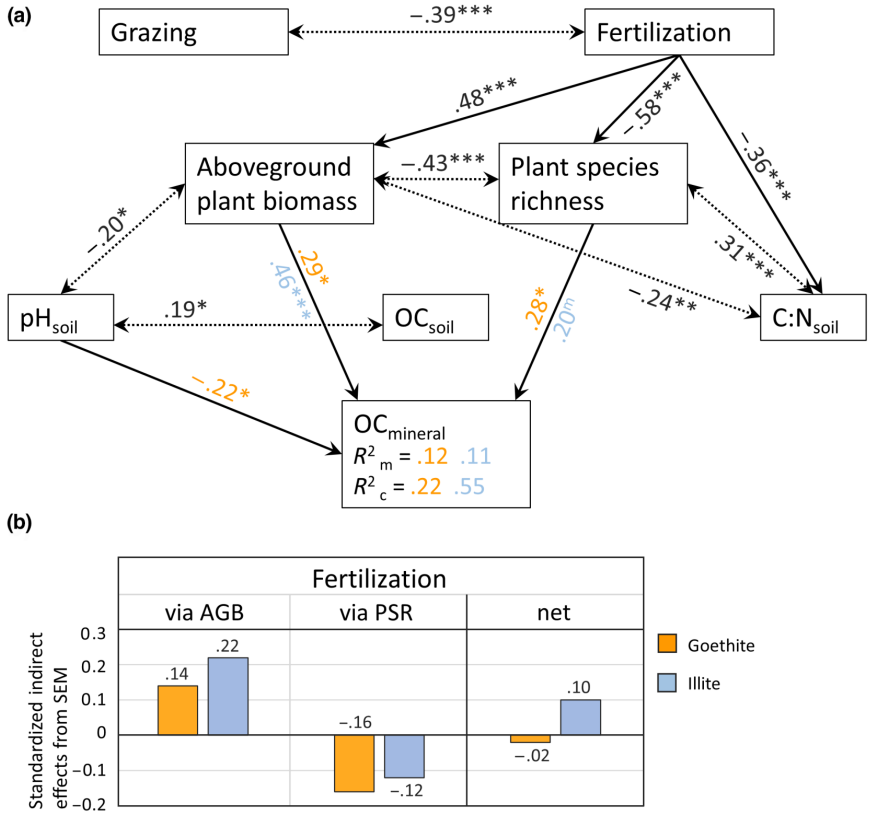

Figure 6-6. Piecewise structural equation model representing the direct and mediated effects of management on MAOM-C accumulation on pristine minerals (goethite and illite) buried for 5 years at 5 cm depth in the topsoil of grasslands across three regions in Germany (a) and the standardized indirect effects of fertilization (b). Organic soils of the SCH region were excluded from the model. AGB, aboveground biomass; C:Nsoil, C:N ratio of the soil; OC mineral, OC content in goethite or illite in mineral containers; OC_{soil}, OC concentration in the soil; pHsoil, pH of the soil; PSR, plant species richness. Single-headed arrows indicate causal relationships (paths) while doubled-headed arrows indicate covariances. Values on top of the arrows are standardized coefficients (β) with significance levels. NS, not significant (p > .1); m.05 > p < .1; *p ≤ .05; **p ≤ .01; ***p ≤ .001. Standardized coefficients in black are relevant for both minerals while those in orange and blue are relevant for goethite and illite respectively. Study region was denoted as a random factor in the model. Two coefficients of determination are given for the response variable—marginal (R^2_m) and conditional R^2 (R^2_c), that is, without and with considering the effect of the random factor respectively. Model parameters: goethite (Fisher's C = 8.906; AIC = 44.91; p value = .35; n = 121; df = 8) and illite (Fisher's C = 11.68; AIC = 47.68; p value = .166; n = 121; df = 8). AIC, Akaike information criterion; C:N, carbon to nitrogen ratio; MAOM, mineral-associated organic matter; OC, organic carbon.

Therefore, the net effect of fertilization was negative for goethite (β = -.02) and positive for illite (β = .10). For goethite, MAOM-C accumulation was further directly and negatively related to soil pH. Grazing was not linked to MAOM-C accumulation. The accumulation of MAOM-C was also not linked to the soil OC concentration if we considered only mineral soils. However, linear regressions revealed a significant relationship between these two variables in the organic soils of the Schorfheide-Chorin reg ion for both minerals (Figure 6-7). The grassland SEMs did not show a link between MAOM-C accumulation and soil C:N ratio, but the latter negatively covaried with aboveground plant biomass and positively with plant species richness (Figure 6-7). The concentration of WEOC in the overlying soil was not relevant for MAOM formation (data not shown). Overall, the grassland SEMs explained 22% and 55% of the variance in MAOM-C accumulation on goethite and illite respectively. Compared to the forest SEMs, less of the total variance was explained by the fixed factors (management, plant and soil properties; R^2_m = .12 and .11 for goethite and illite respectively).

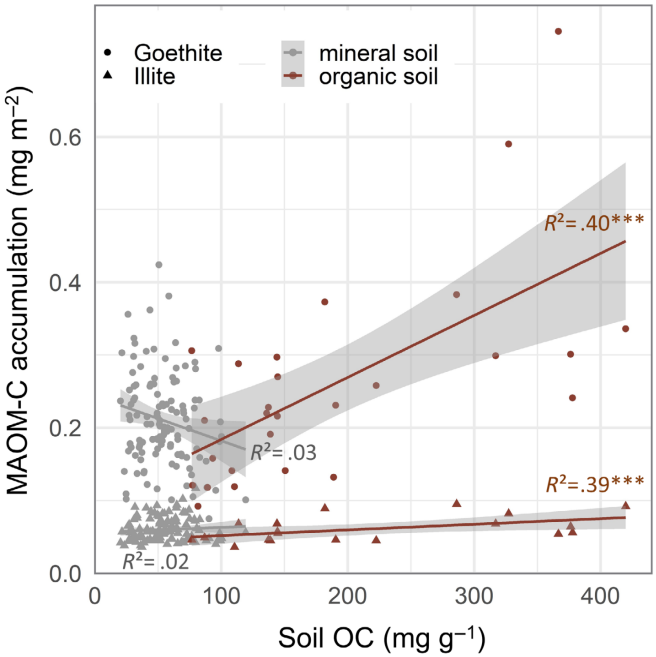

Figure 6-7. Relationship between MAOM-C accumulation on pristine minerals (goethite and illite) over a period of 5 years and soil OC concentration at 5 cm depth in 148 grasslands across Germany. For each mineral, n = 121 for mineral soils and 27 for organic soils. Significance level: ***p ≤ .001. MAOM, mineral-associated organic matter; OC, organic carbon.

Discussion

Mineral type effect

The importance of Fe oxides and their superiority to clays regarding the formation of MAOM has been observed in laboratory studies (Han et al., 2021; Kaiser et al., 2007; Neurath et al., 2021). In a laboratory pre-study on the sorption capacity of the minerals, we also found that goethite was capable of sorbing up to 2.5 mg OC per m² of mineral surface area, while illite only retained 0.07 mg m^{-2} (Figure S6-2). We corroborate the

results of the laboratory experiments in our 5-year field study, finding much higher MAOM-C accumulation on goethite than on illite. The amount of OC that accumulated during the field exposure corresponds to about 86% of the potential sorption capacity of illite determined in the pre-study, suggesting its potential sorption capacity has almost been reached. In turn, goethite only accumulated OC equivalent to about 10% of its potential capacity.

We acknowledge the difference in the ratio of quartz sand to pristine mineral in the two types of mineral containers. While the difference in the content of sand, due to its negligible sorption capacity (Figure S6-2), did not likely directly affect OC in the mineral containers, it might have impacted the water holding capacity, and thus, the time the minerals were in contact with the soil solution. Since sorption of OM to minerals is a relatively fast process (Dahlgren & Marrett, 1991; Kaiser & Zech, 1998), differences in passage time of the soil solution had presumably no significant effect on the overall difference in the OC accumulated in the two types of mineral containers. This assumption is supported by the OC accumulation on illite already approaching the mineral's maximum sorption capacity despite the potentially faster soil solution passage.

Since minerals tend to accumulate C less efficiently when approaching their maximum sorption capacity (Georgiou et al., 2022), the difference in MAOM-C accumulation between goethite and illite should become even greater with longer field exposure time. This underscores that soils dominated by goethite and other oxides-type phases have a greater capacity to accumulate and store C than those dominated by illite and other clay minerals. To our knowledge, this is the first large-scale direct comparison of the OM sorption capacity of these two mineral groups under field conditions.

The higher capacity of oxides to bind OM is often simply attributed to their high SSA (B. Sarkar et al., 2018). However, we found that despite having only half the SSA of illite, goethite accumulated on average two times more OC per gram of mineral than illite. This difference was fourfold when MAOM-C accumulation was normalized to the SSA of the minerals (Figure 6-3). Therefore, the reactivity of the surfaces of the two minerals was likely more decisive for MAOM-C accumulation than their SSA. The goethite used has a variably charged surface with a point of zero charge (PZC) at pH of 7.8 (Table 6-2), below which it is positively charged. Being mainly positively charged in acidic and

neutral soils, oxides—such as goethite—attract negatively charged OM while permanently negatively charged clays—such as illite—rather repel the also mainly negatively charged OM (Kleber et al., 2021; R. Mikutta & Kaiser, 2011). Subsequently, oxides bind OM more strongly than clays via less reversible ligand exchange reactions, while binding to clays is mainly attributed to cation bridging (Kleber et al., 2021; R. Mikutta et al., 2007). Consequently, OM bound to clays is more desorbable and available for microbial consumption and mineralization than OM bound to oxides (Kleber et al., 2021). In a companion study, we observed a higher phospholipid-derived fatty acids (PLFAs) to OC ratio on illite than on goethite (Brandt et al., 2023). This means illite supported a larger microbial biomass per MAOM-C than goethite, which is in line with our idea that the OM bound to illite might have been more bioavailable than that bound to goethite. Consequently, the interplay between the rate of OM desorption and the growth and activity of mineral-associated microorganisms could be an important determinant of OM accumulating on minerals.

Whatever the exact mechanism(s) causing the higher MAOM-C accumulation on goethite than illite may be, we observed a striking consistency in this trend across study regions and land uses (Figure 6-4). Therefore, our study provides strong evidence for the primary role of the soil mineral composition for MAOM formation.

Land use and study region effects

The accumulation of MAOM-C was consistently higher in coniferous forests than in grasslands (Figure 6-4). The wider C:N ratio of coniferous litter leads to its decelerated and incomplete mineralization. This causes accumulation of thick organic layers from which large amounts of DOM can originate (Andivia et al., 2016; Trum et al., 2011). The difference in MAOM-C accumulation between these two ecosystems was more pronounced for goethite than illite. This might be due to the higher sorption capacity of goethite, and the more acidic conditions under coniferous forests amplifying the effect of the higher DOM fluxes by increasing the sorption capacity of goethite (Rasmussen et al., 2018)(Rasmussen et al., 2018). For both minerals, more MAOM-C accumulated under deciduous forests than grasslands in the Schorfheide-Chorin region, but the opposite was true for the Schwäbische Alb and Hainich-Dün (Figure 6-4). These results might reflect differences in the importance of aboveground and belowground OC

inputs for MAOM formation in forests and grasslands, and the modulating effect of soil texture and mineralogical characteristics on the contribution of OC inputs from these sources. Organic inputs in grasslands are probably primarily from belowground sources (Keller, Borer, et al., 2022; Sokol et al., 2019). Inputs from belowground sources are closer to the exposed containers. Therefore, we argue that in the Schwäbische Alb and Hainich-Dün, where the mineral soils are richer in clay and oxides compared to Schorfheide-Chorin (Table 6-1), sorption of aboveground-derived DOM in the soil overlying the mineral containers would reduce OM inputs to the mineral containers more in forests than grasslands. This effect might be more pronounced in deciduous than coniferous forests because of the lower OC stocks in the organic layers in deciduous forests (Table 6-1), and thus, potentially lower OC inputs. It is important to note that the study region effect on MAOM formation could be partially influenced by differences in tree species composition. Nevertheless, even after considering only beech-dominated forests, we found that MAOM-C accumulation remained higher in the coarse-textured soils in Schorfheide-Chorin than the other study regions (Supporting Information Fig. S6-5). Therefore, we suggest that the region effect on MAOM-C accumulation might be more ascribed to the difference in soil texture and soil mineral composition. Thicker organic layers in combination with presumably less sorptive soils seemingly favour increased DOM fluxes into the mineral containers, and thus, the MAOM formation.

Effects of management and soil conditions: Forests

Thinning and harvesting led to reduced litter and hence OC input. This translated into a reduction of the OC stock in the organic layer (Figure 6-5) and likely the DOC flux into the mineral containers, causing less MAOM formation. The OC stocks in the organic layer might have been especially important for MAOM formation in our study as the mineral containers were placed at a shallow depth of 5 cm in the mineral soil. Organic C stored in the soil organic layer is more sensitive to management and global changes than OC stored in the MAOM fraction (Grüneberg et al., 2013; Lugato et al., 2021; Mosier et al., 2019). In previous studies, reduced OC stocks in the soil organic layer did not translate into lower MAOM-C stocks even after several decades of forest management (Grüneberg et al., 2013, 2013; Mosier et al., 2019). Here, we demonstrate that

processes reducing OC stocks in the soil organic layer of forests will also have consequences for the input of OM to the MAOM fraction in the topsoil, and thus likely, MAOM-C stocks in the long term. The formation of MAOM was positively related to the SMIr, which is positively correlated with conifer share (Figure 6-5). Interestingly, in the SEMs, the OC concentration of the overlying mineral soil was not relevant for the amount of OC that accumulated on the minerals. The accumulation of MAOM-C was, however, positively related to the C:N ratio of the soil. This was even the case when only deciduous tree species were considered (data not shown). Thus the quality, not the quantity of the OM in the mineral soil determined the mobility of OC and consequently DOC fluxes (Aitkenhead & McDowell, 2000). We quantified the concentration of WEOC in the overlying soil as a measure of the potential input of OC into the mineral containers. However, this is a static measurement that probably does not reflect the actual fluxes of DOM in the field; hence, it was not a suitable predictor of MAOM-C accumulation in our study (data not shown). Nevertheless, the positive relationship between DOM production and soil C:N ratio is well documented (Cools et al., 2014; Gan et al., 2020; Kindler et al., 2011; Thieme et al., 2019).

Effects of management and soil conditions: Grasslands

Fertilization positively and negatively affected MAOM formation by increasing aboveground plant biomass and decreasing plant species richness respectively (Figure 6-6). When considering both, the effects mediated by aboveground biomass as well as by plant species richness, fertilization had an overall positive effect on MAOM formation for illite (β = .10) and negative effect for goethite (β = -.02). Our study demonstrates that the positive effect of fertilization on MAOM formation can be offset by the fertilization-induced loss of plant diversity.

The aboveground biomass-mediated effect of fertilization might reflect the positive link between nutrient addition, plant productivity and soil C storage (Fornara & Tilman, 2012; X. Huang et al., 2020). Additionally, fertilization improves the quality of organic inputs (Apostolakis et al., 2022; Poeplau et al., 2018). This could have promoted more efficient utilization of OM by the mineral-associated microorganisms and consequently stimulated microbial biomass production (Cotrufo et al., 2013; Poeplau et al., 2019) and ultimately increased MAOM formation (Angst et al., 2021). This statement

is supported by the finding of a positive relationship between PLFAs:MAOM-C ratio and land use intensity (fertilization) in our companion study (Brandt et al., 2023). Brandt et al. (2023) also observed more PLFAs per unit MAOM-C on illite than goethite, which might indicate that microbial-derived OM accounts for a larger share of the OM accumulating on illite. The finding of a stronger positive effect of fertilization (aboveground biomass) on MAOM formation for illite than goethite (Figure 6-6) suggest that MAOM formation via the microbial efficiency-matrix stabilization pathway (see Cotrufo et al., 2013) might be more relevant in soils where the mineral assemblage favours less direct sorptive accumulation and stabilization of OM (Cotrufo et al., 2015). This warrants further exploration given the growing emphasis on the role of microbial necromass in MAOM formation (Angst et al., 2021; Cotrufo & Lavallee, 2022; Rui et al., 2022).

The differential effect of fertilization on MAOM formation for illite and goethite might also be in part explained by fractional sorption of DOM constituents (Han et al., 2021; Lehmann & Kleber, 2015; Schneider et al., 2010). Oxides, such as goethite, are presumed to preferentially sorb aromatic constituents while clay minerals, such as illite, retain less aromatic and smaller compounds of lower molecular weight (Han et al., 2021; Kleber et al., 2015). We suppose fertilization could have reduced the abundance of aromatic compounds (J. Zhang et al., 2019), which are preferentially sorbed by goethite. This could in part explain the slightly negative net effect of fertilization on MAOM formation for goethite, but further research is needed to validate this claim. We were surprised to find a positive link between plant species richness and MAOM-C accumulation despite there was a negative association between plant species richness and plant productivity (aboveground biomass) (Figure 6-6). In previous studies, the link between plant diversity and soil OC storage was mainly ascribed to the positive effect of plant diversity on plant productivity and OC inputs into the soil (Anacker et al., 2021; Chen et al., 2018; Cong et al., 2014; Lange et al., 2015; Prommer et al., 2020). We surmise that while fertilization improves soil nutrition and stimulates aboveground biomass production, it might cause lower belowground investment of C (Keller et al., 2022; Poyda et al., 2021). This is because with increased fertilization intensity plants are able to more easily access nutrients without substantial investment in a dense rooting system (J. Li et al., 2011; Poyda et al., 2021). Lower investment of resources belowground could also result from a shift in plant communities towards more resource

acquisitive, fast-growing species that tend to be more abundant in highly fertilized, species-poor grasslands (Apostolakis et al., 2022; Blüthgen et al., 2012). We could not confirm these mechanisms since there was no correlation between the biomass of roots in the overlying soil and MAOM formation (data not shown).

We, however, acknowledge that the used estimate of belowground biomass did not capture inputs from rhizodeposition and mycorrhizal fungi, which can serve as important belowground sources of C. While further research is needed to elucidate the precise mechanisms that underlie these results, our study highlights the caveat of applying fertilizers as a strategy to increase soil OC stocks in temperate grasslands. Grazing was not an important factor of MAOM formation (Figure 6-6). Unlike fertilization, C and nutrient inputs through urine and dung patches are spatially heterogenous (see Maire et al., 2018), and hence, likely not as relevant for MAOM-C accumulation as fertilization across a regional scale.

While it was not statistically relevant in forests, soil pH had a direct negative effect on MAOM-C accumulation for goethite in grasslands (Figure 6-6). This is likely because the pH of the grassland soils, unlike the forest soils, is in the critical range close to the mineral's PZC where its sorption capacity is significantly reduced (Figure S6-3). Similar to forests, we did not find a link between the OC concentration in the overlying soil and MAOM formation for the mineral grassland soils (Figure 6-6). However, for organic grassland soils in the Schorfheide-Chorin region, MAOM formation increased with soil OC content (Figure 6-7). Possibly, compared to mineral soils, the organic soils facilitated direct fluxes of DOC from immediate surroundings into the mineral containers. The question arises: where did the MAOM-C come from in the mineral grassland soils? We are only able to speculate that because MAOM formation was related to plant properties, direct inputs from roots and mycorrhizal fungi might have been important. Overall, our findings suggest differences in the pathways of MAOM formation in grasslands on mineral soils and those on organic soils. They underscore the need to better constrain the sources of MAOM-C to unravel the enigma of MAOM formation in grasslands.

Implications and outlook

Exposing two pristine soil minerals (goethite and illite) for 5 years in topsoils of managed temperate forest and grassland ecosystems, we found that the type of mineral was the principal factor controlling MAOM formation. Our study underpins the relevance of soil mineralogical properties for the accumulation of soil OM. Irrespective of the environmental conditions, goethite accumulated much more OM than illite (Figure 6-8), even for field conditions previously considered less optimal for oxide–OM interactions (pH >6.5).

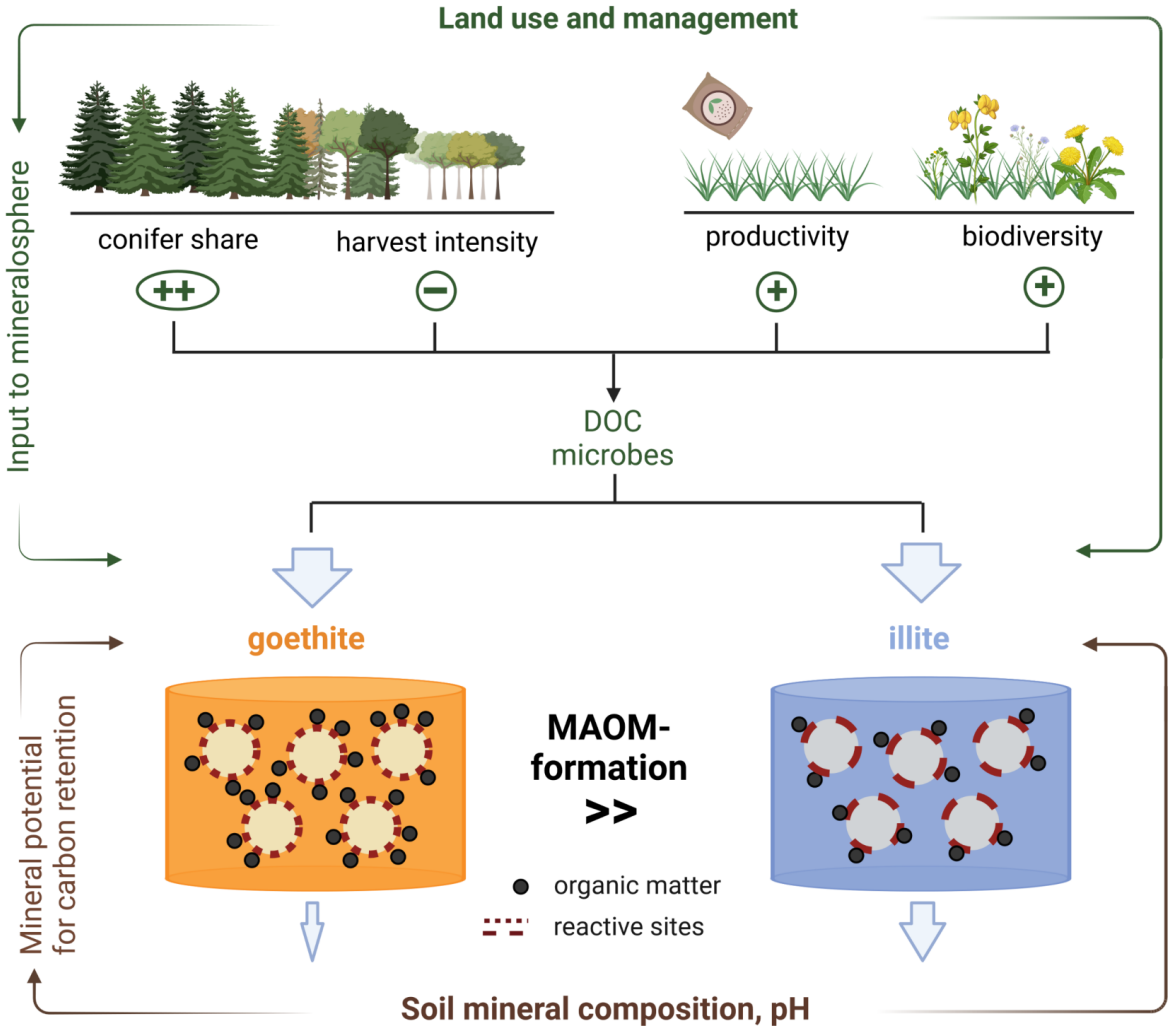

Figure 6-8. Graphical summary of the interplay of land use, management and mineral type in mineral-associated organic matter (MAOM) formation. The upper part of the figure illustrates factors that control the input of OM to the minerals. The double positive sign highlights the much stronger effect of tree species selection (conifer share) than other management practices. The lower part depicts the influence of mineral type for the same level of OM input.

This is consistent with the long-standing observations for the OM retention by Fe oxides in aquatic systems under circumneutral conditions (Tipping, 1981).

Our study provides direct evidence to support the earlier call by Rasmussen et al. (2018) to consider type and reactivity of minerals rather than only the clay content for predicting soil OM content. It adds to the demonstrated superiority of other predictors, such as the concentration of pedogenic oxides (Herold et al., 2014; Kirsten et al., 2021; Rasmussen et al., 2018; Reichenbach et al., 2023).

Within the short time of 5 years, illite already came close to its OM sorption capacity in some cases, despite the amount of accumulated OM being low relative to its SSA. This suggests that not all surfaces of minerals contribute to organo-mineral interactions and underscores the need to go beyond surface area to predict the OM storage capacity of soil minerals (see figure 1 in Kaiser & Guggenberger, 2000). It also suggests that soils dominated by illite (and probably other clay minerals as well) may be relatively limited in their capacity to accumulate and store MAOM-C. In contrast, goethite was nowhere near its sorption capacity and may take decades before reaching saturation. This suggests that soils rich in goethite (and similar oxides and related mineral phases) have a large capacity to store and accumulate MAOM-C. Our findings corroborate the work of Kirsten et al. (2021) who observed a positive relationship between MAOM-C and the ratio of Fe_d: clay. Taken together, these findings suggest that increasing C inputs into soils where oxides are present in appreciable amounts—especially those that are far below their mineralogical capacity to store C (see Georgiou et al., 2022)—may offer great potential to enhance near-term soil C sequestration. Unlike previous studies conducted in natural soils (Grüneberg et al., 2013; Herold et al., 2014; Keller, Borer, et al., 2022; Mosier et al., 2019; Schöning et al., 2013), we were able to detect significant effects of land use and management intensity on MAOM-C after exposing pristine minerals for only 5 years to ambient soil conditions. This demonstrates that land use and management intensification can be relevant for MAOM formation on relatively short time scales. Our findings are thus important in the context of predicting how MAOM-C responds to anthropogenic interferences. In natural soils, these changes occur in the presence of a long-term background of MAOM accumulation, and thus, might be difficult to discern directly on short time scales.

We observed consistently higher MAOM-C accumulation under coniferous forests compared to deciduous forests and grasslands. Since the minerals were exposed in topsoils, subsoil patterns might differ. Thus, future investigations on the effect of land use on MAOM formation in the subsoil are warranted. The container design reduced the influence of roots and macrofauna, which might play a role for MAOM formation especially in grasslands (Angst et al., 2022; Sokol et al., 2019). Our results suggest that in addition to the forest type, the magnitude of difference in MAOM-C between temperate forests and grasslands might depend on the quantity of aboveground-derived C entering the mineral soil.

Management intensity had stronger effects on the MAOM formation in forests than grasslands (Figure 6-8). The much lower variance in MAOM-C accumulation explained in the SEMs for grasslands compared to forests suggests research is particularly needed to deepen our understanding of the key controls of MAOM formation in grasslands. There has been growing emphasis on the role of fine roots, hyphae and microbial necromass for the formation of MAOM (Angst et al., 2021; Cotrufo et al., 2013; Cotrufo & Lavallee, 2022; Rui et al., 2022; See et al., 2022; Zhu et al., 2022). Accurately quantifying the contribution of all these potential OM sources, including belowground inputs, to MAOM formation is not without challenge, but might be an important step towards improving our predictive understanding of the response of MAOM-C to management in grasslands.

Author contributions

De Shorn E. Bramble: Conceptualization; data curation; formal analysis; investigation; visualization; writing – original draft. **Susanne Ulrich:** Conceptualization; data curation; formal analysis; investigation; visualization; writing – original draft. **Ingo Schöning:** Conceptualization; methodology; supervision; writing – review and editing. **Robert Mikutta:** Conceptualization; funding acquisition; writing – review and editing. **Luise Brandt:** Visualization; writing – review and editing. **Christian Poll:** Conceptualization; writing – review and editing. **Ellen Kandeler:** Conceptualization; funding acquisition; writing – review and editing. **Christian Mikutta:** Conceptualization; funding acquisition; writing – review and editing. **Alexander Konrad:** Formal analysis; funding acquisition; writing – review and editing. **Jan Siemens:** Funding acquisition; writing – review and editing. **Yang Yang:** Formal analysis; funding acquisition; writing – review and editing. **Andrea Polle:** Funding acquisition; writing – review and editing. **Peter Schall:** Writing – review and editing. **Christian Ammer:** Writing – review and editing. **Klaus Kaiser:** Conceptualization; funding acquisition; supervision; writing – review and editing. **Marion Schrumpf:** Conceptualization; funding acquisition; methodology; supervision; visualization; writing – review and editing.

Acknowledgements

We thank the managers of the three Exploratories, Kirsten Reichel-Jung, Iris Steitz, Sandra Weithmann, Florian Staub, Julia Bass, Juliane Vogt, Anna K. Franke, Miriam Teuscher, Franca Marian, and all former managers for their work in maintaining the plot and project infrastructure; Christiane Fischer, Jule Mangels and Victoria Grießmaier for support through the central office, Michale Owonibi and Andreas Ostrowski for managing the central data base, and Markus Fischer, Eduard Linsenmair, Dominik Hessenmöller, Daniel Prati, François Buscot, Ernst-Detlef Schulze, Wolfgang W. Weisser and the late Elisabeth Kalko for their role in setting up the Biodiversity Exploratories project. We thank the administration of the Hainich national park, the UNESCO Biosphere Reserve Schwäbische Alb and the UNESCO Biosphere Reserve Schorfheide-Chorin as well as all land owners for the excellent collaboration. We further thank Ines Hilke, Birgit Froehlich and Jessica Heublein of the Routine

Measurements & Analysis of Environmental Samples (ROMA) laboratory at the Max Planck Institute for Biogeochemistry, Alexandra Boritzki, Christine Krenkewitz, Gudrun Nemson-von Koch, Anja Kroner, Miriam Kempe, Steffen Ferber, Marco Pöhlmann, Theresa Klötzing, Iris Kuhlmann, Sarah Pozorski, Uzma Heme, Manuel Rost, Enrico Weber, Adrian Lattacher, Philipp Mäder, Juliette Blum and Marina Patulla for support during sampling and laboratory analyses, Core Project 9 of the Biodiversity Exploratories for setting the experiment up in 2015. We thank Susan Trumbore and Kai-Uwe Totsche for their helpful comments on earlier versions of the manuscript, and Sophie von Fromm for her help with testing random forest models for data exploration. We are also grateful for the helpful feedback from the two anonymous reviewers. Field work permits were issued by the responsible state environmental offices of Baden-Württemberg, Thüringen and Brandenburg. Open Access funding enabled and organized by Projekt DEAL.

Funding information

This work was funded by the DFG Priority Program 1374 'Biodiversity-Exploratories' (DFG project numbers 433273584 and 193957772) and the Max Planck Society. Funding for De Shorn E. Bramble, Alexander Konrad and Yang Yang was provided by the International Max Planck Research School for Biogeochemical Cycles (IMPRS-gBGC), the Justus Liebig University Giessen and the Chinese Scholarship Council (CSC) respectively.

Conflict of interest statement

The authors declare that they have no conflict of interest.

Data availability statement

This work is based on data elaborated by the BEmins project of the Biodiversity Exploratories program (DFG Priority Program 1374). The datasets are publicly available in the Biodiversity Exploratories Information System (http://doi.org/10.17616/R32P9Q); BExIS dataset IDs: 14686 (soil texture), 19346 (dithionite- and oxalate extractable Al and Fe), 20126 (aboveground litter weights), 20127 (aboveground litter CNS), 20826 (elevation and main tree species), 22246 (soil

pH), 24346 (OC stock of soil organic layer), 25046 (SMI), 21187 (aboveground biomass and species richness in 2016), 23486 (aboveground biomass and species richness in 2017), 24166 (aboveground biomass and species richness in 2018), 26747 (aboveground biomass and species richness in 2019), 27426 (aboveground biomass and species richness in 2020), 31251 (C and N contents), 31476 (WEOC), 31475 (root biomass in forests in 2021) and 31477 (root biomass in grasslands in 2021).

Chapter VII

Mineral type and land-use intensity control composition and functions of microorganisms colonizing pristine minerals in grassland soils

Luise Brandt[1], Fabian Stache[1], Christian Poll[1], De Shorn Bramble[2], Ingo Schoning[2],

Marion Schrumpf[2], Susanne Ulrich[3], Klaus Kaiser[3], Robert Mikutta[3], Christian Mikutta[4],

Yvonne Oelmann[5], **Alexander Konrad[6]**, Jan Siemens[6], Ellen Kandeler[1]

[1]Department of Soil Biology, Institute of Soil Science and Land Evaluation, University of Hohenheim, Emil-Wolff-Straße 27, 70599, Stuttgart, Germany [2]Max-Planck-Institute for Biogeochemistry, Jena

[2]Max-Planck-Institute for Biogeochemistry, Hans-Knöll-Straße 10, 07745, Jena, Germany [4]Department of Soil Biology, Institute of Soil Science and Land Evaluation, University of Hohenheim, Stuttgart

[3]Soil Science and Soil Protection, Martin Luther University Halle-Wittenberg, Von-Senckendorff-Platz 3, 06120, Halle (Saale), Germany

[4]Soil Mineralogy, Institute of Mineralogy, Gottfried Wilhelm Leibnitz University Hannover, Callinstraße 3, 30167, Hannover, Germany

[5]Geoecology, University of Tübingen, Rümleinstraße 19-23, 72070, Tübingen, Germany [8]Department of Silvicultur and Forest Ecology of the Temperate Zones, Georg August University Göttingen, Göttingen, Germany

[6]Institute of Soil Science and Soil Conservation, iFZ Research Center for BioSystems, Land Use and Nutrition, Justus Liebig University Giessen, Heinrich-Buff-Ring 26-32, 35392, Giessen, Germany

This is a copy-edited, peer reviewed version of the following article: Mineral type and land-use intensity control composition and functions of microorganisms colonizing pristine minerals in grassland soils Brandt, L., Stache, F., Poll, C., Bramble, D. S., Schöning, I., Schrumpf, M., et al. (2023). *Soil Biology and Biochemistry*, *182*, 109037. https://doi.org/10.1016/j.soilbio.2023.109037

Abstract

Mineral surfaces in soil are an important interface for organic matter (OM) and nutrient cycling, with associated microorganisms contributing to the formation and turnover of mineral-associated OM (MAOM). However, the relevance of intrinsic (mineral type) versus extrinsic (land-use intensity) factors on the co-development of MAOM and microorganisms under natural conditions remains poorly understood. Mineral containers filled with mixtures of quartz-sand and pristine secondary minerals (goethite or illite) were exposed to 50 grassland topsoils of the Schwäbische Alb (Germany) along a land-use intensity gradient for five years. Mineral samples and soils were analyzed for organic carbon (OC) and nutrients (N and P), abundance and composition of major microbial groups based on phospholipid fatty acid profiles, as well as enzyme activities (β-glucosidase, β-xylosidase, N-acetyl glucosaminidase, and acid phosphatase). Microorganisms colonized both mineral samples to the same extent, with goethite samples exhibiting greater MAOM accumulation and higher enzyme activities than illite samples. Both mineral samples differed from the overlying soils with greater relative abundances of fungi and Gram-negative bacteria and greater microbial acquisition of nutrients (N and P) relative to C as indicated by the stoichiometry of enzyme activities. Increasing land-use intensity was associated with decreasing C:N ratios and microbial abundances for goethite samples and increasing β-glucosidase activity for illite samples while the proportion of fungi was reduced in both mineral samples. We conclude that in the studied temperate grasslands the association of OM and microorganisms with secondary minerals is driven more by mineral type and reactivity than by differences in land-use intensity. The different minerals apparently formed distinct microhabitats with unique characteristics that differed in MAOM accumulation and microbial access to OC and nutrients, thus affecting microbial colonization and functionality.

Introduction

The association of organic matter (OM) with minerals is regarded as one of the most important factors contributing to the preservation of organic carbon (OC) in soils (Kaiser & Guggenberger, 2000; Kögel-Knabner et al., 2008). Mineral-associated OM (MAOM) is formed from compounds either derived from decaying plant litter and directly sorbed to mineral surfaces ('*ex-vivo* modification pathway') or from microbial products, including necromass and exudates produced during OM decomposition ('*in vivo* microbial turnover pathway') (Lavallee et al., 2020; Liang et al., 2017). The surfaces of secondary pedogenic minerals represent important interfaces in soil as they not only harbor MAOM but also provide a habitat for microorganisms involved in C and nutrient cycling. Mineral-associated microorganisms contribute to MAOM formation and probably further alter MAOM through microbial degradation and transformation processes, e.g., by the production of enzymes. While the abundance of reactive minerals has been recognized as key to the accumulation of MAOM (Kleber et al., 2015), how mineral composition affects patterns of microbial colonization and subsequent functioning of microbial communities on mineral surfaces is not well understood. The mineral type likely not only controls MAOM formation but also the composition and diversity of associated microorganisms (e. g., Colin et al., 2017; Ditterich et al., 2016; Pronk et al., 2017; Sun et al., 2020; Whitman et al., 2018), due to differences in surface reactivities, chemical composition, or dissolution rates (Uroz et al., 2015). Each mineral may therefore represent a microhabitat (also termed "mineralosphere" according to Uroz et al., 2015) that is colonized by uniquely adapted microorganisms (A. A. Jones & Bennett, 2017). Especially fungi were shown to successfully obtain nutrients from mineral surfaces (Andrino et al., 2021; Balogh-Brunstad et al., 2017; Landeweert et al., 2001), e.g., by excretion of agents promoting chemical weathering (Hoffland et al., 2004). Little information is available on how different types of secondary soil minerals modify the interactions of drivers controlling MAOM formation or microbial abundances, composition, and the production of enzymes, especially under field conditions. Microbial colonization of mineral surfaces was reported to be a nonrandom process not only controlled by intrinsic mineral properties, but also extrinsic environmental conditions (Jones and Bennett, 2017), such as OM inputs. Previous studies investigated

microbial colonization of minerals (goethite-illite mixtures) in grassland soils for up to 31 months in the presence of organic substrates of different complexities, including glucose, citric acid, and fine roots (Boeddinghaus et al., 2021; Kandeler et al., 2019; Vieira et al., 2020). These studies found that functionally distinct and active microbial communities dominated by fungi and specific bacterial communities developed in the OM-mineral mixtures over time, actively using the added labile and complex C sources. Those results highlighted the importance of OM for the growth and activity of mineral-associated microorganisms. Land-use intensity in grasslands is known to control OM and nutrient inputs to soil. This includes the production of dissolved OM as a potential contributor to MAOM formation (Lange et al., 2021) via effects of land-use intensity on soil nutrient status, above- and belowground plant biomass, plant species composition, and productivity (Gilhaus et al., 2017; Schöps et al., 2018). Microorganisms are affected by changes in OM and nutrient availability related to land-use intensity, adapting their biomass production, community structure, and enzyme production patterns in grassland soils (Berner et al., 2011; Herold et al., 2014; Lagerlöf et al., 2014). However, it is unclear whether and how these processes translate to mineral surfaces in the field, as knowledge of underlying mechanisms and long-term effects of land-use intensity is limited.

Our main objective was to clarify how microbial colonization and functioning on different pristine mineral surfaces are linked to newly formed mineral-associated OC and nutrients in response to land-use intensity (see conceptual Fig. 7-1). The current study aimed to determine, after their establishment on pristine minerals, the abundance and composition of major microbial groups and enzyme activities related to cycling of C, nitrogen (N), and phosphorus (P) after five years of exposure to grassland soils under strongly varying land-use intensities. Microbes control the expression of enzymes based on their nutrient demands (Sinsabaugh & Shah, 2012), so enzyme stoichiometry can reveal differences in relative resource allocation to C, N, and P acquisition (Moorhead et al., 2016). In order to mechanistically explain patterns of microbial colonization and potential enzyme activities, we determined bioavailable C, N, and P fractions in both soil and mineral samples using established extraction procedures. To disentangle the effect of individual mineral types, we incubated containers filled with mixtures of quartz-sand and either goethite, an iron oxyhydroxide, or illite, a clay mineral, in 50

grassland soils of the Schwäbische Alb, across a land-use intensity gradient from non-fertilized pastures to fertilized meadows.

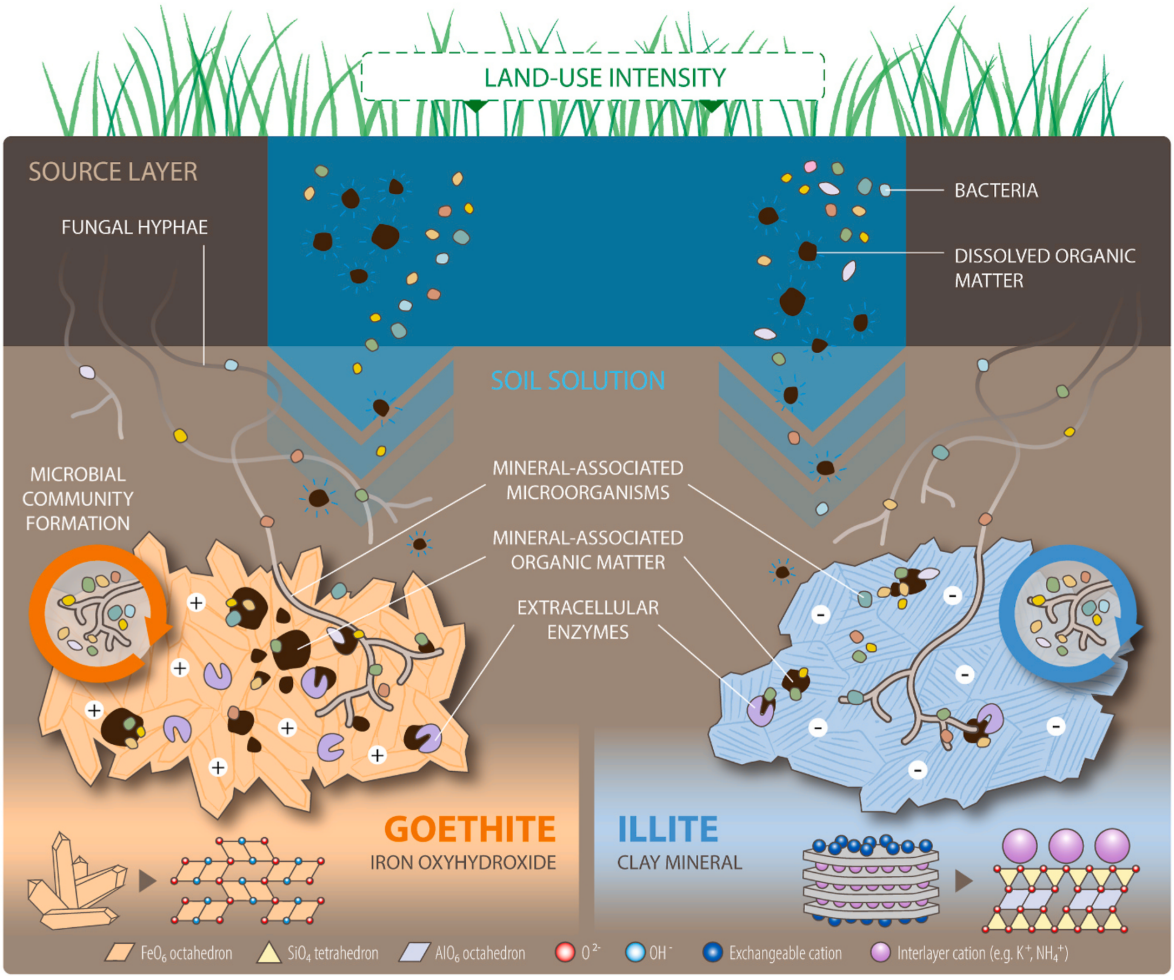

Figure 7-1. In our experiment, mineral-associated organic matter (MAOM) originates either from the source layer (overlying soil), which enters the mineral containers as dissolved organic matter (DOM) via the soil solution and is converted to MAOM by adsorption processes, or from microbes colonizing the mineral surfaces. Microorganisms can colonize the mineral surfaces via passive transport through the percolating soil solution or by actively growing or migrating into the containers (restricted to fungi and motile bacteria). After five years, we propose that in addition to these pioneering colonization strategies, mineral-associated microbes rely on the formed MAOM for maintenance and synthesis of new biomass and thus secrete extracellular enzymes to extract carbon or nutrients from MAOM. Depending on intrinsic mineral properties, such as surface charge, which is dictated primarily by mineral structure, interactions between minerals, OM, and microbes likely differ among mineral types. Goethite and illite have contrasting surface charges, with goethite being positively charged under the given pH conditions, while illite has a permanent negative charge due to isomorphic replacement. This likely results in contrasting microhabitat properties as a basis for microbial community formation. Land-use intensity influences the input of DOM and nutrients and thus further extrinsically affects the described processes at a higher level.

The selected minerals are the most prominent representatives of iron oxides and clay minerals in temperate soils and strongly differ in their physico-chemical properties,

such as sorption capacity for OM, specific surface area, and (pH-dependent) surface charge. We hypothesized that (i) the greater OM sorption capacity of goethite than illite results in higher microbial abundance and enzyme activities; (ii) due to their active hyphal growth, fungi colonize mineral surfaces more intensively than bacteria relative to the soil; (iii) the different mineral types modify the microbial investment into C versus nutrient (N and P) acquisition; and (vi) higher inputs of easily degradable OM and nutrients with increasing land-use intensity translate into higher microbial biomass and enzyme activities, but lower fungal to bacterial (F:B) ratios.

Materials and methods

Study sites

The 50 grassland sites studied are part of the Biodiversity Exploratories project, serving as a platform for large-scale and long-term functional biodiversity research (Fischer et al., 2010). The experimental plots (EPs) located in the UNESCO Biosphere Reserve Schwäbische Alb and the surrounding area are situated in southwest Germany at altitudes of 460–860 m above sea level, with a mean annual temperature of 6–7 °C and annual precipitation of 700–1000 mm (Fischer et al., 2010). The Schwäbische Alb mountain range is formed from calcareous bedrock with karst phenomena (Fischer et al., 2010). On the Jurassic limestones, clay-rich Cambisols and Leptosols (IUSS Working Group WRB, 2015) have developed. The EPs cover a gradient in grassland management intensity, including unfertilized pastures, fertilized pastures, fertilized and mown pastures, as well as unfertilized and fertilized meadows. To quantify land-use intensity, the land-use intensity index (LUI) was calculated for the years 2015–2020 according to Blüthgen et al. (2012). The LUI is defined by Equation (1) as:

$$LUI_i = \frac{F_i}{F_R} + \frac{M_i}{M_R} + \frac{G_i}{G_R}$$

where F_i is the intensity of N fertilization (kg N ha^{-1} year^{-1}), M_i is the mowing frequency year^{-1}, G_i is the density of livestock (livestock units days of grazing ha^{-1} year^{-1}) on each site i for the years 2015–2020, and F_R, M_R, G_R are their respective means within the region R for those years. The calculation is based on information provided by the landowners on mowing, grazing, and fertilization (Vogt et al., 2019) using the LUI

calculation tool (Ostrowski et al., 2020) implemented in the Biodiversity Exploratories Information System (BExIS) (http://doi.org/10.17616 /R32P9Q). The resulting index is a continuous variable, enabling regression analysis.

More detailed information on yearly average grazing density, mowing frequency, fertilization intensity, and the calculated LUI for each site is given in Table S7-1.

Experimental and sampling design

In late 2015, sets of five mineral containers per mineral were buried in 1 × 1 m^2 subplots at all 50 grassland EPs of the Schwäbische Alb exploratory. The mineral containers were filled with mixtures of either 12 g of the iron oxyhydroxide goethite (α-FeOOH; Lanxess, Bayferrox® 920 Z, CAS-No. 51274-00-1) and 12 g washed and annealed sea sand (VWR, CAS-No. 14808-60-7) (in total 24 g) or 12 g of the phyllosilicate illite (Inter-ILI. Engineering Co. Ltd., Kosd, Hungary) and 33 g washed and annealed sea sand (in total 45 g). The different mixing ratios of goethite and illite with sand were used to fill the mineral containers with the same volumes of mineral sample and to enable unhindered passage of the soil solution. Information on physicochemical properties (pH, specific surface area, element concentrations, cation exchange capacity, etc.) of the goethite, illite, and sea sand used are listed in Table S7-2. The mineral containers were placed on beds of quartz-sand (fire-dried at 350°C; AQUAGRAN, EUROQUARZ GmbH, Laußnitz, Germany) at 5 cm soil depth (Fig. 7-2d) in two parallel rows with five replicates per mineral type (Fig. 7-2a). The sand beds (<1 cm thickness) were used to ensure horizontal installation of the mineral containers and optimal contact with the soil without creating large hollow cavities in their vicinity. Each mineral container consisted of a plastic ring filled with the mineral sample, which was sealed on its upper and lower sides by a 50-µm mesh to prevent root ingrowth but allow microbial colonization (Fig. 7-2b and c). This enabled us to experimentally separate the newly developing mineralosphere microhabitat from the rhizosphere and bulk soil environment. The mesh was fixed to the plastic ring with two steel rings, which in turn were firmly connected with galvanized wire. The selected design of the mineral containers limits the horizontal transfer of OM, nutrients, and microorganisms into the mineral samples, while allowing for their vertical transfer from the soil layer above via the soil solution. The 50-µm mesh size limits the contribution of root-derived and particulate OM, so

that OM inputs are mainly through OM dissolved in the percolating soil solution and from microbial sources.

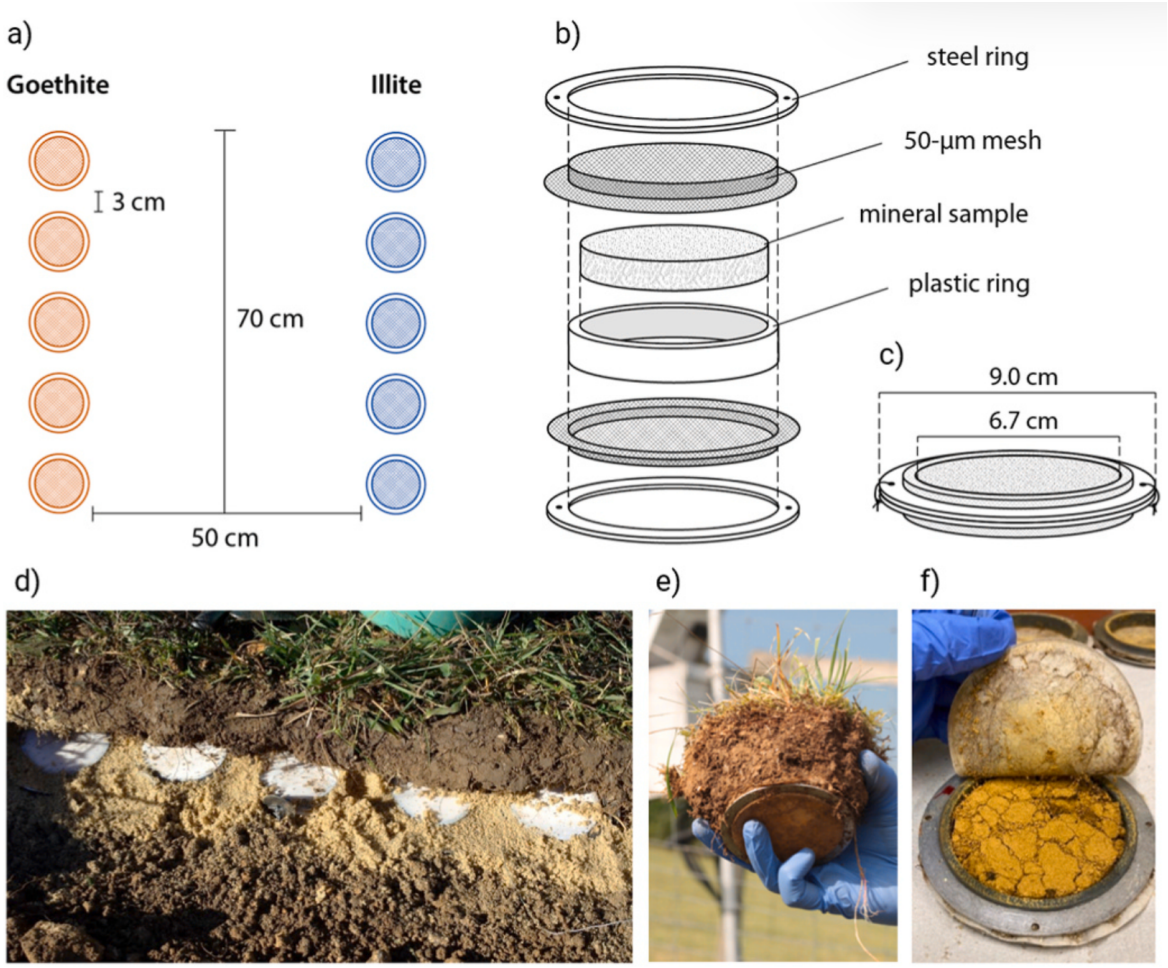

Figure 7-2. a) Schematic top view of the mineral container placement; b) individual parts of a mineral container consisting of a plastic ring holding the mineral sample, two 50-µm meshes, and two steel rings; c) the dimensions of a fully assembled mineral container; d) picture of a row of mineral containers placed at a soil depth of 5 cm on a sand bed during burial of the samples in a grassland site in 2015; e) picture of the removal of a mineral container together with overlying soil during sampling in 2020; f) picture of a freshly opened goethite mineral container during sample preparation in the laboratory.

After five years of exposure, three of the five mineral containers per mineral type were sampled in August 2020 (Fig. 7-2e) to receive an adequate amount of sample to perform all analyses, reserving two mineral containers for later sampling. The samples were placed in cooling boxes and stored at 4°C prior to processing in the laboratory.

The mineral containers were opened (Fig. 7-2d) and controlled for ingrown roots, which were removed with tweezers. The three containers per site were combined into

a homogeneously mixed sample. In addition, soil from up to 5 cm above the three containers was taken separately for goethite and illite to identify the potential sources of OM, nutrient inputs, and microbial colonization. Soil samples were sieved to <4 mm. Aliquots of soil and mineral samples were either air-dried or stored frozen at –20°C until analyses. Consequently, we obtained data of goethite and illite samples as well as the corresponding soil above goethite and illite mineral containers for each site separately.

Laboratory analyses

The dry weight of the soil and mineral samples was determined by drying 2 g soil and 1.5 g mineral sample at 105 °C for 24 h. All data presented are reported on an oven-dry basis.

Organic and inorganic carbon and nitrogen in mineral and soil samples

Total C (TC) and N (TN) contents of the mineral and soil samples were determined by dry combustion at 1100 °C using a varioMax elemental analyzer (Elementar Analysensysteme GmbH, Langenselbold, Germany). Before dry combustion, soil samples were dried at 40 °C and ball-milled, while mineral samples were ground by hand with a mortar and pestle and freeze-dried. The inorganic C (IC) content of the soils was determined with the same analyzer after removing OC by exposing the sample to a temperature of 450 °C for 16 h. Since we anticipated low IC content in the mineral samples, IC was analyzed by suspending 200 mg of the mineral samples in 50 mL of 2 M HCl at 50 °C and subsequent detection of CO_2 released using a soliTIC module interfaced to a varioMax Cube elemental analyzer (Elementar Analysensysteme GmbH). Exchangeable inorganic N was extracted from mineral samples by adding 10 mL of 1 M KCl to 1 g of mineral sample, shaking for 60 min, centrifuging (20 min at 2000×*g*) and passing through ash-free filter papers (Rotilabo 114A, Carl Roth GmbH, Karlsruhe, Germany). The NO_3–N and NH_4–N content of the filtrate was determined photometrically using a SANSplus flow injection analyzer (Skalar Analytical B.V., Breda, The Netherlands). The OC content was calculated as the difference between TC and IC.

Bioavailable phosphorus in mineral and soil samples

Sodium bicarbonate-extractable P in the minerals was determined according to Olsen et al. (1954) and modified after Schoenau and O'Halloran (2007) using 1 g of mineral samples and 20 mL of 0.5 M $NaHCO_3$ solution (1:20, w/v). Extracts were centrifuged (1300×*g*, 10 min), filtered (no. 40, Cytiva-Whatman plc, Maidstone, UK), and analyzed photometrically for PO_4–P at 712 nm on a Cary 60 UV–Vis spectrophotometer (Agilent Technologies) using the ammonium molybdate–antimony potassium tartrate–ascorbic acid method (Murphy & Riley, 1962).

Rare interferences with dissolved OM were reduced by sample dilution. In addition, extracts were analyzed for total P (TP) by ICP-OES (5900 SVDV, Agilent Technologies).

All extractions were carried out in triplicate. Fractions of organic P (OP) were calculated by subtracting inorganic Olsen-PO_4-P (IP) from TP. Information on OP fractions in the soils of the experimental sites was obtained from the Biodiversity Exploratories Information System (BExIS).

Water-extractable organic matter in soil samples

To characterize the input of soluble OM from overlying soil into the mineral containers with percolating water, the soil directly above the containers was analyzed for the amount and composition of water extractable OM (WEOM). Since the amount and composition of WEOM strongly depends on soil moisture conditions, all soil samples were air-dried, subsequently moistened to 50% of their water-holding capacity and incubated for 7 days at 5 °C prior to extraction. By this standardization, the comparability of WEOM concentrations and composition between sites was increased, while minimizing the effect of drying and re-wetting (Akagi et al., 2007). After incubation, moist equivalents of 20 g of dry soil were percolated with 40 mL of 10 mM $CaCl_2$ solution (soil to solution ratio = 1:2, w/v) in triplicate. Eluates were filtered using syringe filters with 0.45 µm polyether sulfone membranes (VWR International GmbH, Darmstadt, Germany). The water-extractable OC (WEOC) concentrations of the eluates were measured with a varioTOC analyzer (Elementar Analysensysteme GmbH). Ammonium-N, NO_3–N, total N (after wet oxidation to NO_3), and PO_4–P concentrations were analyzed photometrically using a continuous flow analyzer (AA500, Seal Analytical, Norderstedt, Germany). The total P concentration of the eluates was determined using inductively coupled plasma-optical emission spectrometry (ICP-OES, 720-ES, Agilent Technologies, Santa Clara, CA, USA). Water-extractable organic N (WEON) concentrations were calculated by subtracting NH_4–N and NO_3–N concentrations from total N concentrations. Water-extractable organic P (WEOP) concentrations were calculated analogously, subtracting PO_4–P concentrations from total P concentrations. The concentrations measured in the eluates were subsequently multiplied with the eluate volume (in L) and normalized to the mass of soil in order to express the amounts of WEOC, WEON, and WEOP in mg kg^{-1} of soil.

Abundances of major microbial groups in mineral and soil samples

Major microbial groups were characterized by phospholipid fatty acid (PLFA) analysis. Lipids were extracted from 2 g of thawed soil and, due to the overall low lipid contents in the mineral samples, an increased weight of 12 g of thawed mineral samples using a single-phase mixture of chloroform, methanol, and aqueous citrate buffer (Bligh and Dyer reagent). Lipids were isolated by subsequent phase separation following Frostegård et al. (1991). Neutral fats, glyco- and phospholipids were separated by solid-phase extraction. The separated phospholipids were then transformed into fatty acid methyl esters (FAMEs) by mild alkaline methanolysis. Extracted FAMEs were measured by gas chromatography (AutoSystem XL, Perkin-Elmer Corporation, Norwalk, CT, USA) equipped with a flame ionization detector using helium as the carrier gas. For additional methodological details, see Kramer et al. (2013). According to Ruess & Chamberlain (2010), the PLFAs i15:0, a15:0, i16:0, and i17:0 were used as indicators of Gram-positive bacteria, cy17:0 and cy19:0 of Gram-negative bacteria. The PLFA 18:2ω6,9 was used as indicator for fungi. The sum of PLFAs derived from Gram-positive and Gram-negative bacteria and the fatty acid 16:1ω7 were used to estimate total bacterial biomass. Total microbial PLFAs were determined as the sum of bacterial and fungal PLFA markers and were used as an indicator of microbial biomass. The PLFAs of individual organism groups were used to calculate the fungal to bacterial ratio (F:B) and Gram-positive to Gram-negative bacterial ratio ($Gram^+$:$Gram^-$).

Potential enzyme activities in mineral and soil samples

We analyzed potential activities of C-, N-, and P-cycling enzymes, i. e., β-glucosidase (BG) (EC 3.2.1.21), β-xylosidase (XYL) (EC 3.2.1.37), N-acetyl-β-glucosaminidase (NAG) (EC 3.2.1.52), and acid phosphatase (AP) (EC 3.1.3.2) to gain insight into microbial functions in response to mineral type and land use. Enzyme activities were determined using fluorogenic substrates according to Marx et al. (2001). The substrates containing the fluorescent compound 4-methylumbelliferone (4-MUF) were obtained from Sigma-Aldrich (St. Louis, MI, USA). Briefly, 1 g soil, 1 g illite sample, or 0.5 g goethite sample was suspended in 50 mL deionized water and disaggregated by sonication

(Ultrasonic Processor UP200S, Hielscher Ultrasonics GmbH, Teltow, Germany) for 120 s at 50 J s^{-1} mL^{-1}. For goethite, the sample weight had to be reduced due to the high optical density of the goethite-water suspension, which interfered with the photometric measurement. Fifty microliters of sample suspension were then transferred into microplates (PP F black 96 well, Greiner Bio-One GmbH, Germany) with three analytical replicates and constantly stirred on a magnetic stirrer to prevent settling of particles. The suspensions were mixed with 50 µL of 0.1 M MES (2-(*N*-morpholino) ethanesulfonic acid) buffer solution (pH 6.1) and 100 µL 1 mM substrate solution. The suspensions with substrate were then preincubated at 30 °C for 30 min (soils) or 60 min (mineral samples). Fluorescence was measured spectroscopically at 360/460 nm (excitation/emission) after 0, 30, 60, 120, and 180 min using a fluorescence microplate reader (Synergy HTX, Agilent Technologies). Since enzyme activities in the mineral suspensions were comparatively low and a linear increase of the fluorescence could only be established after a longer incubation period, mineral suspensions were additionally measured after 240 and 300 min to increase the total developed fluorescence. At the same time, a standard plate with concentrations of 0, 0.5, 1, 2.5, 4, and 6 µM 4-MUF was measured. Between measurements, the samples were kept at 30 °C. Enzyme activities corresponded to an increase in fluorescence and were calculated according to the standards in nmol g^{-1} dry weight soil or mineral sample h^{-1}.

Statistical analyses

Prior to statistical analysis, in addition to regarding absolute total PLFA values only, we normalized total PLFAs to OC content by dividing the content of total PLFAs by OC content (total PLFA:OC ratios). In addition, we calculated biomass- and OM-specific enzyme activities by normalizing enzyme activities to microbial biomass and OC content, respectively. These normalizations were made to link microbial biomass directly to accumulated OM, as well as enzyme activities to OM and microbial biomass to provide indirect insight into OM utilization and potential substrate quality.

To express differences between the mineral samples and the overlaying soils, each variable x in mineral samples was expressed as percentage of variable x in the overlaying soil according to Equation (2).

$$x_{\%\ of\ soil} = \frac{x_{mineral}}{x_{overlaying\ soil}} \times 100$$

We also calculated untransformed proportional enzyme activity vector lengths and angles according to Moorhead et al. (2016) to assess the relative microbial focus on C versus nutrient (N and P) acquisition and P versus N acquisition. Vector length was calculated by Equation (3), where x represents the relative activities of C- versus P-acquiring enzymes (BG/(BG + AP)) and y represents the relative activities of C versus N-acquiring enzymes (BG/(BG + NAG)).

$$Vector\ length = \sqrt{(x^2 + y^2)}$$

The vector angle was calculated as the arctangent of the line extending from the plot origin to point (x, y) according to Equation (4).

$$Vector\ angle\ (°) = atan2(x, y)$$

All statistical analyses were carried out in R 4.0.2 (R Core Team, 2020). To determine differences between goethite and illite samples and the respective overlying soil, we applied linear mixed models with the R function *lme* from the package nlme (Pinheiro et al., 2020) with EP as random factor. The function *emmeans* from the R package emmeans (Lenth, 2017) with a Tukey adjustment for multiple comparisons was used for post hoc analysis. Model assumptions were tested for normal distribution of residuals by graphical inspection of QQ plots and for homogeneity of variances by visual inspection of scatter plots of standardized residuals against fitted values. Response variables were log-transformed when model assumptions were not met (Table S7-3).

To gain insight into the factors controlling microbial variables of the field-exposed mineral samples, we established linear models with the R function *lm* from the package stats (R Core Team, 2022) for each type of mineral separately and determined the most important influencing factors for each variable with backward model selection using the function *stepAIC* from the R package MASS (Venables & Ripley, 2013). Applying the function *vif* from the R package car on the final models revealed negligible multicollinearities between independent variables since the variance inflation factor of all variables was <5. Respective p-values were extracted from subsequent ANOVAs applied to the models (R function *Anova*, R package car). To detect additional correlations

between single factors, we used Pearson correlations by applying the R function *cor.test* from the package stats.

To identify direct and indirect effects of LUI on the properties observed on the two types of mineral samples and to investigate links between mineral-associated OC and nutrients as well as microbial biomass and enzyme activities involved in C- (BG, XYL), N- (NAG), and P-cycling (AP), we fitted multigroup structural equation models (SEMs). The mineral type was used as grouping variable using the R function *sem* from the lavaan package (Rosseel, 2012). The general structure of the SEMs is illustrated in Fig. S1. Standardized path coefficients were extracted with the function *standardizedsolution* and R values with the function *lavInspect* (R package lavaan). To keep the number of variables and paths in a moderate range and secure the quality of SEM outputs, we did not include any additional parameters in the model structure. We tested for effects of LUI on parameters that were not covered by the SEM analysis with additional linear models (R function *lm*) only including LUI as an explanatory variable. Detailed results for all applied models are summarized in Tables S7-3–S7-6.

Results

Organic matter and nutrient contents

The grassland soils in which the mineral containers were buried for five years encompass a wide range of soil properties. For example, OC and TN ranged from 35.0 to 122.2 g kg^{-1} and 3.6–11.6 g kg^{-1}, respectively (Table S7-7). Olsen-extractable OP ranged from 0.3 to 49.1 mg kg^{-1}. Water-extractable OC, ON, and OP represented on average 0.2, 0.2, and 4.4% of soil OC, TN, and Olsen-extractable OP, respectively. Additional information on environmental and soil properties (pH and soil texture) at each site can be found in Table S7-1. Of note, soil samples taken separately from above the goethite and illite containers did not differ significantly in any measured property for each EP (Table 7-1), indicating that the same initial conditions prevailed for the goethite and illite samples throughout their field exposure.

Before exposure to grassland soils, the mineral samples contained no inorganic C and N and little OC and TN (Table S7-8). After five years of field exposure, and when expressed per gram of mineral-sand mixture, goethite samples accumulated on average

2.5- and 1.5-fold more OC and TN than illite samples ($p < 0.001$; Table 7-1). The Olsen-extractable OP content was similar for both mineral samples and accounted for most Olsen-extractable TP (on average 94% in goethite samples and 89% in illite samples).

Since quartz does likely not contribute much to OM and nutrient accumulation (Fig. S7-8), the mixing of minerals with sand can be considered as a dilution of reactive surface area. Thus, we additionally present OC and nutrient concentrations normalized to mass and surface area of goethite and illite (Table S7-7). Nevertheless, bacteria as well as fungi probably colonize the complete samples, including sand. Consequently, we report and discuss microbiological and chemical data per gram of sample of the entire mineral-sand-mixtures. Inorganic C and N contents of the mineral samples were negligible after field exposure, which may suggest exclusive accumulation of OC and ON forms over time. However, the observed C:N ratios of illite (4–9) were substantially lower than those associated with goethite (8–15) and the overlying soils (9–14) ($p < 0.001$). The low C:N ratios of illite samples suggest possible contribution of interlayer NH_4^+ and an increase in both organic and inorganic N, hampering a straightforward interpretation of C:N ratios as proxies for MAOM quality. In the case of goethite, the C:N ratios slightly but significantly exceeded those of the overlying soil ($p < 0.05$). Linear modeling indicated an increase in Olsen-extractable OP with increasing LUI in the soil and on the minerals (goethite: $p < 0.001$, $R^2 = 0.21$; illite: $p < 0.05$, $R^2 = 0.08$; soil: $p < 0.001$, $R^2 = 0.19$). In addition, increasing LUI resulted in decreasing C:N ($soil_{goethite}$: $p < 0.001$, $R^2 = 0.28$; $soil_{illite}$: $p < 0.01$, $R^2 = 0.13$) and WEOC:WEON ratios ($p < 0.01$, $R^2 = 0.17$) in the overlying soils, and decreasing C:N ratios in goethite ($p < 0.05$, $R^2 = 0.06$) but not in illite samples. However, the percentage of variance explained by LUI was considerably smaller for the linear models related to the goethite samples than for the soils.

Microbial biomass and major microbial groups

No microbial PLFAs were detected in the mineral samples before exposure to soil (Table S7-7), implying that all PLFAs present in the soil exposed samples reflected accumulation of new microbial biomass. The average content of total PLFAs were 2.7 and 2.6 nmol g^{-1} in goethite and illite samples, respectively (Table 7-1). The content of mineral-associated PLFAs did not differ between mineral samples and represented only around 1.6% of the PLFAs present in the overlying soils. Backward-selected linear

modeling indicated that the content of mineral-associated OC was the most important factor explaining microbial biomass in both mineral samples ($p < 0.001$; Fig. S7-2a). The ratio of total PLFAs to OC was significantly higher for illite than for either the goethite samples or the overlying soils ($p < 0.001$; Fig. 7-3a). In goethite samples, the total PLFA:OC ratio was lower than in the soils ($p < 0.001$) and decreased with increasing C:N ratios of the newly formed MAOM ($p < 0.05$; Fig. S2b), which was not the case for illite samples. With increasing LUI, linear modeling indicated an increase in microbial biomass ($p < 0.05$, $R^2 = 0.09$; Fig. S7-3a) and in the total PLFA:OC ratio in goethite ($p < 0.05$, $R^2 = 0.07$; Fig. 7-4a) but not in illite samples, however, the percentage of variance explained was low.

Table 7-1. Chemical and microbiological properties of goethite samples, illite samples, and the corresponding overlaying soils averaged for all 50 experimental sites. Standard deviations are given in parentheses; information on the range of values is available in Table S7-8. Superscript numbers in front of values indicate statistically significant differences between samples according to linear mixed modeling (p< 0.05).

	Goethite	Illite	$Soil_{goethite}$	$Soil_{illite}$
C, N, and P contents				
TC (g kg^{-1})	[a]2.2 (0.5)	[b]0.9 (0.2)	[c]73.8 (19.4)	[c]73.7 (18.8)
IC (g kg^{-1})	<0.1	<0.1	[a]3.9 (9.1)	[a]1.5 (7.3)
OC (g kg^{-1})	[a]2.2 (0.5)	[b]0.9 (0.2)	[c]69.9 (16.6)	[c]72.2 (17.7)
TN (g kg^{-1})	[a]0.2 (0.0)	[b]0.1 (0.0)	[c]6.7 (1.8)	[c]6.8 (1.7)
TP (mg kg^{-1})	[a]2.8 (3.4)[a]	[b]3.1 (3.0)	[c]33.2 (21.1)[a]*	
IP (mg kg^{-1})	[a]0.3 (0.7)[a]	[b]0.5 (0.7)[b]	[c]19.3 (16.8)[a]*	
OP (mg kg^{-1})	[a]2.5 (2.7)[a]	[a]2.6 (2.3)[a]	[b]13.9 (8.2)[a]*	
C:N	[a]11.1 (1.7)[a]	[b]6.5 (1.0)[b]	[c]10.5 (0.9)	[ac]10.6 (1.1)
Water-extractable C, N and P contents				
WEOC (mg kg^{-1})	–	–	144.1 (46.2)*	
WEON (mg kg^{-1})	–	–	13.8 (4.6)*	
WEOP (mg kg^{-1})	–	–	0.4 (0.2)*	
WEOC:WEON	–	–	11.0 (3.3)*	
Main microbial groups				
Total PLFAs (nmol g^{-1})	[a]2.7 (1.1)	[a]2.6 (1.0)	[b]163.5 (42.5)	[b]160.1 (39.3)
Fungal PLFAs (nmol g^{-1})	[a]0.4 (0.2)	[a]0.4 (0.2)	[b]15.0 (5.3)	[b]15.1 (6.0)
Bacterial PLFAs (nmol g^{-1})	[a]2.3 (1.0)	[a]2.2 (1.0)	[b]148.5 (40.2)	[b]145.0 (36.8)
$Gram^+$ PLFAs (nmol g^{-1})	[a]1.2 (0.6)	[a]1.1 (0.6)	[b]99.9 (26.7)	[b]97.3 (24.5)
$Gram^-$ PLFAs (nmol g^{-1})	[a]0.5 (0.3)	[a]0.5 (0.3)	[b]20.3 (6.0)	[b]20.1 (5.4)
F:B	[a]0.2 (0.1)	[b]0.2 (0.1)	[c]0.1 (0.0)	[c]0.1 (0.0)
$Gram^+$:$Gram^-$	[a]2.9 (1.1)	[b]2.4 (0.8)	[c]5.0 (0.9)	[c]4.9 (0.6)
Total PLFA:OC (mmol kg^{-1})	[a]1.2 (0.3)	[b]3.0 (0.8)	[c]2.4 (0.5)	[c]2.3 (0.5)
Potential enzyme activities				
BG (nmol g^{-1} h^{-1})	[a]65.3 (38.2)	[b]16.3 (9.1)	[c]1421.5 (587.1)	[c]1548.2 (628.6)
XYL (nmol g^{-1} h^{-1})	[a]34.8 (22.9)	[b]4.7 (4.8)	[c]332.9 (135.7)	[c]379.3 (172.4)
NAG (nmol g^{-1} h^{-1})	[a]60.4 (49.7)	[b]13.4 (8.0)	[c]496.5 (155.4)	[c]564.3 (195.7)
AP (nmol g^{-1} h^{-1})	[a]434.8 (159.7)	[b]49.8 (20.9)	[c]2086.8 (908.5)	[c]2260.1 (1033.3)

TC: total carbon; IC: inorganic carbon; OC: organic carbon; TN: total nitrogen; TP: Olsen-extractable total phosphorus; IP: Olsen-extractable inorganic phosphorus; OP: Olsen-extractable organic phosphorus; C:N: ratio of OC to TN; WEOC: water-extractable organic carbon; WEON: water-extractable organic nitrogen; WEOP: water-extractable organic phosphorus; WEOC:WEON: ratio of water-extractable organic carbon to organic nitrogen; PLFAs: phospholipid fatty acids; F:B: ratio of fungal to bacterial PLFAs; $Gram^+$:$Gram^-$: ratio of grampositive to gramnegative bacterial PLFAs; Total PLFA:OC: ratio of total PLFAs to OC; BG: activity of β-glucosidase; XYL: activity of β-xylosidase; NAG: activity of N-acetyl-β-glucosaminidase; AP: activity of acid phosphatase.
*Data only available for bulk soil without separation into $soil_{goethite}$ and $soil_{illite}$.
[a] Data obtained from Oelmann and Sorkau (2015)

Absolute amounts of bacterial and fungal PLFAs were significantly lower in the mineral samples than in the overlaying soil, but similar for the two mineral samples (Table 7-1). We observed 2-fold higher F:B ratios in the mineral samples than in the overlying soils ($p < 0.001$; Fig. 7-3b) and slightly but significantly lower F:B ratios in goethite than

illite samples ($p < 0.05$). Backward-selected linear modeling analysis indicated increasing F:B ratios with decreasing Olsen-extractable OP in both mineral samples ($p < 0.01$; Table S7-5). In illite samples, F:B ratios were positively correlated with F:B ratios of the overlying soils ($p < 0.05$).

With increasing LUI, the absolute quantity of bacterial PLFAs increased in goethite ($p < 0.05$, $R^2 = 0.09$) but not in illite samples, and the F:B ratio shifted more strongly towards bacteria on both minerals (goethite: $p = 0.061$, $R^2 = 0.05$; illite: $p < 0.05$, $R^2 = 0.08$; Fig. 7-4b). Again, however, the amount of variance explained by the linear models was low.

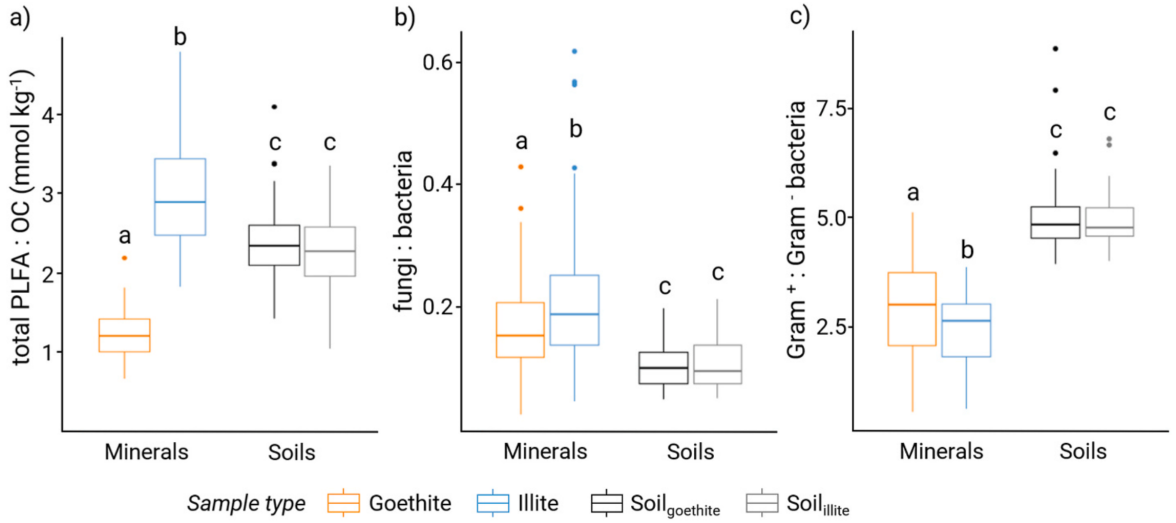

Figure 7-3. Boxplots of a) the ratio of total PLFAs to organic C (OC), b) the ratio of fungal to bacterial PLFAs, and c) the ratio of Gram-positive to Gram negative bacterial PLFAs in mineral samples and overlying soils. Boxes in boxplots represent the median and interquartile range, whiskers extend to 1.5 times the interquartile range (IQR) and points denote outliers. Letters above boxplots depict statistically significant ($p < 0.05$) differences between the sample types according to linear mixed modeling.

In the soils overlying the mineral samples, increasing LUI corresponded with a simultaneous decrease in fungal PLFAs ($soil_{goethite}$: $p < 0.01$, $R^2 = 0.08$; $soil_{illite}$: $p < 0.05$, $R^2 = 0.12$) and increase in bacterial PLFAs ($soil_{goethite}$: $p < 0.05$, $R^2 = 0.06$; soilillite: $p = 0.07$, $R^2 = 0.05$), which also translated into lower F:B ratios ($soil_{goethite}$: $p < 0.001$, $R^2 = 0.28$; $soil_{illite}$: $p < 0.001$, $R^2 = 0.31$; Fig. 7-4e).

The mineral samples displayed lower relative contents of Gram positive as well as higher relative contents of Gram-negative bacteria than the overlying soils ($p < 0.001$; Fig. S7-4), resulting on average in about half as high Gram+:Gram- ratios ($p < 0.001$). Goethite samples had slightly higher relative contents of Gram-positive bacterial PLFAs

than illite samples (p< 0.05; Fig. S7-4), resulting in a higher ratio of Gram$^+$:Gram$^-$ (p< 0.05; Fig. 7-3c). There was no effect of LUI on the abundance of Gram-positive or Gram-negative bacteria in mineral samples or soils (Table S7-4).

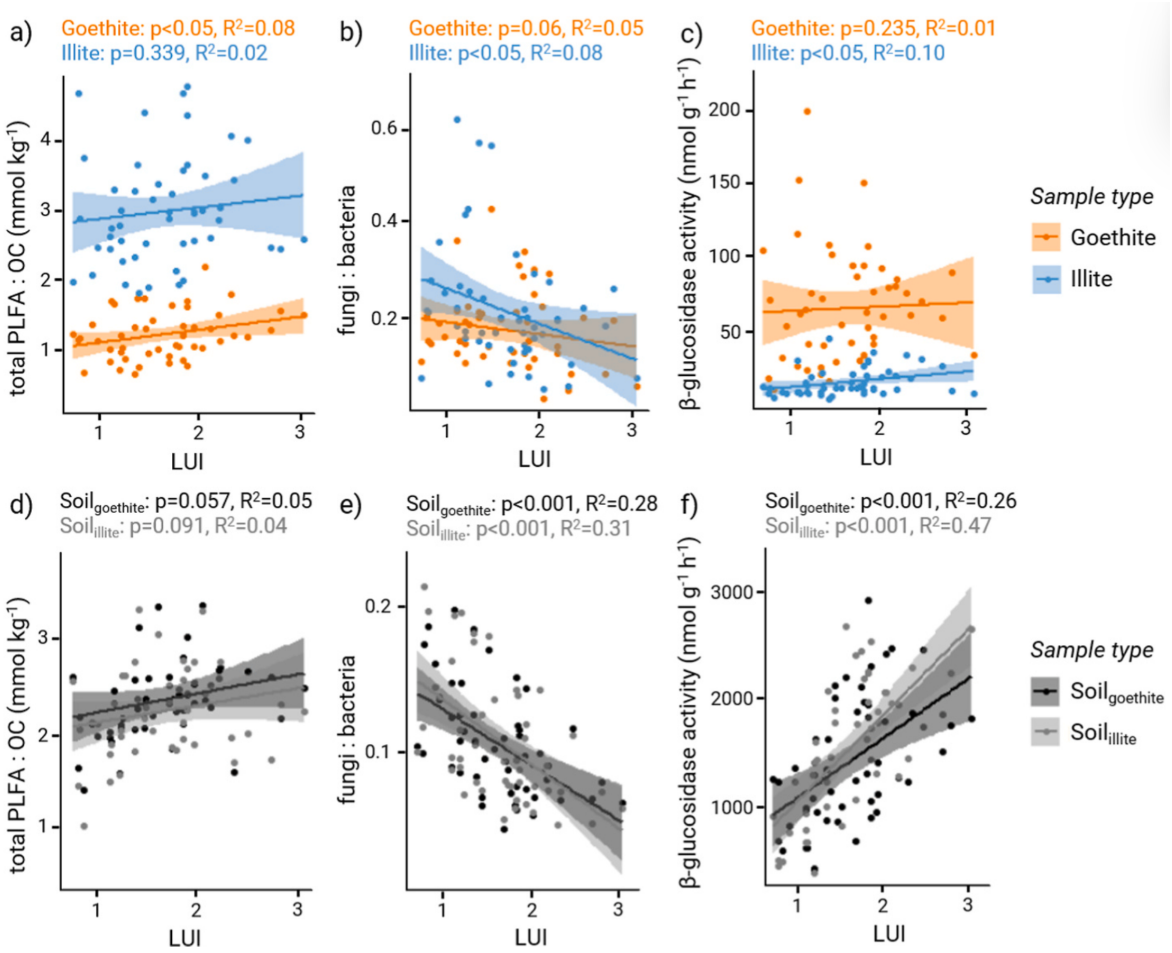

Figure 7-4. Linear regressions between LUI and total PLFA:OC ratios in a) mineral samples and d) soils; Linear regressions between LUI and fungi to bacteria ratios in b) mineral samples, and e) soils; Linear regressions between LUI and the activity of β-glucosidase in c) mineral samples and f) soils. 95% confidence intervals are shown. P-values and R^2 of linear regressions are depicted above each plot.

Enzyme activities

Before exposure to grassland soils, the illite samples were free of enzyme activities, whereas the goethite samples displayed BG and AP activities of 32.8 and 454.1 nmol g^{-1} h^{-1}, respectively (Table S7-7). Since these enzyme activities prevailed even after autoclaving, we suggest some yet to be identified abiotic reason for the substrate cleavage. However, when soil-exposed goethite samples were autoclaved, the AP activities were largely reduced, implying that the observed substrate cleavage in the field-exposed goethite samples derived predominantly from biotic processes.

Goethite samples exhibited 4- to 9-fold higher enzyme activities than illite samples ($p< 0.001$; Table 7-1; Fig. S7-5). When expressed as percentage of enzyme activities in overlaying soil, activities in goethite and illite samples displayed enzyme- and mineral-specific differences. In the case of goethite samples, the mean normalized activities were 5.8% (BG), 12.8% (XYL), 13.2% (NAG), and 23.7% (AP) of those in the overlying soils (Fig. S7-6). In contrast, illite samples exhibited significantly lower normalized activities (1.2–2.8%) for all four enzymes ($p< 0.001$). Biomass-specific and OC-specific enzyme activities were consistently higher in goethite samples than in illite samples ($p< 0.001$). In both mineral samples, biomass-specific enzyme activities (Fig. 7-5) and OC specific enzyme activities (Fig. S7-7) of N- and P-cycling enzymes exceeded those of the soils ($p< 0.001$).

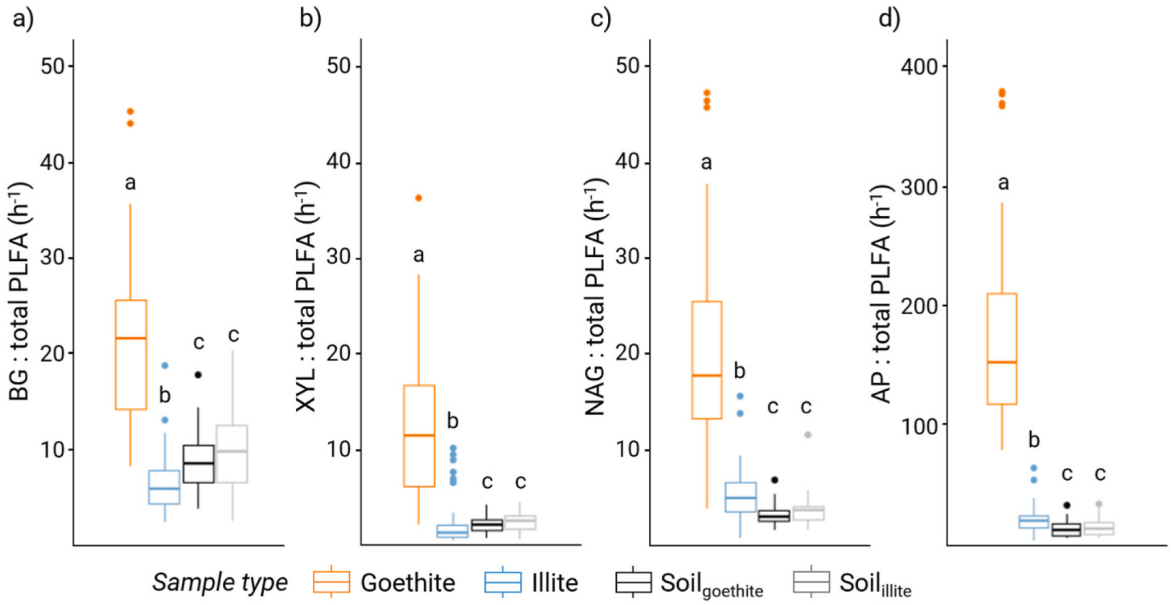

Figure 7-5. Boxplots of a) β-glucosidase (BG), b) β-xylosidase (XYL), c) N-acetylglucosaminidase (NAG), and d) acid phosphatase (AP) activities normalized to the microbial biomass content (total PLFA). Boxes represent the median and interquartile range, whiskers extend to 1.5 times the interquartile range (IQR) and points denote outliers. Letters above boxplots depict statistically significant differences between the sample types according to linear mixed modeling ($p < 0.05$).

In goethite samples, backward-selected linear modeling indicated that activities of all four enzymes were primarily and positively related to the contents of mineral-associated OC (BG, XYL: $p < 0.001$; NAG, AP: $p < 0.05$; Fig. S7-5). This effect of OC was not evident in the illite samples, for which enzyme activities were instead related to the associated microbial biomass content (BG: $p < 0.001$; NAG: $p < 0.01$; AP: $p < 0.05$). In the soils, we found a positive effect of LUI on absolute, biomass-specific, and OC-specific activities of both C-hydrolyzing enzymes ($p < 0.01$; Fig. S7-7h). Similarly, we observed increasing absolute ($p < 0.05$; Fig. S7-7d), biomass-specific ($p < 0.05$), and OC-specific ($p = 0.073$) activity of BG with increasing LUI in illite samples. Enzyme activities in goethite samples were unrelated to LUI.

To gain insight into the relative investments of mineral-associated microorganisms in C as well as N and P acquisition, we calculated enzyme activity vector lengths and angles (Fig. 7-6). Calculated vector lengths, indicating relatively more investment into C than nutrientacquiring (N and P) enzymes, increased in the following order: goethite samples (0.55) < illite samples (0.61) < soils (0.84) (Fig. 7-6b).

In contrast, vector angles, indicating stronger relative focus on P vs. N acquisition, increased in the reverse order: soils (60.8°) < illite samples (65.2°) < goethite samples (76.5°) (Fig. 7-6c).

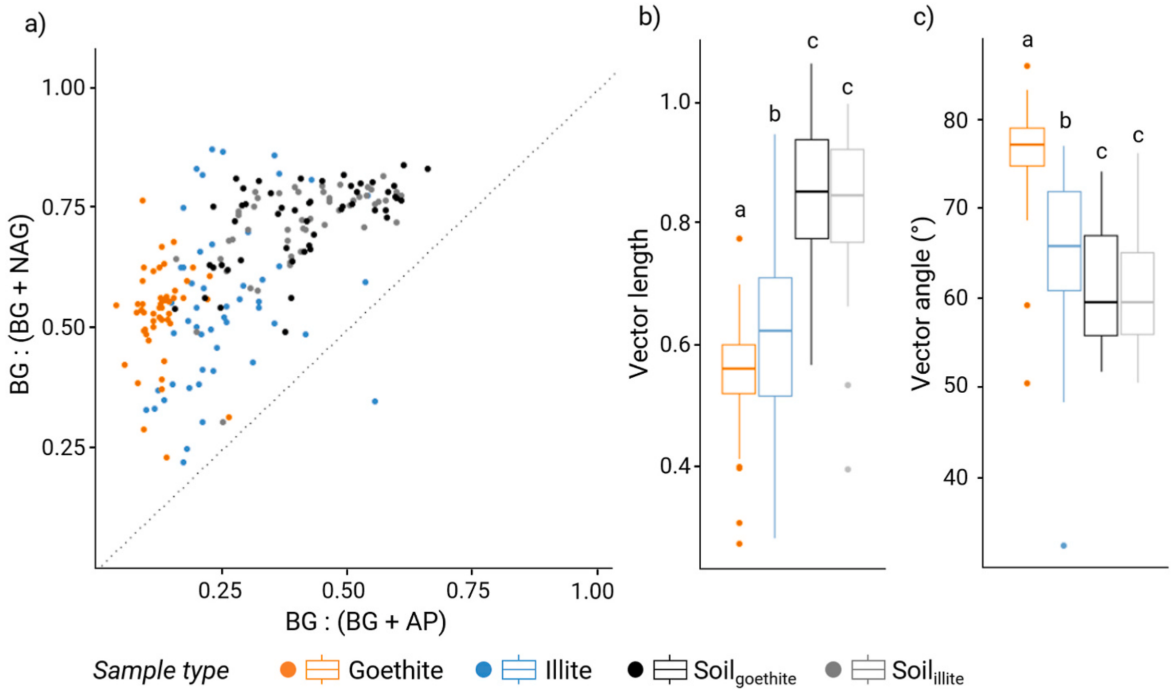

Figure 7-6. Enzyme activity vector analysis showing a) the relationship between the relative enzyme activities as proportions of C to N acquisition versus C to P acquisition. BG:(BG + AP) represents the relative activities of C- versus P-acquiring enzymes (BG: β-glucosidase, AP: acid phosphatase), and (BG:(BG + AP)) represents the relative activities of C- versus N acquiring enzymes (NAG: N-acetylglucosaminidase); b) boxplots of resulting vector lengths and c) vector angles per sample type. Boxes in boxplots represent the median and interquartile range, whiskers extend to 1.5 times the interquartile range (IQR) and points denote outliers. Letters above boxplots depict statistically significant differences between the sample types according to linear mixed modeling ($p < 0.05$).

With increasing LUI, we observed an increase in vector length for illite samples ($p < 0.05$) and soils ($soil_{goethite}$: $p < 0.01$; $soil_{illite}$: $p < 0.001$), while the vector angle remained unaffected.

Direct and indirect effects of land-use intensity

The SEMs focusing on C (Fig. 7-7) and N (Fig. S7-9a) suggested that the processes involved in C- and N-cycling in the exposed mineral samples were not directly controlled by the properties of the overlying soils. Over the exposure period, higher contents of OC, TN, and microbial biomass as well as higher C- and N-hydrolyzing enzyme activities in the soils did not translate into a proportional increase of these properties in the

mineral samples. The only link between mineral samples and overlying soils in the SEMs related to C and N was a positive effect of soil OC on mineral-associated microbial biomass ($p < 0.05$). In contrast, there were several connections between mineral samples and soils for the P-related SEMs (Fig. S7-9b). Activities of AP in the soils were positively related to AP activities ($p < 0.01$) and microbial biomass in the mineral samples (goethite: $p < 0.05$; illite: $p = 0.06$). In addition, soil microbial biomass had a positive effect on the accumulation of Olsen-extractable OP in the mineral samples (goethite: $p < 0.01$; illite: $p = 0.06$).

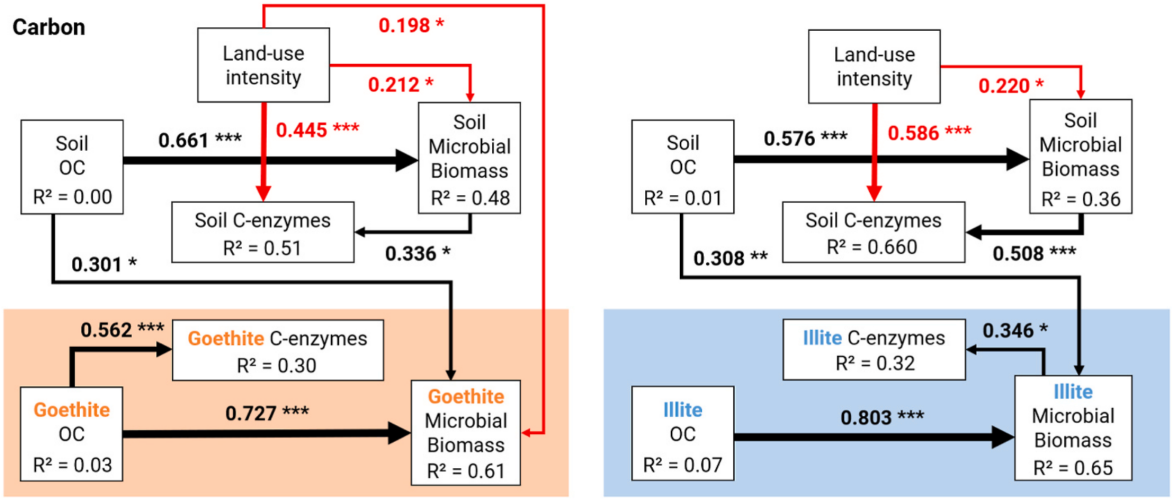

Figure 7-7. Structural equation models showing effects of land-use intensity on organic carbon (OC) accumulation, microbial biomass, and C-cycling enzyme activities in goethite (left column) and illite samples (right column). Path lines indicate only significant ($p < 0.05$) relationships. A continuous line indicates a positive path coefficient, while a dashed line reflects a negative path coefficient. Numbers on arrows are standardized path coefficients and the thickness of arrows is proportional to the effect size of the coefficient. Red arrows symbolize direct effects of LUI on variables. The amount of explained variance of variables is given as R^2 value; variables measured in mineral samples are in orange (goethite) and blue (illite) boxes. The full model output is presented in Table S7-6.

Organic C and TN exerted a strong positive influence on microbial biomass in both soils and mineral samples ($p < 0.001$), whereas Olsen extractable OP was positively related to microbial biomass only in the mineral samples (goethite: $p < 0.06$; illite: $p < 0.001$). In the soils, C hydrolyzing enzyme activities were positively related to microbial biomass (goethite: $p < 0.05$; illite: $p < 0.001$), whereas N- and P-cycling enzymes were related to TN contents (goethite: $p < 0.001$; illite: $p < 0.05$) and Olsen-extractable OP ($p < 0.001$), respectively. In the mineral samples, we observed mineral type-dependent relationships. In the goethite samples, C- and N-hydrolyzing enzyme activities were more

related to the accumulated OC ($p < 0.001$) and TN ($p < 0.05$) than to microbial biomass, whereas all enzyme activities in illite samples were more related to mineral-associated microbial biomass (C and N: $p < 0.01$; P: $p < 0.001$).

The SEM related to C indicated direct positive effects of LUI on microbial biomass in the soil and goethite samples ($p < 0.05$). Via its effect on soil microbial biomass, LUI had a positive indirect effect on soil C hydrolyzing enzyme activities, but there was also a direct positive link between LUI and soil C-hydrolyzing enzyme activities ($p < 0.001$; Fig. 7-7). The SEM related to N suggested a positive effect of LUI on the accumulation of TN in both mineral samples (goethite: $p < 0.001$; illite: $p = 0.09$) but not in the soils, which in turn positively affected microbial biomass and NAG activities. The SEM related to P indicated a positive effect of LUI on Olsen-extractable OP contents in soils ($p < 0.01$) but not in mineral samples. In addition, there was a long indirect effect chain of increasing LUI positively affecting Olsen-extractable OP and subsequently AP activities in the soil. Soil AP activities then had a positive effect on AP activities in the mineral samples.

Discussion

Microbial colonization of mineral surfaces in soil is likely affected by both intrinsic properties of the minerals and by extrinsic environmental conditions (A. A. Jones & Bennett, 2017). The latter affect the mineralosphere on a broader scale and include properties of the surrounding soils and impacts of land-use intensity. The presence of OM and nutrients, mediated by land-use intensity, alters resource availability on mineral surfaces and potentially increases their attractiveness as microbial habitats. The exposure of pristine minerals to topsoils of grassland sites with different management intensities over a five-year period allowed to investigate whether and to what extent mineral type and land-use intensity, and their effects on OM and nutrient contents, influence the abundance, composition, and functionality of mineral-associated microorganisms.

Minerals as microhabitats for microbial colonization

In our experiment, OC and nutrients (N and P) accumulated on the surfaces of the previously pristine minerals probably by adsorption of compounds that derived either from microbial colonization or from soil solution entering the mineral containers. The 50-µm mesh size, which allowed us to experimentally separate the mineralosphere within the soil, prevented roots and particulate OM from entering the mineral containers, limiting potential sources for MAOM formation. Mineral associated OM sorption is subject to saturation, if we assume that MAOM is sorbed as a monolayer and consider that mineral surfaces have a finite surface area (Lavallee et al., 2020). Therefore, mineral samples were presumably limited in their maximum capacity to accumulate OC. The concurrent colonization of the mineral containers can be seen as the combination of two major processes. First, similarly to the transport of DOC, there might be an input of microbes with the soil solution, likely to a similar extent for goethite and illite mineral containers. This process can be considered as partly random but may be complemented by some deterministic processes based on different exploitation strategies of bacteria and fungi. However, microhabitat characteristics determine the initial growth conditions for newly establishing microbial communities and may become increasingly important over time for biomass buildup and community differentiation (Fig. 7-1).

Thus, after five years, we consider the amount of accumulated OM to be an important constraint on the proliferation of established microbes as microbial growth is generally highly dependent on OC and nutrients. Microbial biomass in both mineral samples corresponded to only 1.6% of the microbial biomass in the overlying soils. In contrast, Kandeler et al. (2019) found a 2.5-fold higher microbial biomass (4.1% of the soil) in mineral containers filled with a goethite-illite mixture after a shorter incubation period (31 months) in some of the same grassland soils of the Schwäbische Alb. However, they added labeled root litter of *Dactylis glomerate/Lolium perenne* to the mineral mixture, which could have provided a stronger incentive for microbial colonization from the beginning. The difference in mineral colonization between the present study and the one by Kandeler et al. (2019) emphasizes the importance of available OM for microbial growth on mineral surfaces. Possibly due to the lack of additional substrate during the early stages of our experiment, the OC content in the mineral samples turned out to be the limiting factor for mineral-associated microbial biomass, as indicated by the strong positive relationship between the two variables (Fig. S7-1a). However, in contrast to our expectation that stronger MAOM formation in goethite than in illite samples would result in greater microbial colonization, microbial biomass did not differ between the two mineral samples when expressed per mass of entire mineral samples (Table 7-1). When expressed per unit of OC (total PLFA:OC ratios), it becomes evident that microbes on illite were able to sustain a higher biomass from the same amount of OC than on goethite (Fig. 7-3a). Assuming weaker sorption processes on the clay mineral (Kleber et al., 2015), illite-bound OM may be desorbed more easily than goethite-bound OM, resulting in better access by microbes. This likely contributed to the observed higher total PLFA:OC ratios in illite samples. In addition, illite probably provides a less hostile environment than goethite, since it has been reported that strong sorption processes on goethite result in pronounced activity suppression, and even bacterial cell death (Cai et al., 2018; Mills, 2003; Tavanaee et al., 2017; Wu et al., 2014). Since we found a decrease in microbial biomass and in the ratio of total PLFA:OC with increasing C:N ratio in goethite samples (Fig. S7-2b), we suggest a more efficient utilization of OM in response to increasing resource quality on the iron oxyhydroxide.

This relationship between the C:N ratio and C use efficiency (CUE) has been suggested in the past (Angst et al., 2021) and CUE is assumed to decrease as the resource C:N moves further away from biomass stoichiometry (Kästner et al., 2021).

Contributions of fungi and bacteria to the colonization of pristine minerals

Identifying microbial groups that colonize mineral surfaces is critical for understanding the mechanisms underlying C turnover, as they are tightly connected to MAOM formation and degradation. In accordance with our hypothesis, fungi colonized goethite and illite samples more intensely than bacteria relative to the overlying soils (Fig. 7-3b), indicating that fungi are more capable than bacteria of colonizing pristine mineral surfaces. They may be favored due to different reasons. Firstly, arbuscular mycorrhizal fungi access mineral-protected OM by excreting organic acids that release previously mineral-bound substances (Keiluweit et al., 2015). Secondly, fungi are able to re-allocate nutrients via their hyphal network (Boberg et al., 2014; Frey et al., 2003) and are more independent of C limitations due to their symbiotic relationships with plants (Benito-Carnero et al., 2021; Güsewell & Gessner, 2009). Moreover, fungi can overcome distances by hyphal growth, enabling them to actively grow into the mineral containers. The higher F:B ratios in illite than goethite samples may be explained in part by the acquisition of potassium from the illite interlayer by symbiotic fungi (Garcia & Zimmermann, 2014; Lian et al., 2008). It is additionally possible that fungi were similarly able to release and take up NH_4^+ fixed in the interlayers of illite (Paris et al., 1995). This might have supported faster fungal colonization of illite than goethite samples, where N had to accumulate over time.

Based on these observations, we suggest that fungi colonized the mineral containers first and supported subsequent bacterial colonization by providing exudates and fungal necromass, which were recently suggested to greatly contribute to MAOM formation (See et al., 2022). Moreover, hyphal exploration allows for non-random colonization of minerals by hyphae-associated bacterial taxa via the so-called “fungal highway”, which is a way for bacteria to overcome their restricted mobility in soil (See et al., 2022). To our knowledge, the majority of bacterial groups that have previously been reported as fungiphilic or traveling via fungal hyphae (Simon et al., 2015; Warmink et al., 2011) are classified as Gram-negative bacteria, which is why fungi might serve to promote colonization of minerals by that bacterial group. This is highlighted by the fact that in illite samples, which had higher F:B ratios than goethite samples, the

$Gram^+$:$Gram^-$ ratio was shifted more strongly towards Gram-negative bacteria than in goethite samples.

Also, since the $Gram^+$:$Gram^-$ ratio is suggested as a rough indicator of both relative C availability and energy limitation to bacterial communities (Fanin et al., 2019), the greater proportion of Gram-negative bacteria in illite samples may reflect increased availability of OM as a result of weaker mineral-organic bonds. Moreover, due to their rapid growth properties, Gram-negative bacteria could have had an advantage in the competition for new surface areas upon arrival in the mineral containers (Whitman et al., 2018). This emphasizes how the composition of mineral-associated microorganisms could have been strongly affected by different transport and growth strategies as well as OM and nutrient availability.

Enzyme activities in goethite and illite samples

We expected that the different potential availabilities of OM and nutrients between mineral types also have implications for the overall level of enzyme activities. And indeed, we found that absolute enzyme activities were higher in goethite than illite samples (Table 7-1), which we assume to be related to the stronger sorption of OM by goethite. Enzyme activities were directly and positively linked to accumulated OC and TN in goethite samples, while they were indirectly influenced by OM accumulation in illite samples via the build-up of microbial biomass (Fig. 7-7). In relation to the microbial biomass and OC present, the overall mineral-associated enzyme activities were quite comparable to those of the soil, especially in illite samples. The differences in specific enzyme activities in illite samples were significant but small compared to soil, suggesting that illite-associated microbes likely invested in total enzyme production in a similar manner as microbes in soil. However, the specific enzyme activities in goethite samples were several times higher than in soil and illite samples (Fig.7-5; Fig. S7-7), suggesting that the higher enzyme activities in goethite samples cannot be explained solely by the higher amounts of accumulated OC and do not correspond in a similar way to the microbial biomass as in illite samples. This result might be explained by several additional mechanisms. First, goethite can cause abiotic oxidative cleavages of substrates (Chacon et al., 2019), which may have increased the overall amount of substrates available for hydrolytic enzymes, to which microorganisms could respond with

increased production of hydrolases. Second, iron oxides have higher capacities to adsorb enzymes than clay minerals (Tan et al., 2018; Yang et al., 2019), which supports stabilization, and thus, longer turnover times and protection of enzymes against variations in temperature and pH (Lammirato et al., 2010; Olsson et al., 2011; J. M. Sarkar et al., 1989; Yan et al., 2010). However, mineral sorption can also result in a reduction in enzyme activities due to, e.g., steric limitations, conformational changes, limited substrate diffusion, or changes in enzymatic pH optima (Chacon et al., 2018; Datta et al., 2017; Quiquampoix, 1987; Shirvani et al., 2020; Skujiņš et al., 1974; Tietjen & Wetzel, 2003). Third, weaker sorption of OM, enzymes, and substrates to illite than goethite might have increased the physicochemical and spatial accessibility between microbes, enzymes, and their substrates in illite samples (Kleber et al., 2021). Thus, microbes on illite likely relied less on the excretion of extracellular enzymes for nutrient acquisition than microbes on goethite (Olagoke et al., 2019).

The relative microbial production of enzymes involved in different nutrient cycles is a good indicator of both specific nutrient availability and limitations, as it reflects the stoichiometric needs of the microbial communities. We expected that the relative acquisition of C, N, and P of mineral-associated microorganisms would be affected by the different mineral types and indeed, enzyme activity vector analysis indicated a relatively stronger focus on nutrient (N and P) versus C as well as P versus N acquisition in the mineral samples than in the soil (Fig. 7-6). We suggest that the stronger focus on N and P acquisition in the mineral samples could have been enhanced by the expected high contribution of microbially-derived compounds to MAOM (Lavallee et al., 2020; Liang et al., 2017; R. Mikutta et al., 2019). The high specific NAG activities associated with the mineral samples suggest that the degradation of chitin as a component of fungal necromass is an important process in this habitat, since microbes have been reported to respond to necromass-rich environments with a shift from BG to NAG production (Mori, 2020). Higher relative P acquisition on the minerals than the soils likely resulted from most of the mineral-associated P being in organic form, which was presumably microbially-derived and required enzymatic degradation by AP before the released phosphate could be taken up by microbes. Sorption of P-rich microbial compounds to mineral surfaces prevents its mineralization, which can explain the high relative association of OP forms with reactive minerals (Spohn, 2020).

Since we observed a positive relationship between AP activities in soils and on minerals, the high AP activities on the minerals could also have been a result of leaching of AP from the overlaying soil (Fetzer et al., 2021).

Organic P accumulated in both mineral samples to the same extent. Still, vector angles suggested higher P acquisition in goethite than in illite samples. Thus, not only the degree of sorption but rather the stronger binding of OP or enzymatically released phosphate to goethite than to illite may be decisive for the observed differences in vector an gles between the minerals. Phosphorus-rich compounds are known to have a strong affinity towards iron oxides (Amadou et al., 2022; X. Wang et al., 2019) and inorganic and organic P are only barely bioavailable once bound to goethite (Amadou et al., 2022; Klotzbücher et al., 2020). This may have resulted in lower P availability on goethite than on illite, and thus, in an increased microbial investment into P acquisition to meet nutrient requirements.

Mineral-association of microorganisms and enzyme activities in response to land use

Besides the intrinsic factor of mineral type, it is important to consider extrinsic factors such as land use, which affects processes on mineral surfaces at larger scales due to different OM and nutrient inputs to soil. In the past, higher inputs of high-quality OM and nutrients in response to more intensive land use increased microbial biomass production and enzyme production as well as altered microbial community structure (Berner et al., 2011; Herold et al., 2014; Lagerlöf et al., 2014). We expected that these anticipated effects of LUI on the overlying soil would translate also to the mineral-associated microorganisms, which we accounted for by including direct as well as soil-mediated indirect LUI effects in our SEMs (Fig. S7-1).

Consistent with our expectations, we found increased nutrient levels in both soils and mineral samples with increasing LUI, which we attribute to increased inputs of labile, N-rich litter and exudates from fast-growing plant species (Vries et al., 2012), N and P inputs from fertilization and grazing (Alt et al., 2011), and increased accumulation of N-rich microbial products and necromass due to higher microbial activity and biomass.

The SEM related to C indicated a positive link between LUI and soil microbial biomass, likely a result of microbial growth fostered by more labile OM and higher nutrient inputs (Herold et al., 2014). Accordingly, we observed in goethite samples that an increase in LUI was positively associated with bacterial biomass and PLFA:OC ratios. Similar to the soil, we suggest that this is related to the narrowing of the C:N ratio with increasing LUI of goethite samples, and thus, increased availability of OM and nutrients to microbes. LUI, however, did not affect microbial biomass on illite, perhaps since the influence of NH_4^+ and potassium in the clay interlayers as additional potential nutrient sources lowered the impact of LUI.

Carbon-hydrolyzing enzyme activities and vector lengths in soils increased with increasing LUI, probably due to known positive effects of N addition on cellulose-degrading enzyme activities (Herold et al., 2014; Keeler et al., 2009; Stursova et al., 2006). Accordingly, we observed higher absolute and specific BG activities as well as vector lengths with increasing LUI in illite samples. Enzyme activities in goethite samples were not affected by LUI, possibly because the strong sorption of substrates and enzymes to goethite surfaces overcame management effects.

In line with our hypothesis, F:B ratios decreased in soil and mineral samples with increasing LUI. High land-use intensity was previously shown not only to result in higher bacterial but also in lower fungal biomass in soils (de Vries et al., 2006; Joergensen & Wichern, 2008). This has been attributed to smaller contributions of slow-growing plant species (de Vries et al., 2012) and lower plant species diversity, providing a less diverse input of substrates (Malik et al., 2016) under high land-use intensity. This reduced share of fungi with increasing land-use intensity might have also negatively affected soil structure, as interactions of fungal hyphae with minerals are known to contribute to biotic structuring of soils by promoting aggregation (Jeewani et al., 2021; Vidal et al., 2018; Witzgall et al., 2021). Hyphae might thus promote physical protection of OM through aggregation, and moreover contribute to MAOM formation by transport of rhizodeposits and litter-derived OC and N to mineral surfaces (Jeewani et al., 2021; Vidal et al., 2021). Yet, we could not observe a link between mineral-associated OC accumulation and LUI, or F:B ratios. However, it is possible that reduced aggregation by

fungal hyphae was in turn compensated by increased bacterial production of extracellular polymeric substances under higher LUI (Costa et al., 2018).

Overall, increasing LUI likely altered the quantity and quality of OM and nutrient inputs, resulting in greater nutrient accumulation in mineral samples and mineral-type-dependent adaptations in microbial biomass, composition, and functionality. However, contrary to our expectations, the SEMs focusing on C and N showed that the effects of LUI on OM and microbial parameters in the mineral samples tended not to be mediated via the overlying soil. Instead, LUI impacted them directly. It is also important to note that the effects of LUI, although often significant, were much weaker than other environmental factors.

Conclusions

We examined the colonization by major microbial groups and microbial functions in two different pristine mineral samples (goethite and illite) exposed for five years to grassland topsoils along a land-use intensity gradient. Our findings emphasize that the internal factor of mineral type primarily controls the abundances of major microbial groups as well as functions of mineral-associated microorganisms. This is likely due to contrasting physicochemical properties of the selected minerals controlling the sorption of OM, as well as enzymes, and their reaction products. This led to the establishment of mineral-specific microbial habitats, that were only partly modified by the overlaying soil and land-use intensity. The relatively stronger focus on nutrient (N and P) versus C as well as P versus N acquisition in the mineralosphere than in the overlaying soil supported the hypothesis that microorganisms have different stoichiometric needs in these different habitats. Thus, our findings suggest that the abundance of different reactive minerals in soil regulates OM and nutrient cycling by the extent and strength of sorption processes, forcing mineral-associated microbial communities to adapt their acquisition strategies in order to meet their resource demands. Such mineral-specific interactions could shape spatially distinct microhabitats with unique features. In the future, studies with higher temporal resolution may provide additional knowledge on rates of MAOM formation and possible saturation endpoints. Our study underlined the importance of the quality of the newly formed MAOM for microbial colonization. Thus,

detailed investigations on the contribution of plant and microbial sources, e.g., by using isotope-labeled compounds, in combination with a taxonomically highly resolved analysis of microbial succession would further deepen our process understanding.

Author Contributions

MS, IS, EK, CM, RM, KK, JS; laboratory analyses: LB, FS, DSB, SU, AK, CM's lab; data and statistical analysis: LB; writing – original draft preparation: LB, EK, CP; writing – reviewing and editing: all authors; funding acquisition: EK, MS, CM, KK, AK.

Declaration of competing interest

The authors declare that they have no known competing financial interests or personal relationships that could have appeared to influence the work reported in this paper.

Data availability

This work is based on data elaborated by the BEmins project of the Biodiversity Exploratories program (DFG Priority Program 1374). The datasets are publicly available in the Biodiversity Exploratories Information System (BExIS; http://doi.org/10.17616/R32P9Q). BExIS dataset IDs: 31251 (C and N contents), 31316 (enzyme activities), 31317 (PLFAs), 31318 (WEOM), 31320 (Olsen-P in mineral containers), 19286 (soil Olsen-P), 20826 (elevation, slope, aspect, and coordinates), 14686 (soil texture), 22246 (soil pH), and 19007 (climate data).

Acknowledgements

We thank the managers of the Schwäbische Alb, Kirsten Reichel-Jung, Iris Steitz, Sandra Weithmann, Florian Staub, Julia Bass, Max Müller and all former managers for their work in maintaining the plot and project infrastructure; Christiane Fischer, Jule Mangels, and Victoria Grießmeier for giving support through the central office, Michael Owonibi and Andreas Ostrowski for managing the central data base, and Markus Fischer, Eduard Linsenmair, Dominik Hessenmoller, Daniel Prati, François Buscot, Ernst-Detlef Schulze, Wolfgang W. Weisser and the late Elisabeth Kalko for their role in setting up the Biodiversity Exploratories project. We thank the administration of the

UNESCO Biosphere Reserve Schwäbische Alb as well as all landowners for the excellent collaboration. We further thank Heike Haslwimmer, Sabine Rudolph, Gudrun Nemson-von Koch, Christine Krenkewitz, Theresa Klötzing, Steffen Ferber, and Katja Pursche for support during laboratory analyses, Core Project 9 of the Biodiversity Exploratories (DFG project number 193957772) for setting the experiment up in 2015 and all people assisting in the sampling of the mineral containers in 2020. We further thank Caterina Penone for advice with statistical analysis and Kathleen Regan for proofreading of the manuscript. The work has been funded by the DFG Priority Program 1374 "Biodiversity Exploratories" (DFG project number 433273584) and by a postgraduate scholarship of the Justus Liebig University Giessen for Alexander Konrad. Field work permits were issued by the responsible state environmental office of Baden-Württemberg.

Chapter VIII

Findings and Synthesis

Summarizing Chapter II-VII, adsorption to minerals controls the fate of SOM as demonstrated within this dissertation in laboratory experiments and in the field. Sorptive control is modified by environmental boundary conditions, namely nutrient availability and soil pH, as well as land use (Tab. 8-1). Furthermore, minerals shape how OC is microbially utilized, by providing habitats where microbes are either thriving, or which are hostile to microbial life. The following summarizes these findings and whether they support or oppose my hypotheses.

Table 8-1. Summary of dissertation: title of study, experimental scope, and main findings.

Chapter	Title	Experimental Scope	Main findings
II	Thermodynamics of sorption of organic acids to iron oxyhydroxides	Development of an isothermal titration calorimetry method for carboxylic acid adsorption to iron oxyhydroxide surfaces.	Goethite with increasing specific surface area and lattice disorder made binding less exergonic (rising ΔG from -20.7 to -18.0 kJ mol^{-1}) by shifting enthalpy (ΔH from -23.5 to -27.0 kJ mol^{-1}) and entropy (ΔS = -8.8 to -29.9 kJ mol^{-1}). Salicylic acid adsorption was more strongly exothermic (ΔH =-40.5 kJ mol^{-1}) and entropically unfavorable (ΔS =-65.1 kJ mol^{-1}) than citric acid, likely reflecting chelation to iron sites.
III	Microbial carbon use efficiency of mineral-associated organic matter is related to its desorbability	Batch sorption-desorption experiments on goethite, kaolinite and illite and monomers (glucose, acetylglucosamine, phenylalanine, salicylic acid and citric acid). Incubation of mineral-adsorbed monomers (uniformly ^{14}C labeled) in loamy and sandy arable topsoil, followed by glucose-induced priming. Tracing of monomer-C into microbial biomass and CO_2. Determination of P bioavailability.	Carboxylic acids adsorbed to goethite, kaolinite and illite more strongly, and were retained after water desorption to a greater extent than (amino-) sugars or phenylalanine. Microbial assimilation and CUE of mineral-bound monomers mixed and incubated in loamy and sandy arable top soils rose linearly with the monomer´s desorbability from the mineral phase. Monomers adsorbed to goethite exhibited lower CUEs than those on clay minerals, but carboxylic-acid-goethite complexes yielded the highest total soil C retention. Goethite reduced bioavailable P, limiting microbial CUE. Glucose-priming of incubated soils further mineralized monomer-C, with the strongest priming effect on goethite.
IV	Rapid mineralization of mineral-bound carboxyl-C of salicylic acid and phenylalanine	Reproduction of the incubation experiment from chapter III using mineral-(goethite, kaolinite or illite) adsorbed, carboxyl-^{14}C labeled salicylic acid and phenylalanine.	A greater fraction of the mineral-adsorbed carboxyl-C was bioavailable and mineralized than C bound to other monomer-C, irrespective of mineral or soil type. Enhanced mineralization most likely resulted from competetive desorption of the ligands followd by their preferential microbial degradation. Therefore, factors that increase desorbability in the mineral-soil system can override the presumed stability of ligand-bound carboxyl groups.
V	Forest Soil Colloids Enhance Delivery of P Into a Diffusive Gradient in Thin Films (DGT) Sink	Extraction of natural organo-mineral colloids from forest soils of different nutrient availability. Quantification of P transport through an unsaturated porous medium in sinks mimicking plant roots.	Natural soil colloids enriched in iron minerals and organic matter from a P-poor sandy podzol delivered more P faster into a sink mimicking plant roots than the other portions of the soil solid phase. Both colloid mobility and P-binding strength jointly controlled the contributions of colloids to the bio-available P pool in soil. Colloids can both increase P leaching and enhance P delivery to microbes and plants, underscoring their dual role in soil P dynamics.
VI	Formation of mineral-associated organic matter in temperate soils is primarily controlled by mineral type and modified by land use and management intensity	Quantification of mineral-associated organic matter formation on goethite and illite burried for five years in 150 forest and 150 grassland soils with a gradient in land use intensity.	Goethite accumulated on average nearly four times more organic C than illite (0.23 ± 0.1 mg C m^{-2} vs. 0.06 ± 0.03 mg C m^{-2}). C accumulation on minerals was highest in coniferous forests, intermediate in deciduous forests, and lowest in grasslands, indicating a vegetation-driven gradient in mineral-associated organic matter formation Thinning and harvesting reduced the formation of mineral-bound C, while fertilization in grassland boosted mineral-associated organic matter formation via increased productivity. Mineral type is the primary driver of mineral-associated organic matter formation, modulated by land-use and management practices.
VII	Mineral type and land-use intensity control composition and functions of microorganisms colonizing pristine minerals in grassland soils	Quantification of microbial communities and exoenzymatic acitivites on goethite and illite burried for five years in 150 forest and 150 grassland soils with a gradient in land use intensity.	Microbial communities on goethite produced more exoenzymes involved in the mining of C, N and P compared to illite and surrounding soil, indicating nutrient limitations. Illite and goethite were colonized by a higher abundance of fungi and gram-negative bacteria relative the overlying soil. Increasing land-use intensity reduced microbial abundances on goethite and a declining proportion of funghi on both minerals. Mineral properties outweighed land-use intensity in shaping the microbial colonization.

Microbial bioavailability of mineral-adsorbed organic matter related to sorption strength

Thermodynamics of adsorption of organic monomers to minerals used in soil incubation studies in chapter III and IV were only obtainable for salicylic acid and citric acid adsorbing to goethite surfaces. This is because isothermal titration calorimetry has been applicable only to the binding mechanisms defined by high affinities and large changes in enthalpy (and therefore, measured heat flow), namely ligand-exchange reactions (see chapter II).

Preservation of mineral-adsorbed organic matter against mineralization in soil increases by adsorption mechanism from van der Waals forces < polyvalent exchangeable cation bridging < ligand exchange (Mikutta et al., 2007). Hence, a threshold of sorption strength that prevent microbial cycling of mineral-associated OC, if existing, should be found for the ligand-exchange interactions that could be quantified via ITC. Incubating uniformly ^{14}C labeled monomers adsorbed to minerals in loamy Dikopshof and sandy Thyrow topsoil however revealed that 23 – 60% of goethite-adsorbed citric acid and 53-54% of goethite-adsorbed salicylic acid remained bioavailable to microbes (Chapter III). Therefore a thermodynamic threshold of adsorption - at least for the investigated mineral-OC interactions in these soils – was not observed, or overcome by other means than microbial investment.

Most surprisingly, the mineral-bound carboxyl-^{14}C labeled salicylic acid incubated in Dikopshof and Thyrow soil (Chapter IV) showed that even more (74-82%) carboxyl-C (which was ligand-bound to minerals) than C in other functional groups of monomers becomes bioavailable. Overall, carboxyl-C adsorbed to either clay minerals or iron oxyhydroxide was less protected than C bound in other functional groups against microbial processing and rapidly mineralized. Comparing data from incubated soils in chapter III and IV yielded two primary findings. First, monomers adsorption to mineral surfaces via ligand-exchange is overcome rapidly, and second, C in other functional groups, such as the positively charged amino group (phenylalanine) and the phenyl groups have been demonstrated to be retained in soil longer and thus are more important for the retention of C in soils than initially hypothesized. The former is most likely the

result of anions within soil solution adsorbing to the introduced mineral surfaces and thus, competing with the already ligand-bound carboxyl-C for binding sites. The latter might be the successive step after competitive desorption, namely preferential uptake and processing of carboxyl-C.

Overcoming mineral adsorption by competition with components within the soil solution might also explain why no threshold of adsorption strength was found: continuous equilibration between C adsorbed to minerals and dissolved molecules in soil pore water overcomes the need of the microbiome in investing energy to receive mineral-associated C and nutrients. The other way around, preferential adsorption of otherwise bioavailable nutrients can hamper microbial growth and overall metabolism as shown by Pastore et al. (2020) and phosphate limited use of glucose adsorbed to goethite as shown in chapter III.

The ways of mineral-induced C stabilization

Association with minerals protected monomer-C from microbial processing. Sorptive protection of monomers by goethite exceeded that of kaolinite and illite. The same has been demonstrated in the field for natural OC binding to goethite and illite (Chapter VI). Most interestingly, the adsorption to different minerals strongly influenced monomers CUE in soil. Three main findings here are:

1. CUE for uniformly ^{14}C labeled monomers increased linearly with increasing desorbability,
2. Soil´s boundary conditions altered CUE, and
3. CUE of monomer was always lower when incubated adsorbed to goethite.

The reason for this has been discussed within chapter III and can be summarized by CUEs being limited by the biochemical pathway the monomer is been funneled in, as well as the fact that microbes are regulating biochemistry to cope with environmental stress. One identified environmental factor was mineral-induced nutrient availability for the nearby microbiome, as shown for minerals buried in the field (chapter VII). Here, exoenzymes active in the cycling of C, N and P produced by goethite-settling microbes were significantly higher than from microbes settling on illite, or situated on the

bulk soil around the minerals. This indicates the need for microorganisms near goethite to cleave organic matter to mine nutrients and energy.

Because of goethite's high affinity to adsorb C, and N, but especially P containing molecules (but see Spohn (2024)), goethite-induced nutrient limitations might force cells to burn excess C, which would otherwise been used for anabolic processes when nutrient stoichiometry is met.

Contrary to goethite, clay minerals and illite in particular were not limiting the microbiomes nutrient availability as shown for phosphate in mineral-amended soils. In the field, illite showed even less activity of exoenzymes involved in C-cycling compared to surrounding bulk soil (Fig. 7-3). Thus, the microbiome settling on or nearby illite seems less constrained by nutrients and can process OC with higher CUEs. Therefore the way of mineral-associated organic matter cycling and stabilization differs substantially between illite and goethite: goethite renders large amounts of OC inaccessible to microbial life by adsorption. Illite (and kaolinite) bound OC on the other hand is more easily microbially processed with higher CUE and therefore fewer C loss by mineralization. Findings of this dissertation can be readily integrated into conceptual framework of Lehmann & Kleber (2015), by decipher the fate of mineral-bound OC by mineral type and P availability (Fig. 8-1).

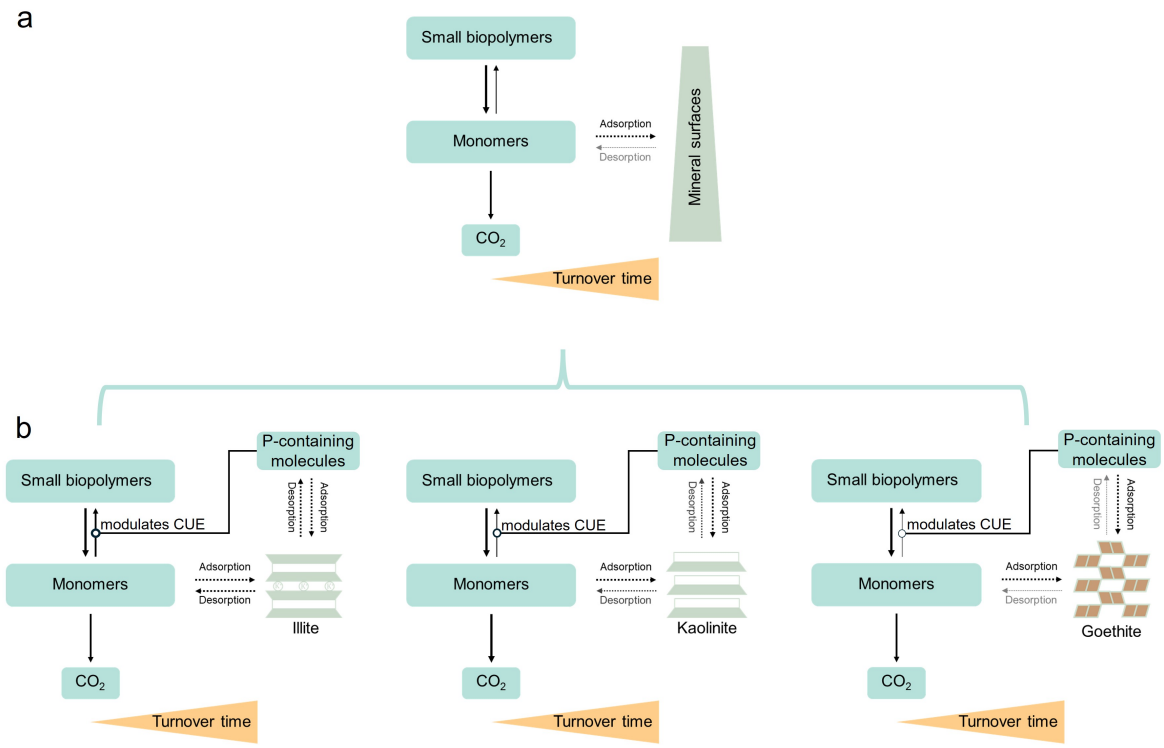

Figure 8-1. a) snippet of the soil continuum model by Lehman & Kleber (2015, with permission), linking microbial processing of small biopolymers to monomers and ultimatively to CO_2, with turnover times increasing from monomers to biopolymers. Biotic transformations (solid arrows) drive biomass synthesis, depolymerization and mineralization, abiotic transfer (dashed arrows) represent adsorption to and desorption from mineral surfaces. (b) Model adaption incorporating dissertation findings: Mineral-specific modulation of microbial carbon use efficiency (CUE) by monomers desorbability and mineral-induced P-availability, thereby tuning turnover times. Thicker arrows denote relatively greater flux rates.

Minerals not only bind P, but can also carry bioavailable forms as shown in chapter V. Interestingly, natural soil colloids highly enriched in Fe and OC delivered large quantities of potentially bioavailable P. This seems contradictory to other results at hand, where Fe oxides are the cause of microbial P deficiencies. However, Fe oxides used for within the other studies of this work were added to soil either pristine or loaded with OC far below sorption capacities. Iron-enriched, P-delivering soil colloids investigated in chapter V however contained large amounts of OC and P and thus oxides might have been saturated by organic matter. In most soil and on a global scale, minerals are rarely saturated with OC and P (Georgiou et al., 2025) (with some even argue that there is no upper limit of saturation, but see Begill et al., 2023). Findings on OC stabilization and cycling presented from slightly OC loaded and pristine minerals are therefore not superficially altered by unnatural mineral conditions. Same is also true for the described

P-delivering forest soil colloids, as they originated from sandy podzolic forest soil, whose soil conditions are typical for this kind of ecosystem but not met on the arable sites used for this dissertation. The process of podzolization led to the removal of almost all oxides except those extracted in the colloidal fraction and are therefore the only mineral sink and source of P. Combining results therefore reveals that the role of Fe oxides like goethite for soils P nutrition and impact on microbial life differ between ecosystems. They can act on a broad scale: as P sinks that hamper microbial growth in arable, fertilized fields, up to the essential sink and source for bioavailable P in nutrient-poor, sandy podzolic forest ecosystems.

Scope and limitations

The work presented here has been performed across arable land, grassland and forest sites. While the main findings were consistent across land use and experimental scales (from laboratory experiments to the field), the influence of climate and time on the fate of soil OC across a larger context was not investigated. Only soils from the warm-temperate, mid-latitude climate zone of Germany were used, restricting the validity of findings to ecosystems at hand. However, a recent study by Von Fromm et al. (2025) found similar relationships between short-range ordered minerals and soil OC. The authors analysed about 11,000 soil profiles, spanning Holdrige Life Zones from polar to tropical ecosystems and from arid to perhumid climates, suggesting the mechanisms identified in this dissertation may be more widely applicable. Besides climatic constraints, laboratory soil incubations in chapter III and IV were performed at constant moisture and temperature. Consequently, the experiments did not capture the effects of fluctuating moisture and temperature, including full wet-dry and freeze-thaw cycles, that are known as important factors in the microbial cycling of C and nutrients (Harrison-Kirk et al., 2014; Huang & Hall, 2017; Jaeger et al., 2023).

Natural soils develop over years to millennia. Globally, topsoil OC age show that mineral-associated OC has a mean turnover time of 129 years (compared to 23 years for particulate OC) (Zhou et al., 2024). The studies at hand trace mineral-OC-microbe interactions over 21-42 days (Chapter III, IV) and up to 5 years (Chapter VI, VII), hence limiting the explanatory power of this findings for larger time scales. This is however only true for OC that was not mineralized in the given time frames: namely, OC which stayed adsorbed to minerals, within the soil matrix, or was assimilated into microbial biomass. Consequently, extending this work to long-term, field-scale observations will be essential for assessing whether the mechanistic patterns identified here persist over decadal to millennial horizons that govern soil OC feedbacks.

Outlook

Future research can build on the strong points of this dissertation and address the limitations of the experimental setups as described above. First, extending the incubation period of labeled mineral-associated organic monomers could reveal the longer-term stability of C assimilated into microbial biomass and residual mineral-associated OC. From here, the boundary conditions of the soil system can be manipulated: field-like changes in environmental factors can be created by subjecting the soil to dry-wet or freeze-thaw cycles, simulating natural environmental fluctuations that drive soil OC transformation. Next, the impact of human activities on mineral-associated organic matter cycling can be tested by physically disrupting incubated soil to mimic plowing, thereby overcoming spatial separation between substrates and microbes. Soil OC studies could also be coupled with pollutant research: for example, adding manure or sewage sludge containing pharmaceuticals to examine their effects on mineral-associated OC dynamics.

Beyond varying boundary conditions and incubation times, both minerals and organic substrates can become more representative to conditions in the fields. A simple, straight-forward approach can be the use of small polymers as substrate, and clay minerals artificially coated with different amounts of (oxyhydr-)oxides as mineral phases, as they are commonly found in the environment. In order to achieve a more accurate representation of real soil conditions, the purification of minerals extracted from soil and subsequent loading with substrates also offers a viable approach.

The concept of burying pristine minerals in grassland and forest soil, as described within the studies in chapter VI and VII could be extended to arable soil as well. Effects of differing nutrient availabilities by otherwise similar soil properties on mineral-associated organic matter cycling can be investigated by burying minerals in long-term fertilization experiments, like the Thyrow field test (see https://www.agrar.hu-berlin.de/de/institut/einrichtungen/freiland/thyrow/dau_versuch). Moreover, pre-loading minerals with labeled OC before burial would allow turnover rates under true field conditions to be tracked: sampling soils above and below the buried minerals would elucidate compound transport and transformation.

Conclusion

The dissertation at hand set out to investigate how sorption to minerals shapes longevity and cycling of organic carbon in soil. This overarching research question was addressed in six studies. The ability to derive the thermodynamics of adsorption of organic ligands to mineral surfaces from calorimetric experiments has been demonstrated for the first time, revealing that mineral crystallinity influences thermodynamics of adsorption (Chapter II). The work presented in Chapter III&IV pioneered a combination of sorption-desorption and incubation experiments. Here, it is shown that the microbial utilization of organic carbon not only differs between molecules, but are decisively influenced by interactions with minerals. Furthermore, the long standing view that that inner-sphere complexation of carboxyl groups with minerals render these carbon sources inaccessible to microbes is being questioned. The ability of fine-grained minerals to not only act as sinks, but also a source and carrier of phosphate was demonstrated within chapter V, linking carbon and phosphorus cycle. Work presented in chapter VI and VII revealed that formation of sub decadal mineral-associated organic matter, microbial communities and there functioning are mineral-dependent and modified by land use. Together, these findings show that minerals shape the cycling and fate of mineral-associated organic matter, by providing habitats that are either supportive or hostile to microbial life.

Utilizing a mix of lab experiments as well as field studies offered robust insights in organic carbon cycling, with special advantages in disentangling the effect of adsorption-desorption processes of organic molecules to minerals and its subsequent microbial processing. However, limitations remain by the restricted timeframes investigated (minutes up to five years vs. OC persisting in soil up to millennia), limited geographical variety (soils only from humid, temperate Germany), and the separation of minerals used compared to the complex mixtures found within the natural soil environments may affect generalizability. Therefore, this dissertation lay a foundation for future research, to confirm or disprove its main findings by investigating organo-mineral-microbe relationships in soils on a global scale, on longer time frames, and by the study of complex boundary conditions. In summary, this work provides new insights and refines existing theories on mineral-associated organic matter cycling by highlighting

how the interplay between inanimate organic matter, minerals, and microbes shape carbon accumulation and turnover in soil.

References

Achard, F. K. (1786). *Chemische Untersuchung des Torfs.* Crell's Chem. Ann, 2, 391-403.

Aitkenhead, J. A., & McDowell, W. H. (2000). Soil C:N ratio as a predictor of annual riverine DOC flux at local and global scales. *Global Biogeochemical Cycles*, *14*(1), 127–138. https://doi.org/10.1029/1999GB900083

Akagi, J., Zsolnay, Á., & Bastida, F. (2007). Quantity and spectroscopic properties of soil dissolved organic matter (DOM) as a function of soil sample treatments: Air-drying and pre-incubation. *Chemosphere*, *69*(7), 1040–1046. https://doi.org/10.1016/j.chemosphere.2007.04.036

Alef, K., & Nannipieri, P. (1995). *Methods in applied soil microbiology and biochemistry*. Academic Press.

Alt, F., Oelmann, Y., Herold, N., Schrumpf, M., & Wilcke, W. (2011). Phosphorus partitioning in grassland and forest soils of Germany as related to land-use type, management intensity, and land use–related pH. *Journal of Plant Nutrition and Soil Science*, *174*(2), 195–209. https://doi.org/10.1002/jpln.201000142

Amadou, I., Faucon, M.-P., & Houben, D. (2022). Role of soil minerals on organic phosphorus availability and phosphorus uptake by plants. *Geoderma*, *428*, 116125. https://doi.org/10.1016/j.geoderma.2022.116125

Anacker, B. L., Seastedt, T. R., Halward, T. M., & Lezberg, A. L. (2021). Soil carbon and plant richness relationships differ among grassland types, disturbance history and plant functional groups. *Oecologia*, *196*(4), 1153–1166. https://doi.org/10.1007/s00442-021-04992-x

Andivia, E., Rolo, V., Jonard, M., Formánek, P., & Ponette, Q. (2016). Tree species identity mediates mechanisms of top soil carbon sequestration in a Norway spruce and European beech mixed forest. *Annals of Forest Science*, *73*(2), Article 2. https://doi.org/10.1007/s13595-015-0536-z

Andrino, A., Guggenberger, G., Kernchen, S., Mikutta, R., Sauheitl, L., & Boy, J. (2021). Production of Organic Acids by Arbuscular Mycorrhizal Fungi and Their Contribution in the Mobilization of Phosphorus Bound to Iron Oxides. *Frontiers in Plant Science*, *12*. https://doi.org/10.3389/fpls.2021.661842

Angst, G., Frouz, J., van Groenigen, J. W., Scheu, S., Kögel-Knabner, I., & Eisenhauer, N. (2022). Earthworms as catalysts in the formation and stabilization of soil microbial necromass. *Global Change Biology*, *28*(16), 4775–4782. https://doi.org/10.1111/gcb.16208

Angst, G., Messinger, J., Greiner, M., Häusler, W., Hertel, D., Kirfel, K., Kögel-Knabner, I., Leuschner, C., Rethemeyer, J., & Mueller, C. W. (2018). Soil organic carbon stocks in topsoil and subsoil controlled by parent material, carbon input in the rhizosphere, and microbial-derived compounds. *Soil Biology and Biochemistry*, *122*, 19–30. https://doi.org/10.1016/j.soilbio.2018.03.026

Angst, G., Mueller, K. E., Castellano, M. J., Vogel, C., Wiesmeier, M., & Mueller, C. W. (2023). Unlocking complex soil systems as carbon sinks: Multi-pool management as the key. *Nature Communications*, *14*(1), 2967. https://doi.org/10.1038/s41467-023-38700-5

Angst, G., Mueller, K. E., Nierop, K. G. J., & Simpson, M. J. (2021). Plant- or microbial-derived? A review on the molecular composition of stabilized soil organic matter. *Soil Biology and Biochemistry*, *156*, 108189. https://doi.org/10.1016/j.soilbio.2021.108189

Antelo, J., Avena, M., Fiol, S., López, R., & Arce, F. (2005). Effects of pH and ionic strength on the adsorption of phosphate and arsenate at the goethite–water interface. *Journal of Colloid and Interface Science*, *285*(2), 476–486. https://doi.org/10.1016/j.jcis.2004.12.032

Apostolakis, A., Schöning, I., Klaus, V. H., Michalzik, B., Bischoff, W.-A., Boeddinghaus, R. S., Bolliger, R., Fischer, M., Hölzel, N., Kandeler, E., Kleinebecker, T., Manning, P., Marhan, S., Neyret, M., Oelmann, Y., Prati, D., van Kleunen, M., Schwarz, A., Schurig, E., & Schrumpf, M. (2022). Direct and plant community mediated effects of management intensity on annual nutrient leaching risk in temperate grasslands. *Nutrient Cycling in Agroecosystems*, *123*(3), 83–104. https://doi.org/10.1007/s10705-022-10209-1

Atkins, P. W., & de Paula, J. (2013). *Physikalische Chemie* (Fünfte Auflage). Wiley-VCH.

Bailey, S. W. (1991). *Hydrous phyllosilicates: Exclusive of micas*. Mineralogical society of America.

Baldwin, D. S. (1998). Reactive “organic” phosphorus revisited. *Water Research*, *32*(8), 2265–2270. https://doi.org/10.1016/S0043-1354(97)00474-0

Balesdent, J., Chenu, C., & Balabane, M. (2000). Relationship of soil organic matter dynamics to physical protection and tillage. *Soil and Tillage Research*, *53*(3–4), 215–230. https://doi.org/10.1016/S0167-1987(99)00107-5

Balogh-Brunstad, Z., Keller, C. K., Shi, Z., Wallander, H., & Stipp, S. L. S. (2017). Ectomycorrhizal Fungi and Mineral Interactions in the Rhizosphere of Scots and Red Pine Seedlings. *Soils*, *1*(1), Article 1. https://doi.org/10.3390/soils1010005

Banchio, A. J., Nägele, G., & Bergenholtz, J. (1999). Viscoelasticity and generalized Stokes–Einstein relations of colloidal dispersions. *The Journal of Chemical Physics*, *111*(18), 8721–8740. https://doi.org/10.1063/1.480212

Bartlett, M. S., & Fowler, R. H. (1997). Properties of sufficiency and statistical tests. *Proceedings of the Royal Society of London. Series A - Mathematical and Physical Sciences*, *160*(901), 268–282. https://doi.org/10.1098/rspa.1937.0109

Bastos, M., Abian, O., Johnson, C. M., Ferreira-da-Silva, F., Vega, S., Jimenez-Alesanco, A., Ortega-Alarcon, D., & Velazquez-Campoy, A. (2023). Isothermal titration calorimetry. *Nature Reviews Methods Primers*, *3*(1), 17. https://doi.org/10.1038/s43586-023-00199-x

Batjes, N. H. (2014). Total carbon and nitrogen in the soils of the world. *European Journal of Soil Science*, *65*(1), 10–21. https://doi.org/10.1111/ejss.12114_2

Begill, N., Don, A., & Poeplau, C. (2023). No detectable upper limit of mineral-associated organic carbon in temperate agricultural soils. *Global Change Biology*, *29*(16), 4662–4669. https://doi.org/10.1111/gcb.16804

Benito-Carnero, G., Gartzia-Bengoetxea, N., Arias-González, A., & Rousk, J. (2021). Low-quality carbon and lack of nutrients result in a stronger fungal than bacterial home-field advantage during the decomposition of leaf litter. *Functional Ecology*, *35*(8), 1783–1796. https://doi.org/10.1111/1365-2435.13822

Benjamini, Y., & Hochberg, Y. (1995). Controlling the False Discovery Rate: A Practical and Powerful Approach to Multiple Testing. *Journal of the Royal Statistical Society. Series B (Methodological)*, *57*(1), 289–300.

Berendsen, R. L., Pieterse, C. M. J., & Bakker, P. A. H. M. (2012). The rhizosphere microbiome and plant health. *Trends in Plant Science*, *17*(8), 478–486. https://doi.org/10.1016/j.tplants.2012.04.001

Bergaya, F., & Lagaly, G. (Eds.). (2013). *Handbook of clay science* (2nd ed). Elsevier.

Berner, D., Marhan, S., Keil, D., Poll, C., Schützenmeister, A., Piepho, H.-P., & Kandeler, E. (2011). Land-use intensity modifies spatial distribution and function of soil microorganisms in grasslands. *Pedobiologia*, *54*(5), 341–351. https://doi.org/10.1016/j.pedobi.2011.08.001

Blagodatskaya, E. V., Blagodatsky, S. A., Anderson, T. -H., & Kuzyakov, Y. (2009). Contrasting effects of glucose, living roots and maize straw on microbial growth kinetics and substrate availability in soil. *European Journal of Soil Science*, *60*(2), 186–197. https://doi.org/10.1111/j.1365-2389.2008.01103.x

Blakey, B. C., & James, D. F. (2003). The viscous behaviour and structure of aqueous suspensions of goethite. *Colloids and Surfaces A: Physicochemical and Engineering Aspects*, *231*(1–3), 19–30. https://doi.org/10.1016/j.colsurfa.2003.08.019

Blüthgen, N., Dormann, C. F., Prati, D., Klaus, V. H., Kleinebecker, T., Hölzel, N., Alt, F., Boch, S., Gockel, S., Hemp, A., Müller, J., Nieschulze, J., Renner, S. C., Schöning, I., Schumacher, U., Socher, S. A., Wells, K., Birkhofer, K., Buscot, F., … Weisser, W. W. (2012). A quantitative index of land-use intensity in grasslands: Integrating mowing, grazing and fertilization. *Basic and Applied Ecology*, *13*(3), 207–220. https://doi.org/10.1016/j.baae.2012.04.001

Boberg, J. B., Finlay, R. D., Stenlid, J., Ekblad, A., & Lindahl, B. D. (2014). Nitrogen and Carbon Reallocation in Fungal Mycelia during Decomposition of Boreal Forest Litter. *PLOS ONE*, *9*(3), e92897. https://doi.org/10.1371/journal.pone.0092897

Boeddinghaus, R. S., Marhan, S., Gebala, A., Haslwimmer, H., Vieira, S., Sikorski, J., Overmann, J., Soares, M., Rousk, J., Rennert, T., & Kandeler, E. (2021). The mineralosphere—Interactive zone of microbial colonization and carbon use in grassland soils. *Biology and Fertility of Soils*, *57*(5), 587–601. https://doi.org/10.1007/s00374-021-01551-7

Bolan, N. S., Adriano, D. C., Kunhikrishnan, A., James, T., McDowell, R., & Senesi, N. (2011). Dissolved Organic Matter. In *Advances in Agronomy* (Vol. 110, pp. 1–75). Elsevier. https://doi.org/10.1016/B978-0-12-385531-2.00001-3

Bollyn, J., Castelein, L., & Smolders, E. (2019). Fate and bioavailability of phosphorus loaded to iron oxyhydroxide nanoparticles added to weathered soils. *Plant and Soil*, *438*(1), 297–311. https://doi.org/10.1007/s11104-019-04008-x

Bollyn, J., Faes, J., Fritzsche, A., & Smolders, E. (2017). Colloidal-Bound Polyphosphates and Organic Phosphates Are Bioavailable: A Nutrient Solution Study. *Journal of Agricultural and Food Chemistry*, *65*(32), 6762–6770. https://doi.org/10.1021/acs.jafc.7b01483

Boos, E. F., Bruun, S., & Magid, J. (2023). Priming is frequently overestimated in studies using 14C-labelled substrates due to underestimation of 14CO2 activity. *Soil Biology and Biochemistry*, *181*, 109020. https://doi.org/10.1016/j.soilbio.2023.109020

Boos, E. F., Magid, J., Bruun, S., & Jørgensen, N. O. G. (2022). Liquid scintillation counting can underestimate 14C-activity of 14CO2 trapped in NaOH. *Soil Biology and Biochemistry*, *166*, 108576. https://doi.org/10.1016/j.soilbio.2022.108576

Bradford, M. A., Davies, C. A., Frey, S. D., Maddox, T. R., Melillo, J. M., Mohan, J. E., Reynolds, J. F., Treseder, K. K., & Wallenstein, M. D. (2008). Thermal adaptation of soil microbial respiration to elevated temperature. *Ecology Letters*, *11*(12), 1316–1327. https://doi.org/10.1111/j.1461-0248.2008.01251.x

Bramble, D. S. E., Ulrich, S., Schöning, I., Mikutta, R., Brandt, L., Poll, C., Kandeler, E., Mikutta, C., Konrad, A., Siemens, J., Yang, Y., Polle, A., Schall, P., Ammer, C., Kaiser, K., & Schrumpf, M. (2024). Formation of mineral-associated organic matter in temperate soils is primarily controlled by mineral type and modified by land use and management intensity. *Global Change Biology*, *30*(1), e17024. https://doi.org/10.1111/gcb.17024

Brandt, L., Stache, F., Poll, C., Bramble, D. S., Schöning, I., Schrumpf, M., Ulrich, S., Kaiser, K., Mikutta, R., Mikutta, C., Oelmann, Y., Konrad, A., Siemens, J., & Kandeler, E. (2023). Mineral type and land-use intensity control composition and functions of microorganisms colonizing pristine minerals in grassland soils. *Soil Biology and Biochemistry*, *182*, 109037. https://doi.org/10.1016/j.soilbio.2023.109037

Brown, R. W., & Jones, D. L. (2024). Plasticity of microbial substrate carbon use efficiency in response to changes in plant carbon input and soil organic matter status. *Soil Biology and Biochemistry*, *188*, 109230. https://doi.org/10.1016/j.soilbio.2023.109230

Cabrol, L., Quéméneur, M., & Misson, B. (2017). Inhibitory effects of sodium azide on microbial growth in experimental resuspension of marine sediment. *Journal of Microbiological Methods*, *133*, 62–65. https://doi.org/10.1016/j.mimet.2016.12.021

Cai, P., Liu, X., Ji, D., Yang, S., Walker, S. L., Wu, Y., Gao, C., & Huang, Q. (2018). Impact of soil clay minerals on growth, biofilm formation, and virulence gene expression of Escherichia coli O157:H7. *Environmental Pollution*, *243*, 953–960. https://doi.org/10.1016/j.envpol.2018.09.032

Camenzind, T., Mason-Jones, K., Mansour, I., Rillig, M. C., & Lehmann, J. (2023). Formation of necromass-derived soil organic carbon determined by microbial death pathways. *Nature Geoscience*, *16*(2), 115–122. https://doi.org/10.1038/s41561-022-01100-3

Celi, L., Cerli, C., Turner, B. L., Santoni, S., & Bonifacio, E. (2013). Biogeochemical cycling of soil phosphorus during natural revegetation of Pinus sylvestris on disused sand quarries in Northwestern Russia. *Plant and Soil*, *367*(1), 121–134. https://doi.org/10.1007/s11104-013-1627-y

Chacon, S. S., García-Jaramillo, M., Liu, S. Y., Ahmed, M., & Kleber, M. (2018). Differential capacity of kaolinite and birnessite to protect surface associated proteins against thermal degradation. *Soil Biology and Biochemistry*, *119*, 101–109. https://doi.org/10.1016/j.soilbio.2018.01.020

Chacon, S. S., Reardon, P. N., Burgess, C. J., Purvine, S., Chu, R. K., Clauss, T. R., Walter, E., Myrold, D. D., Washton, N., & Kleber, M. (2019). Mineral Surfaces as Agents of Environmental Proteolysis: Mechanisms and Controls. *Environmental Science & Technology*, *53*(6), 3018–3026. https://doi.org/10.1021/acs.est.8b05583

Chappell, A., Baldock, J., & Sanderman, J. (2016). The global significance of omitting soil erosion from soil organic carbon cycling schemes. *Nature Climate Change*, *6*(2), 187–191. https://doi.org/10.1038/nclimate2829

Chen, S., Wang, W., Xu, W., Wang, Y., Wan, H., Chen, D., Tang, Z., Tang, X., Zhou, G., Xie, Z., Zhou, D., Shangguan, Z., Huang, J., He, J.-S., Wang, Y., Sheng, J., Tang, L., Li, X., Dong, M., … Bai, Y. (2018). Plant diversity enhances productivity and soil carbon storage. *Proceedings of the National Academy of Sciences*, *115*(16), 4027–4032. https://doi.org/10.1073/pnas.1700298114

Cheng, T., & Saiers, J. E. (2015). Effects of dissolved organic matter on the co-transport of mineral colloids and sorptive contaminants. *Journal of Contaminant Hydrology*, *177–178*, 148–157. https://doi.org/10.1016/j.jconhyd.2015.04.005

Claveria-Gimeno, R., Lanuza, P. M., Morales-Chueca, I., Jorge-Torres, O. C., Vega, S., Abian, O., Esteller, M., & Velazquez-Campoy, A. (2017). The intervening domain from MeCP2 enhances the DNA affinity of the methyl binding domain and provides an independent DNA interaction site. *Scientific Reports*, *7*(1), 41635. https://doi.org/10.1038/srep41635

Colin, Y., Nicolitch, O., Turpault, M.-P., & Uroz, S. (2017). Mineral Types and Tree Species Determine the Functional and Taxonomic Structures of Forest Soil Bacterial Communities. *Applied and Environmental Microbiology*, *83*(5), e02684-16. https://doi.org/10.1128/AEM.02684-16

Conant, R. T., Cerri, C. E. P., Osborne, B. B., & Paustian, K. (2017). Grassland management impacts on soil carbon stocks: A new synthesis. *Ecological Applications*, *27*(2), 662–668. https://doi.org/10.1002/eap.1473

Cong, W.-F., van Ruijven, J., Mommer, L., De Deyn, G. B., Berendse, F., & Hoffland, E. (2014). Plant species richness promotes soil carbon and nitrogen stocks in grasslands without legumes. *Journal of Ecology*, *102*(5), 1163–1170. https://doi.org/10.1111/1365-2745.12280

Cools, N., Vesterdal, L., De Vos, B., Vanguelova, E., & Hansen, K. (2014). Tree species is the major factor explaining C:N ratios in European forest soils. *Forest Ecology and Management*, *311*, 3–16. https://doi.org/10.1016/j.foreco.2013.06.047

Córdova, S. C., Olk, D. C., Dietzel, R. N., Mueller, K. E., Archontouilis, S. V., & Castellano, M. J. (2018). Plant litter quality affects the accumulation rate, composition, and stability of mineral-associated soil organic matter. *Soil Biology and Biochemistry*, *125*, 115–124. https://doi.org/10.1016/j.soilbio.2018.07.010

Cornell, R. M., & Schwertmann, U. (2003). *The iron oxides: Structure, properties, reactions, occurrences and uses* (2., compl. rev. and extended ed., repr). Wiley-VCH.

Costa, O. Y. A., Raaijmakers, J. M., & Kuramae, E. E. (2018). Microbial Extracellular Polymeric Substances: Ecological Function and Impact on Soil Aggregation. *Frontiers in Microbiology*, *9*. https://doi.org/10.3389/fmicb.2018.01636

Cotrufo, M. F., Haddix, M. L., Kroeger, M. E., & Stewart, C. E. (2022). The role of plant input physical-chemical properties, and microbial and soil chemical diversity on the formation of particulate and mineral-associated organic matter. *Soil Biology and Biochemistry*, *168*, 108648. https://doi.org/10.1016/j.soilbio.2022.108648

Cotrufo, M. F., & Lavallee, J. M. (2022). Chapter One - Soil organic matter formation, persistence, and functioning: A synthesis of current understanding to inform its conservation and regeneration. In D. L. Sparks (Ed.), *Advances in Agronomy* (Vol. 172, pp. 1–66). Academic Press. https://doi.org/10.1016/bs.agron.2021.11.002

Cotrufo, M. F., Soong, J. L., Horton, A. J., Campbell, E. E., Haddix, M. L., Wall, D. H., & Parton, W. J. (2015). Formation of soil organic matter via biochemical and physical pathways of litter mass loss. *Nature Geoscience*, *8*(10), 776–779. https://doi.org/10.1038/ngeo2520

Cotrufo, M. F., Wallenstein, M. D., Boot, C. M., Denef, K., & Paul, E. (2013). The Microbial Efficiency-Matrix Stabilization (MEMS) framework integrates plant litter decomposition with soil organic matter stabilization: Do labile plant inputs form stable soil organic matter? *Global Change Biology*, *19*(4), 988–995. https://doi.org/10.1111/gcb.12113

Creamer, C. A., Foster, A. L., Lawrence, C., McFarland, J., Schulz, M., & Waldrop, M. P. (2019). Mineralogy dictates the initial mechanism of microbial necromass association. *Geochimica et Cosmochimica Acta*, *260*, 161–176. https://doi.org/10.1016/j.gca.2019.06.028

Crow, S. E., Lajtha, K., Filley, T. R., Swanston, C. W., Bowden, R. D., & Caldwell, B. A. (2009). Sources of plant-derived carbon and stability of organic matter in soil: Implications for global change. *Global Change Biology*, *15*(8), 2003–2019. https://doi.org/10.1111/j.1365-2486.2009.01850.x

Dahlgren, R. A., & Marrett, D. J. (1991). Organic Carbon Sorption in Arctic and Subalpine Spodosol B Horizons. *Soil Science Society of America Journal*, *55*(5), 1382–1390. https://doi.org/10.2136/sssaj1991.03615995005500050030x

Dalkmann, P., Willaschek, E., Schiedung, H., Bornemann, L., Siebe, C., & Siemens, J. (2014). Long-term Wastewater Irrigation Reduces Sulfamethoxazole Sorption, but Not Ciprofloxacin Binding, in Mexican Soils. *Journal of Environmental Quality*, *43*(3), 964–970. https://doi.org/10.2134/jeq2013.11.0473

Datta, R., Anand, S., Moulick, A., Baraniya, D., Pathan, S. I., Rejsek, K., Vranova, V., Sharma, M., Sharma, D., Kelkar, A., & Formanek, P. (2017). How enzymes are adsorbed on soil solid phase and factors limiting its activity: A Review. *International Agrophysics*, *31*(2), 287–302. https://doi.org/10.1515/intag-2016-0049

Davis, J. A., & Hayes, K. F. (Eds.). (1987). *Geochemical Processes at Mineral Surfaces* (Vol. 323). American Chemical Society. https://doi.org/10.1021/bk-1987-0323

Davison, W., & Zhang, H. (2012). Progress in understanding the use of diffusive gradients in thin films (DGT) – back to basics. *Environmental Chemistry*, *9*(1), 1–13. https://doi.org/10.1071/EN11084

de Jonge, L. W., Moldrup, P., Rubæk, G. H., Schelde, K., & Djurhuus, J. (2004). Particle Leaching and Particle-Facilitated Transport of Phosphorus at Field Scale. *Vadose Zone Journal*, *3*(2), 462–470. https://doi.org/10.2136/vzj2004.0462

de Vries, F. T., Hoffland, E., van Eekeren, N., Brussaard, L., & Bloem, J. (2006). Fungal/bacterial ratios in grasslands with contrasting nitrogen management. *Soil Biology and Biochemistry*, *38*(8), 2092–2103. https://doi.org/10.1016/j.soilbio.2006.01.008

Degryse, F., Smolders, E., Zhang, H., & Davison, W. (2009). Predicting availability of mineral elements to plants with the DGT technique: A review of experimental data and interpretation by modelling. *Environmental Chemistry*, *6*(3), 198–218. https://doi.org/10.1071/EN09010

Dippold, M. A., & Kuzyakov, Y. (2013). Biogeochemical transformations of amino acids in soil assessed by position-specific labelling. *Plant and Soil*, *373*(1–2), 385–401. https://doi.org/10.1007/s11104-013-1764-3

Dippold, M., Biryukov, M., & Kuzyakov, Y. (2014). Sorption affects amino acid pathways in soil: Implications from position-specific labeling of alanine. *Soil Biology and Biochemistry*, *72*, 180–192. https://doi.org/10.1016/j.soilbio.2014.01.015

Ditterich, F., Poll, C., Pronk, G. J., Heister, K., Chandran, A., Rennert, T., Kögel-Knabner, I., & Kandeler, E. (2016). Succession of soil microbial communities and enzyme activities in artificial soils. *Pedobiologia*, *59*(3), 93–104. https://doi.org/10.1016/j.pedobi.2016.03.002

Dong, H., Huang, L., Zhao, L., Zeng, Q., Liu, X., Sheng, Y., Shi, L., Wu, G., Jiang, H., Li, F., Zhang, L., Guo, D., Li, G., Hou, W., & Chen, H. (2022). A critical review of mineral–microbe interaction and co-evolution: Mechanisms and applications. *National Science Review*, *9*(10), nwac128. https://doi.org/10.1093/nsr/nwac128

Dultz, S., Woche, S. K., Mikutta, R., Schrapel, M., & Guggenberger, G. (2019). Size and charge constraints in microaggregation: Model experiments with mineral particle size fractions. *Applied Clay Science*, *170*, 29–40. https://doi.org/10.1016/j.clay.2019.01.002

Dunphy Guzman, K. A., Finnegan, M. P., & Banfield, J. F. (2006). Influence of Surface Potential on Aggregation and Transport of Titania Nanoparticles. *Environmental Science & Technology*, *40*(24), 7688–7693. https://doi.org/10.1021/es060847g

Echigo, T., Hatta, T., Nemoto, S., & Takizawa, S. (2012). X-ray photoelectron spectroscopic study on the goethites with variations in crystallinity and morphology: Their effects on surface hydroxyl concentration. *Physics and Chemistry of Minerals*, *39*(9), 769–778. https://doi.org/10.1007/s00269-012-0531-y

Eilers, P. H. C., & Boelens, H. F. M. (2005). *Baseline Correction with Asymmetric Least Squares Smoothing*. *Leiden-. Univ. Med. Cent. Rep. 1, 5 (2005)*.

Eze, S., Palmer, S. M., & Chapman, P. J. (2018). Soil organic carbon stock in grasslands: Effects of inorganic fertilizers, liming and grazing in different climate settings. *Journal of Environmental Management*, *223*, 74–84. https://doi.org/10.1016/j.jenvman.2018.06.013

Fageria, N. K. (2012). Role of Soil Organic Matter in Maintaining Sustainability of Cropping Systems. *Communications in Soil Science and Plant Analysis*, *43*(16), 2063–2113. https://doi.org/10.1080/00103624.2012.697234

Fang, Y., Fu, J., Tao, C., Liu, P., & Cui, B. (2020). Mechanical properties and antibacterial activities of novel starch-based composite films incorporated with salicylic acid. *International Journal of Biological Macromolecules*, *155*, 1350–1358. https://doi.org/10.1016/j.ijbiomac.2019.11.110

Fanin, N., Kardol, P., Farrell, M., Nilsson, M.-C., Gundale, M. J., & Wardle, D. A. (2019). The ratio of Gram-positive to Gram-negative bacterial PLFA markers as an indicator of carbon availability in organic soils. *Soil Biology and Biochemistry*, *128*, 111–114. https://doi.org/10.1016/j.soilbio.2018.10.010

Feng, W., Plante, A. F., & Six, J. (2013). Improving estimates of maximal organic carbon stabilization by fine soil particles. *Biogeochemistry*, *112*(1–3), 81–93. https://doi.org/10.1007/s10533-011-9679-7

Fetzer, J., Loeppmann, S., Frossard, E., Manzoor, A., Brödlin, D., Kaiser, K., & Hagedorn, F. (2021). Leaching of Phosphomonoesterase Activities in Beech Forest Soils: Consequences for Phosphorus Forms and Mobility. *Frontiers in Forests and Global Change*, *4*. https://doi.org/10.3389/ffgc.2021.684069

Filius, J. D., Lumsdon, D. G., Meeussen, J. C. L., Hiemstra, T., & Van Riemsdijk, W. H. (2000). Adsorption of fulvic acid on goethite. *Geochimica et Cosmochimica Acta*, *64*(1), 51–60. https://doi.org/10.1016/S0016-7037(99)00176-3

Fischer, M., Bossdorf, O., Gockel, S., Hänsel, F., Hemp, A., Hessenmöller, D., Korte, G., Nieschulze, J., Pfeiffer, S., Prati, D., Renner, S., Schöning, I., Schumacher, U., Wells, K., Buscot, F., Kalko, E. K. V., Linsenmair, K. E., Schulze, E.-D., & Weisser, W. W. (2010). Implementing large-scale and long-term functional biodiversity research: The Biodiversity Exploratories. *Basic and Applied Ecology*, *11*(6), 473–485. https://doi.org/10.1016/j.baae.2010.07.009

Flury, M., & Aramrak, S. (2017). Role of air-water interfaces in colloid transport in porous media: A review. *Water Resources Research*, *53*(7), 5247–5275. https://doi.org/10.1002/2017WR020597

Fornara, D. A., & Tilman, D. (2012). Soil carbon sequestration in prairie grasslands increased by chronic nitrogen addition. *Ecology*, *93*(9), 2030–2036. https://doi.org/10.1890/12-0292.1

Franzluebbers, A. J., & Stuedemann, J. A. (2009). Soil-profile organic carbon and total nitrogen during 12 years of pasture management in the Southern Piedmont USA. *Agriculture, Ecosystems & Environment*, *129*(1), 28–36. https://doi.org/10.1016/j.agee.2008.06.013

Freire, E., Mayorga, O. L., & Straume, M. (1990). Isothermal titration calorimetry. *Analytical Chemistry*, *62*(18), 950A-959A. https://doi.org/10.1021/ac00217a002

Freundlich, H. (1907). Über die Adsorption in Lösungen. *Zeitschrift für Physikalische Chemie*, *57U*(1), 385–470. https://doi.org/10.1515/zpch-1907-5723

Frey, S. D., Six, J., & Elliott, E. T. (2003). Reciprocal transfer of carbon and nitrogen by decomposer fungi at the soil–litter interface. *Soil Biology and Biochemistry*, *35*(7), 1001–1004. https://doi.org/10.1016/S0038-0717(03)00155-X

Friedlingstein, P., O'Sullivan, M., Jones, M. W., Andrew, R. M., Gregor, L., Hauck, J., Le Quéré, C., Luijkx, I. T., Olsen, A., Peters, G. P., Peters, W., Pongratz, J., Schwingshackl, C., Sitch, S., Canadell, J. G., Ciais, P., Jackson, R. B., Alin, S. R., Alkama, R., … Zheng, B. (2022). Global Carbon Budget 2022. *Earth System Science Data*, *14*(11), 4811–4900. https://doi.org/10.5194/essd-14-4811-2022

Frissel, M. J. (1961). *THE ADSORPTION OF SOME ORGANIC COMPOUNDS, ESPECIALLY HERBICIDES, ON CLAY MINERALS*.

Frostegård, Å., Tunlid, A., & Bååth, E. (1991). Microbial biomass measured as total lipid phosphate in soils of different organic content. *Journal of Microbiological Methods*, *14*(3), 151–163. https://doi.org/10.1016/0167-7012(91)90018-L

Gallego-Urrea, J. A., Tuoriniemi, J., & Hassellöv, M. (2011). Applications of particle-tracking analysis to the determination of size distributions and concentrations of nanoparticles in environmental, biological and food samples. *TrAC Trends in Analytical Chemistry*, *30*(3), 473–483. https://doi.org/10.1016/j.trac.2011.01.005

Gan, H. Y., Schöning, I., Schall, P., Ammer, C., & Schrumpf, M. (2020). Soil Organic Matter Mineralization as Driven by Nutrient Stoichiometry in Soils Under Differently Managed Forest Stands. *Frontiers in Forests and Global Change*, *3*. https://doi.org/10.3389/ffgc.2020.00099

Gao, J., Jansen, B., Cerli, C., Helmus, R., Mikutta, R., Dultz, S., Guggenberger, G., Vogel, C., & Kalbitz, K. (2018). Organic matter coatings of soil minerals affect adsorptive interactions with phenolic and amino acids. *European Journal of Soil Science*, *69*(4), 613–624. https://doi.org/10.1111/ejss.12562

Garcia, K., & Zimmermann, S. D. (2014). The role of mycorrhizal associations in plant potassium nutrition. *Frontiers in Plant Science*, *5*. https://doi.org/10.3389/fpls.2014.00337

Geelhoed, J. S., Hiemstra, T., & Van Riemsdijk, W. H. (1998). Competitive Interaction between Phosphate and Citrate on Goethite. *Environmental Science & Technology*, *32*(14), 2119–2123. https://doi.org/10.1021/es970908y

Georgiou, K., Angers, D., Champiny, R. E., Cotrufo, M. F., Craig, M. E., Doetterl, S., Grandy, A. S., Lavallee, J. M., Lin, Y., Lugato, E., Poeplau, C., Rocci, K. S., Schweizer, S. A., Six, J., & Wieder, W. R. (2025). Soil Carbon Saturation: What Do We Really Know? *Global Change Biology*, *31*(5), e70197. https://doi.org/10.1111/gcb.70197

Georgiou, K., Jackson, R. B., Vindušková, O., Abramoff, R. Z., Ahlström, A., Feng, W., Harden, J. W., Pellegrini, A. F. A., Polley, H. W., Soong, J. L., Riley, W. J., & Torn, M. S. (2022). Global stocks and capacity of mineral-associated soil organic carbon. *Nature Communications*, *13*(1), 3797. https://doi.org/10.1038/s41467-022-31540-9

Gerke, J. (2010). Humic (Organic Matter)-Al(Fe)-Phosphate Complexes: An Underestimated Phosphate Form in Soils and Source of Plant-Available Phosphate. *Soil Science*, *175*(9), 417. https://doi.org/10.1097/SS.0b013e3181f1b4dd

Gilhaus, K., Boch, S., Fischer, M., Hölzel, N., Kleinebecker, T., Prati, D., Rupprecht, D., Schmitt, B., & Klaus, V. H. (2017). *Grassland management in Germany: Effects on plant diversity and vegetation composition* [PDF]. https://doi.org/10.14471/2017.37.010

Glasauer, S., Langley, S., & Beveridge, T. J. (2001). Sorption of Fe (Hydr)Oxides to the Surface of *Shewanella putrefaciens*: Cell-Bound Fine-Grained Minerals Are Not Always Formed De Novo. *Applied and Environmental Microbiology*, *67*(12), 5544–5550. https://doi.org/10.1128/AEM.67.12.5544-5550.2001

Goodman, B. A., & Lewis, D. G. (1981). MÖSSBAUER SPECTRA OF ALUMINOUS GOETHITES (α-FeOOH). *Journal of Soil Science*, *32*(3), 351–364. https://doi.org/10.1111/j.1365-2389.1981.tb01711.x

Gottselig, N., Amelung, W., Kirchner, J. W., Bol, R., Eugster, W., Granger, S. J., Hernández-Crespo, C., Herrmann, F., Keizer, J. J., Korkiakoski, M., Laudon, H., Lehner, I., Löfgren, S., Lohila, A., Macleod, C. J. A., Mölder, M., Müller, C., Nasta, P., Nischwitz, V., … Klumpp, E. (2017). Elemental Composition of Natural Nanoparticles and Fine Colloids in European Forest Stream Waters and Their Role as Phosphorus Carriers. *Global Biogeochemical Cycles*, *31*(10), 1592–1607. https://doi.org/10.1002/2017GB005657

Gottselig, N., Sohrt, J., Uhlig, D., Nischwitz, V., Weiler, M., & Amelung, W. (2020). Groundwater controls on colloidal transport in forest stream waters. *Science of The Total Environment*, *717*, 134638. https://doi.org/10.1016/j.scitotenv.2019.134638

Grüneberg, E., Schöning, I., Hessenmöller, D., Schulze, E.-D., & Weisser, W. W. (2013). Organic layer and clay content control soil organic carbon stocks in density fractions of differently managed German beech forests. *Forest Ecology and Management*, *303*, 1–10. https://doi.org/10.1016/j.foreco.2013.03.014

Gu, B., Mehlhorn, T. L., Liang, L., & McCarthy, J. F. (1996). Competitive adsorption, displacement, and transport of organic matter on iron oxide: I. Competitive adsorption. *Geochimica et Cosmochimica Acta*, *60*(11), 1943–1950. https://doi.org/10.1016/0016-7037(96)00059-2

Gu, Baohua., Schmitt, Juergen., Chen, Zhihong., Liang, Liyuan., & McCarthy, J. F. (1994). Adsorption and desorption of natural organic matter on iron oxide: Mechanisms and models. *Environmental Science & Technology*, *28*(1), 38–46. https://doi.org/10.1021/es00050a007

Gunina, A., & Kuzyakov, Y. (2015). Sugars in soil and sweets for microorganisms: Review of origin, content, composition and fate. *Soil Biology and Biochemistry*, *90*, 87–100. https://doi.org/10.1016/j.soilbio.2015.07.021

Guo, H., & Barnard, A. S. (2013). Naturally occurring iron oxide nanoparticles: Morphology, surface chemistry and environmental stability. *J. Mater. Chem. A*, *1*(1), 27–42. https://doi.org/10.1039/C2TA00523A

Güsewell, S., & Gessner, M. O. (2009). N: P ratios influence litter decomposition and colonization by fungi and bacteria in microcosms. *Functional Ecology*, *23*(1), 211–219. https://doi.org/10.1111/j.1365-2435.2008.01478.x

Han, L., Yang, Y., Sun, K., Zhang, B., Chen, Y., Fang, L., & Xing, B. (2021). Different mechanisms driving the preferential adsorption of dissolved organic matter by goethite and montmorillonite. *Chemical Geology*, *585*, 120560. https://doi.org/10.1016/j.chemgeo.2021.120560

Harrison-Kirk, T., Beare, M. H., Meenken, E. D., & Condron, L. M. (2014). Soil organic matter and texture affect responses to dry/wet cycles: Changes in soil organic matter fractions and relationships with C and N mineralisation. *Soil Biology and Biochemistry*, *74*, 50–60. https://doi.org/10.1016/j.soilbio.2014.02.021

Hartmann, M., & Six, J. (2022). Soil structure and microbiome functions in agroecosystems. *Nature Reviews Earth & Environment*, *4*(1), 4–18. https://doi.org/10.1038/s43017-022-00366-w

Hathaway, J. C. (1956). Procedure for clay mineral analyses used in the sedimentary petrology laboratory of the U.S. Geological Survey. *Clay Minerals Bulletin*, *3*(15), 8–13. https://doi.org/10.1180/claymin.1956.003.15.05

Haygarth, P. M., Warwick, M. S., & House, W. A. (1997). Size distribution of colloidal molybdate reactive phosphorus in river waters and soil solution. *Water Research*, *31*(3), 439–448. https://doi.org/10.1016/S0043-1354(96)00270-9

H. J. C. (1936). Humus: By Selman A. Waksman, Baltimore: Williams … Wilkins Co. XI + 494 pages, illus. 1936. *Agronomy Journal*, *28*(6), 488–489. https://doi.org/10.2134/agronj1936.00021962002800060016x

Heathwaite, L., Haygarth, P., Matthews, R., Preedy, N., & Butler, P. (2005). Evaluating Colloidal Phosphorus Delivery to Surface Waters from Diffuse Agricultural Sources. *Journal of Environmental Quality*, *34*(1), 287–298. https://doi.org/10.2134/jeq2005.0287a

Hedges, J. I., & Keil, R. G. (1999). Organic geochemical perspectives on estuarine processes: Sorption reactions and consequences. *Marine Chemistry*, *65*(1–2), 55–65. https://doi.org/10.1016/S0304-4203(99)00010-9

Helling, C. S., Chesters, G., & Corey, R. B. (1964). Contribution of Organic Matter and Clay to Soil Cation-Exchange Capacity as Affected by the pH of the Saturating Solution. *Soil Science Society of America Journal*, *28*(4), 517–520. https://doi.org/10.2136/sssaj1964.03615995002800040020x

Herold, N., Schöning, I., Michalzik, B., Trumbore, S., & Schrumpf, M. (2014). Controls on soil carbon storage and turnover in German landscapes. *Biogeochemistry*, *119*(1), 435–451. https://doi.org/10.1007/s10533-014-9978-x

Herrmann, L., Anongrak, N., Zarei, M., Schuler, U., & Spohrer, K. (2007). Factors and processes of gibbsite formation in Northern Thailand. *CATENA*, *71*(2), 279–291. https://doi.org/10.1016/j.catena.2007.01.007

Hoffland, E., Kuyper, T. W., Wallander, H., Plassard, C., Gorbushina, A. A., Haselwandter, K., Holmström, S., Landeweert, R., Lundström, U. S., Rosling, A., Sen, R., Smits, M. M., van Hees, P. A., & van Breemen, N. (2004). The role of fungi in weathering. *Frontiers in Ecology and the Environment*, *2*(5), 258–264. https://doi.org/10.1890/1540-9295(2004)002[0258:TROFIW]2.0.CO;2

Holm, S. (1979). A Simple Sequentially Rejective Multiple Test Procedure. *Scand J Statist*. https://doi.org/10.2307/4615733

Hong, Z., Yan, J., Jiang, J., Li, J., & Xu, R. (2020). Isothermal titration calorimetry as a useful tool to examine adsorption mechanisms of phosphate on gibbsite at various solution conditions. *Soil Science Society of America Journal*, *84*(4), 1110–1124. https://doi.org/10.1002/saj2.20101

Hong, Z., Yan, J., Jiang, J., Li, J., & Xu, R. (2021). Direct Quantification of Sorption Thermodynamics of Phosphate on Four Soil Colloids through Isothermal Titration Calorimetry. *ACS Earth and Space Chemistry*, *5*(2), 295–304. https://doi.org/10.1021/acsearthspacechem.0c00281

Hou, J., Tan, X., Xiang, Y., Zheng, Q., Chen, C., Sha, Z., Ren, L., Wang, M., & Tan, W. (2022). Insights into the underlying effect of Fe vacancy defects on the adsorption affinity of goethite for arsenic immobilization. *Environmental Pollution*, *314*, 120268. https://doi.org/10.1016/j.envpol.2022.120268

Houghton, J. & IPCC (Eds.). (2001). *Climate change 2001: The scientific basis ; contribution of Working Group I to the third assessment report of the Intergovernmental Panel on Climate Change*. Cambridge Univ. Press.

Hu, P., Liu, S., Ye, Y., Zhang, W., Wang, K., & Su, Y. (2018). Effects of environmental factors on soil organic carbon under natural or managed vegetation restoration. *Land Degradation & Development*, *29*(3), 387–397. https://doi.org/10.1002/ldr.2876

Huang, W., & Hall, S. J. (2017). Elevated moisture stimulates carbon loss from mineral soils by releasing protected organic matter. *Nature Communications*, *8*(1), 1774. https://doi.org/10.1038/s41467-017-01998-z

Huang, X., Terrer, C., Dijkstra, F. A., Hungate, B. A., Zhang, W., & van Groenigen, K. J. (2020). New soil carbon sequestration with nitrogen enrichment: A meta-analysis. *Plant and Soil*, *454*(1), 299–310. https://doi.org/10.1007/s11104-020-04617-x

Hussain, M. Z., Robertson, G. P., Basso, B., & Hamilton, S. K. (2020). Leaching losses of dissolved organic carbon and nitrogen from agricultural soils in the upper US Midwest. *Science of The Total Environment*, *734*, 139379. https://doi.org/10.1016/j.scitotenv.2020.139379

Hütsch, B. W., Augustin, J., & Merbach, W. (2002). Plant rhizodeposition—An important source for carbon turnover in soils. *Journal of Plant Nutrition and Soil Science*, *165*(4), 397–407. https://doi.org/10.1002/1522-2624(200208)165:4<397::AID-JPLN397>3.0.CO;2-C

Ilg, K., Siemens, J., & Kaupenjohann, M. (2005). Colloidal and Dissolved Phosphorus in Sandy Soils as Affected by Phosphorus Saturation. *Journal of Environmental Quality*, *34*(3), 926–935. https://doi.org/10.2134/jeq2004.0101

Ito, A., & Wagai, R. (2017). Global distribution of clay-size minerals on land surface for biogeochemical and climatological studies. *Scientific Data*, *4*(1), 170103. https://doi.org/10.1038/sdata.2017.103

Jackson, R. B., Lajtha, K., Crow, S. E., Hugelius, G., Kramer, M. G., & Piñeiro, G. (2017). The Ecology of Soil Carbon: Pools, Vulnerabilities, and Biotic and Abiotic Controls. *Annual Review of Ecology, Evolution, and Systematics*, *48*(1), 419–445. https://doi.org/10.1146/annurev-ecolsys-112414-054234

Jacobsen, O. H., Moldrup, P., Larsen, C., Konnerup, L., & Petersen, L. W. (1997). Particle transport in macropores of undisturbed soil columns. *Journal of Hydrology*, *196*(1), 185–203. https://doi.org/10.1016/S0022-1694(96)03291-X

Jaeger, A. C. H., Hartmann, M., Six, J., & Solly, E. F. (2023). Contrasting sensitivity of soil bacterial and fungal community composition to one year of water limitation in Scots pine mesocosms. *FEMS Microbiology Ecology*, *99*(6), fiad051. https://doi.org/10.1093/femsec/fiad051

Jeewani, P. H., Luo, Y., Yu, G., Fu, Y., He, X., Van Zwieten, L., Liang, C., Kumar, A., He, Y., Kuzyakov, Y., Qin, H., Guggenberger, G., & Xu, J. (2021). Arbuscular mycorrhizal fungi and goethite promote carbon sequestration via hyphal-aggregate

mineral interactions. *Soil Biology and Biochemistry*, *162*, 108417. https://doi.org/10.1016/j.soilbio.2021.108417

Jiang, X., Bol, R., Cade-Menun, B. J., Nischwitz, V., Willbold, S., Bauke, S. L., Vereecken, H., Amelung, W., & Klumpp, E. (2017). Colloid-bound and dissolved phosphorus species in topsoil water extracts along a grassland transect from Cambisol to Stagnosol. *Biogeosciences*, *14*(5), 1153–1164. https://doi.org/10.5194/bg-14-1153-2017

Jiang, X., Bol, R., Nischwitz, V., Siebers, N., Willbold, S., Vereecken, H., Amelung, W., & Klumpp, E. (2015). Phosphorus Containing Water Dispersible Nanoparticles in Arable Soil. *Journal of Environmental Quality*, *44*(6), 1772–1781. https://doi.org/10.2134/jeq2015.02.0085

Jilling, A., Keiluweit, M., Gutknecht, J. L. M., & Grandy, A. S. (2021). Priming mechanisms providing plants and microbes access to mineral-associated organic matter. *Soil Biology and Biochemistry*, *158*, 108265. https://doi.org/10.1016/j.soilbio.2021.108265

Jobbágy, E. G., & Jackson, R. B. (2000). THE VERTICAL DISTRIBUTION OF SOIL ORGANIC CARBON AND ITS RELATION TO CLIMATE AND VEGETATION. *Ecological Applications*, *10*(2), 423–436. https://doi.org/10.1890/1051-0761(2000)010[0423:TVDOSO]2.0.CO;2

Jódar-Reyes, A. B., Martín-Rodríguez, A., & Ortega-Vinuesa, J. L. (2001). An Enthalpic Analysis on the Aggregation of Colloidal Particles Studied by Microcalorimetry. *Journal of Colloid and Interface Science*, *237*(1), 6–10. https://doi.org/10.1006/jcis.2001.7429

Joergensen, R. G., & Wichern, F. (2008). Quantitative assessment of the fungal contribution to microbial tissue in soil. *Soil Biology and Biochemistry*, *40*(12), 2977–2991. https://doi.org/10.1016/j.soilbio.2008.08.017

Jonard, M., Fürst, A., Verstraeten, A., Thimonier, A., Timmermann, V., Potočić, N., Waldner, P., Benham, S., Hansen, K., Merilä, P., Ponette, Q., de la Cruz, A. C., Roskams, P., Nicolas, M., Croisé, L., Ingerslev, M., Matteucci, G., Decinti, B., Bascietto, M., & Rautio, P. (2015). Tree mineral nutrition is deteriorating in Europe. *Global Change Biology*, *21*(1), 418–430. https://doi.org/10.1111/gcb.12657

Jones, A. A., & Bennett, P. C. (2017). Mineral Ecology: Surface Specific Colonization and Geochemical Drivers of Biofilm Accumulation, Composition, and Phylogeny. *Frontiers in Microbiology*, *8*. https://doi.org/10.3389/fmicb.2017.00491

Jones, D. L., & Edwards, A. C. (1998). Influence of sorption on the biological utilization of two simple carbon substrates. *Soil Biology and Biochemistry*, *30*(14), 1895–1902. https://doi.org/10.1016/S0038-0717(98)00060-1

Jones, D. L., Hill, P. W., Smith, A. R., Farrell, M., Ge, T., Banning, N. C., & Murphy, D. V. (2018). Role of substrate supply on microbial carbon use efficiency and its role in interpreting soil microbial community-level physiological profiles (CLPP). *Soil Biology and Biochemistry*, *123*, 1–6. https://doi.org/10.1016/j.soilbio.2018.04.014

Joshi, H., Shirude, P. S., Bansal, V., Ganesh, K. N., & Sastry, M. (2004). Isothermal Titration Calorimetry Studies on the Binding of Amino Acids to Gold Nanoparticles. *The Journal of Physical Chemistry B*, *108*(31), 11535–11540. https://doi.org/10.1021/jp048766z

Journet, E., Balkanski, Y., & Harrison, S. P. (2014). A new data set of soil mineralogy for dust-cycle modeling. *Atmospheric Chemistry and Physics*, *14*(8), 3801–3816. https://doi.org/10.5194/acp-14-3801-2014

Kaiser, K., & Guggenberger, G. (2000). The role of DOM sorption to mineral surfaces in the preservation of organic matter in soils. *Organic Geochemistry*, *31*(7), 711–725. https://doi.org/10.1016/S0146-6380(00)00046-2

Kaiser, K., & Guggenberger, G. (2003). Mineral surfaces and soil organic matter. *European Journal of Soil Science*, *54*(2), 219–236. https://doi.org/10.1046/j.1365-2389.2003.00544.x

Kaiser, K., & Guggenberger, G. (2007). Sorptive stabilization of organic matter by microporous goethite: Sorption into small pores vs. surface complexation. *European Journal of Soil Science*, *58*(1), 45–59. https://doi.org/10.1111/j.1365-2389.2006.00799.x

Kaiser, K., Guggenberger, G., Haumaier, L., & Zech, W. (1997). Dissolved organic matter sorption on sub soils and minerals studied by ^{13}C-NMR and DRIFT spectroscopy. *European Journal of Soil Science*, *48*(2), 301–310. https://doi.org/10.1111/j.1365-2389.1997.tb00550.x

Kaiser, K., & Kalbitz, K. (2012). Cycling downwards – dissolved organic matter in soils. *Soil Biology and Biochemistry*, *52*, 29–32. https://doi.org/10.1016/j.soilbio.2012.04.002

Kaiser, K., Mikutta, R., & Guggenberger, G. (2007). Increased Stability of Organic Matter Sorbed to Ferrihydrite and Goethite on Aging. *Soil Science Society of America Journal*, *71*(3), 711–719. https://doi.org/10.2136/sssaj2006.0189

Kaiser, K., & Zech, W. (1997). Competitive Sorption of Dissolved Organic Matter Fractions to Soils and Related Mineral Phases. *Soil Science Society of America Journal*, *61*(1), 64–69. https://doi.org/10.2136/sssaj1997.03615995006100010011x

Kaiser, K., & Zech, W. (1998). Rates of Dissolved Organic Matter Release and Sorption in Forest Soils. *Soil Science*, *163*, 714–725. https://doi.org/10.1097/00010694-199809000-00005

Kalbitz, K., Schwesig, D., Rethemeyer, J., & Matzner, E. (2005). Stabilization of dissolved organic matter by sorption to the mineral soil. *Soil Biology and Biochemistry*, *37*(7), 1319–1331. https://doi.org/10.1016/j.soilbio.2004.11.028

Kandeler, E., Gebala, A., Boeddinghaus, R. S., Müller, K., Rennert, T., Soares, M., Rousk, J., & Marhan, S. (2019). The mineralosphere – Succession and physiology of bacteria and fungi colonising pristine minerals in grassland soils under different land-use intensities. *Soil Biology and Biochemistry*, *136*, 107534. https://doi.org/10.1016/j.soilbio.2019.107534

Kästner, M., Miltner, A., Thiele-Bruhn, S., & Liang, C. (2021). Microbial Necromass in Soils—Linking Microbes to Soil Processes and Carbon Turnover. *Frontiers in Environmental Science*, *9*, 756378. https://doi.org/10.3389/fenvs.2021.756378

Kavanagh, B. V., Posner, A. M., & Quirk, J. P. (1976). THE ADSORPTION OF POLYVINYL ALCOHOL ON GIBBSITE AND GOETHITE. *Journal of Soil Science*, *27*(4), 467–477. https://doi.org/10.1111/j.1365-2389.1976.tb02016.x

Keeler, B. L., Hobbie, S. E., & Kellogg, L. E. (2009). Effects of Long-Term Nitrogen Addition on Microbial Enzyme Activity in Eight Forested and Grassland Sites: Implications for Litter and Soil Organic Matter Decomposition. *Ecosystems*, *12*(1), 1–15. https://doi.org/10.1007/s10021-008-9199-z

Keiluweit, M., Bougoure, J. J., Nico, P. S., Pett-Ridge, J., Weber, P. K., & Kleber, M. (2015). Mineral protection of soil carbon counteracted by root exudates. *Nature Climate Change*, *5*(6), 588–595. https://doi.org/10.1038/nclimate2580

Keiluweit, M., & Kleber, M. (2009). Molecular-Level Interactions in Soils and Sediments: The Role of Aromatic π-Systems. *Environmental Science & Technology*, *43*(10), 3421–3429. https://doi.org/10.1021/es8033044

Keller, A. B., Borer, E. T., Collins, S. L., DeLancey, L. C., Fay, P. A., Hofmockel, K. S., Leakey, A. D. B., Mayes, M. A., Seabloom, E. W., Walter, C. A., Wang, Y., Zhao, Q., & Hobbie, S. E. (2022). Soil carbon stocks in temperate grasslands differ strongly across sites but are insensitive to decade-long fertilization. *Global Change Biology*, *28*(4), 1659–1677. https://doi.org/10.1111/gcb.15988

Khan, N., Bano, A., & Curá, J. A. (2020). Role of Beneficial Microorganisms and Salicylic Acid in Improving Rainfed Agriculture and Future Food Safety. *Microorganisms*, *8*(7), 1018. https://doi.org/10.3390/microorganisms8071018

Khomo, L., Trumbore, S., Bern, C. R., & Chadwick, O. A. (2017). Timescales of carbon turnover in soils with mixed crystalline mineralogies. *SOIL*, *3*(1), 17–30. https://doi.org/10.5194/soil-3-17-2017

Kindler, R., Siemens, J., Kaiser, K., Walmsley, D. C., Bernhofer, C., Buchmann, N., Cellier, P., Eugster, W., Gleixner, G., Grũnwald, T., Heim, A., Ibrom, A., Jones, S. K., Jones, M., Klumpp, K., Kutsch, W., Larsen, K. S., Lehuger, S., Loubet, B., … Kaupenjohann, M. (2011). Dissolved carbon leaching from soil is a crucial component of the net ecosystem carbon balance: DISSOLVED CARBON LEACHING. *Global Change Biology*, *17*(2), 1167–1185. https://doi.org/10.1111/j.1365-2486.2010.02282.x

Kirsten, M., Mikutta, R., Vogel, C., Thompson, A., Mueller, C. W., Kimaro, D. N., Bergsma, H. L. T., Feger, K.-H., & Kalbitz, K. (2021). Iron oxides and aluminous clays selectively control soil carbon storage and stability in the humid tropics. *Scientific Reports*, *11*(1), Article 1. https://doi.org/10.1038/s41598-021-84777-7

Klaus, V. H., Kleinebecker, T., Busch, V., Fischer, M., Hölzel, N., Nowak, S., Prati, D., Schäfer, D., Schöning, I., Schrumpf, M., & Hamer, U. (2018). Land use intensity, rather than plant species richness, affects the leaching risk of multiple nutrients from permanent grasslands. *Global Change Biology*, *24*(7), 2828–2840. https://doi.org/10.1111/gcb.14123

Kleber, M., Bourg, I. C., Coward, E. K., Hansel, C. M., Myneni, S. C. B., & Nunan, N. (2021). Dynamic interactions at the mineral–organic matter interface. *Nature Reviews Earth & Environment*, *2*(6), 402–421. https://doi.org/10.1038/s43017-021-00162-y

Kleber, M., Mikutta, R., Torn, M. S., & Jahn, R. (2005). Poorly crystalline mineral phases protect organic matter in acid subsoil horizons. *European Journal of Soil Science*, *0*(0), 050912034650054. https://doi.org/10.1111/j.1365-2389.2005.00706.x

Klotzbücher, A., Schunck, F., Klotzbücher, T., Kaiser, K., Glaser, B., Spohn, M., Widdig, M., & Mikutta, R. (2020). Goethite-Bound Phosphorus in an Acidic Subsoil Is Not Available to Beech (Fagus sylvatica L.). *Frontiers in Forests and Global Change*, *3*. https://doi.org/10.3389/ffgc.2020.00094

Kögel-Knabner, I., Guggenberger, G., Kleber, M., Kandeler, E., Kalbitz, K., Scheu, S., Eusterhues, K., & Leinweber, P. (2008). Organo-mineral associations in temperate soils: Integrating biology, mineralogy, and organic matter chemistry. *Journal of Plant Nutrition and Soil Science*, *171*(1), 61–82. https://doi.org/10.1002/jpln.200700048

Kong, A. Y. Y., Six, J., Bryant, D. C., Denison, R. F., & van Kessel, C. (2005). The Relationship between Carbon Input, Aggregation, and Soil Organic Carbon Stabilization in Sustainable Cropping Systems. *Soil Science Society of America Journal*, *69*(4), 1078–1085. https://doi.org/10.2136/sssaj2004.0215

Konrad, A., Hofmann, D., Siemens, J., Stutz, K. P., Lang, F., & Mulder, I. (2025). Microbial carbon use efficiency of mineral-associated organic matter is related to its desorbability. *Soil Biology and Biochemistry*, *203*, 109740. https://doi.org/10.1016/j.soilbio.2025.109740

Kramer, S., Marhan, S., Haslwimmer, H., Ruess, L., & Kandeler, E. (2013). Temporal variation in surface and subsoil abundance and function of the soil microbial community in an arable soil. *Soil Biology and Biochemistry*, *61*, 76–85. https://doi.org/10.1016/j.soilbio.2013.02.006

Krause, A., Papastefanou, P., Gregor, K., Layritz, L. S., Zang, C. S., Buras, A., Li, X., Xiao, J., & Rammig, A. (2022). Quantifying the impacts of land cover change on gross primary productivity globally. *Scientific Reports*, *12*(1), 18398. https://doi.org/10.1038/s41598-022-23120-0

Kretzschmar, R., Borkovec, M., Grolimund, D., & Elimelech, M. (1999). Mobile Subsurface Colloids and Their Role in Contaminant Transport. In D. L. Sparks (Ed.), *Advances in Agronomy* (Vol. 66, pp. 121–193). Academic Press. https://doi.org/10.1016/S0065-2113(08)60427-7

Kretzschmar, R., Robarge, W. P., & Amoozegar, A. (1995). Influence of Natural Organic Matter on Colloid Transport Through Saprolite. *Water Resources Research*, *31*(3), 435–445. https://doi.org/10.1029/94WR02676

Kruse, J., Abraham, M., Amelung, W., Baum, C., Bol, R., Kühn, O., Lewandowski, H., Niederberger, J., Oelmann, Y., Rüger, C., Santner, J., Siebers, M., Siebers, N., Spohn, M., Vestergren, J., Vogts, A., & Leinweber, P. (2015). Innovative methods in soil phosphorus research: A review. *Journal of Plant Nutrition and Soil Science*, *178*(1), 43–88. https://doi.org/10.1002/jpln.201400327

Kumar, S., Dumpala, R. M. R., Chandane, A., & Bahadur, J. (2022). Elucidation of the sorbent role in sorption thermodynamics of uranium(VI) on goethite. *Environmental Science: Processes & Impacts*, *24*(4), 567–575. https://doi.org/10.1039/D1EM00380A

Kuzyakov, Y., & Domanski, G. (2000). Carbon input by plants into the soil. Review. *Journal of Plant Nutrition and Soil Science*, *163*(4), 421–431. https://doi.org/10.1002/1522-2624(200008)163:4<421::AID-JPLN421>3.0.CO;2-R

L. Fischer, Brümmer, G. W., & Barrow, N. J. (1998). *Zur Kinetik der Sorption von Schwermetallen an Bodenkomponenten. I. Sorptions- und Diffusionsprozesse an/in Goethitpartikeln*. Mittelg. Dtsch. Bodenkdl. Ges. 88, 171-174.

Lagerlöf, J., Adolfsson, L., Börjesson, G., Ehlers, K., Vinyoles, G. P., & Sundh, I. (2014). Land-use intensification and agroforestry in the Kenyan highland: Impacts on soil microbial community composition and functional capacity. *Applied Soil Ecology*, *82*, 93–99. https://doi.org/10.1016/j.apsoil.2014.05.015

Lair, G. J., Gerzabek, M. H., & Haberhauer, G. (2007). Sorption of heavy metals on organic and inorganic soil constituents. *Environmental Chemistry Letters*, *5*(1), 23–27. https://doi.org/10.1007/s10311-006-0059-9

Lajtha, K., Bowden, R. D., & Nadelhoffer, K. (2014). Litter and Root Manipulations Provide Insights into Soil Organic Matter Dynamics and Stability. *Soil Science Society of America Journal*, *78*(S1), S261–S269. https://doi.org/10.2136/sssaj2013.08.0370nafsc

Lammirato, C., Miltner, A., Wick, L. Y., & Kästner, M. (2010). Hydrolysis of cellobiose by β-glucosidase in the presence of soil minerals – Interactions at solid–liquid interfaces and effects on enzyme activity levels. *Soil Biology and Biochemistry*, *42*(12), 2203–2210. https://doi.org/10.1016/j.soilbio.2010.08.018

Landeweert, R., Hoffland, E., Finlay, R. D., Kuyper, T. W., & Breemen, N. van. (2001). Linking plants to rocks: Ectomycorrhizal fungi mobilize nutrients from minerals. *Trends in Ecology & Evolution*, *16*(5), 248–254. https://doi.org/10.1016/S0169-5347(01)02122-X

Lang, F., Bauhus, J., Frossard, E., George, E., Kaiser, K., Kaupenjohann, M., Krüger, J., Matzner, E., Polle, A., Prietzel, J., Rennenberg, H., & Wellbrock, N. (2016). Phosphorus in forest ecosystems: New insights from an ecosystem nutrition perspective. *Journal of Plant Nutrition and Soil Science*, *179*(2), 129–135. https://doi.org/10.1002/jpln.201500541

Lang, F., Krüger, J., Amelung, W., Willbold, S., Frossard, E., Bünemann, E. K., Bauhus, J., Nitschke, R., Kandeler, E., Marhan, S., Schulz, S., Bergkemper, F., Schloter, M., Luster, J., Guggisberg, F., Kaiser, K., Mikutta, R., Guggenberger, G., Polle, A., … Chmara, I. (2017). Soil phosphorus supply controls P nutrition strategies of beech forest ecosystems in Central Europe. *Biogeochemistry*, *136*(1), 5–29. https://doi.org/10.1007/s10533-017-0375-0

Lange, M., Eisenhauer, N., Sierra, C. A., Bessler, H., Engels, C., Griffiths, R. I., Mellado-Vázquez, P. G., Malik, A. A., Roy, J., Scheu, S., Steinbeiss, S., Thomson, B. C., Trumbore, S. E., & Gleixner, G. (2015). Plant diversity increases soil microbial activity and soil carbon storage. *Nature Communications*, *6*(1), 6707. https://doi.org/10.1038/ncomms7707

Lange, M., Roth, V., Eisenhauer, N., Roscher, C., Dittmar, T., Fischer-Bedtke, C., González Macé, O., Hildebrandt, A., Milcu, A., Mommer, L., Oram, N. J., Ravenek, J., Scheu, S., Schmid, B., Strecker, T., Wagg, C., Weigelt, A., & Gleixner, G. (2021). Plant diversity enhances production and downward transport of biodegradable dissolved organic matter. *Journal of Ecology*, *109*(3), 1284–1297. https://doi.org/10.1111/1365-2745.13556

Lavallee, J. M., Soong, J. L., & Cotrufo, M. F. (2020). Conceptualizing soil organic matter into particulate and mineral-associated forms to address global change in the 21st century. *Global Change Biology*, *26*(1), 261–273. https://doi.org/10.1111/gcb.14859

Lefcheck, J. S. (2016). piecewiseSEM: Piecewise structural equation modelling in r for ecology, evolution, and systematics. *Methods in Ecology and Evolution*, *7*(5), 573–579. https://doi.org/10.1111/2041-210X.12512

Lehmann, J., Hansel, C. M., Kaiser, C., Kleber, M., Maher, K., Manzoni, S., Nunan, N., Reichstein, M., Schimel, J. P., Torn, M. S., Wieder, W. R., & Kögel-Knabner, I. (2020). Persistence of soil organic carbon caused by functional complexity. *Nature Geoscience*, *13*(8), 529–534. https://doi.org/10.1038/s41561-020-0612-3

Lehmann, J., & Kleber, M. (2015). The contentious nature of soil organic matter. *Nature*, *528*(7580), 60–68. https://doi.org/10.1038/nature16069

Lenth, R. V. (2017). *emmeans: Estimated Marginal Means, aka Least-Squares Means* (p. 1.11.1) [Dataset]. https://doi.org/10.32614/CRAN.package.emmeans

Li, H., Bölscher, T., Winnick, M., Tfaily, M. M., Cardon, Z. G., & Keiluweit, M. (2021). Simple Plant and Microbial Exudates Destabilize Mineral-Associated Organic Matter via Multiple Pathways. *Environmental Science & Technology*, *55*(5), 3389–3398. https://doi.org/10.1021/acs.est.0c04592

Li, J., Lin, S., Taube, F., Pan, Q., & Dittert, K. (2011). Above and belowground net primary productivity of grassland influenced by supplemental water and nitrogen in Inner Mongolia. *Plant and Soil*, *340*(1), 253–264. https://doi.org/10.1007/s11104-010-0612-y

Li, Y., Wang, T., Camps-Arbestain, M., Suárez-Abelenda, M., & Whitby, C. P. (2020). Lime and/or Phosphate Application Affects the Stability of Soil Organic Carbon: Evidence from Changes in Quantity and Chemistry of the Soil Water-Extractable Organic Matter. *Environmental Science & Technology*, *54*(21), 13908–13916. https://doi.org/10.1021/acs.est.0c01341

Lian, B., Wang, B., Pan, M., Liu, C., & Teng, H. H. (2008). Microbial release of potassium from K-bearing minerals by thermophilic fungus *Aspergillus fumigatus*. *Geochimica et Cosmochimica Acta*, *72*(1), 87–98. https://doi.org/10.1016/j.gca.2007.10.005

Liang, C., Schimel, J. P., & Jastrow, J. D. (2017). The importance of anabolism in microbial control over soil carbon storage. *Nature Microbiology*, *2*(8), 17105. https://doi.org/10.1038/nmicrobiol.2017.105

Liebmann, P., Mikutta, R., Kalbitz, K., Wordell-Dietrich, P., Leinemann, T., Preusser, S., Mewes, O., Perrin, E., Bachmann, J., Don, A., Kandeler, E., Marschner, B., Schaarschmidt, F., & Guggenberger, G. (2022). Biogeochemical limitations of carbon stabilization in forest subsoils. *Journal of Plant Nutrition and Soil Science*, *185*(1), 35–43. https://doi.org/10.1002/jpln.202100295

Lorenz, M., Blagodatskaya, E., Finn, D., Fricke, C., Hüging, H., Kandeler, E., Kaiser, K., Kästner, M., Lechtenfeld, O., Marhan, S., Maskow, T., Mayer, J., Miltner, A., Normant-Saremba, M., Poll, C., Resseguier, C., Rupp, A., Schrumpf, M., Schweitzer, K., … Thiele-Bruhn, S. (2024). *Database for the Priority Program 2322 SoilSystems – Soils and substrates used in the first phase (2021-2024)* [Dataset]. Zenodo. https://doi.org/10.5281/zenodo.11207502

Lugato, E., Lavallee, J. M., Haddix, M. L., Panagos, P., & Cotrufo, M. F. (2021). Different climate sensitivity of particulate and mineral-associated soil organic matter. *Nature Geoscience*, *14*(5), 295–300. https://doi.org/10.1038/s41561-021-00744-x

Ma, C., & Eggleton, R. A. (1999). Cation Exchange Capacity of Kaolinite. *Clays and Clay Minerals*, *47*(2), 174–180. https://doi.org/10.1346/CCMN.1999.0470207

Ma, S., Cao, Y., Lu, J., Ren, T., Cong, R., Lu, Z., Zhu, J., & Li, X. (2024). Response of soil aggregation and associated organic carbon to organic amendment and its controls: A global meta-analysis. *CATENA*, *237*, 107774. https://doi.org/10.1016/j.catena.2023.107774

Madsen, D. E., Cervera-Gontard, L., Kasama, T., Dunin-Borkowski, R. E., Koch, C. B., Hansen, M. F., Frandsen, C., & Mørup, S. (2009). Magnetic fluctuations in nanosized goethite (α-FeOOH) grains. *Journal of Physics: Condensed Matter*, *21*(1), 016007. https://doi.org/10.1088/0953-8984/21/1/016007

Maire, J., Gibson-Poole, S., Cowan, N., Reay, D. S., Richards, K. G., Skiba, U., Rees, R. M., & Lanigan, G. J. (2018). Identifying Urine Patches on Intensively Managed Grassland Using Aerial Imagery Captured From Remotely Piloted Aircraft Systems. *Frontiers in Sustainable Food Systems*, *2*. https://doi.org/10.3389/fsufs.2018.00010

Malik, A. A., Chowdhury, S., Schlager, V., Oliver, A., Puissant, J., Vazquez, P. G. M., Jehmlich, N., von Bergen, M., Griffiths, R. I., & Gleixner, G. (2016). Soil Fungal:Bacterial Ratios Are Linked to Altered Carbon Cycling. *Frontiers in Microbiology*, *7*. https://doi.org/10.3389/fmicb.2016.01247

Mann, H. B., & Whitney, D. R. (1947). On a Test of Whether one of Two Random Variables is Stochastically Larger than the Other. *The Annals of Mathematical Statistics*, *18*(1), 50–60. https://doi.org/10.1214/aoms/1177730491

Marx, M.-C., Wood, M., & Jarvis, S. C. (2001). A microplate fluorimetric assay for the study of enzyme diversity in soils. *Soil Biology and Biochemistry*, *33*(12), 1633–1640. https://doi.org/10.1016/S0038-0717(01)00079-7

Mason, S. D., McLaughlin, M. J., Johnston, C., & McNeill, A. (2013). Soil test measures of available P (Colwell, resin and DGT) compared with plant P uptake using isotope dilution. *Plant and Soil*, *373*(1), 711–722. https://doi.org/10.1007/s11104-013-1833-7

Mayer, M., Prescott, C. E., Abaker, W. E. A., Augusto, L., Cécillon, L., Ferreira, G. W. D., James, J., Jandl, R., Katzensteiner, K., Laclau, J.-P., Laganière, J., Nouvellon, Y., Paré, D., Stanturf, J. A., Vanguelova, E. I., & Vesterdal, L. (2020). Tamm Review: Influence of forest management activities on soil organic carbon stocks: A knowledge synthesis. *Forest Ecology and Management*, *466*, 118127. https://doi.org/10.1016/j.foreco.2020.118127

Meyers, P. A., & Quinn, J. G. (1974). Organic matter on clay minerals and marine sediments—Effect on adsorption of dissolved copper, phosphate, and lipids from saline solutions. *Chemical Geology*, *13*(1), 63–68. https://doi.org/10.1016/0009-2541(74)90050-3

Mikutta, C., Lang, F., & Kaupenjohann, M. (2004). Soil Organic Matter Clogs Mineral Pores: Evidence from^{1} H-NMR and N_2 Adsorption. *Soil Science Society of America Journal*, *68*(6), 1853–1862. https://doi.org/10.2136/sssaj2004.1853

Mikutta, R., & Kaiser, K. (2011). Organic matter bound to mineral surfaces: Resistance to chemical and biological oxidation. *Soil Biology and Biochemistry*, *43*(8), 1738–1741. https://doi.org/10.1016/j.soilbio.2011.04.012

Mikutta, R., Mikutta, C., Kalbitz, K., Scheel, T., Kaiser, K., & Jahn, R. (2007). Biodegradation of forest floor organic matter bound to minerals via different binding mechanisms. *Geochimica et Cosmochimica Acta*, *71*(10), 2569–2590. https://doi.org/10.1016/j.gca.2007.03.002

Mikutta, R., Turner, S., Schippers, A., Gentsch, N., Meyer-Stüve, S., Condron, L. M., Peltzer, D. A., Richardson, S. J., Eger, A., Hempel, G., Kaiser, K., Klotzbücher, T., & Guggenberger, G. (2019). Microbial and abiotic controls on mineral-associated organic matter in soil profiles along an ecosystem gradient. *Scientific Reports*, *9*(1), 10294. https://doi.org/10.1038/s41598-019-46501-4

Mills, A. L. (2003). Keeping in Touch: Microbial Life on Soil Particle Surfaces. In *Advances in Agronomy* (Vol. 78, pp. 1–43). Academic Press. https://doi.org/10.1016/S0065-2113(02)78001-2

Missong, A., Bol, R., Nischwitz, V., Krüger, J., Lang, F., Siemens, J., & Klumpp, E. (2018a). Phosphorus in water dispersible-colloids of forest soil profiles. *Plant and Soil*, *427*(1), 71–86. https://doi.org/10.1007/s11104-017-3430-7

Missong, A., Bol, R., Willbold, S., Siemens, J., & Klumpp, E. (2016). Phosphorus forms in forest soil colloids as revealed by liquid-state 31P-NMR. *Journal of Plant Nutrition and Soil Science*, *179*(2), 159–167. https://doi.org/10.1002/jpln.201500119

Missong, A., Holzmann, S., Bol, R., Nischwitz, V., Puhlmann, H., v. Wilpert, K., Siemens, J., & Klumpp, E. (2018b). Leaching of natural colloids from forest topsoils and their relevance for phosphorus mobility. *Science of The Total Environment*, *634*, 305–315. https://doi.org/10.1016/j.scitotenv.2018.03.265

Molnar, I. L., Pensini, E., Asad, M. A., Mitchell, C. A., Nitsche, L. C., Pyrak-Nolte, L. J., Miño, G. L., & Krol, M. M. (2019). Colloid Transport in Porous Media: A Review of Classical Mechanisms and Emerging Topics. *Transport in Porous Media*, *130*(1), 129–156. https://doi.org/10.1007/s11242-019-01270-6

Montalvo, D., Degryse, F., & McLaughlin, M. J. (2015). Natural Colloidal P and Its Contribution to Plant P Uptake. *Environmental Science & Technology*, *49*(6), 3427–3434. https://doi.org/10.1021/es504643f

Montalvo, D., McLaughlin, M. J., & Degryse, F. (2015). Efficacy of Hydroxyapatite Nanoparticles as Phosphorus Fertilizer in Andisols and Oxisols. *Soil Science Society of America Journal*, *79*(2), 551–558. https://doi.org/10.2136/sssaj2014.09.0373

Moore, D. M., & Reynolds, R. C. (1997). *X-ray diffraction and the identification and analysis of clay minerals* (2. ed). Oxford University Press.

Moorhead, D. L., Sinsabaugh, R. L., Hill, B. H., & Weintraub, M. N. (2016). Vector analysis of ecoenzyme activities reveal constraints on coupled C, N and P dynamics. *Soil Biology and Biochemistry*, *93*, 1–7. https://doi.org/10.1016/j.soilbio.2015.10.019

Mori, T. (2020). Does ecoenzymatic stoichiometry really determine microbial nutrient limitations? *Soil Biology and Biochemistry*, *146*, 107816. https://doi.org/10.1016/j.soilbio.2020.107816

Mosier, S., Paustian, K., Davies, C., Kane, M., & Cotrufo, M. F. (2019). Soil organic matter pools under management intensification of loblolly pine plantations. *Forest Ecology and Management*, *447*, 60–66. https://doi.org/10.1016/j.foreco.2019.05.056

Mossou, E., Teixeira, S. C. M., Mitchell, E. P., Mason, S. A., Adler-Abramovich, L., Gazit, E., & Forsyth, V. T. (2014). The self-assembling zwitterionic form of L -phenylalanine at neutral pH. *Acta Crystallographica Section C Structural Chemistry*, *70*(3), 326–331. https://doi.org/10.1107/S2053229614002563

Moyano, F. E., Vasilyeva, N., & Menichetti, L. (2018). Diffusion limitations and Michaelis–Menten kinetics as drivers of combined temperature and moisture effects on carbon fluxes of mineral soils. *Biogeosciences*, *15*(16), 5031–5045. https://doi.org/10.5194/bg-15-5031-2018

Murage, E. W., & Voroney, P. R. (2007). Modification of the original chloroform fumigation extraction technique to allow measurement of δ13C of soil microbial biomass carbon. *Soil Biology and Biochemistry*, *39*(7), 1724–1729. https://doi.org/10.1016/j.soilbio.2007.01.026

Murphy, J., & Riley, J. P. (1962). A modified single solution method for the determination of phosphate in natural waters. *Analytica Chimica Acta*, *27*, 31–36. https://doi.org/10.1016/S0003-2670(00)88444-5

Neurath, R. A., Pett-Ridge, J., Chu-Jacoby, I., Herman, D., Whitman, T., Nico, P. S., Lipton, A. S., Kyle, J., Tfaily, M. M., Thompson, A., & Firestone, M. K. (2021). Root Carbon Interaction with Soil Minerals Is Dynamic, Leaving a Legacy of Microbially Derived Residues. *Environmental Science & Technology*, acs.est.1c00300. https://doi.org/10.1021/acs.est.1c00300

Oades, J. M. (1989). An Introduction to Organic Matter in Mineral Soils. In J. B. Dixon & S. B. Weed (Eds.), *SSSA Book Series* (pp. 89–159). Madison, WI, USA: Soil Science Society of America. https://doi.org/10.2136/sssabookser1.2ed.c3

Odom, I. E. (1984). Smectite clay minerals: Properties and uses. *Philosophical Transactions of the Royal Society of London. Series A, Mathematical and Physical Sciences*, *311*(1517), 391–409. https://doi.org/10.1098/rsta.1984.0036

OECD. (2000). *Test No. 106: Adsorption -- Desorption Using a Batch Equilibrium Method*. OECD. https://doi.org/10.1787/9789264069602-en

OECD. (2002). *Test No. 307: Aerobic and Anaerobic Transformation in Soil*. OECD. https://doi.org/10.1787/9789264070509-en

Olagoke, F. K., Kalbitz, K., & Vogel, C. (2019). Control of Soil Extracellular Enzyme Activities by Clay Minerals—Perspectives on Microbial Responses. *Soil Systems*, *3*(4), Article 4. https://doi.org/10.3390/soilsystems3040064

Olsson, R., Giesler, R., & Persson, P. (2011). Adsorption mechanisms of glucose in aqueous goethite suspensions. *Journal of Colloid and Interface Science*, *353*(1), 263–268. https://doi.org/10.1016/j.jcis.2010.09.023

Ostrowski, A., Lorenzen, K., Petzold, E., & Schindler, S. (2020). *Land use intensity index (LUI) calculation tool of the Biodiversity Exploratories project for grassland survey data from three different regions in Germany since 2006, BEXIS 2 module* [Computer software]. Zenodo. https://doi.org/10.5281/zenodo.3865579

Öztan, S., & Düring, R.-A. (2012). Microwave assisted EDTA extraction—Determination of pseudo total contents of distinct trace elements in solid environmental matrices. *Talanta*, *99*, 594–602. https://doi.org/10.1016/j.talanta.2012.06.042

Paris, F., Bonnaud, P., Ranger, J., Robert, M., & Lapeyrie, F. (1995). Weathering of ammonium- or calcium-saturated 2:1 phyllosilicates by ectomycorrhizal fungi *in vitro*. *Soil Biology and Biochemistry*, *27*(10), 1237–1244. https://doi.org/10.1016/0038-0717(95)00061-I

Pastore, G., Kaiser, K., Kernchen, S., & Spohn, M. (2020). Microbial release of apatite- and goethite-bound phosphate in acidic forest soils. *Geoderma*, *370*, 114360. https://doi.org/10.1016/j.geoderma.2020.114360

Paustian, K., Lehmann, J., Ogle, S., Reay, D., Robertson, G. P., & Smith, P. (2016). Climate-smart soils. *Nature*, *532*(7597), 49–57. https://doi.org/10.1038/nature17174

Paz-Kagan, T., Ohana-Levi, N., Herrmann, I., Zaady, E., Henkin, Z., & Karnieli, A. (2016). Grazing intensity effects on soil quality: A spatial analysis of a Mediterranean grassland. *CATENA*, *146*, 100–110. https://doi.org/10.1016/j.catena.2016.04.020

Pellegrini, A. F. A., Harden, J., Georgiou, K., Hemes, K. S., Malhotra, A., Nolan, C. J., & Jackson, R. B. (2022). Fire effects on the persistence of soil organic matter and long-term carbon storage. *Nature Geoscience*, *15*(1), 5–13. https://doi.org/10.1038/s41561-021-00867-1

Penn, C. J., & Warren, J. G. (2009). Investigating Phosphorus Sorption onto Kaolinite Using Isothermal Titration Calorimetry. *Soil Science Society of America Journal*, *73*(2), 560–568. https://doi.org/10.2136/sssaj2008.0198

Penn, C. J., & Zhang, H. (2010). Isothermal Titration Calorimetry as an Indicator of Phosphorus Sorption Behavior. *Soil Science Society of America Journal*, *74*(2), 502–511. https://doi.org/10.2136/sssaj2009.0199

Philippe, A., & Schaumann, G. E. (2014). Interactions of Dissolved Organic Matter with Natural and Engineered Inorganic Colloids: A Review. *Environmental Science & Technology*, *48*(16), 8946–8962. https://doi.org/10.1021/es502342r

Pignatello, J. J. (1998). Soil organic matter as a nanoporous sorbent of organic pollutants. *Advances in Colloid and Interface Science*, *76–77*, 445–467. https://doi.org/10.1016/S0001-8686(98)00055-4

Pignatello, J. J., & Xing, B. (1996). Mechanisms of Slow Sorption of Organic Chemicals to Natural Particles. *Environmental Science & Technology*, *30*(1), 1–11. https://doi.org/10.1021/es940683g

Piñeiro, G., Paruelo, J. M., Oesterheld, M., & Jobbágy, E. G. (2010). Pathways of Grazing Effects on Soil Organic Carbon and Nitrogen. *Rangeland Ecology & Management*, *63*(1), 109–119. https://doi.org/10.2111/08-255.1

Pinheiro, J., Bates, D., & R Core Team. (1999). *nlme: Linear and Nonlinear Mixed Effects Models* (p. 3.1-168) [Dataset]. https://doi.org/10.32614/CRAN.package.nlme

Plante, A. F., & Parton, W. J. (2007). THE DYNAMICS OF SOIL ORGANIC MATTER AND NUTRIENT CYCLING. In *Soil Microbiology, Ecology and Biochemistry* (pp. 433–467). Elsevier. https://doi.org/10.1016/B978-0-08-047514-1.50020-2

Poeplau, C., Helfrich, M., Dechow, R., Szoboszlay, M., Tebbe, C. C., Don, A., Greiner, B., Zopf, D., Thumm, U., Korevaar, H., & Geerts, R. (2019). Increased microbial anabolism contributes to soil carbon sequestration by mineral fertilization in temperate grasslands. *Soil Biology and Biochemistry*, *130*, 167–176. https://doi.org/10.1016/j.soilbio.2018.12.019

Poeplau, C., Zopf, D., Greiner, B., Geerts, R., Korvaar, H., Thumm, U., Don, A., Heidkamp, A., & Flessa, H. (2018). Why does mineral fertilization increase soil carbon stocks in temperate grasslands? *Agriculture, Ecosystems & Environment*, *265*, 144–155. https://doi.org/10.1016/j.agee.2018.06.003

Potapov, A. M. (2022). Multifunctionality of belowground food webs: Resource, size and spatial energy channels. *Biological Reviews*, *97*(4), 1691–1711. https://doi.org/10.1111/brv.12857

Poyda, A., Reinsch, T., Struck, I. J., Skinner, R. H., Kluß, C., & Taube, F. (2021). Low assimilate partitioning to root biomass is associated with carbon losses at an intensively managed temperate grassland. *Plant and Soil*, *460*(1), 31–50. https://doi.org/10.1007/s11104-020-04771-2

Prietzel, J., Klysubun, W., & Werner, F. (2016). Speciation of phosphorus in temperate zone forest soils as assessed by combined wet-chemical fractionation and XANES spectroscopy. *Journal of Plant Nutrition and Soil Science*, *179*(2), 168–185. https://doi.org/10.1002/jpln.201500472

Prommer, J., Walker, T. W. N., Wanek, W., Braun, J., Zezula, D., Hu, Y., Hofhansl, F., & Richter, A. (2020). Increased microbial growth, biomass, and turnover drive soil organic carbon accumulation at higher plant diversity. *Global Change Biology*, *26*(2), 669–681. https://doi.org/10.1111/gcb.14777

Pronk, G. J., Heister, K., Vogel, C., Babin, D., Bachmann, J., Ding, G.-C., Ditterich, F., Gerzabek, M. H., Giebler, J., Hemkemeyer, M., Kandeler, E., Kunhi Mouvenchery, Y., Miltner, A., Poll, C., Schaumann, G. E., Smalla, K., Steinbach, A., Tanuwidjaja, I., Tebbe, C. C., … Kögel-Knabner, I. (2017). Interaction of minerals, organic matter, and microorganisms during biogeochemical interface formation as shown by a series of artificial soil experiments. *Biology and Fertility of Soils*, *53*(1), 9–22. https://doi.org/10.1007/s00374-016-1161-1

Prozeller, D., Morsbach, S., & Landfester, K. (2019). Isothermal titration calorimetry as a complementary method for investigating nanoparticle–protein interactions. *Nanoscale*, *11*(41), 19265–19273. https://doi.org/10.1039/C9NR05790K

Quiquampoix, H. (1987). A stepwise approach to the understanding of extracellular enzyme activity in soil I. Effect of electrostatic interactions on the conformation of a β-d-glucosidase adsorbed on different mineral surfaces. *Biochimie*, *69*(6), 753–763. https://doi.org/10.1016/0300-9084(87)90196-9

R Core Team, 2022. (n.d.). *R: A language and environment for statistical computing. R Foundation for Statistical Computing, Vienna, Austra.* https://www.R-project.org/

Rasmussen, C., Heckman, K., Wieder, W. R., Keiluweit, M., Lawrence, C. R., Berhe, A. A., Blankinship, J. C., Crow, S. E., Druhan, J. L., Hicks Pries, C. E., Marin-Spiotta, E., Plante, A. F., Schädel, C., Schimel, J. P., Sierra, C. A., Thompson, A., & Wagai, R. (2018). Beyond clay: Towards an improved set of variables for predicting soil organic matter content. *Biogeochemistry*, *137*(3), 297–306. https://doi.org/10.1007/s10533-018-0424-3

Rasmussen, C., Torn, M. S., & Southard, R. J. (2005). Mineral Assemblage and Aggregates Control Carbon Dynamics in a California Conifer Forest. *Soil Science Society of America Journal*, *69*(6), 1711–1721. https://doi.org/10.2136/sssaj2005.0040

Rawls, W. J., Pachepsky, Y. A., Ritchie, J. C., Sobecki, T. M., & Bloodworth, H. (2003). Effect of soil organic carbon on soil water retention. *Geoderma*, *116*(1–2), 61–76. https://doi.org/10.1016/S0016-7061(03)00094-6

Reichard, P. U., Kretzschmar, R., & Kraemer, S. M. (2007). Dissolution mechanisms of goethite in the presence of siderophores and organic acids. *Geochimica et Cosmochimica Acta*, *71*(23), 5635–5650. https://doi.org/10.1016/j.gca.2006.12.022

Reichenbach, M., Fiener, P., Hoyt, A., Trumbore, S., Six, J., & Doetterl, S. (2023). Soil carbon stocks in stable tropical landforms are dominated by geochemical controls and not by land use. *Global Change Biology*, *29*(9), 2591–2607. https://doi.org/10.1111/gcb.16622

Rosseel, Y. (2012). lavaan: An R Package for Structural Equation Modeling. *Journal of Statistical Software*, *48*, 1–36. https://doi.org/10.18637/jss.v048.i02

Ruess, L., & Chamberlain, P. M. (2010). The fat that matters: Soil food web analysis using fatty acids and their carbon stable isotope signature. *Soil Biology and Biochemistry*, *42*(11), 1898–1910. https://doi.org/10.1016/j.soilbio.2010.07.020

Rui, Y., Jackson, R. D., Cotrufo, M. F., Sanford, G. R., Spiesman, B. J., Deiss, L., Culman, S. W., Liang, C., & Ruark, M. D. (2022). Persistent soil carbon enhanced in Mollisols by well-managed grasslands but not annual grain or dairy forage cropping systems. *Proceedings of the National Academy of Sciences*, *119*(7), e2118931119. https://doi.org/10.1073/pnas.2118931119

Saidy, A. R., Smernik, R. J., Baldock, J. A., Kaiser, K., & Sanderman, J. (2013). The sorption of organic carbon onto differing clay minerals in the presence and absence of hydrous iron oxide. *Geoderma*, *209–210*, 15–21. https://doi.org/10.1016/j.geoderma.2013.05.026

Saidy, A. R., Smernik, R. J., Baldock, J. A., Kaiser, K., & Sanderman, J. (2015). Microbial degradation of organic carbon sorbed to phyllosilicate clays with and without hydrous iron oxide coating: Mineralization of OC-clay-oxide associations. *European Journal of Soil Science*, *66*(1), 83–94. https://doi.org/10.1111/ejss.12180

Saidy, A. R., Smernik, R. J., Baldock, J. A., Kaiser, K., Sanderman, J., & Macdonald, L. M. (2012). Effects of clay mineralogy and hydrous iron oxides on labile organic carbon stabilisation. *Geoderma*, *173–174*, 104–110. https://doi.org/10.1016/j.geoderma.2011.12.030

Sarkar, B., Singh, M., Mandal, S., Churchman, G. J., & Bolan, N. S. (2018). Chapter 3—Clay Minerals—Organic Matter Interactions in Relation to Carbon Stabilization in Soils. In C. Garcia, P. Nannipieri, & T. Hernandez (Eds.), *The Future of Soil Carbon* (pp. 71–86). Academic Press. https://doi.org/10.1016/B978-0-12-811687-6.00003-1

Sarkar, J. M., Leonowicz, A., & Bollag, J.-M. (1989). Immobilization of enzymes on clays and soils. *Soil Biology and Biochemistry*, *21*(2), 223–230. https://doi.org/10.1016/0038-0717(89)90098-9

Sarker, T. C., Zotti, M., Fang, Y., Giannino, F., Mazzoleni, S., Bonanomi, G., Cai, Y., & Chang, S. X. (2022). Soil Aggregation in Relation to Organic Amendment: A Synthesis. *Journal of Soil Science and Plant Nutrition*, *22*(2), 2481–2502. https://doi.org/10.1007/s42729-022-00822-y

Schall, P., & Ammer, C. (2013). How to quantify forest management intensity in Central European forests. *European Journal of Forest Research*, *132*(2), 379–396. https://doi.org/10.1007/s10342-013-0681-6

Schall, P., Schulze, E.-D., Fischer, M., Ayasse, M., & Ammer, C. (2018). Relations between forest management, stand structure and productivity across different types of Central European forests. *Basic and Applied Ecology*, *32*, 39–52. https://doi.org/10.1016/j.baae.2018.02.007

Schimel, J. (2023). Modeling ecosystem-scale carbon dynamics in soil: The microbial dimension. *Soil Biology and Biochemistry*, *178*, 108948. https://doi.org/10.1016/j.soilbio.2023.108948

Schmidt, M. W. I., Torn, M. S., Abiven, S., Dittmar, T., Guggenberger, G., Janssens, I. A., Kleber, M., Kögel-Knabner, I., Lehmann, J., Manning, D. A. C., Nannipieri, P., Rasse, D. P., Weiner, S., & Trumbore, S. E. (2011). Persistence of soil organic matter as an ecosystem property. *Nature*, *478*(7367), 49–56. https://doi.org/10.1038/nature10386

Schneider, M. P. W., Scheel, T., Mikutta, R., Van Hees, P., Kaiser, K., & Kalbitz, K. (2010). Sorptive stabilization of organic matter by amorphous Al hydroxide. *Geochimica et Cosmochimica Acta*, *74*(5), 1606–1619. https://doi.org/10.1016/j.gca.2009.12.017

Schöning, I., Grüneberg, E., Sierra, C. A., Hessenmöller, D., Schrumpf, M., Weisser, W. W., & Schulze, E.-D. (2013). Causes of variation in mineral soil C content and turnover in differently managed beech dominated forests. *Plant and Soil*, *370*(1), 625–639. https://doi.org/10.1007/s11104-013-1654-8

Schöps, R., Goldmann, K., Herz, K., Lentendu, G., Schöning, I., Bruelheide, H., Wubet, T., & Buscot, F. (2018). Land-Use Intensity Rather Than Plant Functional Identity Shapes Bacterial and Fungal Rhizosphere Communities. *Frontiers in Microbiology*, *9*. https://doi.org/10.3389/fmicb.2018.02711

Schrumpf, M., Kaiser, K., Guggenberger, G., Persson, T., Kögel-Knabner, I., & Schulze, E.-D. (2013). Storage and stability of organic carbon in soils as related to depth, occlusion within aggregates, and attachment to minerals. *Biogeosciences*, *10*(3), 1675–1691. https://doi.org/10.5194/bg-10-1675-2013

Schwertmann, U. (1964). Differenzierung der Eisenoxide des Bodens durch Extraktion mit Ammoniumoxalat-Lösung. *Zeitschrift für Pflanzenernährung, Düngung, Bodenkunde*, *105*(3), 194–202. https://doi.org/10.1002/jpln.3591050303

Schwertmann, U., Cambier, P., & Murad, E. (1985). Properties of Goethites of Varying Crystallinity. *Clays and Clay Minerals*, *33*(5), 369–378. https://doi.org/10.1346/CCMN.1985.0330501

See, C. R., Keller, A. B., Hobbie, S. E., Kennedy, P. G., Weber, P. K., & Pett-Ridge, J. (2022). Hyphae move matter and microbes to mineral microsites: Integrating the hyphosphere into conceptual models of soil organic matter stabilization. *Global Change Biology*, *28*(8), 2527–2540. https://doi.org/10.1111/gcb.16073

Séquaris, J.-M., & Lewandowski, H. (2003). Physicochemical characterization of potential colloids from agricultural topsoils. *Colloids and Surfaces A: Physicochemical and Engineering Aspects*, *217*(1), 93–99. https://doi.org/10.1016/S0927-7757(02)00563-0

Shiga, Y. (1961). Studies on the Complexes of Montmorines with Urea and its Derivatives. *Soil Science and Plant Nutrition*, *7*(3), 119–124. https://doi.org/10.1080/00380768.1961.10430967

Shirvani, M., Khalili, B., Kalbasi, M., Shariatmadari, H., & Nourbakhsh, F. (2020). Adsorption of Alkaline Phosphates on Palygorskite and Sepiolite: A Tradeoff Between Enzyme Protection and Inhibition. *Clays and Clay Minerals*, *68*(4), 287–295. https://doi.org/10.1007/s42860-020-00066-w

Simon, A., Bindschedler, S., Job, D., Wick, L. Y., Filippidou, S., Kooli, W. M., Verrecchia, E. P., & Junier, P. (2015). Exploiting the fungal highway: Development of a novel tool for the in situ isolation of bacteria migrating along fungal mycelium. *FEMS Microbiology Ecology*, *91*(11), fiv116. https://doi.org/10.1093/femsec/fiv116

Simon, C., Miltner, A., Mulder, I., Kaiser, K., Lorenz, M., Thiele-Bruhn, S., & Lechtenfeld, O. (2025). Long-term effects of manure addition on soil organic matter molecular composition: Carbon transformation as a major driver of energetic potential. *Soil Biology and Biochemistry*, 109755. https://doi.org/10.1016/j.soilbio.2025.109755

Sinsabaugh, R. L., & Shah, J. J. F. (2012). Ecoenzymatic Stoichiometry and Ecological Theory. *Annual Review of Ecology, Evolution, and Systematics*, *43*(Volume 43, 2012), 313–343. https://doi.org/10.1146/annurev-ecolsys-071112-124414

Six, J., Bossuyt, H., Degryze, S., & Denef, K. (2004). A history of research on the link between (micro)aggregates, soil biota, and soil organic matter dynamics. *Soil and Tillage Research*, *79*(1), 7–31. https://doi.org/10.1016/j.still.2004.03.008

Six, J., Elliott, E. T., & Paustian, K. (2000). Soil macroaggregate turnover and microaggregate formation: A mechanism for C sequestration under no-tillage agriculture. *Soil Biology and Biochemistry*, *32*(14), 2099–2103. https://doi.org/10.1016/S0038-0717(00)00179-6

Six, J., Guggenberger, G., Paustian, K., Haumaier, L., Elliott, E. T., & Zech, W. (2001). Sources and composition of soil organic matter fractions between and within soil aggregates: *Sources and composition of soil organic matter fractions*. *European Journal of Soil Science*, *52*(4), 607–618. https://doi.org/10.1046/j.1365-2389.2001.00406.x

Six, L., Pypers, P., Degryse, F., Smolders, E., & Merckx, R. (2012). The performance of DGT versus conventional soil phosphorus tests in tropical soils—An isotope dilution study. *Plant and Soil*, *359*(1), 267–279. https://doi.org/10.1007/s11104-012-1192-9

Skujiņš, J., Puķite, A., & McLaren, A. D. (1974). Adsorption and activity of chitinase on kaolinite. *Soil Biology and Biochemistry*, *6*(3), 179–182. https://doi.org/10.1016/0038-0717(74)90024-8

Socher, S. A., Prati, D., Boch, S., Müller, J., Klaus, V. H., Hölzel, N., & Fischer, M. (2012). Direct and productivity-mediated indirect effects of fertilization, mowing and grazing on grassland species richness. *Journal of Ecology*, *100*(6), 1391–1399. https://doi.org/10.1111/j.1365-2745.2012.02020.x

Sokol, N. W., Sanderman, J., & Bradford, M. A. (2019). Pathways of mineral-associated soil organic matter formation: Integrating the role of plant carbon source, chemistry, and point of entry. *Global Change Biology*, *25*(1), 12–24. https://doi.org/10.1111/gcb.14482

Sokol, N. W., Whalen, E. D., Jilling, A., Kallenbach, C., Pett-Ridge, J., & Georgiou, K. (2022). Global distribution, formation and fate of mineral-associated soil organic matter under a changing climate: A trait-based perspective. *Functional Ecology*, *36*(6), 1411–1429. https://doi.org/10.1111/1365-2435.14040

Spielvogel, S., Prietzel, J., & Kgel-Knabner, I. (2008). Soil organic matter stabilization in acidic forest soils is preferential and soil type-specific. *European Journal of Soil Science*, *59*(4), 674–692. https://doi.org/10.1111/j.1365-2389.2008.01030.x

Spohn, M. (2020). Increasing the organic carbon stocks in mineral soils sequesters large amounts of phosphorus. *Global Change Biology*, *26*(8), 4169–4177. https://doi.org/10.1111/gcb.15154

Spohn, M. (2024). Preferential adsorption of nitrogen- and phosphorus-containing organic compounds to minerals in soils: A review. *Soil Biology and Biochemistry*, *194*, 109428. https://doi.org/10.1016/j.soilbio.2024.109428

Sposito, G. (2020). *The chemistry of soils* (Third edition). Oxford University Press. https://doi.org/10.1093/oso/9780190630881.001.0001

Sposito, G., Skipper, N. T., Sutton, R., Park, S., Soper, A. K., & Greathouse, J. A. (1999). Surface geochemistry of the clay minerals. *Proceedings of the National Academy of Sciences*, *96*(7), 3358–3364. https://doi.org/10.1073/pnas.96.7.3358

Stainton, M. P. (1980). Errors in Molybdenum Blue Methods for Determining Orthophosphate in Freshwater. *Canadian Journal of Fisheries and Aquatic Sciences*, *37*(3), 472–478. https://doi.org/10.1139/f80-061

Stoner, S. W., Hoyt, A. M., Trumbore, S., Sierra, C. A., Schrumpf, M., Doetterl, S., Baisden, W. T., & Schipper, L. A. (2021). Soil organic matter turnover rates increase to match increased inputs in grazed grasslands. *Biogeochemistry*, *156*(1), 145–160. https://doi.org/10.1007/s10533-021-00838-z

Strauss, R., Brümmer, G. W., & Barrow, N. J. (1997). Effects of crystallinity of goethite: II. Rates of sorption and desorption of phosphate. *European Journal of Soil Science*, *48*(1), 101–114. https://doi.org/10.1111/j.1365-2389.1997.tb00189.x

Stursova, M., Crenshaw, C. L., & Sinsabaugh, R. L. (2006). Microbial Responses to Long-Term N Deposition in a Semiarid Grassland. *Microbial Ecology*, *51*(1), 90–98. https://doi.org/10.1007/s00248-005-5156-y

Stutz, K. P. (2023). Perspectives of the Fritz-Scheffer Awardee 2021: Profile- to ecosystem-scale perspectives on soil organic matter formation as demonstrated by woody debris in forest dynamics. *Journal of Plant Nutrition and Soil Science*, *186*(3), 241–252. https://doi.org/10.1002/jpln.202300031

Sugai, S. F., & Schimel, J. P. (1993). Decomposition and biomass incorporation of 14c-labeled glucose and phenolics in taiga forest floor: Effect of substrate quality, successional state, and season. *Soil Biology and Biochemistry*, *25*(10), 1379–1389. https://doi.org/10.1016/0038-0717(93)90052-D

Sulman, B. N., Phillips, R. P., Oishi, A. C., Shevliakova, E., & Pacala, S. W. (2014). Microbe-driven turnover offsets mineral-mediated storage of soil carbon under elevated CO2. *Nature Climate Change*, *4*(12), 1099–1102. https://doi.org/10.1038/nclimate2436

Sun, Q., Liu, X., Wang, S., & Lian, B. (2020). Effects of mineral substrate on ectomycorrhizal fungal colonization and bacterial community structure. *Science of The Total Environment*, *721*, 137663. https://doi.org/10.1016/j.scitotenv.2020.137663

Swift, M. J., Heal, O. W., & Anderson, J. M. (1979). *Decomposition in terrestrial ecosystems*. Univ. of Calif. Pr.

Taitel-Goldman, N., Bender Koch, C., & Singer, A. (2004). Si-Associated Goethite in Hydrothermal Sediments of the Atlantis II and Thetis Deeps, Red Sea. *Clays and Clay Minerals*, *52*(1), 115–129. https://doi.org/10.1346/CCMN.2004.0520111

Tan, X., He, Y., Wang, Z., Li, C., Kong, L., Tian, H., Shen, W., Megharaj, M., & He, W. (2018). Soil mineral alters the effect of Cd on the alkaline phosphatase activity. *Ecotoxicology and Environmental Safety*, *161*, 78–84. https://doi.org/10.1016/j.ecoenv.2018.05.069

Tavanaee, M., Shirvani, M., & Bakhtiary, S. (2017). Adhesion of *Pseudomonas putida* onto Palygorskite and Sepiolite Clay Minerals. *Geomicrobiology Journal*, *34*(8), 677–686. https://doi.org/10.1080/01490451.2016.1238982

Thieme, L., Graeber, D., Hofmann, D., Bischoff, S., Schwarz, M. T., Steffen, B., Meyer, U.-N., Kaupenjohann, M., Wilcke, W., Michalzik, B., & Siemens, J. (2019). Dissolved organic matter characteristics of deciduous and coniferous forests with variable management: Different at the source, aligned in the soil. *Biogeosciences*, *16*(7), 1411–1432. https://doi.org/10.5194/bg-16-1411-2019

Tietjen, T., & Wetzel, R. G. (2003). Extracellular enzyme-clay mineral complexes: Enzyme adsorption, alteration of enzyme activity, and protection from photodegradation. *Aquatic Ecology*, *37*(4), 331–339. https://doi.org/10.1023/B:AECO.0000007044.52801.6b

Tipping, E. (1981). The adsorption of aquatic humic substances by iron oxides. *Geochimica et Cosmochimica Acta*, *45*(2), 191–199. https://doi.org/10.1016/0016-7037(81)90162-9

Tisdall, J. M., & Oades, J. M. (1982). Organic matter and water-stable aggregates in soils. *Journal of Soil Science*, *33*(2), 141–163. https://doi.org/10.1111/j.1365-2389.1982.tb01755.x

Todd-Brown, K. E. O., Randerson, J. T., Post, W. M., Hoffman, F. M., Tarnocai, C., Schuur, E. A. G., & Allison, S. D. (2013). Causes of variation in soil carbon simulations from CMIP5 Earth system models and comparison with observations. *Biogeosciences*, *10*(3), 1717–1736. https://doi.org/10.5194/bg-10-1717-2013

Tombácz, E., Libor, Z., Illés, E., Majzik, A., & Klumpp, E. (2004). The role of reactive surface sites and complexation by humic acids in the interaction of clay mineral and iron oxide particles. *Organic Geochemistry*, *35*(3), 257–267. https://doi.org/10.1016/j.orggeochem.2003.11.002

Tributh, H., & Lagaly, G. (1986). *Aufbereitung und Identifizierung von Boden- und Lagerstättentonen. I. Aufbereitung der Proben im Labor.* GIT-Fachzeitschrift für das Laboratorium 30, S. 524-529.

Trum, F., Titeux, H., Ranger, J., & Delvaux, B. (2011). Influence of tree species on carbon and nitrogen transformation patterns in forest floor profiles. *Annals of Forest Science*, *68*(4), Article 4. https://doi.org/10.1007/s13595-011-0080-4

Turner, B. L., Condron, L. M., Wells, A., & Andersen, K. M. (2012). Soil nutrient dynamics during podzol development under lowland temperate rain forest in New Zealand. *CATENA*, *97*, 50–62. https://doi.org/10.1016/j.catena.2012.05.007

Uroz, S., Kelly, L. C., Turpault, M.-P., Lepleux, C., & Frey-Klett, P. (2015). The Mineralosphere Concept: Mineralogical Control of the Distribution and Function of Mineral-associated Bacterial Communities. *Trends in Microbiology*, *23*(12), 751–762. https://doi.org/10.1016/j.tim.2015.10.004

van der Veeken, P. L. R., Pinheiro, J. P., & van Leeuwen, H. P. (2008). Metal Speciation by DGT/DET in Colloidal Complex Systems. *Environmental Science & Technology*, *42*(23), 8835–8840. https://doi.org/10.1021/es801654s

Van Veldhoven, P. P., & Mannaerts, G. P. (1987). Inorganic and organic phosphate measurements in the nanomolar range. *Analytical Biochemistry*, *161*(1), 45–48. https://doi.org/10.1016/0003-2697(87)90649-X

Vance, E. D., Brookes, P. C., & Jenkinson, D. S. (1987). An extraction method for measuring soil microbial biomass C. *Soil Biology and Biochemistry*, *19*(6), 703–707. https://doi.org/10.1016/0038-0717(87)90052-6

Venables, W. N., & Ripley, B. D. (2013). *Modern Applied Statistics with S-PLUS*. Springer Science & Business Media.

Vidal, A., Hirte, J., Bender, S. F., Mayer, J., Gattinger, A., Höschen, C., Schädler, S., Iqbal, T. M., & Mueller, C. W. (2018). Linking 3D Soil Structure and Plant-Microbe-Soil Carbon Transfer in the Rhizosphere. *Frontiers in Environmental Science*, *6*. https://doi.org/10.3389/fenvs.2018.00009

Vidal, A., Klöffel, T., Guigue, J., Angst, G., Steffens, M., Hoeschen, C., & Mueller, C. W. (2021). Visualizing the transfer of organic matter from decaying plant residues to soil mineral surfaces controlled by microorganisms. *Soil Biology and Biochemistry*, *160*, 108347. https://doi.org/10.1016/j.soilbio.2021.108347

Vieira, S., Sikorski, J., Gebala, A., Boeddinghaus, R. S., Marhan, S., Rennert, T., Kandeler, E., & Overmann, J. (2020). Bacterial colonization of minerals in grassland soils is selective and highly dynamic. *Environmental Microbiology*, *22*(3), 917–933. https://doi.org/10.1111/1462-2920.14751

Vogt, J., Klaus, V. H., Both, S., Fürstenau, C., Gockel, S., Gossner, M. M., Heinze, J., Hemp, A., Hölzel, N., Jung, K., Kleinebecker, T., Lauterbach, R., Lorenzen, K., Ostrowski, A., Otto, N., Prati, D., Renner, S., Schumacher, U., Seibold, S., … Weisser, W. W. (2019). Eleven years' data of grassland management in Germany. *Biodiversity Data Journal*, *7*, e36387. https://doi.org/10.3897/BDJ.7.e36387

Von Fromm, S. F., Jungkunst, H. F., Amenkhienan, B., Hall, S. J., Georgiou, K., Pries, C. H., Montaño-López, F., Quesada, C. A., Rasmussen, C., Schrumpf, M., Singh, B., Thompson, A., Wagai, R., & Fiedler, S. (2025). Moisture and soil depth govern relationships between soil organic carbon and oxalate-extractable metals at the global scale. *Biogeochemistry*, *168*(1), 20. https://doi.org/10.1007/s10533-025-01208-9

Vries, F. T. de, Bloem, J., Quirk, H., Stevens, C. J., Bol, R., & Bardgett, R. D. (2012). Extensive Management Promotes Plant and Microbial Nitrogen Retention in Temperate Grassland. *PLOS ONE*, *7*(12), e51201. https://doi.org/10.1371/journal.pone.0051201

Wada, K., & and Aomine, S. (1966). Occurrence of gibbsite in weathering of volcanic materials at Kuroishibaru, Kumamoto. *Soil Science and Plant Nutrition*, *12*(4), 25–31. https://doi.org/10.1080/00380768.1966.10431950

Wang, G., Post, W. M., & Mayes, M. A. (2013). Development of microbial-enzyme-mediated decomposition model parameters through steady-state and dynamic analyses. *Ecological Applications*, *23*(1), 255–272. https://doi.org/10.1890/12-0681.1

Wang, L., Missong, A., Amelung, W., Willbold, S., Prietzel, J., & Klumpp, E. (2020). Dissolved and colloidal phosphorus affect P cycling in calcareous forest soils. *Geoderma*, *375*, 114507. https://doi.org/10.1016/j.geoderma.2020.114507

Wang, X., Toner, B. M., & Yoo, K. (2019). Mineral vs. Organic matter supply as a limiting factor for the formation of mineral-associated organic matter in forest and agricultural soils. *Science of The Total Environment*, *692*, 344–353. https://doi.org/10.1016/j.scitotenv.2019.07.219

Waring, B., Gee, A., Liang, G., & Adkins, S. (2022). A quantitative analysis of microbial community structure-function relationships in plant litter decay. *iScience*, *25*(7). https://doi.org/10.1016/j.isci.2022.104523

Warmink, J. A., Nazir, R., Corten, B., & van Elsas, J. D. (2011). Hitchhikers on the fungal highway: The helper effect for bacterial migration via fungal hyphae. *Soil Biology and Biochemistry*, *43*(4), 760–765. https://doi.org/10.1016/j.soilbio.2010.12.009

Welch, B. L. (1947). The Generalization of `Student's' Problem when Several Different Population Variances are Involved. *Biometrika*, *34*(1/2), 28. https://doi.org/10.2307/2332510

Whitman, T., Neurath, R., Perera, A., Chu-Jacoby, I., Ning, D., Zhou, J., Nico, P., Pett-Ridge, J., & Firestone, M. (2018). Microbial community assembly differs across minerals in a rhizosphere microcosm. *Environmental Microbiology*, *20*(12), 4444–4460. https://doi.org/10.1111/1462-2920.14366

Wickham, H. (2016). *Ggplot2*. Springer International Publishing. https://doi.org/10.1007/978-3-319-24277-4

Wilcoxon, F. (1945). *Individual Comparisons by Ranking Methods*. *Vol. 1*(No.6), 80–83.

Wiseman, T., Williston, S., Brandts, J. F., & Lin, L.-N. (1989). Rapid measurement of binding constants and heats of binding using a new titration calorimeter. *Analytical Biochemistry*, *179*(1), 131–137. https://doi.org/10.1016/0003-2697(89)90213-3

Witzgall, K., Vidal, A., Schubert, D. I., Höschen, C., Schweizer, S. A., Buegger, F., Pouteau, V., Chenu, C., & Mueller, C. W. (2021). Particulate organic matter as a functional soil component for persistent soil organic carbon. *Nature Communications*, *12*(1), 4115. https://doi.org/10.1038/s41467-021-24192-8

Wood, T., Bormann, F. H., & Voigt, G. K. (1984). Phosphorus Cycling in a Northern Hardwood Forest: Biological and Chemical Control. *Science*, *223*(4634), 391–393. https://doi.org/10.1126/science.223.4634.391

Wright, A. L., Hons, F. M., & Rouquette, F. M. (2004). Long-term management impacts on soil carbon and nitrogen dynamics of grazed bermudagrass pastures. *Soil Biology and Biochemistry*, *36*(11), 1809–1816. https://doi.org/10.1016/j.soilbio.2004.05.004

Wu, Y., Prietzel, J., Zhou, J., Bing, H., Luo, J., Yu, D., Sun, S., Liang, J., & Sun, H. (2014). Soil phosphorus bioavailability assessed by XANES and Hedley sequential fractionation technique in a glacier foreland chronosequence in Gongga Mountain, Southwestern China. *Science China Earth Sciences*, *57*(8), 1860–1868. https://doi.org/10.1007/s11430-013-4741-z

Yan, J., Pan, G., Li, L., Quan, G., Ding, C., & Luo, A. (2010). Adsorption, immobilization, and activity of β-glucosidase on different soil colloids. *Journal of Colloid and Interface Science*, *348*(2), 565–570. https://doi.org/10.1016/j.jcis.2010.04.044

Yang, Z., Liao, Y., Fu, X., Zaporski, J., Peters, S., Jamison, M., Liu, Y., Wullschleger, S. D., Graham, D. E., & Gu, B. (2019). Temperature sensitivity of mineral-enzyme interactions on the hydrolysis of cellobiose and indican by β-glucosidase. *Science of The Total Environment*, *686*, 1194–1201. https://doi.org/10.1016/j.scitotenv.2019.05.479

Yeasmin, S., Singh, B., Kookana, R. S., Farrell, M., Sparks, D. L., & Johnston, C. T. (2014). Influence of mineral characteristics on the retention of low molecular weight organic compounds: A batch sorption–desorption and ATR-FTIR study. *Journal of Colloid and Interface Science*, *432*, 246–257. https://doi.org/10.1016/j.jcis.2014.06.036

Yi, S., Chen, X., Cao, X., Yi, B., & He, W. (2022). Influencing factors and environmental effects of interactions between goethite and organic matter: A critical review. *Frontiers in Environmental Science*, *10*, 1023277. https://doi.org/10.3389/fenvs.2022.1023277

Yost, E. C., Tejedor-Tejedor, M. I., & Anderson, M. A. (1990). In situ CIR-FTIR characterization of salicylate complexes at the goethite/aqueous solution interface. *Environmental Science & Technology*, *24*(6), 822–828. https://doi.org/10.1021/es00076a005

Yun, D., Krutpijit, C., Jongsomjit, B., & Herrera, J. E. (2018). Asymmetrical coexistence of associatively and dissociatively adsorbed alcohol species over α-Fe2O3 iron oxide nanoparticles. *Surface Science*, *677*, 203–212. https://doi.org/10.1016/j.susc.2018.07.005

Zhang, H., & Davison, W. (1999). Diffusional characteristics of hydrogels used in DGT and DET techniques. *Analytica Chimica Acta*, *398*(2), 329–340. https://doi.org/10.1016/S0003-2670(99)00458-4

Zhang, H., Davison, W., Gadi, R., & Kobayashi, T. (1998). In situ measurement of dissolved phosphorus in natural waters using DGT. *Analytica Chimica Acta*, *370*(1), 29–38. https://doi.org/10.1016/S0003-2670(98)00250-5

Zhang, J., Chi, F., Wei, D., Zhou, B., Cai, S., Li, Y., Kuang, E., Sun, L., & Li, L.-J. (2019). Impacts of Long-term Fertilization on the Molecular Structure of Humic Acid and Organic Carbon Content in Soil Aggregates in Black Soil. *Scientific Reports*, *9*(1), 11908. https://doi.org/10.1038/s41598-019-48406-8

Zhang, Y., Kallay, N., & Matijevic, E. (1985). Interaction of metal hydrous oxides with chelating agents. 7. Hematite-oxalic acid and -citric acid systems. *Langmuir*, *1*(2), 201–206. https://doi.org/10.1021/la00062a004

Zhou, Z., Ren, C., Wang, C., Delgado-Baquerizo, M., Luo, Y., Luo, Z., Du, Z., Zhu, B., Yang, Y., Jiao, S., Zhao, F., Cai, A., Yang, G., & Wei, G. (2024). Global turnover of soil mineral-associated and particulate organic carbon. *Nature Communications*, *15*(1), 5329. https://doi.org/10.1038/s41467-024-49743-7

Zhu, X., Zhang, Z., Wang, Q., Peñuelas, J., Sardans, J., Lambers, H., Li, N., Liu, Q., Yin, H., & Liu, Z. (2022). More soil organic carbon is sequestered through the mycelium pathway than through the root pathway under nitrogen enrichment in an alpine forest. *Global Change Biology*, *28*(16), 4947–4961. https://doi.org/10.1111/gcb.16263

Supplementary material Chapter II

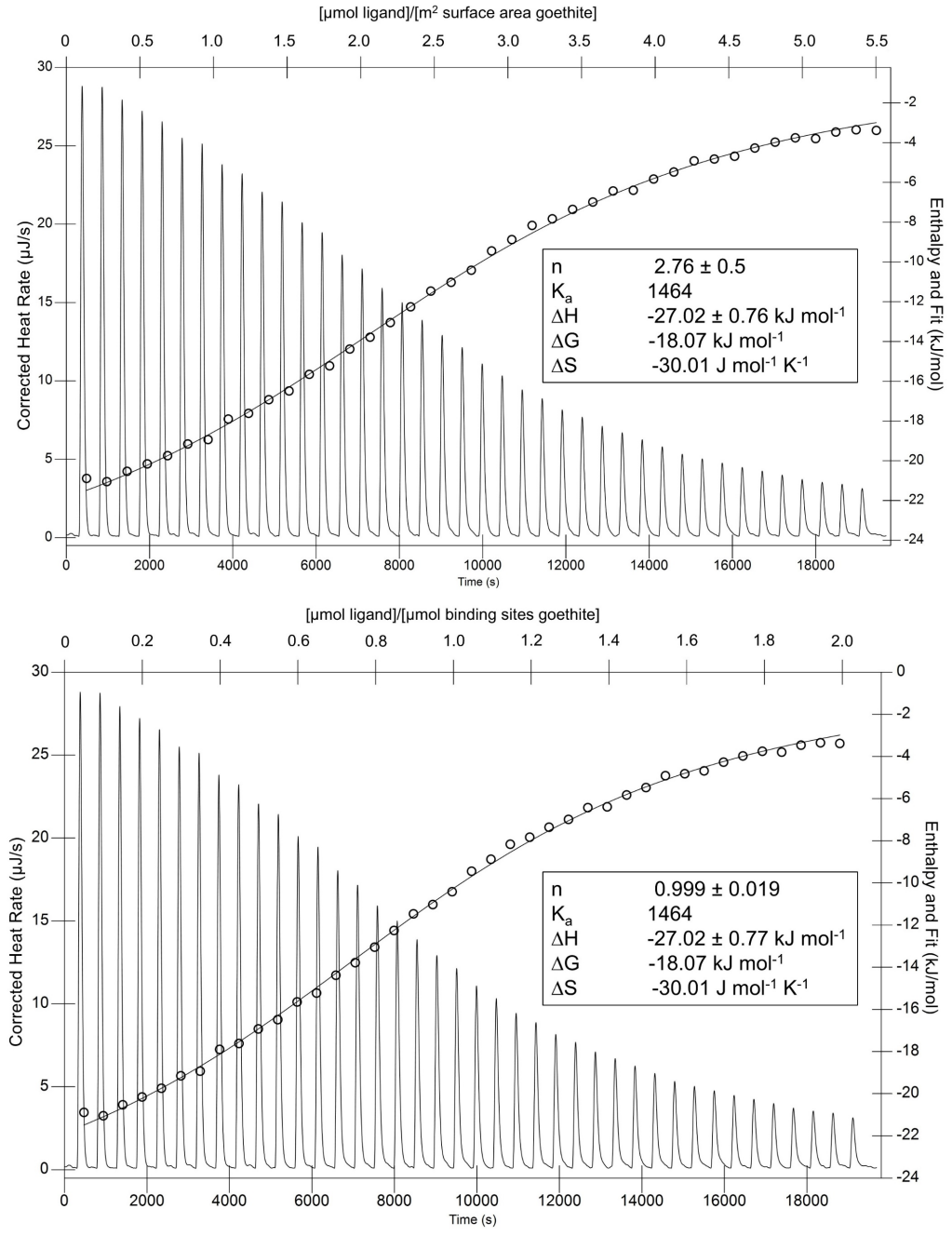

Figure S2-1. Thermograms and independent one-site model fits of citric acid adsorption at pH 5.5 to goethite with a surface area of 119.56 m^2 g^{-1} with different inputs for the concentration of sorbent: top shows stoichiometry n as binding sites goethite per m^2 surface area with concentration of sorbent expressed in the unit [m^2 mineral surface L^{-1}]. The bottom model uses the stoichiometry from the top shown model [µmol m^{-2}] multiplied by the mineral surface area per liter suspension to yield the sorbent concentration in the unit [µmol binding sites L^{-1}] as input. The thermodynamics derived from both models are identical, with n from the first model (top) giving the sorption capacity, while the second models n yields the typical , unitless 1:1 binding stoichiometry.

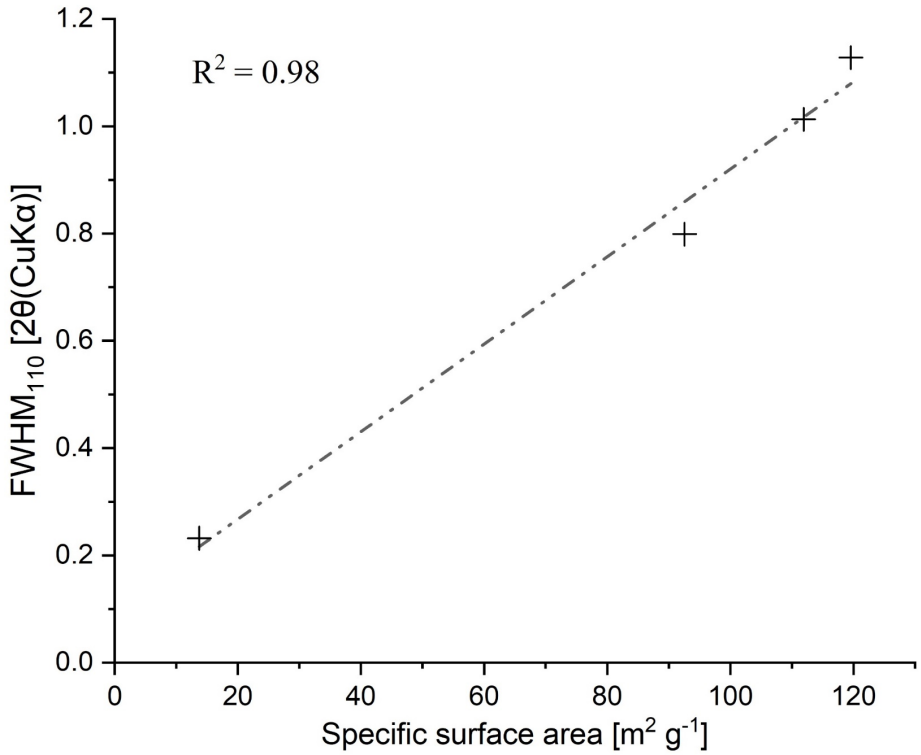

Figure S2-2. Linear regression between specific surface area and full width at half maximum of the 110 diffraction peak ($FWHM_{110}$) of the goethite samples used for this study.

Figure S2-3. Agitator modifications to overcome flocculation of mineral suspension during titration experiments. Left shows double-stacked standard agitators with shortened shafts from TA Instruments Inc. (Newcastle, Delaware, USA). Right shows 3D-printed helical polypropylene agitator.

Supplementary material Chapter III

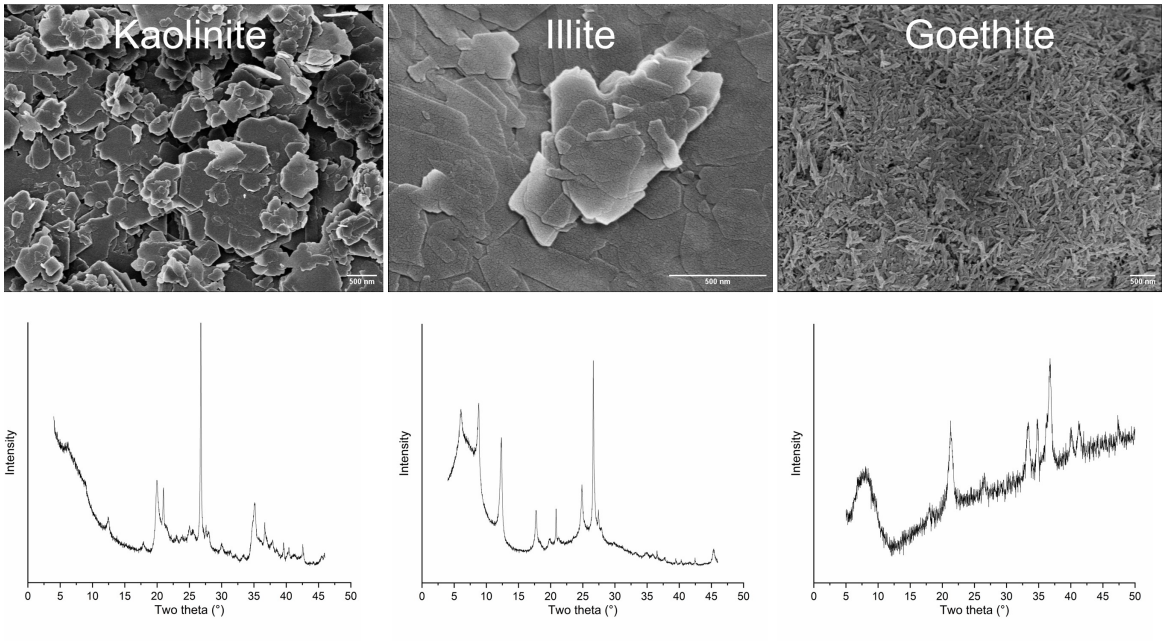

Figure S3-1. Scanning electron microscope images and XRD spectra of kaolinite (BET surface area = 17.2 $m^2 g^{-1}$), illite (43.7 $m^2 g^{-1}$) and goethite (92.5 $m^2 g^{-1}$).

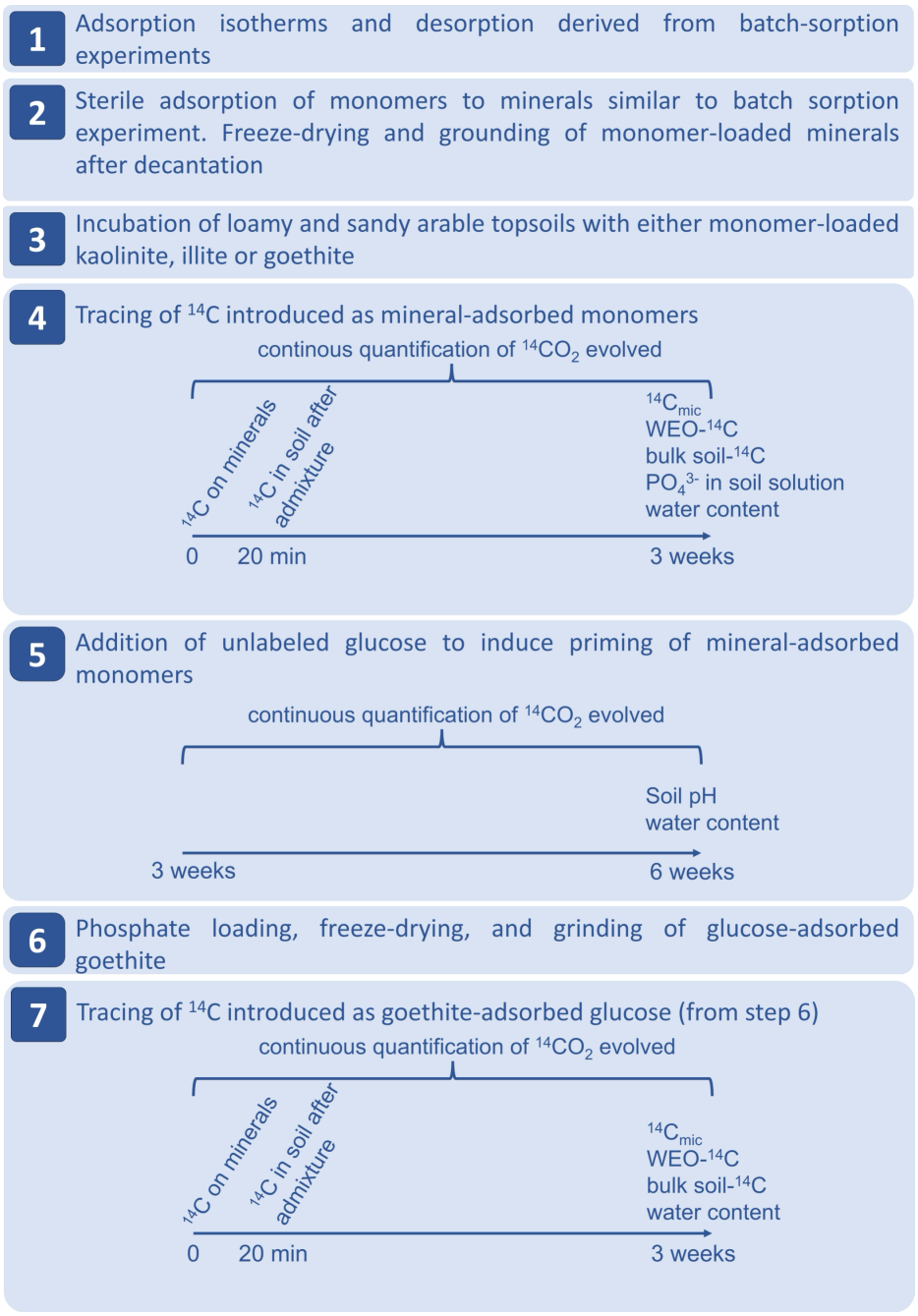

Figure S3-2. Schematic workflow of interlinked experiments investigating monomer-mineral interactions and microbial processing. Initial sorption-desorption studies were conducted with minerals (goethite, kaolinite, illite) and ^{14}C-labeled monomers to characterize binding properties (1). The same monomer-mineral combinations were prepared for soil incubation by adsorbing monomers onto sterilized mineral surfaces, removing excess solution, freeze-drying, and grinding (2). Monomer-loaded minerals were then incubated in sandy and loamy soils (3), with continuous $^{14}CO_2$ tracking over 21 days, after which ^{14}C in microbial biomass, residual soil, and phosphate-P were quantified (4). Following a glucose addition to induce priming of monomer-^{14}C (5), a parallel experiment was performed where phosphate-loaded, glucose-adsorbed goethite (6) was incubated in Dikopshof soil, replicating the 21-day incubation to assess phosphate effects on microbial monomer processing (7).

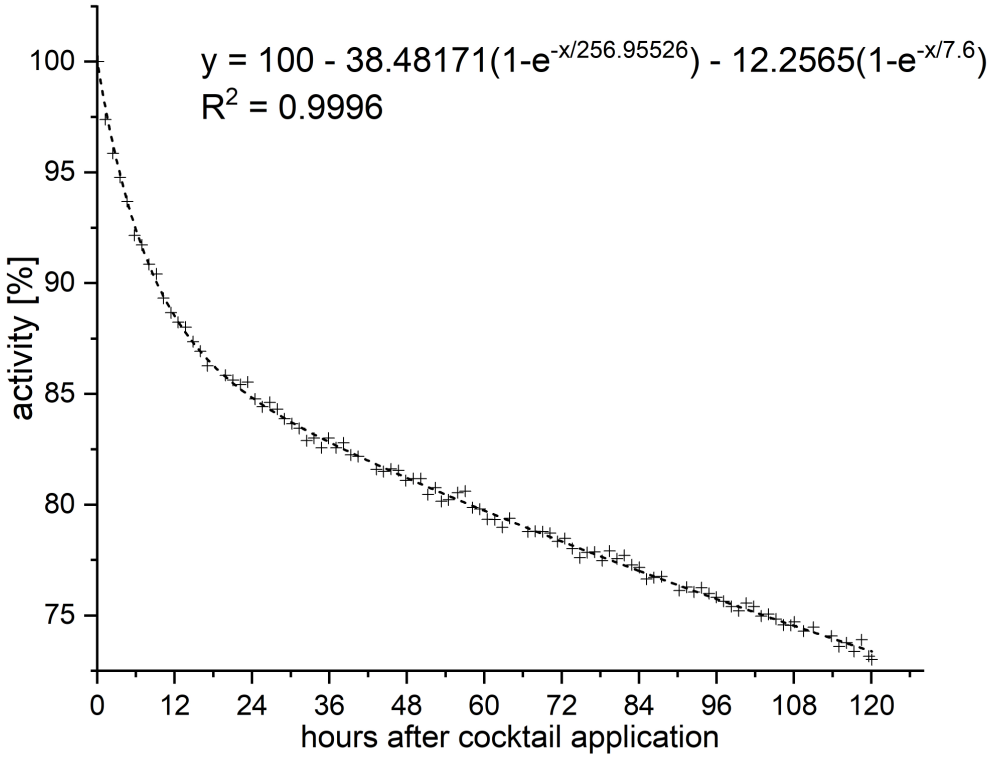

Figure S3-3. Declining activity over time by volatilization of $^{14}CO_2$ trapped in mixture of 1 mL 1 M NaOH together with 10 mL Ultima Gold XR scintillation cocktail.

Table S3-1. Parameters of Freundlich isotherms for citric acid, salicylic acid, phenylalanine, acetylglucosamine and glucose to goethite, kaolinite and illite.

Monomers	Goethite			Kaolinite			Illite		
	K_F	n	R^2	K_F	n	R^2	K_F	n	R^2
Citric acid	2523 ± 621	2.9 ± 0.6	0.937	205 ± 20.9	7.8 ± 2.4	0.819	63.5 ± 2.0	5.5 ± 0.5	0.984
Salicylic acid	773 ± 23	2.2 ± 0.1	0.995	108.9 ± 2.8	3.6 ± 0.2	0.991	25.6 ± 0.7	5.1 ± 1.8	0.999
Phenylalanine	1000	1.0 ± 0.0	1.000	394 ± 3.0	0.9 ± 0.0	0.999	122.6 ± 0.5	1.0 ± 0.0	0.999
N-Acetylglucosamine	12.3 ± 0.2	1.0 ± 0.0	0.998	32.7 ± 0.2	1.0 ± 0.0	0.999	18.8 ± 0.8	0.8 ± 0.1	0.999
Glucose	124.1 ± 1.9	1.1 ± 0.0	0.999	17.9 ± 2.9	2.5 ± 0.9	0.808	12.7 ± 1.8	2.3 ± 0.6	0.860

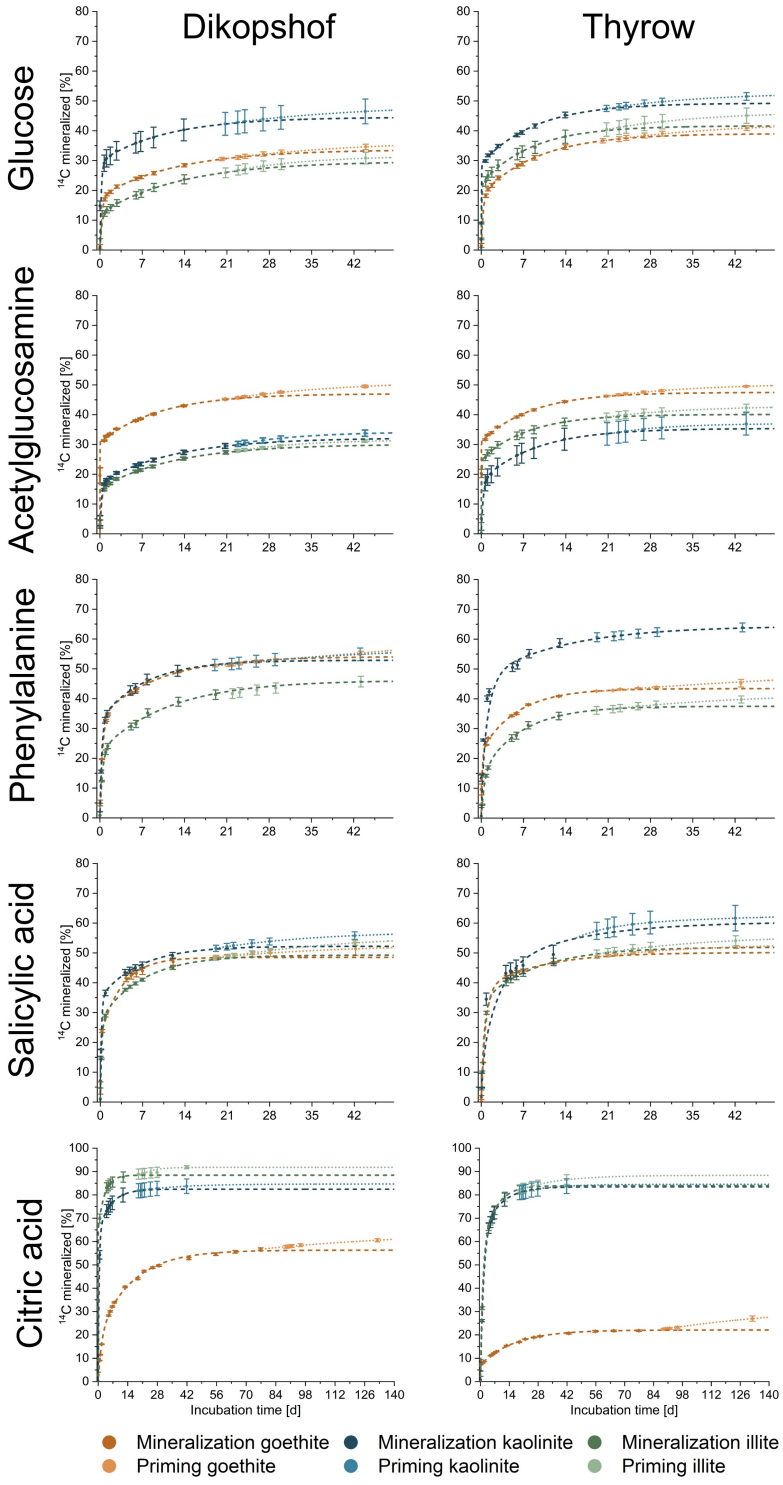

Figure S3-4. Fraction of labeled OC mineralized in percent of ^{14}C added per experiment during incubation of Dikopshof (left) and Thyrow soil (right) with uniformly ^{14}C-labeled monomers adsorbed to goethite (brown), kaolinite (blue) or illite (green) over 21 days in triplicates, followed by glucose priming and additional 21 days of incubation.

Table S3-2. Double pseudo first order fitting parameters for incubation and glucose priming of mineral adsorbed monomers in Dikopshof and Thyrow soil.

Dikopshof		Incubation						Priming						Priming effect
Monomer	Mineral	qe1 [% ^{14}C]	qe2 [% ^{14}C]	∑ [% ^{14}C]	k1	k2	R^2	qe1 [% ^{14}C]	qe2 [% ^{14}C]	∑ [% ^{14}C]	k1	k2	R^2	$\sum qe_{Priming} - \sum qe_{Incubation}$ [% ^{14}C]
Glucose	Goethite	17.8 ± 0.3	15.9 ± 0.6	33.7 ± 0.9	2.96 ± 0.19	0.08 ± 0.01	1.000	21.2 ± 2.6	15.6 ± 1.6	36.8 ± 4.1		0.04 ± 0.01	0.995	3.13 ± 4.99
Glucose	Illite	17.5 ± 0.9	12.3 ± 0.2	29.8 ± 1.1	0.07 ± 0.01	3.28 ± 0.34	0.999	31.6 ± 0.1		31.6 ± 0.1	0.92 ± 0.01		0.999	1.83 ± 1.21
Glucose	Kaolinite	29.6 ± 0.3	14.9 ± 0.6	44.5 ± 1	4.45 ± 0.64	14.92 ± 0.65	1.000	32.2 ± 1.1	16.6 ± 0.7	48.7 ± 1.8	294596 ± 0	0.05 ± 0	0.999	4.2 ± 2.8
Acetylglucosamine	Goethite	30.8 ± 0.3	16.3 ± 0.9	47.1 ± 1.2	72.68 ± 34.31	0.01 ± 0.01	0.994	33.3 ± 2.8	18.2 ± 2.1	51.5 ± 4.9	196.71 ± 2.52	0.05 ± 0.01	0.997	4.41 ± 6.12
Acetylglucosamine	Illite	15.2 ± 0.4	14.9 ± 1.1	30.1 ± 1.5	3.76 ± 0.56	0.08 ± 0.01	0.995	31.6 ± 0.2		31.6 ± 0.2	0.09 ± 0		0.989	1.51 ± 1.76
Acetylglucosamine	Kaolinite	17.1 ± 0.5	15.1 ± 1.9	32.2 ± 2.4	3.72 ± 0.6	0.08 ± 0.02	0.991	34.3 ± 0.2		34.3 ± 0.2	0.09 ± 0		0.988	2.04 ± 2.61
Phenylalanine	Goethite	33.7 ± 1.5	20.4 ± 2	54.1 ± 3.5	2.29 ± 0.15	0.1 ± 0.03	0.998	46.9 ± 1.1	29.2 ± 42.4	76.1 ± 43.5		0.01 ± 0.01	0.993	22 ± 47.06
Phenylalanine	Illite	23.7 ± 7.5	24.4 ± 1.6	48.1 ± 9.1	0.07 ± 0.04	24.38 ± 1.57	0.996	28.5 ± 0.8	19.1 ± 0.6	47.6 ± 1.4		0.05 ± 0	1.000	-0.46 ± 10.5
Phenylalanine	Kaolinite	18.4 ± 2.8	34.2 ± 1.7	52.6 ± 4.4	0.11 ± 0.06	2.92 ± 0.23	0.997	45.8 ± 1.5	12.6 ± 0.8	58.4 ± 2.3		0.03 ± 0.01	0.994	5.78 ± 6.78
Salicylic acid	Goethite	26.7 ± 0.6	21.8 ± 0.5	48.5 ± 1.1	0.28 ± 0.02	16.74 ± 5.62	0.999	43.1 ± 0.8	10.1 ± 0.3	53.2 ± 1.1	314.57 ± 2.25	0.04 ± 0.01	0.998	4.66 ± 2.16
Salicylic acid	Illite	27.7 ± 0.5	21.6 ± 0.6	49.3 ± 1.1	3.6 ± 0.13	0.14 ± 0.01	1.000	36.8 ± 1.8	19.4 ± 1.1	56.2 ± 2.9	53.41 ± 0.52	0.05 ± 0.01	0.997	6.9 ± 3.98
Salicylic acid	Kaolinite	35.1 ± 0.6	17.6 ± 0.7	52.6 ± 1.2	5.1 ± 0.11	0.15 ± 0.02	1.000	39.8 ± 0.9	17.6 ± 0.8	57.3 ± 1.7	3.2 ± 0.42	0.06 ± 0	0.999	4.68 ± 2.94
Citric acid	Goethite	19.6 ± 1.4	36.5 ± 1.2	56.1 ± 2.6	0.6 ± 0.04	0.06 ± 0.01	0.999	61.2 ± 2.5		61.2 ± 2.5	0.24 ± 0.01		1.000	5.15 ± 5.12
Citric acid	Illite	63.1 ± 1	24.2 ± 0.9	87.3 ± 0		0.35 ± 0.03	0.995	91.8 ± 0.3		91.8 ± 0.3	0.17 ± 0.1		0.848	4.5 ± 0.3
Citric acid	Kaolinite	18.7 ± 0.3	63.7 ± 0.4	82.4 ± 0.7	0.17 ± 0.01	2.18 ± 0.07	1.000	77.1 ± 0.8	7.5 ± 0.5	84.7 ± 1.3		0.05 ± 0.01	0.998	2.23 ± 2
Thyrow														
Glucose	Goethite	20.6 ± 0.7	18.4 ± 0.5	39 ± 1.2	0.11 ± 0.01	3.14 ± 0.38	0.999	26.2 ± 2.6	16.7 ± 1.8	42.9 ± 4.4	5.6 ± 0.02	0.05 ± 0.01	0.997	3.88 ± 5.58
Glucose	Illite	22.1 ± 0.4	19.6 ± 1	41.6 ± 1.4	19.56 ± 0.96	13.21 ± 0.43	1.000	23.7 ± 1.7	22.8 ± 1.5	46.5 ± 3.2	23.68 ± 1.7	0.06 ± 0	1.000	4.83 ± 4.59
Glucose	Kaolinite	28.9 ± 0.4	20.4 ± 1.3	49.3 ± 1.7	26.99 ± 1.02	0.11 ± 0.02	0.999	34.2 ± 1.6	18.7 ± 1.3	52.9 ± 2.9		0.06 ± 0.01	0.999	3.62 ± 4.61
Acetylglucosamine	Goethite	31.3 ± 0.2	16.6 ± 0.1	47.9 ± 0.3	6.26 ± 1.69	0.11 ± 0	1.000	35.3 ± 0.8	15.3 ± 0.7	50.6 ± 1.4	5.68 ± 5.05	0.06 ± 0	1.000	2.76 ± 1.77
Acetylglucosamine	Illite	24.8 ± 0.3	15.2 ± 0.6	40.1 ± 0.9	16.47 ± 1.66	0.13 ± 0.01	0.999	26.7 ± 1.1	16.3 ± 1	43 ± 2.1		0.07 ± 0	1.000	2.92 ± 3.07
Acetylglucosamine	Kaolinite	17.8 ± 1.2	17.6 ± 1.6	35.4 ± 2.8	2.93 ± 0.64	0.11 ± 0.03	0.998	37 ± 0.2		37 ± 0.2	0.11 ± 0		0.987	1.65 ± 2.97
Phenylalanine	Goethite	22.5 ± 0.6	20.9 ± 0.7	43.4 ± 1.3	5.94 ± 0.28	0.17 ± 0.02	0.999	38.9 ± 3.6	14.7 ± 42.5	53.6 ± 46.1		0.01 ± 0.06	0.930	10.17 ± 47.44
Phenylalanine	Illite	22.4 ± 0.6	15.1 ± 0.6	37.5 ± 1.3	0.15 ± 0.01	1.82 ± 0.09	1.000	29.1 ± 1.4	13.1 ± 0.7	42.2 ± 2.1		0.04 ± 0.01	0.997	4.67 ± 3.38
Phenylalanine	Kaolinite	34.7 ± 0.6	29.8 ± 1.1	64.4 ± 1.7	0.84 ± 0.22	3.34 ± 0.15	0.909	54.9 ± 1.9	11.7 ± 0.7	66.5 ± 2.5		0.03 ± 0.01	0.994	2.11 ± 4.22
Salicylic acid	Goethite	37.6 ± 1	12.5 ± 0.6	50.2 ± 1.6	1.44 ± 0.04	0.11 ± 0.02	1.000	38.2 ± 1	14.8 ± 0.9	53 ± 1.9	2729 ± 1.25	0.06 ± 0	1.000	2.85 ± 3.5
Salicylic acid	Illite	33.6 ± 0.2	18.3 ± 0.3	52 ± 0.5	2.08 ± 0.02	0.11 ± 0.01	1.000	38 ± 1.5	17.9 ± 1.1	55.9 ± 2.6		0.05 ± 0.01	0.999	3.95 ± 3.1
Salicylic acid	Kaolinite	30.7 ± 5	29.8 ± 3.3	60.5 ± 8.4	0.32 ± 0.14	3.34 ± 0.02	0.963	32.8 ± 0.1	29.8 ± 3.3	62.5 ± 3.4	3.34 ± 0.02	0.19 ± 0.01	0.956	2.07 ± 11.8
Citric acid	Goethite	15 ± 0.2	7.1 ± 0	22.1 ± 0.2	0.06 ± 0	2.11 ± 0	0.999	33.3 ± 0.1		33.3 ± 0.1	0.1 ± 0		0.999	11.18 ± 0.34
Citric acid	Illite	52.7 ± 21.9	31.2 ± 12.3	83.9 ± 34.2	0.96 ± 0.3	0.16 ± 0.21	0.999	71.5 ± 1.3	16.9 ± 0.8	88.4 ± 2.1	211.78 ± 0.12	0.05 ± 0.01	0.995	4.44 ± 36.34
Citric acid	Kaolinite	62.9 ± 2.8	21.2 ± 1.3	84.1 ± 4.1	0.65 ± 0.02	0.1 ± 0.03	1.000	70.6 ± 2.6	13.9 ± 2.3	84.5 ± 4.8		0.07 ± 0	0.996	0.46 ± 8.91

Table S3-3. Mass balances in percent of monomers added as mineral adsorbed monomers into Dikopshof and Thyrow soil after three weeks of incubation.

Dikopshof	Mineral	initial mineralization [%]	mineralized [%]	biomass [%]	WEOC [%]	residual [%]	microbial processed [%]	CUE [%]	mass balance [%]
Glucose	Goethite	1.0 ± 0.8	30.5 ± 0.5	2.1 ± 0.1	0.6 ± 0.0	62.3 ± 2.7	32.7 ± 0.5	6.5 ± 0.3	95.5 ± 2.2
Glucose	Kaolinite	14.8 ± 1.6	42.3 ± 5.4	14.1 ± 1.0	4.0 ± 0.1	38.9 ± 0.8	56.4 ± 4.5	25.3 ± 3.6	99.3 ± 4.0
Glucose	Illite	1.7 ± 2.4	27.1 ± 3.8	39.5 ± 6.5	1.9 ± 0.1	31.9 ± 4.1	66.6 ± 3.6	59.1 ± 6.9	100.4 ± 2.2
Acetylglucosamine	Goethite	19.6 ± 2.6	45.2 ± 2.4	12.8 ± 1.4	3.3 ± 0.1	33.9 ± 2.5	58 ± 1.0	22.1 ± 2.9	95.2 ± 2.0
Acetylglucosamine	Kaolinite	4.4 ± 1.7	29.5 ± 1.9	22.7 ± 0.9	8.1 ± 0.3	38.7 ± 11.4	52.2 ± 2.4	43.6 ± 1.5	99.1 ± 13.1
Acetylglucosamine	Illite	3.3 ± 1.4	27.3 ± 1.6	16.1 ± 1.4	2.7 ± 0.2	56 ± 14.3	43.4 ± 0.7	37.1 ± 3.3	102.2 ± 14.6
Phenylalanine	Goethite	5 ± 0.9	46.5 ± 0.9	4.2 ± 0.1	1.3 ± 0.9	40.9 ± 3.4	49.3 ± 2.4	5.5 ± 3.9	91.6 ± 0.4
Phenylalanine	Kaolinite	1 ± 1.0	46.5 ± 1.5	9.1 ± 1.5	2.5 ± 0.0	33.4 ± 7.9	55.6 ± 2.5	16.4 ± 2.0	91.5 ± 10.1
Phenylalanine	Illite	2.7 ± 2.0	38 ± 3.4	3.7 ± 0.4	1.4 ± 0.1	49.6 ± 4.0	41.6 ± 3.0	8.9 ± 1.7	92.6 ± 1.1
Salicylic acid	Goethite	4.7 ± 2.1	48.9 ± 1.4	6.2 ± 0.2	2.2 ± 0.1	38.7 ± 0.3	53 ± 2.9	7.6 ± 5.4	95.8 ± 1.6
Salicylic acid	Kaolinite	8.4 ± 6.5	52.9 ± 6.3	9.9 ± 0.7	4.4 ± 0.2	28.1 ± 2.3	62.8 ± 5.8	16 ± 2.5	95.3 ± 3.9
Salicylic acid	Illite	2.0 ± 2.9	49.2 ± 3	8.1 ± 1.0	3 ± 0.1	38.1 ± 0.8	57.3 ± 3.8	14.1 ± 1.1	98.4 ± 4.0
Citric acid	Goethite	1.6 ± 2.2	59.3 ± 1.7	0.3 ± 0.0	0.1 ± 0.0	38.6 ± 2.7	59.5 ± 1.7	0.5 ± 0.0	98.2 ± 1.2
Citric acid	Kaolinite	3.6 ± 2.7	78.4 ± 1.0	1.0 ± 0.2	0.6 ± 0.1	9.3 ± 1.6	79.4 ± 1.1	1.3 ± 0.2	89.3 ± 2.3
Citric acid	Illite	9.6 ± 2.9	84.1 ± 3.8	0.8 ± 0.0	0.5 ± 0.0	7.2 ± 1.4	84.9 ± 3.7	0.9 ± 0.1	92.6 ± 3.9
Thyrow									
Glucose	Goethite	1.6 ± 0.7	36.6 ± 0.7	10.8 ± 0.6	2.8 ± 0.1	51.1 ± 0.7	47.4 ± 0.5	22.7 ± 1.2	101.3 ± 0.7
Glucose	Kaolinite	9.1 ± 0.3	47.5 ± 0.7	17 ± 2.1	7.3 ± 0.4	25.3 ± 1.1	64.5 ± 1.4	26.3 ± 2.7	97.1 ± 1.4
Glucose	Illite	3.7 ± 0.3	40.4 ± 2.5	39.7 ± 1.7	5.4 ± 0.2	11.7 ± 2.1	80.1 ± 0.9	49.6 ± 2.6	97.2 ± 1.9
Acetylglucosamine	Goethite	20.3 ± 1.4	46.2 ± 1.5	9.7 ± 0.9	4.5 ± 0.1	36.9 ± 0.7	55.9 ± 1.0	17.4 ± 1.8	97.4 ± 1.1
Acetylglucosamine	Kaolinite	0.6 ± 0.4	34.0 ± 4.0	67.4 ± 5.1	10.8 ± 0.6	0.0 ± 0.2	101.4 ± 3.4	66.4 ± 4.0	101.4 ± 6.8
Acetylglucosamine	Illite	5.1 ± 1.3	39.2 ± 2.6	40.8 ± 1.3	5.1 ± 0.1	15.5 ± 13.6	80.0 ± 1.8	51.1 ± 2.3	100.6 ± 13.8
Phenylalanine	Goethite	9.6 ± 1.8	37.7 ± 1.8	3.3 ± 0.1	0.6 ± 0.0	49.5 ± 0.3	41 ± 1.8	8.2 ± 0.4	91.1 ± 2.1
Phenylalanine	Kaolinite	3.3 ± 4.7	45.4 ± 5.9	8.2 ± 0.6	5.6 ± 2.4	36.2 ± 1.7	53.6 ± 5.4	15.5 ± 2.5	95.3 ± 4.5
Phenylalanine	Illite	1.8 ± 1.4	30.9 ± 2.2	11.6 ± 1.3	4.2 ± 0.3	51.1 ± 3.8	42.5 ± 1.0	27.3 ± 3.6	97.8 ± 3.1
Salicylic acid	Goethite	1.5 ± 0.7	48.6 ± 1	5.1 ± 0.2	3.8 ± 0.1	35.7 ± 0.3	53.7 ± 0.8	9.5 ± 0.6	93.2 ± 0.6
Salicylic acid	Kaolinite	3.8 ± 3.4	61.2 ± 5.6	8.4 ± 0.7	5.7 ± 0.2	26.5 ± 1.6	69.7 ± 5.3	12.2 ± 1.6	101.9 ± 4.8
Salicylic acid	Illite	1.7 ± 2.4	51.3 ± 3.5	6.5 ± 0.1	4.2 ± 0.2	34.6 ± 2	57.8 ± 3.6	11.3 ± 0.5	96.7 ± 5.6
Citric acid	Goethite	6.9 ± 2.5	22.4 ± 2.1	0.3 ± 0.0	0.2 ± 0.0	70.5 ± 1.8	22.7 ± 2.1	1.3 ± 0.1	93.5 ± 2.5
Citric acid	Kaolinite	2.1 ± 2.3	82.2 ± 5.1	1.3 ± 0.3	1.1 ± 0.2	12.9 ± 1	83.6 ± 5.4	1.6 ± 0.3	97.5 ± 6.5
Citric acid	Illite	4.7 ± 2.5	82.3 ± 0.6	0.9 ± 0.0	0.7 ± 0.0	11.7 ± 0.1	83.2 ± 0.6	1.1 ± 0.0	95.5 ± 0.7
Glucose	PO_4^{3-} loaded goethite	0.0 ± 0.0	35.6	11.1 ± 0.1	1.7 ± 0.0	50 ± 1.6	46.6 ± 0.1	23.7 ± 0.2	98.3 ± 1.8

Table S3-4. ^{14}C activity in < 450 nm filtered 2 M KCl extracts of chloroform gas fumigated and non-fumigated soil samples of Dikopshof soil amended with glucose adsorbed to goethite. Extraction residues were sequentially extracted using acidic oxalate solution for 4 h in the dark and filtered < 450 nm prior to liquid scintillation counting.

Treatment	Extractant	Replicate 1	Replicate 2 [Bq g^{-1} soil]	Replicate 3	Mean ± STD [Bq g^{-1} soil]
Non-fumigated soil	2M KCl	3.22	3.08	2.85	3.05 ± 0.2
Fumigated soil	2M KCl	23.39	22.88	22.57	22.95 ± 0.3
Non-fumigated soil	acidic oxalate	71.70	76.60	70.20	72.83 ± 2.7
Fumgated soil	acidic oxalate	50.10	49.20	47.40	48.9 ± 1.1
Non-fumigated soil	∑KCl + oxalate	74.92	79.68	73.05	75.88 ± 2.8
Fumgated soil	∑KCl + oxalate	73.49	72.08	69.97	71.85 ± 1.4

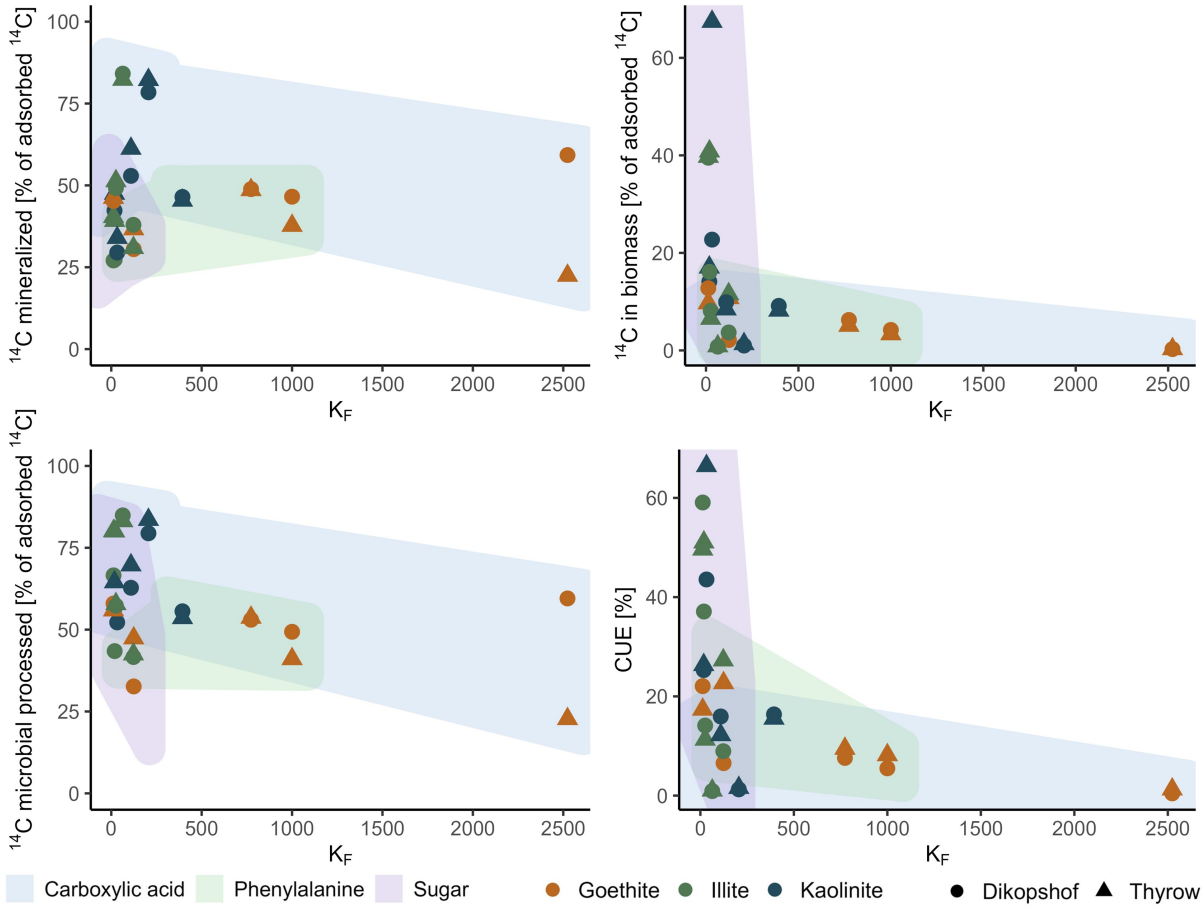

Figure S3-5. Freundlich coefficient K_F plotted against percentage of mineral adsorbed monomer C mineralized (a), assimilated into biomass (b), microbial metabolized (c) and microbial carbon use efficiency (CUE) (d) after three weeks of incubation in Dikopshof and Thyrow soil, respectively.

Supplementary material Chapter IV

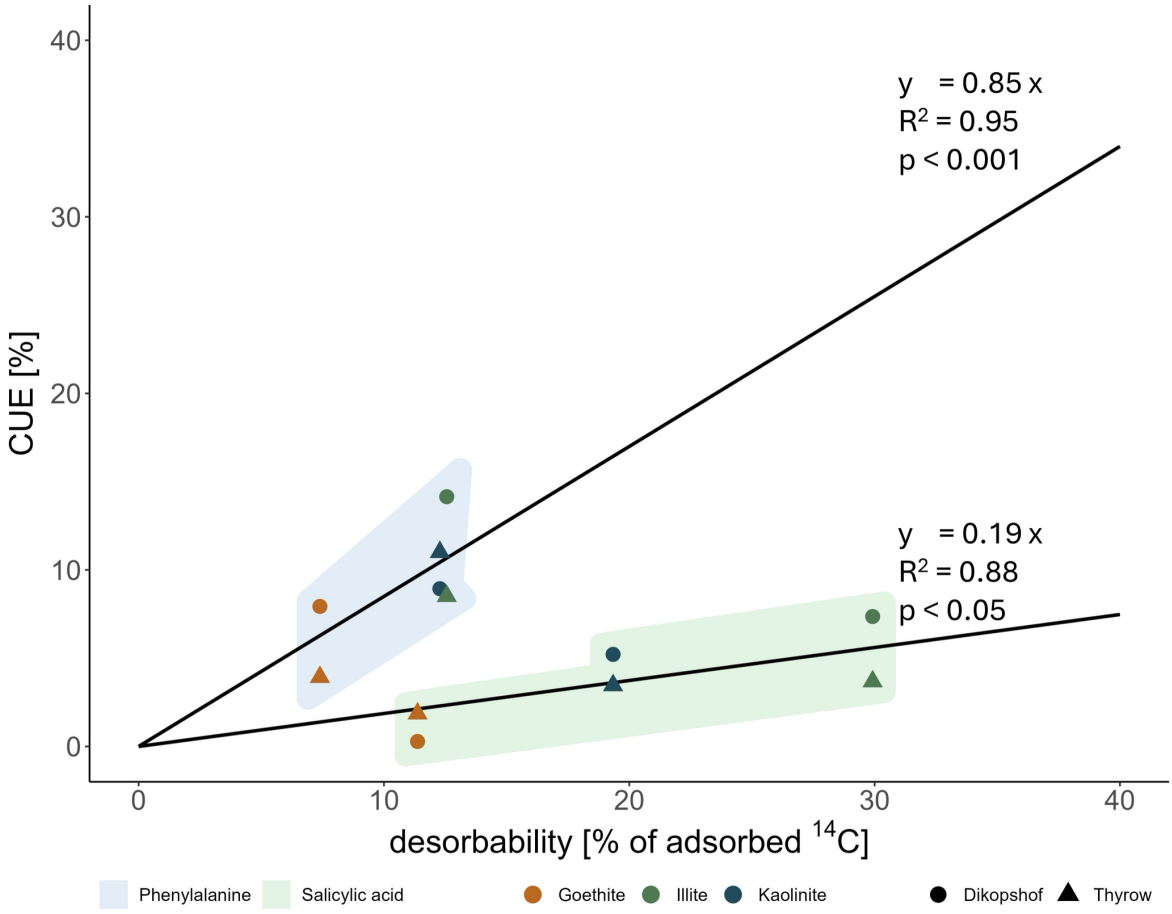

4 Relationship between the desorbability of monomers (expressed as the ratio of desorbable to mineral sorbed amounts as in (Konrad et al., 2025) and the microbial carbon use efficiency (CUE) of the respective substrate.

Supplementary material Chapter V

We calculated the potential flux of colloids into the DGT. To this end we assumed a mean density of the WDC of 2 g cm^{-3}. We calculated WDC of three different fractions: (1) 1/3 of WDC were small particles with 2.5 nm radius, (2) 1/3 were medium particles with 40 nm radius and (3) were large particles with 100 nm radius. We used the mass of colloids added in our experiment (0.523 g), as well as the amount of water added (5.8 ml) to reach 90% waterholding capacity. Based on this assumptions we calculated the following conditions (Tab. 1)

Table S5-1. Boundary conditions for the calculation of diffusional fluxes.

Description	Unit	Value
Volume of one small particle	cm3	6.54498E-20
Volume of one medium particle	cm3	2.68083E-16
Volume of one larger particle	cm3	4.18879E-15
Mass of one small particle	g	1.309E-19
Mass of one medium particle	g	5.36165E-16
Mass of one larger particle	g	8.37758E-15
Total number of particles	absolute number	1.77472E+14
Total number of small particles	absolute number	5.85658E+13
Total number of medium particles	absolute number	6.03405E+13
Total number of larger particles	absolute number	5.85658E+13
Concentration of small particles	number/Liter	1.00976E+16
Concentration of medium particles	number/Liter	1.04035E+16
Concentration of larger particles	number/Liter	1.00976E+16
Total number of small particles	mol	2.94699E-10
Total number of medium particles	mol	1.00198E-10
Total number of larger particles	mol	9.72508E-11
Concentration of small particles	mol/Liter	5.08103E-08
Concentration of medium particles	mol/Liter	1.72755E-08
Concentration of larger particles	mol/Liter	1.67674E-08

We calculated the Diffusion coefficients (D) based on the Stokes-Einstein Equation:

$$D = \frac{k_B \times T}{6\pi \times \mu \times r}$$

with the Boltzmann-constant (kB) (1.3806 x 10^{-23} kg m^2 s^{-2} K^{-1}), the temperature (T) (296.15 K), the viscosity of water at 23° C (μ) (0.00093216 kg m^{-1} s^{-1} and the radii of the particles (m). The calculated coefficients are displayed in Tab. 2.

Table S5-2. Diffusion coefficients of colloids of different sizes.

Description	Unit	Value
Diffusion coefficient small particles	m2 s-1	9.30812E-11
Diffusion coefficient medium particles	m2 s-1	5.81757E-12
Diffusion coefficient larger particles	m2 s-1	2.32703E-12

We calculated the mean square displacement for Brownian particles in one dimension (MSD) based on the calculated Diffusion coefficients (https://en.wikipedia.org/wiki/Mean_squared_displacement) with t as the time of diffusion (s):

$$MSD = 2Dt$$

With results displayed in Tab.3.

Table S5-3. Mean square displacement and mean displacements of colloids of different sizes.

Description	Unit	Value
mean squared displacement small particles	m2	0.000112591
mean squared displacement medium particles	m2	7.03694E-06
mean squared displacement larger particles	m2	2.81477E-06
mean displacement small particles	m	0.010610889
mean displacement medium particles	m	0.002652722
mean displacement larger particles	m	0.001677729

Assuming that the porosity, tortuosity and viscosity of the DGT gels have no influence on the diffusion rate of the colloids, 98% of the small colloids, 21% of the medium colloids and 9% of the large colloids can diffuse through the 0.8 mm thick diffusion layer

into the DGT sink over 168 hours. The underlying calculations can be obtained from the corresponding author (Alexander.Konrad@umwelt.uni-giessen.de)

Supplementary material Chapter VI

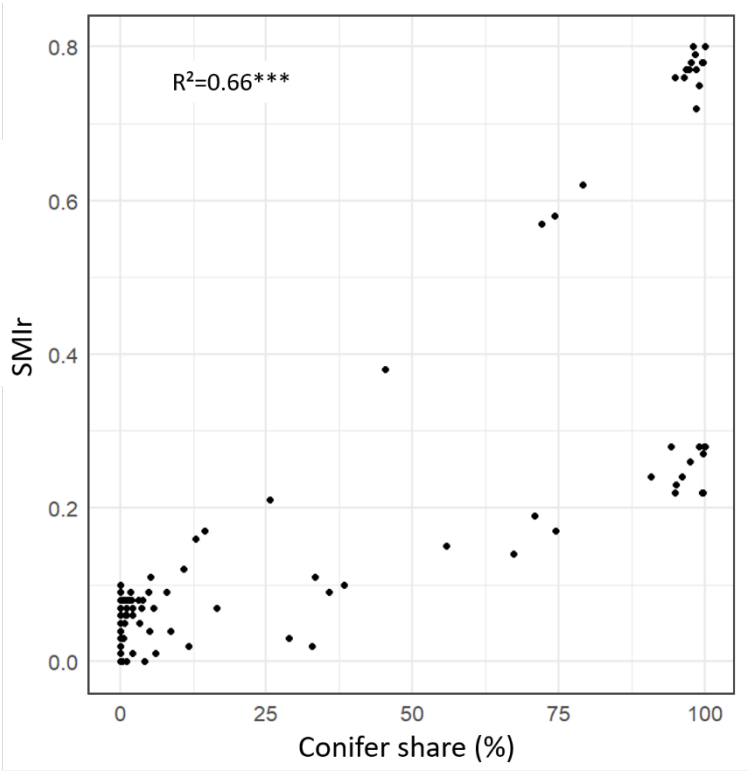

Figure S6-1. Correlation of SMIr – the Silvicultural Management Intensity index reflecting the risk of stand loss – and conifer share. *** denotes a significant correlation at P ≤ 0.001 between the two variables. The splitting of the data points in two groups can be explained by the higher risk of stand loss attributed to spruce stands (upper group) compared to pine stands (lower group).

S2 Characterization of pre-field incubated minerals

Reactions

For pH determination, 10 g of pristine mineral was suspended in 25 ml of 0.01 M $CaCl_2$. The suspension was agitated for 1 hour on a horizontal shaker and centrifuged for 10 minutes at 2500 *g*, and the pH of the supernatant was then measured potentiometrically. The concentration of acid oxalate extractable Al, Fe, Mn, and Si was determined according to Schwertmann (1964). This entailed the extraction of 100 mg of material in 100 ml of 0.2 M NH_4 oxalate (pH 7) for 2 hours in the dark, followed by centrifugation at 2500 *g* for 20 minutes. The supernatants were passed through ash-free paper filters (Rotilabo 114A, Carl Roth GmbH, Karlsruhe, Germany), and Al, Fe, Mn, Si in the extracts were analysed by inductively coupled plasma–optical emission spectrometry (ICP–OES, Ultima 2, Horiba Jobin-Yvon, Longjumeau, France). The concentration of Al, Fe, and Mn in dithionite–citrate–bicarbonate extracts was also analysed by ICP-OES. For this extraction, 100 mg of material (for goethite 20 mg) was mixed with 40 ml 0.3 M Na citrate buffered to pH 8.3 with 10 ml 1 M

$NaHCO_3$. One gram of $Na_2S_2O_4$ was then added to the suspension, before heating to 80°C for 15 minutes. The suspension was centrifuged at 2500 *g* for 20 minutes and the supernatant was passed through an ash-free filter paper (Rotilabo 114A). The procedure was repeated with half the chemicals, and finally the residues (if any) were extracted with 25 ml of 0.05 M $MgCl_2$ (Mehra, 1958). The specific surface area (SSA) of the minerals and quartz sand were calculated by applying the Brunnauer–Emmett–Teller (BET) to N_2 adsorption at 77 K at the relative pressure p/p_0 range of 0.05 to 0.35 (Autosorb IQ MP, Quantachrome Instruments, Boynton Beach, USA). Since N_2 gas cannot access the interlayer spaces of phyllosilicate clays, the BET method estimates the SSA of the external surfaces (Saidy et al., 2013; Baham and Sposito, 1994). The point of zero charge (isoelectric point) of goethite was estimated by determining the electrophoretic mobility of suspended minerals by dynamic light scattering at different pH (Zetasizer Nano ZS, Malvern Panalytical, Malvern, UK).

Element concentrations

Total carbon and nitrogen concentrations of 800 mg sample aliquots was determined by dry combustion elemental analyser (Vario Max Cube, Elementar Analysensysteme GmbH, Langenselbold, Germany). Samples were also tested for inorganic carbon by treating ground 200 mg sample aliquots with 50 ml 2 M HCl at 50 °C and subsequent detection of the released CO_2 (soliTIC modul interfaced to Vario Max Cube, Elementar Analysensysteme GmbH, Langenselbold, Germany). Since none of the samples had detectable contents of inorganic carbon, total carbon was considered to represent exclusively organic carbon (organic C). Total element concentrations were determined by sequential wave length-dispersive X-ray fluorescence spectroscopy (S8 Tiger Series 2, Bruker AXS, Karlsruhe, Germany) using fused beads prepared with 1 g sample aliquots ashed at 1000 °C; analyses were corrected for loss of ignition (including losses of organic C) during ashing.

Cation exchange capacity (CEC) and exchangeable cations

Total cation exchange capacity was determined according to Hendershot et al. (2008). All binding sites available to cations at pH 7 were saturated by equilibrating 500 mg aliquots in 20 ml of 1 M NH_4 acetate (pH 7) solution for 1 hour. Excess NH_4^+ was removed by rinsing with 20 ml of isopropanol. Ammonium ions bound to the mineral surfaces were then extracted by agitation for 1 hour with 20 ml 1 M KCl. Each of the aforementioned steps were repeated three times, with suspensions being centrifuged at 2500 *g* for 20 minutes, and supernatants passed through ash-free paper filters (Rotilabo 114A). The concentration of extracted NH_4^+ was determined photometrically with a continuous flow analyser (SANplus, Skalar Analytical B.V., Breda, The Netherlands). Exchangeable cations were extracted by suspending 1 g aliquots of mineral material in 100 ml 1 M NH_4Cl; shaking horizontally for 60 minutes; and centrifuging at 2500 *g* for 20 minutes. The supernatants were passed through

ash-free paper filters (Rotilabo 114A), and Al, Fe, Mn, Ca, Mg, K, Na in the extracts were analysed by inductively coupled plasma–optical emission spectrometry (ICP–OES, Ultima 2, Horiba Jobin-Yvon, Longjumeau, France). We calculated the Ca, Mg, K, Na saturation by dividing the sum of exchangeable Ca, Mg, K, Na by the total cation exchange capacity. Exchangeable ammonium was extracted by suspending 4 g aliquots of mineral material in 20 ml 1 M KCl; shaking horizontally for 60 minutes; and centrifuging at 2500 *g* for 20 minutes. The supernatants were then passed through ash-free paper filters (Rotilabo 114A), and NH_4^+ in the extracts was analysed photometrically with a continuous flow analyser (SANplus, Skalar Analytical B.V., Breda, The Netherlands).

DOC sorption capacity

Sorption of dissolved organic C (DOC) was tested with leachate solutions (membrane-filtered to <0.45 µm, SUPOR-450, Pall Corp., Port Washington, NY, USA) from different source material (i.e., Spruce Oa DOC, Beech litter DOC and Ryegrass DOC). Increasing amounts of mineral material were added to pH-adjusted 50 ml aliquots of leachate solutions, suspensions were horizontally shaken for 18 hours, centrifuged at 2500 *g* for 20 minutes, and then passed through 0.45-µm membrane filters (SUPOR-450). Solutions were analysed for DOC using a multi N/C 3100 analyser (Analytik Jena AG, Jena, Germany), and sorbed amounts were calculated by the difference in concentrations of initial and equilibrium solutions. The results of this sorption experiment are presented in Figure S6-2. In a similar manner we determined the DOC sorption capacity to goethite and illite across a pH gradient by adding DOC (spruce Oa) solutions that were adjusted to different pH. These results are presented in Figure S.

X-ray diffraction (XRD)

Powder diffractograms were collected in Bragg-Brentano geometry on a D8 Advance instrument (Bruker AXS, Karlsruhe, Germany) equipped with a LYNXEYE XE-T detector. Scans (q-q) were collected at 0.006°2θ step size and 0.9 s/step measuring time using Cu K_a radiation (tube settings: 40 kV and 20 mA for illite and goethite, and 40 kV and 40 mA for sea sand). Samples were rotated (30 rpm) during measurements to minimize preferential orientation effects. Prior to measurements, illite and sea sand samples were ground (10 minutes) to <5 mm particle size using a McCrone micronizing mill. Diffractograms were background-corrected, stripped of K_{a2}, and analysed by the Match! v. 3.12 software (Crystal Impact, Bonn, Germany) utilizing the crystallographic open database (COD). These results are presented in Figure S4.

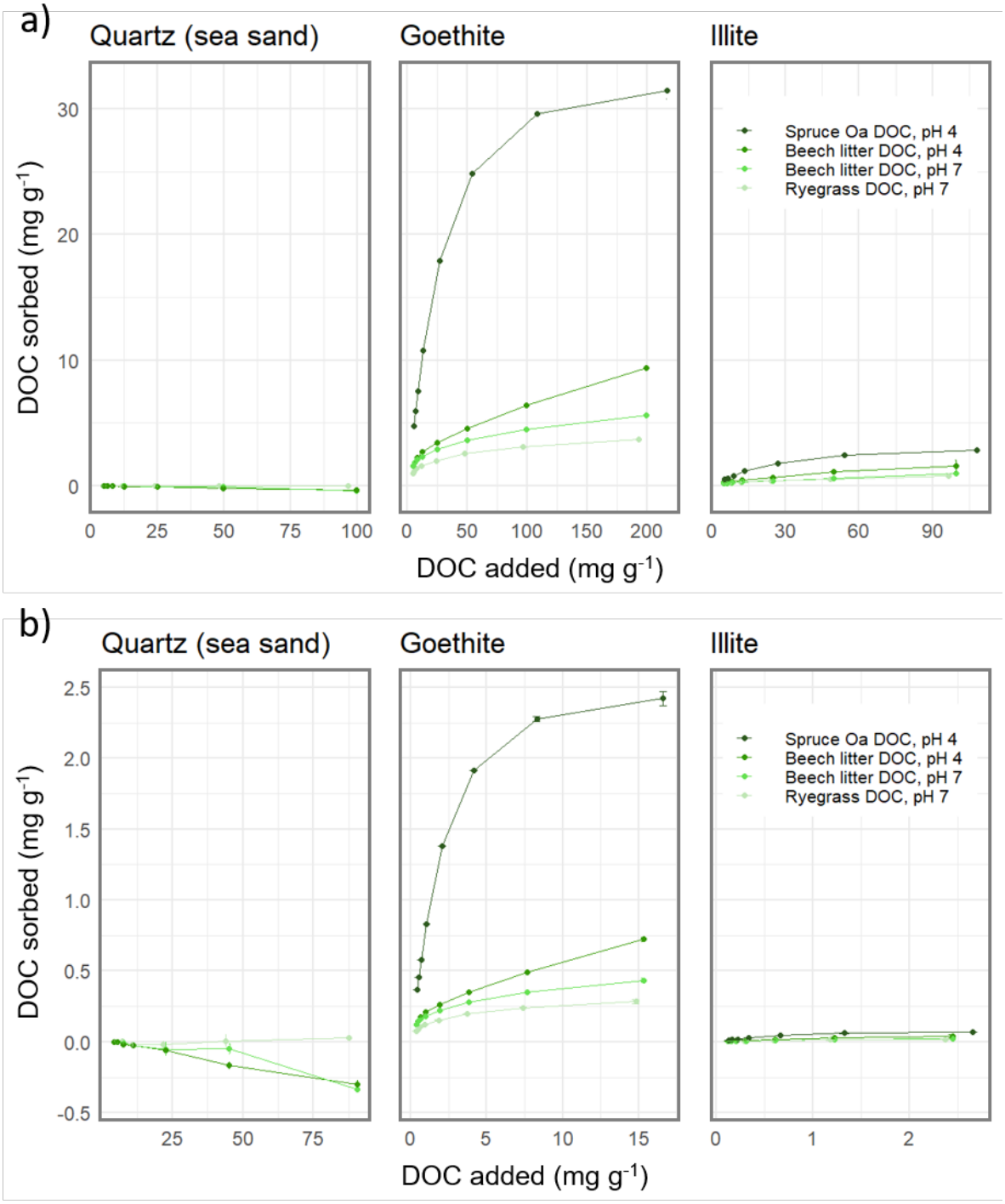

Figure S6-2. Sorption of dissolved organic carbon (DOC) from different sources to sea sand, goethite, and illite at different pH normalized to a) the weight, b) the specific surface area (SSA) of the respective mineral. Since the SSA of the sea sand is very small, values fluctuating around zero when normalized to the weight appear improbably large when normalized to the SSA.

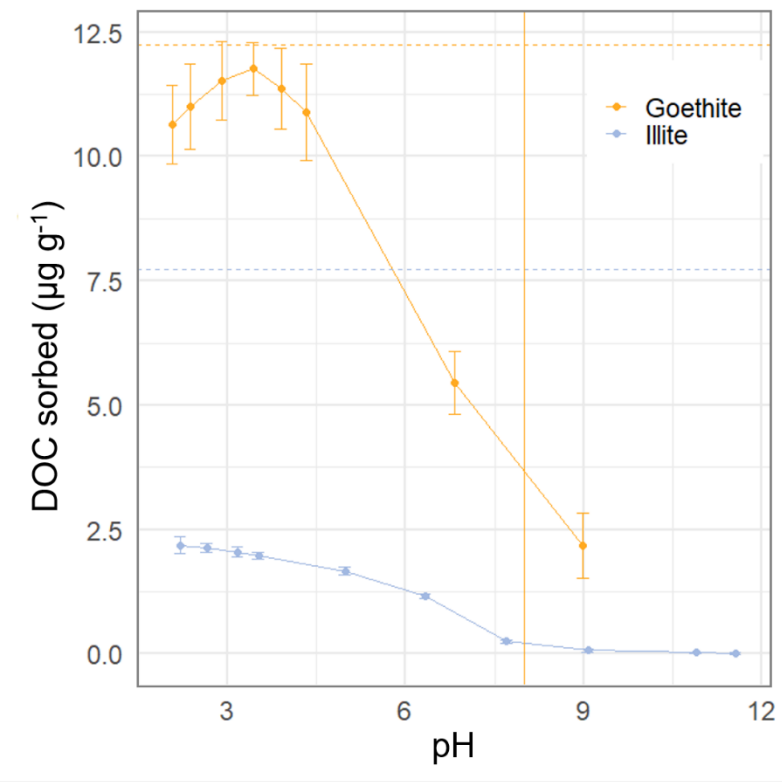

Figure S6-3. Sorption of dissolved organic carbon (DOC) from the Oa horizon of a spruce forest to goethite and illite at differing pH. The orange vertical line depicts the point of zero charge (PZC) of goethite.

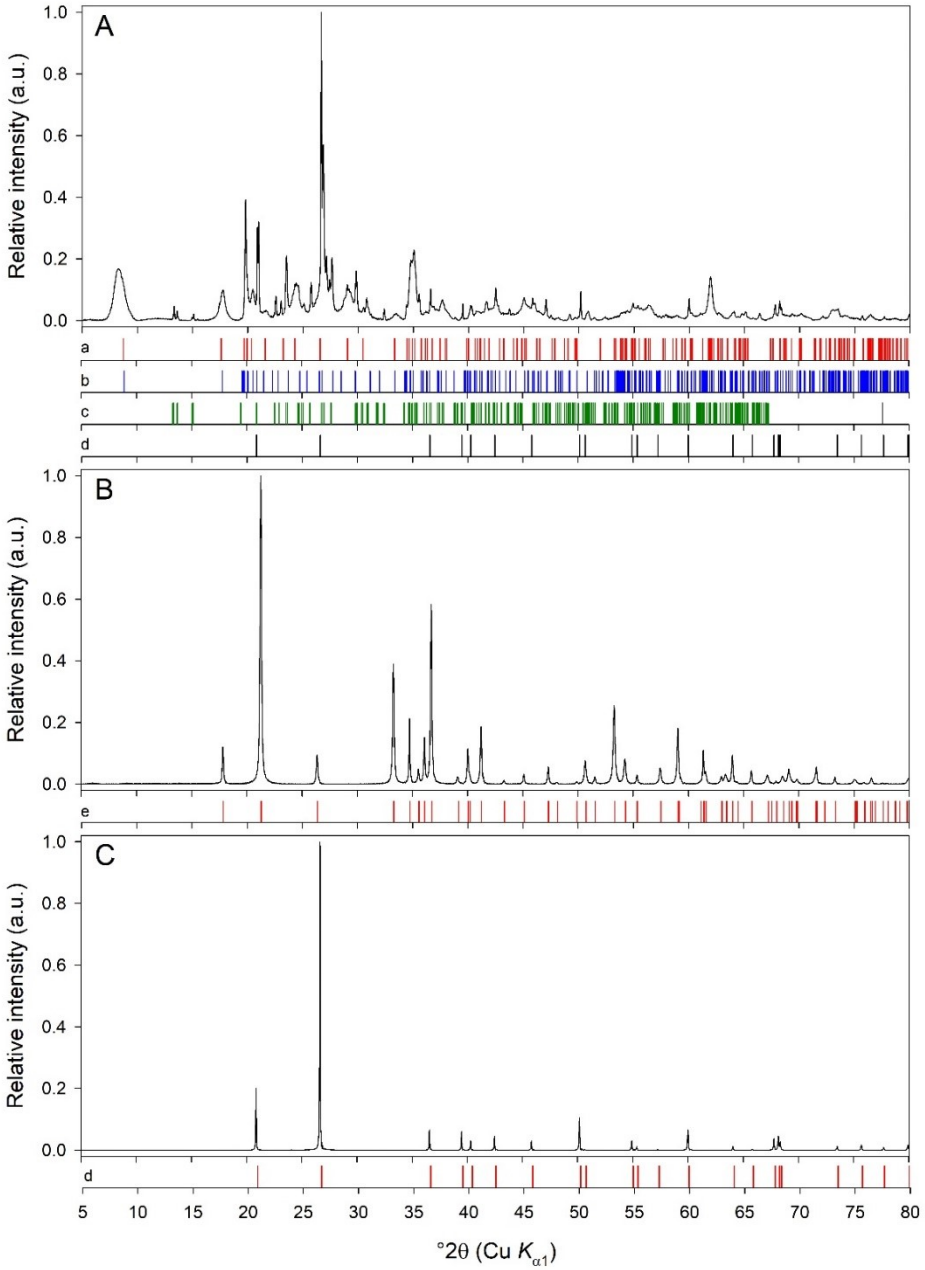

Figure S6-4. Normalized and background-corrected powder X-ray diffractograms of (A) illite, (B) goethite, and (C) sea sand. Reference patterns are (a) illite (COD entry: 96-901-3720), (b) phengite (COD entry: 96-900-5488), (c) microcline (COD entry: 96-900-0702), (d) low-quartz (α-SiO2) (COD entry: 96-101-1098), and (e) goethite (COD entry: 96-221-1653). Goethite is phase pure and the sea sand is phase-pure α-quartz. The illite sample contains micaceous minerals (illite and phengite – a series between muscovite and caledonite; dioctahedral micas), K-feldspar (microcline), and α-quartz.

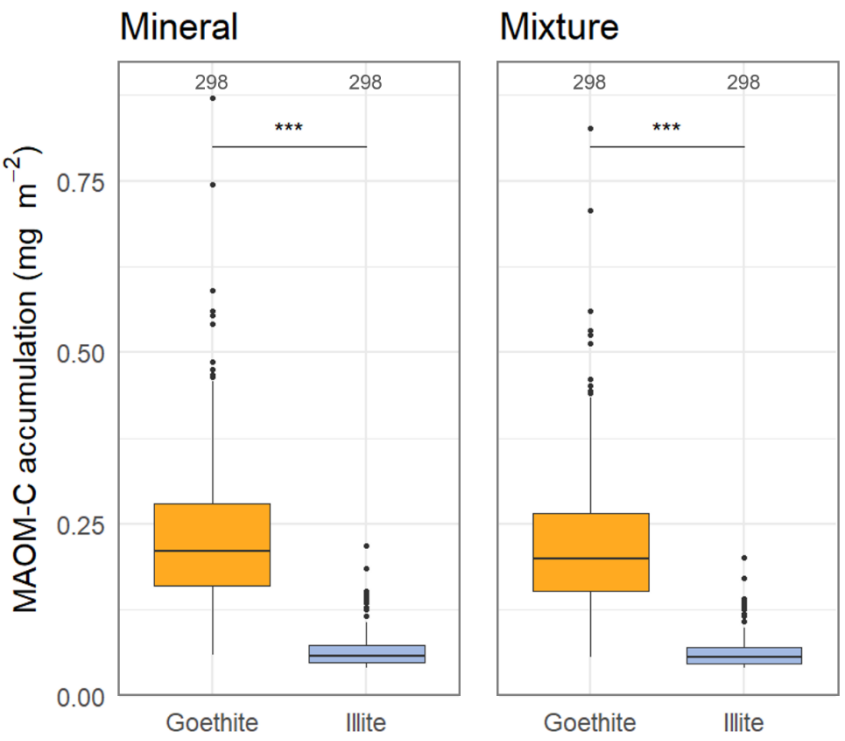

Figure S6-5: Comparison MAOM-C accumulation standardized to the surface area of the minerals goethite and illite (left-hand side) and standardized to the specific surface area of the respective mineral-sand mixtures (right-hand side). The horizontal line represents the median. Outliers are represented by black dots outside the whisker of the plot. *** denotes a significant difference at $P \leq 0.001$ between the two minerals. The number of replicates per box are at the top of the plots.

Determination of other soil properties

We extracted OM from the soils overlying the mineral containers with 0.01 M $CaCl_2$ to quantify the potential input of soluble OM to our mineral containers. Prior to performing the extractions, soil samples were air-dried, moistened to 50% water holding capacity (WHC) and then incubated for 7 days at 5 °C. Air-drying ensured that the WEOM concentrations from different soil samples could be compared (Akagi et al., 2007). After incubation, moist equivalents of 20 g of dry soil were percolated with 40 ml 0.01 M $CaCl_2$ solution in triplicate. The eluates were filtered with syringe filters with 0.45-µm polyether sulfone membranes (VWR International GmbH, Darmstadt, Germany). The concentration of water-extractable organic C (WEOC) in the eluate was measured with a varioTOC analyzer (Elementar Analysensysteme GmbH, Langenselbold, Germany).

In 2017, organic material (<5mm) in the soil organic layer of each forest plot was sampled 14 times along two intersecting 40 m transects with a 225 cm^2 metal frame. We prepared one composite sample for each plot and then dried it at 60 °C for 72 hours

for dry matter content determination. An aliquot of the dried sample was ball milled and analysed for C and N. Organic C stocks were calculated by considering the dry weight of the sample and the area sampled. In the forest plots, 14 core samples of the upper 10 cm of the mineral soil were also taken along the 40 m transects with a split tube auger (diameter of 5 cm). In grasslands, we also took 14 core samples at 10 cm depth along a 20 m transects. One composite sample was prepared for each plot in forests and grasslands. These samples were air dried and sieved to <2 mm after the removal of visible roots. The pH of the mineral soil was then measured on 1:2.5 soil: 0.01 M $CaCl_2$ slurries using a pre-calibrated pH meter (pH meter 538, WTW, Weilheim, Germany) after shaking for 1 hour.

Soil textural analysis was performed using the pipette method (DIN ISO 11277, 2002) on samples collected in 2011. On the same samples, we also measured the concentration of oxalate-extractable Fe and Al (Schwertmann, 1964; Herold et al., 2014) and dithionite-extractable Fe and Al (Holmgren, 1967; Herold et al., 2014).

Plant properties

At all forest plots, we installed five circular litter traps with a diameter of 0.8 m that covered an area of 0.51 m^2 each to quantify litter C inputs. The litter traps were aligned along two 40 m transects. The two transects were at right angle to each other with an intersection at their centre. The litter traps were located at the endpoints of the two transects and at the intersection. The minimum distance between the litter traps was 20 m. Forty-one plots in each region were equipped with litter traps in winter 2015. We installed litter traps at nine additional plots per region in autumn 2016. We collected accumulated litter fall at all plots three times a year in March, June and November in polyester nets with a mesh size of <2 mm that allowed water to penetrate. Immediately, after collection, the litter was oven dried at 60 °C to constant weight. The litter was then sorted into four litter fractions including branches >1 cm in diameter, twigs <1 cm in diameter, fruits and miscellaneous material including mainly leaves and flowers. The mass of each litter component was recorded. In each autumn a separate leaf litter sample was taken. All litter fractions and leaves were shredded and ground in a ball mill (MM300 or MM400, Retsch GmbH, Haan, Germany). The concentrations of total carbon (C) and total nitrogen (N) in aboveground litter were subsequently determined by dry combustion using an elemental analyzer Vario EL (Elementar Analysensysteme GmbH, Langenselbold, Germany). The input of litter C and N was calculated by considering the total dry mass of litter input and the concentration of C and N in the sample. A forest inventory of all 150 forest sites was conducted between 2014 and 2016. The conifer share (%) was calculated as the cumulative basal area of conifer trees over the total basal area.

Plant communities in all 150 grasslands were surveyed every May from 2016-2020. Above ground biomass plant biomass was measured in eight 0.5 m × 0.5 m subplots, which were fenced to prevent livestock grazing or mowing prior to harvest (Apostolakis et al., 2022). In a nearby 4 m × 4 m subplot, we recorded all vascular plant species and calculated the plant species richness for each grassland plot (Apostolakis et al., 2022).

In 2021, we sampled soils from all 150 forests and 150 grasslands using the procedures described above and determined the mass of washed coarse and fine roots after oven-drying at 40 °C for 72 hours (Solly et al., 2014). Total root biomass was calculated as the sum of the mass of coarse and fines roots per unit area.

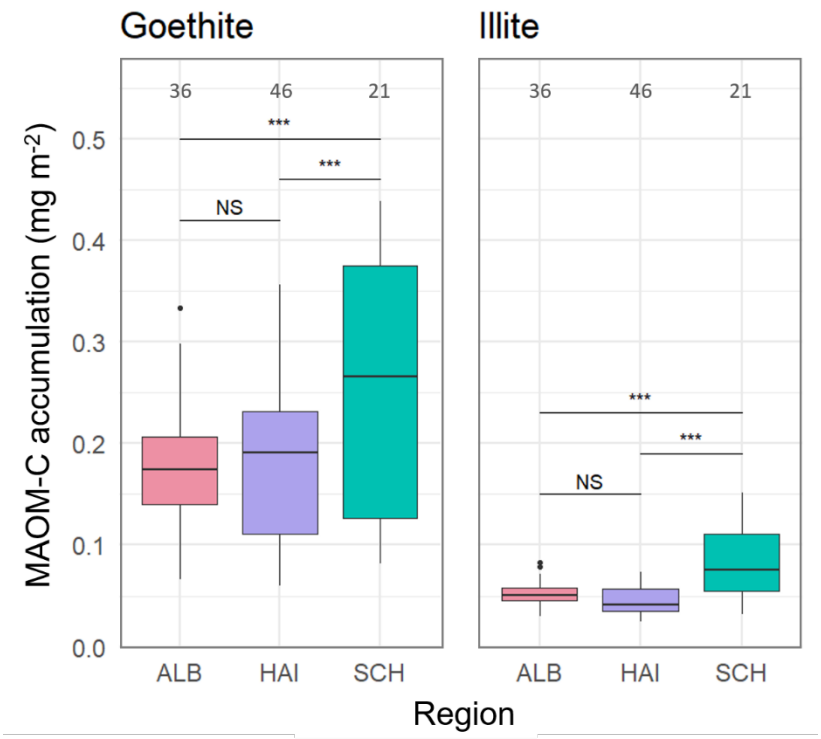

Figure S6-6. Effect of study region on mineral associated organic matter-carbon (MAOM-C) accumulation over 5 years in mineral containers buried at 5cm depth in the mineral soil of beech forests in Germany. The MAOM-C concentration is expressed per m2 of pristine mineral (goethite and illite). Data for each mineral are further separated by study region: Schwäbische Alb (ALB), Hainich Dün (HAI), and Schorfheide-Chorin (SCH). The horizontal line represents the median. Outliers are represented by black dots outside the whisker of the plot. Significance levels: * $P \leq 0.05$; *** $P \leq 0.001$; and NS not significant ($P > 0.05$). The number of replicates per box are at the top of the plots.

Supplementary material Chapter VII

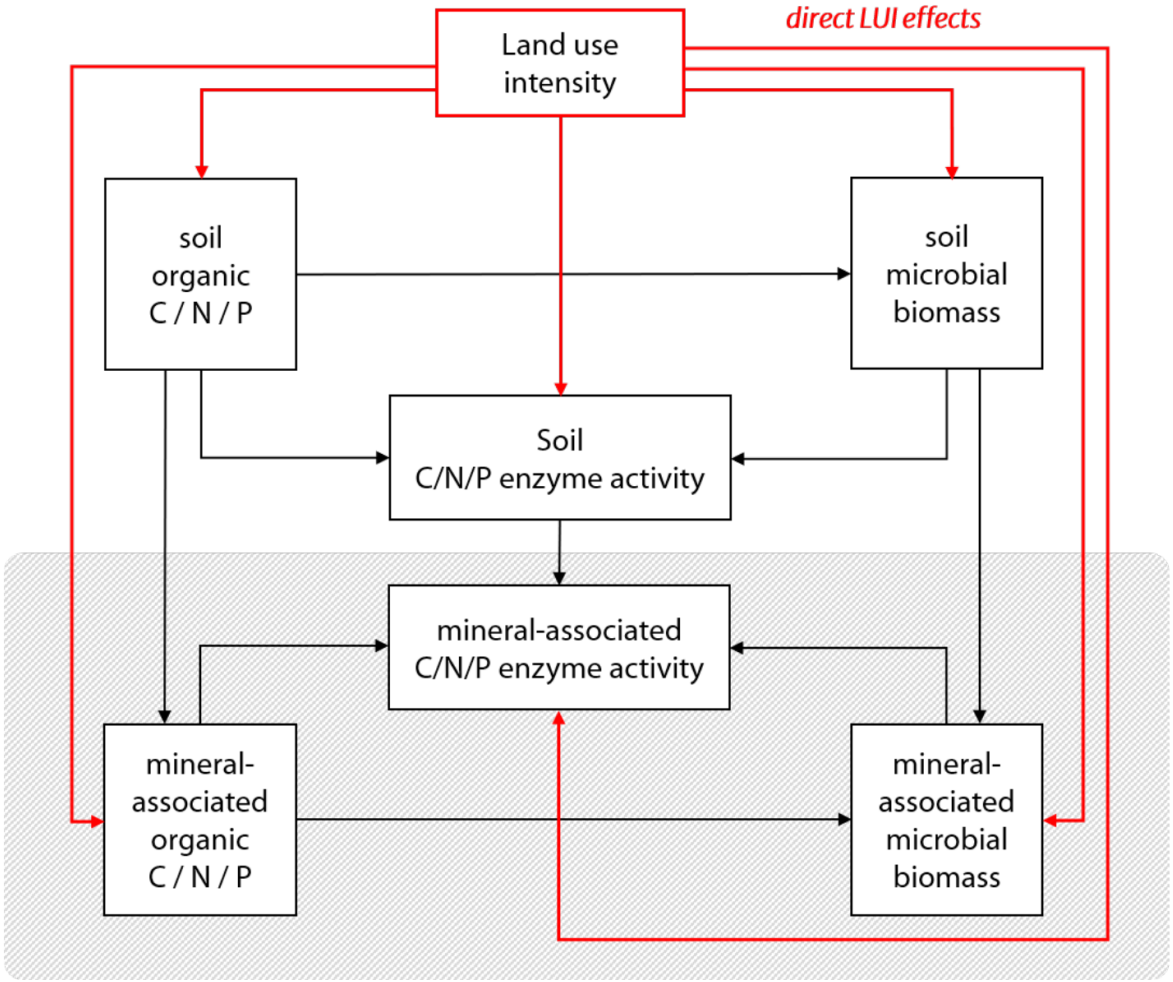

Figure S7-1 General structure of the multi-group SEMs applied separately for the C, N and P cycle; Path lines: red lines show direct effects of land use intensity; grey box indicates mineral associated parameters.

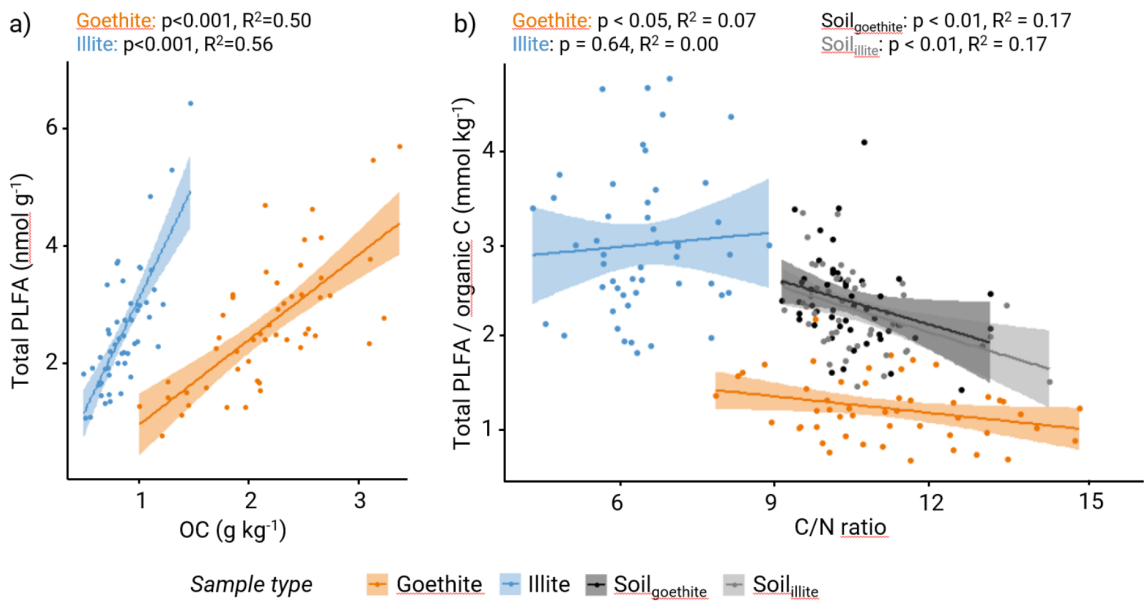

Figure S7-2. Linear regressions between a) microbial biomass and OC content on the minerals, and b) the ratio of total PLFA to organic C and the C/N ratio on minerals and in soils; 95% confidence intervals are shown; statistical significance of linear regressions is depicted above each plot.

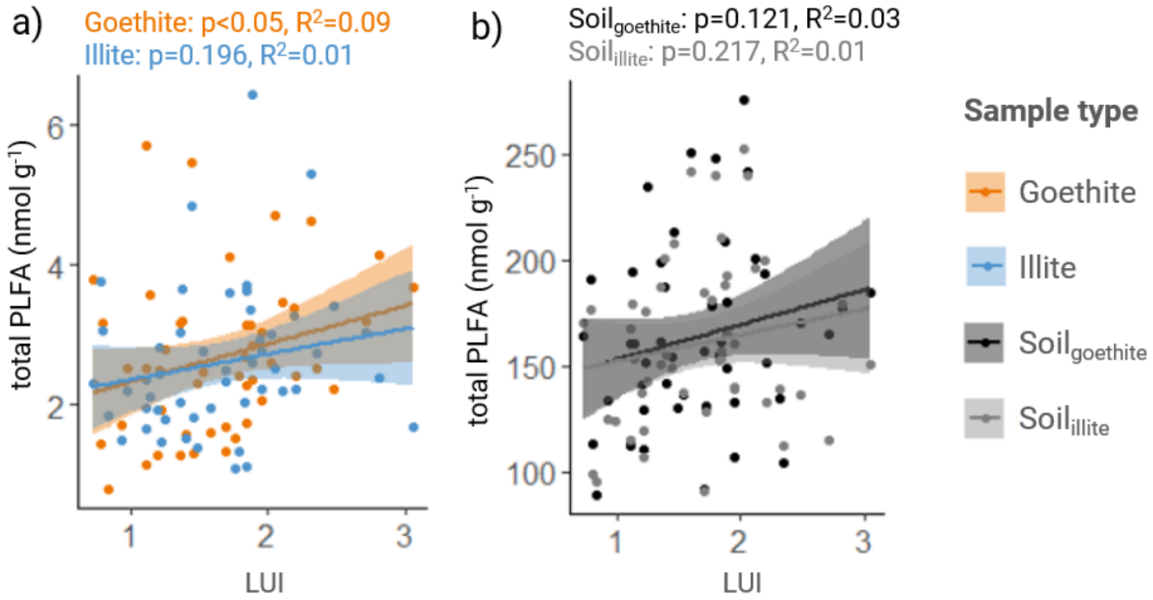

Figure S7-3. Linear regressions between LUI and microbial biomass on minerals (a) and soils (e), LUI and total PLFA / OC ratios on minerals (b) and in soils (f), LUI and fungi to bacteria ratios on minerals (c) and in soils (g) as well as LUI and the activity of β-glucosidase on minerals (d) and in soils (h); 95% confidence intervals are shown; statistical significance of linear regressions is depicted above each plot.

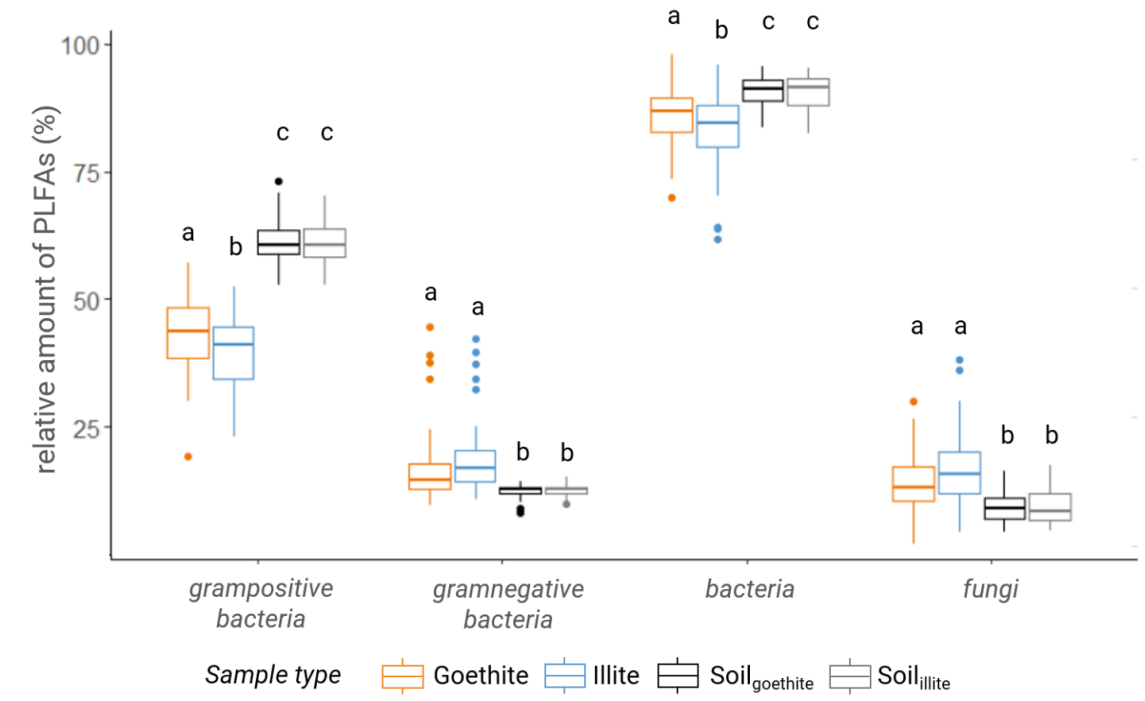

Figure S7-4. Boxplots of the relative contents of PLFAs (%) for main microbial groups; boxes in boxplots represent the median and interquartile range, whiskers extent to 1.5 times the interquartile range (IQR) and points denote outliers; letters above boxplots depict statistically significant ($p<0.05$) differences between the sample types according to linear mixed modeling.

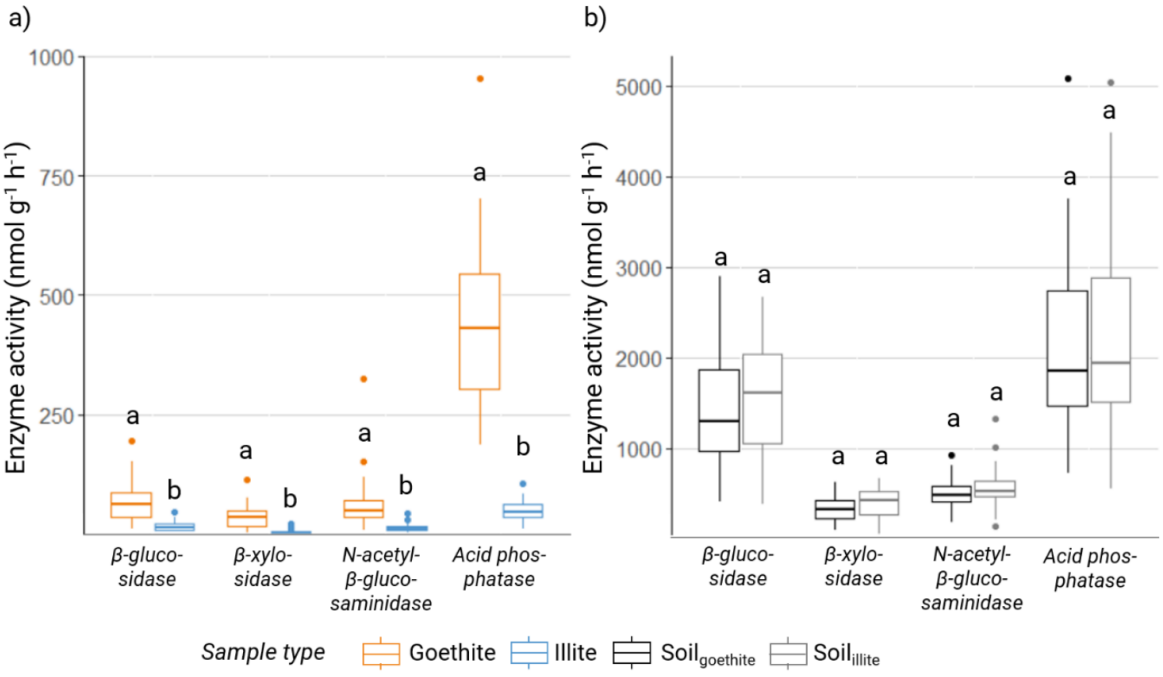

Figure S7-5. Boxplots of absolute enzyme activities a) on minerals and b) in soils; boxes in boxplots represent the median and interquartile range, whiskers extent to 1.5 times the interquartile range (IQR) and points denote outliers; letters above boxplots depict statistically significant ($p<0.05$) differences between the sample types according to linear mixed modeling.

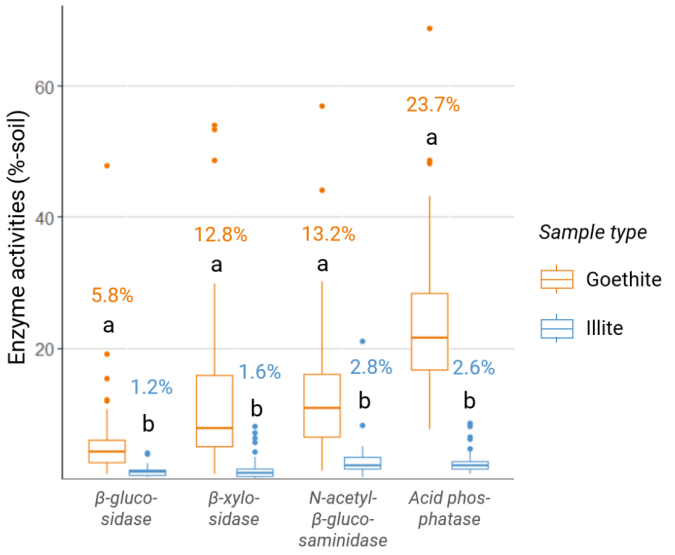

Figure S7-6. Boxplots of enzyme activities expressed as %-soil values; boxes in boxplots represent the median and interquartile range, whiskers extent to 1.5 times the interquartile range (IQR) and points denote outliers; letters above boxplots depict statistically significant ($p<0.05$) differences between the sample types according to linear mixed modeling.

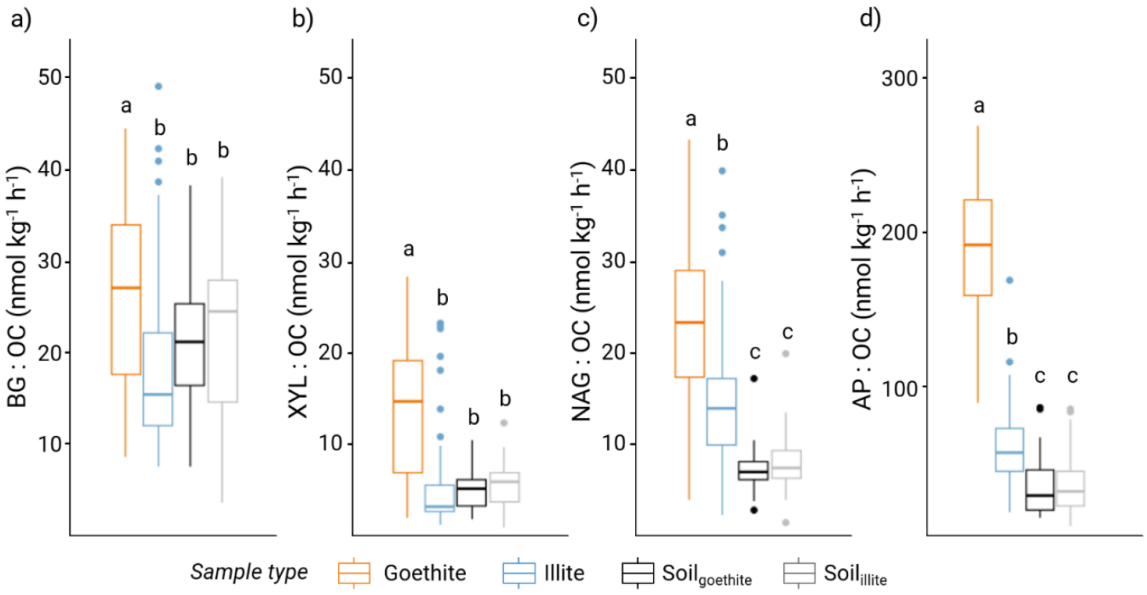

Figure S7-7. Boxplots of the ratio of enzyme activities to organic carbon for a) β-glucosidase, b) β- xylosidase, c) N-acetyl-β-glucosaminidase and d) acid phosphatase; boxes in boxplots represent the median and interquartile range, whiskers extent to 1.5 times the interquartile range (IQR) and points denote outliers; letters above boxplots depict statistically significant ($p<0.05$) differences between the sample types according to linear mixed modeling.

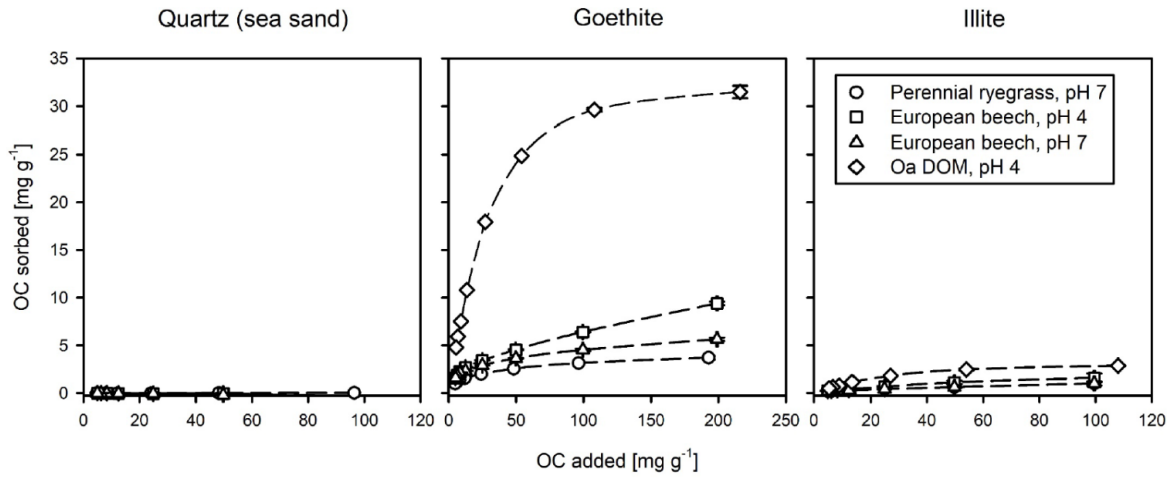

Figure S7-8. Sorption of dissolved OC, either from the Oa horizon of a mor-type organic forest floor layer (pH 4), ryegrass (pH 7), or senescent beech leaves (pH 4 and 7) to quartz sand, goethite and illite.

Methods

Sorption isotherms of dissolved organic carbon from different sources to the three test minerals (goethite, illite, quartz). Error bars represent the standard Error of the mean for triplicate analyses. Sorption was tested using leachate solutions (membrane-filtered to <0.45 µm, SUPOR-450, Pall Corp., Port Washington, NY, USA) either from the Oa horizon of a mor-type organic forest floor layer (pH 4), ryegrass (pH 7), or senescent beech leaves (pH 4 and 7). Increasing amounts of mineral material were added to pH-adjusted 50 ml aliquots of leachate solutions of about 100 mg dissolved organic carbon ml^{-1}. Suspensions were horizontally shaken for 18 hours, centrifuged at 2500 *g* for 20 minutes, and then passed through 0.45-µm membrane filters. Solutions were analysed for dissolved organic carbon using a multi N/C 3100 analyser (Analytik Jena AG, Jena, Germany), and sorbed amounts of organic carbon were calculated by the difference in concentrations of initial and equilibrium solutions.

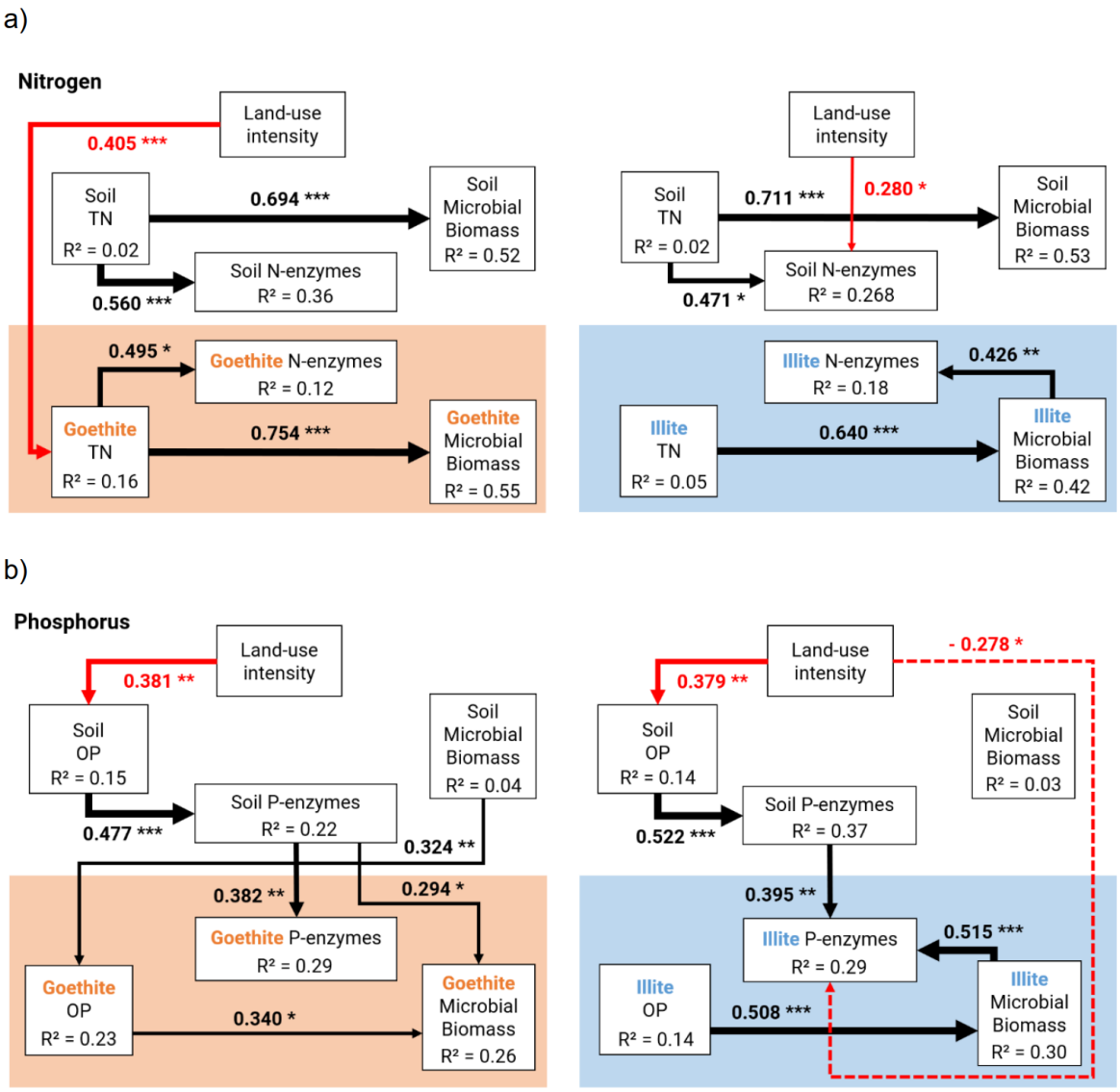

Figure S7-9. Structural equation models showing effects of land use intensity on total nitrogen (TN) and Olsen-extractable organic phosphorus (OP) accumulation, microbial biomass, and enzyme activities, performed separately for elements a) nitrogen and b) phosphorus in goethite (left column) and illite samples (right column). Path lines indicate only significant ($p<0.05$) relationships. A continuous line indicates a positive path coefficient, while a dashed line reflects a negative path coefficient. Numbers on arrows are standardized path coefficients and the thickness of arrows is proportional to the effect size of the coefficient. Red arrows symbolize direct effects of LUI on variables. The amount of explained variance of variables is given as R2 value; variables measured in mineral samples are in orange (goethite) and blue (illite) boxes. The full model output is presented in Table S7-6.

Table S7-1. Site, soil, environmental, and land use intensity-related characteristics of the 50 experimental plots.

EP	Lat	Lon	Elevation (m asl)	Slope (°)	precipitation (mm)	Soil type	pH	Clay (%)	Silt (%)	Sand (%)	average grazing (LU d ha^{-1} $year^{-1}$)	average mowing (times $year^{-1}$)	average fertilization (kg N ha^{-1} $year^{-1}$)	LUI
AEG1	48°40'	9°34'	691.03	2.9	3649	Leptosol	6.8	64.3	32.4	3.3	0.0	2.0	104.9	1.84
AEG2	48°38'	9°47'	752.63	6.2	3649	Leptosol	6.9	51.2	41.1	7.7	0.0	3.0	316.8	2.81
AEG3	48°41'	9°53'	807.72	3.2	3649	Leptosol	6.1	67.2	29.8	3	11.8	1.7	5.1	1.23
AEG4	48°38'	9°42'	660.1	10.6	3649	Leptosol	5.3	48.8	42.7	8.5	108.0	1.0	69.6	1.84
AEG5	48°40'	9°44'	717.79	2.8	3649	Leptosol	6.3	36.5	51.8	11.7	130.5	0.7	56.6	1.79
AEG6	48°40'	9°44'	711.07	7.2	3649	Leptosol	6.0	58.8	38	3.2	129.9	1.0	51.7	1.83
AEG7	48°39'	9°38'	794.66	10.2	3649	Leptosol	7.3	38.5	42.7	18.8	66.9	0.0	0.0	0.93
AEG8	48°42'	9°49'	760.28	3.7	3649	Leptosol	6.6	67.3	31.9	0.8	42.5	1.2	0.0	1.20
AEG9	48°39'	9°50'	742.5	13.3	3465	Leptosol	6.6	55.6	41.7	2.7	101.7	0.0	0.0	1.14
AEG10	48°38'	9°21'	750.27	11.1	3520	Leptosol	5.9	64.7	32.7	2.6	7.6	1.5	0.0	1.12
AEG11	48°49'	9°35'	764.48	5.1	3520	Leptosol	5.4	64.3	32.7	3	0.0	3.2	114.6	2.11
AEG12	48°39'	9°35'	713.08	4.9	3520	Leptosol	6.6	43.6	51.2	5.2	0.0	2.0	111.5	1.87
AEG13	48°39'	9°36'	740.46	7.1	3520	Leptosol	6.3	64.3	31.1	4.6	0.0	2.0	112.3	1.88
AEG14	48°38'	9°52'	729.05	6.1	3969	Leptosol	6.6	52.1	45.3	2.6	0.0	2.3	210.0	2.35
AEG15	48°49'	9°45'	746.77	6.8	3969	Leptosol	5.7	64.2	34	1.8	0.0	3.0	283.5	2.71
AEG16	48°40'	9°46'	723.85	5.8	3969	Leptosol	6.0	52.8	44.9	2.3	274.2	0.7	45.4	2.20
AEG17	48°40'	9°52'	813.11	5.7	3969	Leptosol	6.9	61.8	36.5	1.7	0.0	2.2	39.1	1.53
AEG18	48°38'	9°52'	765.07	3.8	3573	Leptosol	6.9	64.9	33.2	1.9	0.0	2.8	224.5	2.48
AEG19	48°40'	9°45'	719.71	6.1	3573	Leptosol	5.8	63.7	32.7	3.6	242.6	0.5	35.6	2.03
AEG20	48°49'	9°36'	520.63	15.1	3573	Leptosol	6.7	59.7	33.4	6.9	164.7	0.0	0.0	1.46
AEG21	48°44'	9°36'	732.75	3.0	3573	Leptosol	5.8	58.7	39.1	2.2	554.8	1.0	77.5	3.05
AEG22	48°40'	9°51'	796.64	8.5	3625	Leptosol	5.7	70.8	27	2.2	6.6	1.3	20.8	1.21
AEG23	48°42'	9°51'	716.16	1.5	3625	Leptosol	7.1	56.6	38.7	4.7	0.0	2.2	10.3	1.36
AEG24	48°40'	9°49'	768.85	2.8	3625	Leptosol	6.1	63.8	32.9	3.3	34.0	2.7	161.3	2.31
AEG25	48°40'	9°26'	786.12	9.7	3625	Leptosol	7.2	46.3	40.6	13.1	48.2	0.0	0.0	0.79
AEG26	48°40'	9°40'	704.18	13.1	3614	Leptosol	6.8	67.9	24.1	8	291.4	0.0	0.0	1.94
AEG27	48°42'	9°48'	767.26	6.0	3614	Leptosol	6.0	57.6	41	1.4	144.1	0.0	0.0	1.36
AEG28	48°46'	9°49'	783.88	3.4	3614	Leptosol	6.1	59.9	38.5	1.6	74.6	0.0	0.0	0.98
AEG29	48°42'	9°36'	684.93	4.1	3614	Cambisol	5.9	56.6	34.3	9.1	123.1	0.8	0.0	1.49
AEG30	48°46'	9°46'	696.6	6.4	3979	Leptosol	6.6	55.6	37.5	6.9	56.4	1.0	3.7	1.25
AEG31	48°46'	9°46'	728.03	8.1	3979	Leptosol	6.7	59.5	38.1	2.4	89.3	1.0	0.0	1.38
AEG32	48°47'	9°49'	715.44	3.8	3979	Leptosol	5.4	46.1	46.6	7.3	41.8	0.0	0.0	0.73
AEG33	48°45'	9°49'	801.64	5.2	3979	Leptosol	6.0	59.7	38.8	1.5	49.2	0.0	0.0	0.80
AEG34	48°46'	9°50'	773.89	6.4	3699	Leptosol	6.3	42.3	55.4	2.3	84.6	0.5	0.0	1.21
AEG35	48°48'	9°29'	752.49	3.4	3699	Cambisol	5.3	44.6	50.3	5.1	0.0	2.3	114.3	1.95
AEG36	48°48'	9°30'	757.26	3.7	3699	Cambisol	6.0	58.8	21.3	19.9	0.0	2.3	114.3	1.95
AEG37	48°40'	9°41'	714.9	10.0	3699	Cambisol	6.3	56.6	33.4	10	4.2	2.0	109.3	1.88
AEG38	48°44'	9°43'	815.76	1.7	3422	Cambisol	5.6	45.1	46.8	8.1	0.0	2.0	24.2	1.40
AEG39	48°39'	9°43'	702.4	6.1	3422	Cambisol	6.0	46.3	49.3	4.4	4.2	2.0	76.7	1.72
AEG40	48°41'	9°57'	779.4	7.9	3422	Cambisol	6.9	69.8	26.9	3.3	11.4	2.3	81.1	1.84
AEG41	48°37'	9°40'	697.25	8.3	3422	Cambisol	6.3	54.1	40.7	5.2	2.2	2.5	161.0	2.19
AEG42	48°40'	9°38'	707.45	11.1	3605	Cambisol	7.1	15.9	75.7	8.4	15.7	2.8	40.4	1.76
AEG43	48°41'	9°54'	764.28	8.0	3605	Cambisol	6.9	61.3	34.9	3.8	146.0	0.8	0.0	1.59
AEG44	48°38'	9°43'	682.37	13.9	3605	Cambisol	7.3	15.2	73.5	11.3	225.2	0.0	0.0	1.70
AEG45	48°40'	9°46'	733.72	4.3	3605	Cambisol	5.4	52.9	41.7	5.4	21.6	2.7	31.9	1.70
AEG46	48°40'	9°43'	681.49	8.2	3661	Cambisol	6.0	65.9	28.7	5.4	325.9	0.0	0.0	2.05
AEG47	48°42'	9°45'	720.08	16.6	3661	Cambisol	7.5	14.6	70.4	15	95.1	0.0	0.0	1.11
AEG48	48°42'	9°50'	748.76	10.2	3661	Cambisol	7.6	29.5	56.5	14	55.1	0.0	0.0	0.84
AEG49	48°46'	9°50'	809.81	2.7	3661	Cambisol	6.0	45.1	52.2	2.7	95.6	0.0	0.0	1.11
AEG50	48°41'	9°47'	720.1	6.0	3967	Cambisol	6.0	58.9	38.2	2.9	7.0	2.4	15.7	1.45

Table S7-2. Characteristics of the pristine goethite, illite and sea sand.

	unit	Goethite	Illite	Sea sand
Reaction (pH in CaCl2 solution); oxalate- and dithionite–citrate–bicarbonate (DCB)-extractable Al, Fe, and Mn; specific surface area (SSA); point of zero charge (PZC)				
pH (in $CaCl_2$ solution)	-	7.3	7	6.7
Al oxalate	g kg^{-1}	0.17	0.26	n.d.
Fe oxalate	g kg^{-1}	1.82	0.12	n.d.
Al DCB	g kg^{-1}	1.36	n.d.	n.d.
Fe DCB	g kg^{-1}	614.52	0.25	n.d.
Mn DCB	g kg^{-1}	0.28	n.d.	n.d.
SSA (N2-BET)	m^2 g^{-1}	20.4	40.7	1.1
PZC	-	7.8	n.a.	n.a.
Element concentrations				
C	g kg^{-1}	0.4	0.42	0.1
N	g kg^{-1}	0.19	0.38	0.04
C:N	-	2.1	1.1	2.5
Fe	g kg^{-1}	613.49	4.07	n.d.
Mn	g kg^{-1}	0.46	0.07	0.02
Al	g kg^{-1}	2.15	149.33	5.02
Si	g kg^{-1}	0.24	265.58	460.59
K	g kg^{-1}	1	70.24	1.24
Mg	g kg^{-1}	0.28	7.5	0.56
Ca	g kg^{-1}	0.36	2.31	0.29
P	g kg^{-1}	0.12	0.21	0.03
Cation exchange capacity (CEC) and exchangeable cations				
CEC (pH 7)	$mmol_c$ kg^{-1}	n.a.	165.5	4.8
Al^{3+}	$mmol_c$ kg^{-1}	n.a.	<0.01	n.d.
Fe^{3+}	$mmol_c$ kg^{-1}	n.a.	3.7	n.d.
Ca^{2+}	$mmol_c$ kg^{-1}	n.a.	110.4	3.5
Mg^{2+}	$mmol_c$ kg^{-1}	n.a.	33.2	0.4
K^+	$mmol_c$ kg^{-1}	n.a.	14.5	0.5
Na^+	$mmol_c$ kg^{-1}	n.a.	2.6	0.4
NH_4^+	$mmol_c$ kg^{-1}	n.a.	0.03	n.d.
Ca, Mg, K, Na saturation of CEC (pH 7)	%	n.a.	>97	100

n.d. = not detectable; n.a. = not analysed

Methods used for data collected in table S7-2:

Reaction:

Determined by suspending 10 g of material in 25 ml of 0.01 M CaCl2, horizontal agitation for 1 hour, centrifugation for 10 minutes at 2500 g, and potentiometric measurement of pH in the supernatant.

Acid oxalate extraction (Schwertmann 1964):

Extraction of 100 mg of material in 100 ml of 0.2 M NH4 oxalate (pH 7) for 2 hours in the dark, then centrifugation at 2500 g for 20 minutes, supernatants were passed through ash-free paper filters, and Al, Fe, Mn, Si in the extracts were analysed by inductively coupled plasma-optical emission spectrometry (ICP-OES, Ultima 2, Horiba Jobin-Yvon, Longjumeau, France).

Dithionite-citrate-bicarbonate extraction (Mehra & Jackson 1960):

Extraction of 100 mg of material (for goethite 20 mg) with 40 ml 0.3 M Na citrate buffered to pH 8.3 with 10 ml 1 M NaHCO3, with addition of 1 g of Na2S2O4 and heating to 80°C for 15 minutes, centrifugation at 2500 g for 20 minutes; supernatants were passed through ash-free paper filters; the procedure was repeated with half the chemicals, and finally the residues (if any) were extracted with 25 ml of 0.05 M MgCl2. Extracts were analysed for Al, Fe, Mn by inductively coupled plasma-optical emission spectrometry (ICP-OES, Ultima 2, Horiba Jobin-Yvon, Longjumeau, France).

Specific surface area:

Specific surface areas were calculated by applying the Brunnauer-Emmett-Teller (BET) to N2 adsorption at 77 K at the relative pressure p/p0 range of 0.05 to 0.35 (Autosorb IQ MP, Quantachrome Instruments, Boynton Beach, USA).

Organic carbon and total nitrogen:

Determination of total carbon and nitrogen on 800 mg sample aliquots by dry combustion elemental analyser (Vario Max Cube, Elementar Analysensysteme GmbH, Langenselbold, Germany). Samples were also tested for inorganic carbon by treating ground 200 mg sample aliquots with 50 ml 2 M HCl at 50°C and subsequent detection of the released CO2 (soliTIC modul interfaced to Vario Max Cube, Elementar Analysensysteme GmbH, Langenselbold, Germany). Since none of the samples had detectable contents of inorganic carbon, total carbon was considered to represent exclusively organic carbon (OC).

Total element concentrations:

Total element concentrations were determined by sequential wave length-dispersive X-ray fluorescence spectroscopy (S8 Tiger Series 2, Bruker AXS, Karlsruhe, Germany) using fused beads prepared with 1 g sample aliquots ashed at 1000°C; analyses were corrected for loss of ignition (including losses of OC) during ashing.

Total cation exchange capacity at pH 7 (Hendershot et al. 2008):

Saturation of all binding sites available to cations at pH 7 by equilibration of 500 mg aliquots in 20 ml of 1 M NH4 acetate (pH 7) solution for 1 hour (3 times repeated), removal of excess NH4+ by rinsing with 20 ml of isopropanol (3 times repeated), extraction of NH4+ with 20 ml 1 M KCl for 1 hour (3 times repeated), photometric determination of extracted NH4+ with a continuous flow analyser (SANplus, Skalar Analytical B.V., Breda, The Netherlands).

Exchangeable cations:

Mineral materials were extracted by suspending 1 g aliquots in 100 ml 1 M NH4Cl, horizontal agitation for 60 minutes, centrifugation at 2500 g for 20 minutes; the supernatants were passed through ash-free paper filters, and Al, Fe, Mn, Ca, Mg, K, Na in the extracts were analysed by inductively coupled plasma-optical emission spectrometry (ICP-OES, Ultima 2, Horiba Jobin-Yvon, Longjumeau, France).

Exchangeable ammonium:

Mineral materials were extracted by suspending 4 g aliquots in 20 ml 1 M KCl, horizontal agitation for 60 minutes, centrifugation at 2500 g for 20 minutes; the supernatants were then passed through ash-free paper filters, and NH4+ in the extracts was analysed photometrically with a continuous flow analyser (SANplus, Skalar Analytical B.V., Breda, The Netherlands).

Ca, Mg, K, Na saturation: The Ca, Mg, K, Na saturation is the sum of exchangeable Ca, Mg, K, Na divided by the total cation exchange capacity.

Point of zero charge (isoelectric point):

The point of zero charge (isoelectric point) was estimated by determining the electrophoretic mobility of suspended minerals by dynamic light scattering at different pH (Zetasizer Nano ZS, Malvern Panalytical, Malvern, UK). *References* Hendershot W.H., Lalande H., Duquette M. (2008). Chapter 18 Ion exchange and exchangeable cations (p. 197–206). In: Soil Sampling and Methods of Analysis, 2nd edition (Eds. Carter M.R., Gregorich E.G.). CRC Press, Boca Raton, FL, USA. Mehra O.P., Jackson M.L. (1960): Iron oxide removal from soils and clays by a dithionite–citrate system buffered with sodium bicarbonate. Clays and Clay Minerals 7, 317–327. Schwertmann U. (1964). Differenzierung der Eisenoxide des Bodens durch Extraktion mit Ammoniumoxalat-Lösung. Zeitschrift für Pflanzenernährung, Düngung und Bodenkunde 105, 194–202.

Table S7-3. Linear mixed-effects models fit by REML (R function lme) with subsequent comparison of estimated marginal means (EMMs) (R function emmeans).

		class EMM (confidence level 0.95)						pairwise differences of class EMM					
Variable	**Transf.**	**class**	**emmean**	**SE**	**df**	**lower CL**	**upper CL**	**classes**	**estimate**	**SE**	**df**	**t.ratio**	**p.value**
total PLFA	log()	Goethite	0.899	0.0476	49	0.803	0.994	Goethite - Illite	0.0195	0.0600	146	0.325	0.9881
		Illite	0.879	0.0476	49	0.783	0.975	Goethite - $Soil_{goethite}$	-4.1655	0.0600	146	-69.439	<.0001
		$Soil_{goethite}$	5,064	0.0476	49	4,968	5,160	Goethite - $Soil_{illite}$	-4.1452	0.0603	146	-68.701	<.0001
		$Soil_{illite}$	5,044	0.0481	49	4,947	5,140	Illite - $Soil_{goethite}$	-4.1850	0.0600	146	-69.764	<.0001
								Illite - $Soil_{illite}$	-4.1647	0.0603	146	-69.023	<.0001
								$Soil_{goethite}$ - $Soil_{illite}$	0.0203	0.0603	146	0.336	0.9868
gram+:gram- bacteria ratio	-	Goethite	2.91	0.124	49	2.66	3.16	Goethite - Illite	0.544	0.145	146	3.767	0.0014
		Illite	2.36	0.124	49	2.11	2.61	Goethite - $Soil_{goethite}$	-2.124	0.145	146	-14.695	<.0001
		$Soil_{goethite}$	5.03	0.124	49	4.78	5.28	Goethite - $Soil_{illite}$	-2.003	0.145	146	-13.778	<.0001
		$Soil_{illite}$	4.91	0.125	49	4.66	5.16	Illite - $Soil_{goethite}$	-2.668	0.145	146	-18.461	<.0001
								Illite - $Soil_{illite}$	-2.548	0.145	146	-17.523	<.0001
								$Soil_{goethite}$ - $Soil_{illite}$	0.120	0.145	146	0.827	0.8414
fungi:bacteria ratio	log()	Goethite	-1.92	0.0701	49	-2.06	-1.77	Goethite - Illite	-0.1842	0.0697	146	-2.644	0.0445
		Illite	-1.73	0.0701	49	-1.87	-1.59	Goethite - $Soil_{goethite}$	0.4082	0.0697	146	5.858	<.0001
		$Soil_{goethite}$	-2.32	0.0701	49	-2.46	-2.18	Goethite - $Soil_{illite}$	0.3870	0.0701	146	5.519	<.0001
		$Soil_{illite}$	-2.30	0.0705	49	-2.44	-2.16	Illite - $Soil_{goethite}$	0.5924	0.0697	146	8.502	<.0001
								Illite - $Soil_{illite}$	0.5712	0.0701	146	8.146	<.0001
								$Soil_{goethite}$ - $Soil_{illite}$	-0.0212	0.0701	146	-0.302	0.9904
BG activity	log()	Goethite	4.00	0.0753	49	3.85	4.15	Goethite - Illite	1.3422	0.0886	146	15.151	<.0001
		Illite	2.65	0.0753	49	2.50	2.81	Goethite - $Soil_{goethite}$	-3.1714	0.0886	146	-35.799	<.0001
		$Soil_{goethite}$	7.17	0.0753	49	7.02	7.32	Goethite - $Soil_{illite}$	-3.2396	0.0891	146	-36.349	<.0001
		$Soil_{illite}$	7.24	0.0759	49	7.08	7.39	Illite - $Soil_{goethite}$	-4.5136	0.0886	146	-50.950	<.0001
								Illite - $Soil_{illite}$	-4.5818	0.0891	146	-51.409	<.0001
								$Soil_{goethite}$ - $Soil_{illite}$	-0.0682	0.0891	146	-0.765	0.8699
XYL activity	log()	Goethite	3.26	0.0989	49	3.06	3.46	Goethite - Illite	2.0446	0.12	146	17.099	<.0001
		Illite	1.21	0.0989	49	1.02	1.41	Goethite - $Soil_{goethite}$	-2.4530	0.12	146	-20.515	<.0001
		$Soil_{goethite}$	5.71	0.0989	49	5.51	5.91	Goethite - $Soil_{illite}$	-2.5361	0.12	146	-21.084	<.0001
		$Soil_{illite}$	5.80	0.0998	49	5.59	6.00	Illite - $Soil_{goethite}$	-4.4976	0.12	146	-37.614	<.0001
								Illite - $Soil_{illite}$	-4.5807	0.12	146	-38.081	<.0001
								$Soil_{goethite}$ - $Soil_{illite}$	-0.0831	0.12	146	-0.691	0.9004
NAG activity	log()	Goethite	3.87	0.0774	49	3.71	4.02	Goethite - Illite	1.463	0.101	146	14.534	<.0001
		Illite	2.40	0.0774	49	2.25	2.56	Goethite - $Soil_{goethite}$	-2.288	0.101	146	-22.723	<.0001
		$Soil_{goethite}$	6.16	0.0774	49	6.00	6.31	Goethite - $Soil_{illite}$	-2.410	0.101	146	-23.803	<.0001
		$Soil_{illite}$	6.28	0.0782	49	6.12	6.43	Illite - $Soil_{goethite}$	-3.751	0.101	146	-37.257	<.0001
								Illite - $Soil_{illite}$	-3.873	0.101	146	-38.254	<.0001
								$Soil_{goethite}$ - $Soil_{illite}$	-0.122	0.101	146	-1.208	0.6229
AP activity	log()	Goethite	6.01	0.0611	49	5.88	6.13	Goethite - Illite	2.1895	0.0673	146	32.553	<.0001
		Illite	3.82	0.0611	49	3.69	3.94	Goethite - $Soil_{goethite}$	-1.5446	0.0673	146	-22.965	<.0001
		$Soil_{goethite}$	7.55	0.0611	49	7.43	7.67	Goethite - $Soil_{illite}$	-1.6180	0.0677	146	-23.907	<.0001
		$Soil_{illite}$	7.62	0.0616	49	7.50	7.75	Illite - $Soil_{goethite}$	-3.7341	0.0673	146	-55.518	<.0001
								Illite - $Soil_{illite}$	-3.8075	0.0677	146	-56.259	<.0001
								$Soil_{goethite}$ - $Soil_{illite}$	-0.0734	0.0677	146	-1.084	0.6998

Table S7-3. Linear mixed-effects models fit by REML (R function lme) with subsequent comparison of estimated marginal means (EMMs) (R function emmeans).

		class EMM (confidence level 0.95)						pairwise differences of class EMM					
Variable	**Transf.**	**class**	**emmean**	**SE**	**df**	**lower CL**	**upper CL**	**classes**	**estimate**	**SE**	**df**	**t.ratio**	**p.value**
total PLFA:OC	log()	Goethite	0.154	0.0342	49	0.0853	0.223	Goethite - Illite	-0.9079	0.0453	146	-20.050	<.0001
		Illite	1.062	0.0342	49	0.9932	1.131	Goethite - $Soil_{goethite}$	-0.6909	0.0453	146	-15.257	<.0001
		$Soil_{goethite}$	0.845	0.0342	49	0.7762	0.914	Goethite - $Soil_{illite}$	-0.6340	0.0455	146	-13.923	<.0001
		$Soil_{illite}$	0.788	0.0346	49	0.7186	0.858	Illite - $Soil_{goethite}$	0.2170	0.0453	146	4.793	<.0001
								Illite - $Soil_{illite}$	0.2739	0.0455	146	6.016	<.0001
								$Soil_{goethite}$ - $Soil_{illite}$	0.0569	0.0455	146	1.250	0.5963
BG/total PLFA	log()	Goethite	3.10	0.0642	49	2.97	3.23	Goethite - Illite	1.323	0.0811	146	16.315	<.0001
		Illite	1.78	0.0642	49	1.65	1.90	Goethite - $Soil_{goethite}$	0.994	0.0811	146	12.261	<.0001
		$Soil_{goethite}$	2.10	0.0642	49	1.98	2.23	Goethite - $Soil_{illite}$	0.905	0.0815	146	11.099	<.0001
		$Soil_{illite}$	2.19	0.0648	49	2.06	2.32	Illite - $Soil_{goethite}$	-0.329	0.0811	146	-4.054	0.0005
								Illite - $Soil_{illite}$	-0.418	0.0815	146	-5.121	<.0001
								$Soil_{goethite}$ - $Soil_{illite}$	-0.089	0.0815	146	-1.091	0.6956
XYL/ total PLFA	log()	Goethite	2.360	0.0925	49	2.174	2.546	Goethite - Illite	2.025	0.116	146	17.471	<.0001
		Illite	0.335	0.0925	49	0.149	0.521	Goethite - $Soil_{goethite}$	1.712	0.116	146	14.774	<.0001
		$Soil_{goethite}$	0.648	0.0925	49	0.462	0.834	Goethite - $Soil_{illite}$	1.609	0.117	146	13.800	<.0001
		$Soil_{illite}$	0.751	0.0934	49	0.564	0.939	Illite - $Soil_{goethite}$	-0.313	0.116	146	-2.697	0.0387
								Illite - $Soil_{illite}$	-0.416	0.117	146	-3.569	0.0027
								$Soil_{goethite}$ - $Soil_{illite}$	-0.104	0.117	146	-0.888	0.8111
NAG/total PLFA	log()	Goethite	2.97	0.0719	49	2.824	3.11	Goethite - Illite	1.444	0.0907	146	15.926	<.0001
		Illite	1.52	0.0719	49	1.380	1.67	Goethite - $Soil_{goethite}$	1.878	0.0907	146	20.711	<.0001
		$Soil_{goethite}$	1.09	0.0719	49	0.946	1.24	Goethite - $Soil_{illite}$	1.735	0.0912	146	19.023	<.0001
		$Soil_{illite}$	1.23	0.0726	49	1.088	1.38	Illite - $Soil_{goethite}$	0.434	0.0907	146	4.785	<.0001
								Illite - $Soil_{illite}$	0.291	0.0912	146	3.189	0.0094
								$Soil_{goethite}$ - $Soil_{illite}$	-0.143	0.0912	146	-1.568	0.4002
AP/total PLFA	log()	Goethite	5.11	0.0686	49	4.97	5.25	Goethite - Illite	2.1701	0.0773	146	28.064	<.0001
		Illite	2.94	0.0686	49	2.80	3.08	Goethite - $Soil_{goethite}$	2.6209	0.0773	146	33.894	<.0001
		$Soil_{goethite}$	2.49	0.0686	49	2.35	2.63	Goethite - $Soil_{illite}$	2.5263	0.0778	146	32.471	<.0001
		$Soil_{illite}$	2.58	0.0691	49	2.44	2.72	Illite - $Soil_{goethite}$	0.4508	0.0773	146	5.830	<.0001
								Illite - $Soil_{illite}$	0.3562	0.0778	146	4.579	0.0001
								$Soil_{goethite}$ - $Soil_{illite}$	-0.0946	0.0778	146	-1.215	0.6180
BG/OC	log()	Goethite	3.25	0.0680	49	3.12	3.39	Goethite - Illite	0.4148	0.0800	146	5.188	<.0001
		Illite	2.84	0.0680	49	2.70	2.97	Goethite - $Soil_{goethite}$	0.3032	0.0800	146	3.792	0.0012
		$Soil_{goethite}$	2.95	0.0680	49	2.81	3.09	Goethite - $Soil_{illite}$	0.2719	0.0804	146	3.380	0.0051
		$Soil_{illite}$	2.98	0.0685	49	2.84	3.12	Illite - $Soil_{goethite}$	-0.1116	0.0800	146	-1.396	0.5037
								Illite - $Soil_{illite}$	-0.1430	0.0804	146	-1.777	0.2884
								$Soil_{goethite}$ - $Soil_{illite}$	-0.0313	0.0804	146	-0.390	0.9799
XYL/OC	log()	Goethite	2.51	0.0939	49	2.33	2.70	Goethite - Illite	1.1172	0.114	146	9.832	<.0001
		Illite	1.40	0.0939	49	1.21	1.59	Goethite - $Soil_{goethite}$	1.0216	0.114	146	8.991	<.0001
		$Soil_{goethite}$	1.49	0.0939	49	1.30	1.68	Goethite - $Soil_{illite}$	0.9754	0.114	146	8.534	<.0001
		$Soil_{illite}$	1.54	0.0948	49	1.35	1.73	Illite - $Soil_{goethite}$	-0.0956	0.114	146	-0.841	0.8347
								Illite - $Soil_{illite}$	-0.1417	0.114	146	-1.240	0.6025
								$Soil_{goethite}$ - $Soil_{illite}$	-0.0462	0.114	146	-0.404	0.9777

Table S7-3. Linear mixed-effects models fit by REML (R function lme) with subsequent comparison of estimated marginal means (EMMs) (R function emmeans).

		class EMM (confidence level 0.95)						pairwise differences of class EMM					
Variable	**Transf.**	**class**	**emmean**	**SE**	**df**	**lower CL**	**upper CL**	**classes**	**estimate**	**SE**	**df**	**t.ratio**	**p.value**
NAG/OC	log()	Goethite	3.12	0.0718	49	2.98	3.27	Goethite - Illite	0.5359	0.0926	146	5.785	<.0001
		Illite	2.59	0.0718	49	2.44	2.73	Goethite - $Soil_{goethite}$	1.1867	0.0926	146	12.811	<.0001
		$Soil_{goethite}$	1.94	0.0718	49	1.79	2.08	Goethite - $Soil_{illite}$	1.1015	0.0932	146	11.824	<.0001
		$Soil_{illite}$	2.02	0.0725	49	1.88	2.17	Illite - $Soil_{goethite}$	0.6508	0.0926	146	7.026	<.0001
								Illite - $Soil_{illite}$	0.5656	0.0932	146	6.071	<.0001
								$Soil_{goethite}$ - $Soil_{illite}$	-0.0852	0.0932	146	-0.914	0.7973
AP/OC	log()	Goethite	5.26	0.0679	49	5.13	5.40	Goethite - Illite	1.2621	0.0822	146	15.347	<.0001
		Illite	4.00	0.0679	49	3.86	4.14	Goethite - $Soil_{goethite}$	1.9300	0.0822	146	23.467	<.0001
		$Soil_{goethite}$	3.33	0.0679	49	3.20	3.47	Goethite - $Soil_{illite}$	1.8945	0.0827	146	22.898	<.0001
		$Soil_{illite}$	3.37	0.0685	49	3.23	3.51	Illite - $Soil_{goethite}$	0.6678	0.0822	146	8.120	<.0001
								Illite - $Soil_{illite}$	0.6323	0.0827	146	7.643	<.0001
								$Soil_{goethite}$ - $Soil_{illite}$	-0.0355	0.0827	146	-0.429	0.9734
Vector length	-	Goethite	0.549	0.0187	49	0.511	0.586	Goethite - Illite	-0.0646	0.0221	146	-2.926	0.0206
		Illite	0.613	0.0187	49	0.576	0.651	Goethite - $Soil_{goethite}$	-0.2922	0.0221	146	-13.236	<.0001
		$Soil_{goethite}$	0.841	0.0187	49	0.803	0.878	Goethite - $Soil_{illite}$	-0.2816	0.0222	146	-12.679	<.0001
		$Soil_{illite}$	0.830	0.0188	49	0.792	0.868	Illite - $Soil_{goethite}$	-0.2276	0.0221	146	-10.310	<.0001
								Illite - $Soil_{illite}$	-0.2170	0.0222	146	-9.770	<.0001
								$Soil_{goethite}$ - $Soil_{illite}$	0.0106	0.0222	146	0.478	0.9639
Vector angle	-	Goethite	76.5	0.977	49	74.5	78.4	Goethite - Illite	11.26	1.1	146	10.264	<.0001
		Illite	65.2	0.977	49	63.3	67.2	Goethite - $Soil_{goethite}$	15.451	1.1	146	14.084	<.0001
		$Soil_{goethite}$	61.0	0.977	49	59.1	63.0	Goethite - $Soil_{illite}$	15.843	1.1	146	14.353	<.0001
		$Soil_{illite}$	60.6	0.984	49	58.7	62.6	Illite - $Soil_{goethite}$	4.191	1.1	146	3.820	0.0011
								Illite - $Soil_{illite}$	4.583	1.1	146	4.152	0.0003
								$Soil_{goethite}$ - $Soil_{illite}$	0.392	1.1	146	0.355	0.9846
BG mineral: BG soil	log()	Goethite	1.4338	0.0958	48	1.241	1.626	Goethite - Illite	1.38	0.086	48	16.104	<.0001
		Illite	0.0489	0.0965	48	-0.145	0.243						
XYL mineral: XYL soil	log()	Goethite	2.1522	0.129	49	1.893	2.411	Goethite - Illite	2.1	0.114	48	18.491	<.0001
		Illite	0.0516	0.130	48	-0.209	0.312						
NAG mineral:NAG soil	log()	Goethite	2.317	0.107	49	2.102	2.532	Goethite - Illite	1.58	0.121	48	13.123	<.0001
		Illite	0.734	0.108	48	0.517	0.951						
AP mineral:AP soil	log()	Goethite	3.061	0.0710	49	2.918	3.203	Goethite - Illite	2.26	0.074	48	30.525	<.0001
		Illite	0.802	0.0716	48	0.658	0.946						
fungal PLFAs	log()	Goethite	-1.17	0.0635	49	-1.30	-1.04	Goethite - Illite	-0.13309	0.0716	146	-1.859	0.2503
		Illite	-1.04	0.0635	49	-1.17	-0.91	Goethite - $Soil_{goethite}$	-3.81240	0.0716	146	-53.258	<.0001
		$Soil_{goethite}$	2.64	0.0635	49	2.51	2.77	Goethite - $Soil_{illite}$	-3.80631	0.0720	146	-52.848	<.0001
		$Soil_{illite}$	2.64	0.0640	49	2.51	2.76	Illite - $Soil_{goethite}$	-3.67931	0.0716	146	-51.399	<.0001
								Illite - $Soil_{illite}$	-3.67321	0.0720	146	-51.000	<.0001
								$Soil_{goethite}$ - $Soil_{illite}$	0.00609	0.0720	146	0.085	0.9998

Table S7-3. Linear mixed-effects models fit by REML (R function lme) with subsequent comparison of estimated marginal means (EMMs) (R function emmeans).

		class EMM (confidence level 0.95)						pairwise differences of class EMM					
Variable	**Transf.**	**class**	**emmean**	**SE**	**df**	**lower CL**	**upper CL**	**classes**	**estimate**	**SE**	**df**	**t.ratio**	**p.value**
bacterial PLFAs	log()	Goethite	0.745	0.0517	49	0.641	0.849	Goethite - Illite	0.0511	0.0637	146	0.802	0.8533
		Illite	0.694	0.0517	49	0.590	0.798	Goethite - $Soil_{goethite}$	-4.2206	0.0637	146	-66.206	<.0001
		$Soil_{goethite}$	4.965	0.0517	49	4.862	5.069	Goethite - $Soil_{illite}$	-4.1964	0.0641	146	-65.440	<.0001
		$Soil_{illite}$	4.941	0.0521	49	4.837	5.046	Illite - $Soil_{goethite}$	-4.2717	0.0637	146	-67.008	<.0001
								Illite - $Soil_{illite}$	-4.2476	0.0641	146	-66.237	<.0001
								$Soil_{goethite}$ - $Soil_{illite}$	0.0242	0.0641	146	0.377	0.9817
gram+ PLFAs	log()	Goethite	0.0393	0.0573	49	-0.0759	0.1544	Goethite - Illite	0.1066	0.0727	146	1.466	0.4605
		Illite	-0.0673	0.0573	49	-0.1825	0.0478	Goethite - $Soil_{goethite}$	-4.5312	0.0727	146	-62.321	<.0001
		$Soil_{goethite}$	4.5705	0.0573	49	4.4554	4.6857	Goethite - $Soil_{illite}$	-4.5044	0.0731	146	-61.595	<.0001
		$Soil_{illite}$	4.5437	0.0578	49	4.4275	4.6599	Illite - $Soil_{goethite}$	-4.6378	0.0727	146	-63.787	<.0001
								Illite - $Soil_{illite}$	-4.6111	0.0731	146	-63.053	<.0001
								$Soil_{goethite}$ - $Soil_{illite}$	0.0268	0.0731	146	0.366	0.9831
gram- PLFAs	log()	Goethite	-0.93	0.0588	49	-1.048	-0.812	Goethite - Illite	-0.07953	0.0683	146	-1.164	0.6504
		Illite	-0.85	0.0588	49	-0.968	-0.732	Goethite - $Soil_{goethite}$	-3.89740	0.0683	146	-57.045	<.0001
		$Soil_{goethite}$	2.97	0.0588	49	2.850	3.086	Goethite - $Soil_{illite}$	-3.88882	0.0687	146	-56.575	<.0001
		$Soil_{illite}$	2.96	0.0592	49	2.840	3.078	Illite - $Soil_{goethite}$	-3.81787	0.0683	146	-55.881	<.0001
								Illite - $Soil_{illite}$	-3.80929	0.0687	146	-55.418	<.0001
								$Soil_{goethite}$ - $Soil_{illite}$	0.00858	0.0687	146	0.125	0.9993
relative fungal PLFAs	log()	Goethite	2.54	0.0614	49	2.41	2.66	Goethite - Illite	-0.1526	0.0605	146	-2.524	0.0604
		Illite	2.69	0.0614	49	2.56	2.81	Goethite - $Soil_{goethite}$	0.3531	0.0605	146	5.840	<.0001
		$Soil_{goethite}$	2.18	0.0614	49	2.06	2.31	Goethite - $Soil_{illite}$	0.3363	0.0608	146	5.527	<.0001
		$Soil_{illite}$	2.20	0.0618	49	2.08	2.32	Illite - $Soil_{goethite}$	0.5056	0.0605	146	8.364	<.0001
								Illite - $Soil_{illite}$	0.4888	0.0608	146	8.035	<.0001
								$Soil_{goethite}$ - $Soil_{illite}$	-0.0168	0.0608	146	-0.276	0.9926
relative bacterial PLFAs	log()	Goethite	4.451	0.009459	49	4.432	4.470	Goethite - Illite	0.03166	0.0104	146	3.055	0.0141
		Illite	4.420	0.009459	49	4.401	4.439	Goethite - $Soil_{goethite}$	-0.05512	0.0104	146	-5.318	<.0001
		$Soil_{goethite}$	4.507	0.009459	49	4.488	4.526	Goethite - $Soil_{illite}$	-0.05093	0.0104	146	-4.884	<.0001
		$Soil_{illite}$	4.502	0.009529	49	4.483	4.522	Illite - $Soil_{goethite}$	-0.08678	0.0104	146	-8.373	<.0001
								Illite - $Soil_{illite}$	-0.08259	0.0104	146	-7.920	<.0001
								$Soil_{goethite}$ - $Soil_{illite}$	0.00418	0.0104	146	0.401	0.9781
relative gram+ PLFAs	log()	Goethite	3.75	0.0208	49	3.70	3.79	Goethite - Illite	0.08713	0.0242	146	3.600	0.0024
		Illite	3.66	0.0208	49	3.62	3.70	Goethite - $Soil_{goethite}$	-0.36576	0.0242	146	-15.113	<.0001
		$Soil_{goethite}$	4.11	0.0208	49	4.07	4.15	Goethite - $Soil_{illite}$	-0.35892	0.0243	146	-14.741	<.0001
		$Soil_{illite}$	4.10	0.0210	49	4.06	4.15	Illite - $Soil_{goethite}$	-0.45290	0.0242	146	-18.714	<.0001
								Illite - $Soil_{illite}$	-0.44605	0.0243	146	-18.320	<.0001
								$Soil_{goethite}$ - $Soil_{illite}$	0.00684	0.0243	146	0.281	0.9922
relative gram- PLFAs	log()	Goethite	-0.93	0.0588	49	-1.048	-0.812	Goethite - Illite	-0.07953	0.0683	146	-1.164	0.6504
		Illite	-0.85	0.0588	49	-0.968	-0.732	Goethite - $Soil_{goethite}$	-3.89740	0.0683	146	-57.045	<.0001
		$Soil_{goethite}$	2.97	0.0588	49	2.850	3.086	Goethite - $Soil_{illite}$	-3.88882	0.0687	146	-56.575	<.0001
		$Soil_{illite}$	2.96	0.0592	49	2.840	3.078	Illite - $Soil_{goethite}$	-3.81787	0.0683	146	-55.881	<.0001
								Illite - $Soil_{illite}$	-3.80929	0.0687	146	-55.418	<.0001
								$Soil_{goethite}$ - $Soil_{illite}$	0.00858	0.0687	146	0.125	0.9993

Table S7-3. Linear mixed-effects models fit by REML (R function lme) with subsequent comparison of estimated marginal means (EMMs) (R function emmeans).

		class EMM (confidence level 0.95)						pairwise differences of class EMM					
Variable	**Transf.**	**class**	**emmean**	**SE**	**df**	**lower CL**	**upper CL**	**classes**	**estimate**	**SE**	**df**	**t.ratio**	**p.value**
TC (mineral-sand)	log()	Goethite	0.746	0.0358	49	0.674	0.8180	Goethite - Illite	0.917385	0.0504	147	18.216	<.0001
		Illite	-0.171	0.0358	49	-0.243	-0.0994	Goethite - $Soil_{goethite}$	-3.521073	0.0504	147	-69.917	<.0001
		$Soil_{goethite}$	4.267	0.0358	49	4.195	4.3391	Goethite - $Soil_{illite}$	-3.521494	0.0504	147	-69.925	<.0001
		$Soil_{illite}$	4.267	0.0358	49	4.195	4.3395	Illite - $Soil_{goethite}$	-4.438458	0.0504	147	-88.133	<.0001
								Illite - $Soil_{illite}$	-4.438879	0.0504	147	-88.141	<.0001
								$Soil_{goethite}$ - $Soil_{illite}$	-0.000421	0.0504	147	-0.008	1
TC (mineral)	log()	Goethite	1.44	0.0358	49	1.37	1.51	Goethite - Illite	0.288776	0.0504	147	5.734	<.0001
		Illite	1.15	0.0358	49	1.08	1.22	Goethite - $Soil_{goethite}$	-4.149682	0.0504	147	-82.399	<.0001
		$Soil_{goethite}$	5.59	0.0358	49	5.52	5.66	Goethite - $Soil_{illite}$	-4.150103	0.0504	147	-82.407	<.0001
		$Soil_{illite}$	5.59	0.0358	49	5.52	5.66	Illite - $Soil_{goethite}$	-4.438458	0.0504	147	-88.133	<.0001
								Illite - $Soil_{illite}$	-4.438879	0.0504	147	-88.141	<.0001
								$Soil_{goethite}$ - $Soil_{illite}$	-0.000421	0.0504	147	-0.008	1
IC (mineral-sand	-	Goethite	0.0018	0.824	49	-1.655	1.66	Goethite - Illite	-0.0052	1.02	147	-0.005	1.0000
		Illite	0.0070	0.824	49	-1.650	1.66	Goethite - $Soil_{goethite}$	-3.9241	1.02	147	-3.857	0.0010
		$Soil_{goethite}$	3.9259	0.824	49	2.269	5.58	Goethite - $Soil_{illite}$	-1.4884	1.02	147	-1.463	0.4625
		$Soil_{illite}$	1.4902	0.824	49	-0.167	3.15	Illite - $Soil_{goethite}$	-3.9189	1.02	147	-3.852	0.0010
								Illite - $Soil_{illite}$	-1.4832	1.02	147	-1.458	0.4656
								$Soil_{goethite}$ - $Soil_{illite}$	2.4357	1.02	147	2.394	0.0827
IC (mineral)	-	Goethite	0.0036	3.09	49	-6.209	6.22	Goethite - Illite	-0.0226	3.82	147	-0.006	1.0000
		Illite	0.0262	3.09	49	-6.187	6.24	Goethite - $Soil_{goethite}$	-14.7184	3.82	147	-3.858	0.0010
		$Soil_{goethite}$	14.7220	3.09	49	8.509	20.93	Goethite - $Soil_{illite}$	-5.5845	3.82	147	-1.464	0.4621
		$Soil_{illite}$	5.5881	3.09	49	-0.625	11.80	Illite - $Soil_{goethite}$	-14.6958	3.82	147	-3.852	0.0010
								Illite - $Soil_{illite}$	-5.5619	3.82	147	-1.458	0.4657
								$Soil_{goethite}$ - $Soil_{illite}$	9.1339	3.82	147	2.394	0.0827
OC (mineral-sand)	log()	Goethite	1.44	0.0351	49	1.37	1.51	Goethite - Illite	0.2988	0.0476	147	6.273	<.0001
		Illite	1.14	0.0351	49	1.07	1.21	Goethite - $Soil_{goethite}$	-4.1032	0.0476	147	-86.144	<.0001
		$Soil_{goethite}$	5.54	0.0351	49	5.47	5.61	Goethite - $Soil_{illite}$	-4.1337	0.0476	147	-86.784	<.0001
		$Soil_{illite}$	5.57	0.0351	49	5.50	5.64	Illite - $Soil_{goethite}$	-4.4020	0.0476	147	-92.417	<.0001
								Illite - $Soil_{illite}$	-4.4324	0.0476	147	-93.057	<.0001
								$Soil_{goethite}$ - $Soil_{illite}$	-0.0305	0.0476	147	-0.64	0.9189
OC (mineral)	log()	Goethite	0.745	0.0351	49	0.674	0.815	Goethite - Illite	0.9274	0.0476	147	19.470	<.0001
		Illite	-0.183	0.0351	49	-0.253	-0.112	Goethite - $Soil_{goethite}$	-3.4746	0.0476	147	-72.947	<.0001
		$Soil_{goethite}$	4.219	0.0351	49	4.149	4.290	Goethite - $Soil_{illite}$	-3.5051	0.0476	147	-73.587	<.0001
		$Soil_{illite}$	4.250	0.0351	49	4.179	4.320	Illite - $Soil_{goethite}$	-4.4020	0.0476	147	-92.417	<.0001
								Illite - $Soil_{illite}$	-4.4324	0.0476	147	-93.057	<.0001
								$Soil_{goethite}$ - $Soil_{illite}$	-0.0305	0.0476	147	-0.640	0.9189
TN (mineral-sand)	log()	Goethite	-1.66	0.0327	49	-1.72	-1.59	Goethite - Illite	0.3851	0.0407	147	9.464	<.0001
		Illite	-2.04	0.0327	49	-2.11	-1.98	Goethite - $Soil_{goethite}$	-3.5311	0.0407	147	-86.768	<.0001
		$Soil_{goethite}$	1.88	0.0327	49	1.81	1.94	Goethite - $Soil_{illite}$	-3.5379	0.0407	147	-86.935	<.0001
		$Soil_{illite}$	1.88	0.0327	49	1.82	1.95	Illite - $Soil_{goethite}$	-3.9163	0.0407	147	-96.231	<.0001
								Illite - $Soil_{illite}$	-3.9231	0.0407	147	-96.399	<.0001
								$Soil_{goethite}$ - $Soil_{illite}$	-0.0068	0.0407	147	-0.167	0.9983

Table S7-3. Linear mixed-effects models fit by REML (R function lme) with subsequent comparison of estimated marginal means (EMMs) (R function emmeans).

		class EMM (confidence level 0.95)						pairwise differences of class EMM					
Variable	**Transf.**	**class**	**emmean**	**SE**	**df**	**lower CL**	**upper CL**	**classes**	**estimate**	**SE**	**df**	**t.ratio**	**p.value**
TN (mineral)	log()	Goethite	-0.963	0.0327	49	-1.028	-0.897	Goethite - Illite	-0.2435	0.0407	147	-5.983	<.0001
		Illite	-0.719	0.0327	49	-0.785	-0.654	Goethite - $Soil_{goethite}$	-4.1597	0.0407	147	-102.214	<.0001
		$Soil_{goethite}$	3.197	0.0327	49	3.131	3.263	Goethite - $Soil_{illite}$	-4.1666	0.0407	147	-102.381	<.0001
		$Soil_{illite}$	3.204	0.0327	49	3.138	3.270	Illite - $Soil_{goethite}$	-3.9163	0.0407	147	-96.231	<.0001
								Illite - $Soil_{illite}$	-3.9231	0.0407	147	-96.399	<.0001
								$Soil_{goethite}$ - $Soil_{illite}$	-0.0068	0.0407	147	-0.167	0.9983
TP (mineral)	log()	Goethite	0.735	0.103	49	0.527	0.943	Goethite - Illite	-1.41	0.0655	146	-21.544	<.0001
		Illite	2.146	0.103	49	1.938	2.354	Goethite - Soil	-3.84	0.0660	146	-58.258	<.0001
		Soil	4.578	0.104	49	4.370	4.787	Illite - Soil	-2.43	0.0660	146	-36.871	<.0001
TP (mineral-sand)	log()	Goethite	2.40	0.0175	49	2.37	2.44	Goethite - Illite	0.5423	0.0199	146	27.217	<.0001
		Illite	1.86	0.0175	49	1.82	1.89	Goethite - $Soil_{goethite}$	0.0566	0.0199	146	2.839	0.0263
		$Soil_{goethite}$	2.34	0.0175	49	2.31	2.38	Goethite - $Soil_{illite}$	0.0437	0.0200	146	2.182	0.1330
		$Soil_{illite}$	2.36	0.0177	49	2.32	2.39	Illite - $Soil_{goethite}$	-0.4857	0.0199	146	-24.378	<.0001
								Illite - $Soil_{illite}$	-0.4985	0.0200	146	-24.869	<.0001
								$Soil_{goethite}$ - $Soil_{illite}$	-0.0128	0.0200	146	-0.640	0.9190
IP (mineral-sand)	-	Goethite	-5.074	0.418	49	-5.91	-4.235	Goethite - Illite	-4.52	0.485	145	-9.322	<.0001
		Illite	-0.555	0.418	49	-1.39	0.284	Goethite - Soil	-8.93	0.488	145	-18.303	<.0001
		Soil	3.853	0.421	49	3.01	4.700	Illite - Soil	-4.41	0.488	145	-9.039	<.0001
OP (mineral-sand)	log()	Goethite	0.674	0.102	49	0.468	0.880	Goethite - Illite	-0.0271	0.0848	145	-0.320	0.9886
		Illite	0.701	0.102	49	0.495	0.907	Goethite - $Soil_{goethite}$	-1.7449	0.0854	145	-20.440	<.0001
		$Soil_{goethite}$	2.419	0.103	49	2.212	2.626	Goethite - $Soil_{illite}$	-1.7449	0.0854	145	-20.440	<.0001
		$Soil_{illite}$	2.419	0.103	49	2.212	2.626	Illite - $Soil_{goethite}$	-1.7178	0.0854	145	-20.122	<.0001
								Illite - $Soil_{illite}$	-1.7178	0.0854	145	-20.122	<.0001
								$Soil_{goethite}$ - $Soil_{illite}$	0.0000	0.0856	145	0.000	1.0000
OP (mineral)	log()	Goethite	1.37	0.102	49	1.16	1.57	Goethite - Illite	-0.656	0.0848	145	-7.736	<.0001
		Illite	2.02	0.102	49	1.82	2.23	Goethite - Soil	-2.374	0.0854	145	-27.803	<.0001
		Soil	3.74	0.103	49	3.53	3.95	Illite - Soil	-1.718	0.0854	145	-20.122	<.0001
C:N ratio	log()	Goethite	2.40	0.0175	49	2.37	2.44	Goethite - Illite	0.5423	0.0199	146	27.217	<.0001
		Illite	1.86	0.0175	49	1.82	1.89	Goethite - $Soil_{goethite}$	0.0566	0.0199	146	2.839	0.0263
		$Soil_{goethite}$	2.34	0.0175	49	2.31	2.38	Goethite - $Soil_{illite}$	0.0437	0.0200	146	2.182	0.1330
		$Soil_{illite}$	2.36	0.0177	49	2.32	2.39	Illite - $Soil_{goethite}$	-0.4857	0.0199	146	-24.378	<.0001
								Illite - $Soil_{illite}$	-0.4985	0.0200	146	-24.869	<.0001
								$Soil_{goethite}$ - $Soil_{illite}$	-0.0128	0.0200	146	-0.640	0.9190

Table S7-4. Linear model outputs (R function lm).

Response	Predictor	Transformation	class	estimate	STD.Error	t value	Adjusted R2	F	df	p-value
F:B ratio	LUI	log()	Goethite	-0.284	0.148	-1.917	0.05	3.673	48	0.061
		log()	Illite	-0.359	0.154	-2.336	0.08	5.456	48	0.024
		log()	$Soil_{goethite}$	-0.364	0.081	-4.479	0.28	20.060	48	< 0.001
		log()	$Soil_{illite}$	-0.415	0.087	-4.776	0.31	22.810	47	< 0.001
G+:G- ratio	LUI	log()	Goethite	-0.024	0.134	-0.179	-0.02	0.032	48	0.858
		log()	Illite	-0.038	0.117	-0.322	-0.02	0.104	48	0.749
		log()	$Soil_{goethite}$	0.027	0.042	0.647	-0.01	0.418	48	0.521
		log()	$Soil_{illite}$	0.017	0.033	0.509	-0.02	0.259	47	0.613
fungal PLFAs	LUI	log()	Goethite	0.003	0.141	0.024	-0.02	0.001	48	0.981
		log()	Illite	-0.169	0.118	-1.426	0.02	2.034	48	0.160
		log()	$Soil_{goethite}$	-0.223	0.098	-2.263	0.08	5.120	48	0.028
		log()	$Soil_{illite}$	-0.294	0.105	0.007	0.12	7.842	47	0.007
bacterial PLFAs	LUI	log()	Goethite	0.287	0.114	2.515	0.10	6.327	48	0.015
		log()	Illite	0.190	0.114	1.666	0.03	2.776	48	0.102
		log()	$Soil_{goethite}$	0.141	0.069	2.047	0.06	4.191	48	0.046
		log()	$Soil_{illite}$	0.121	0.066	1.833	0.05	3.359	47	0.073
total PLFA	LUI	log()	Goethite	0.264	0.108	2.448	0.09	5.995	48	0.018
		log()	Illite	0.131	0.100	1.311	0.01	1.719	48	0.196
		log()	$Soil_{goethite}$	0.107	0.068	1.578	0.03	2.490	48	0.121
		log()	$Soil_{illite}$	0.082	0.065	1.251	0.01	1.565	47	0.217
total PLFA/OC	LUI	log()	Goethite	0.163	0.073	2.242	0.08	5.026	48	0.030
		log()	Illite	0.066	0.068	0.966	0.00	0.933	48	0.339
		log()	$Soil_{goethite}$	0.100	0.051	1.954	0.05	3.819	48	0.057
		log()	$Soil_{illite}$	0.100	0.058	1.724	0.04	2.973	47	0.091
vector length	LUI	log()	Goethite	0.015	0.052	0.284	-0.02	0.081	48	0.778
		log()	Illite	0.204	0.076	2.669	0.11	7.125	48	0.010
		log()	$Soil_{goethite}$	0.127	0.037	3.415	0.18	11.660	48	0.001
		log()	$Soil_{illite}$	0.148	0.040	3.692	0.21	13.630	47	< 0.001
vector angle	LUI	log()	Goethite	-0.005	0.022	-0.236	-0.02	0.056	48	0.814
		log()	Illite	-0.035	0.041	-0.847	-0.01	0.717	48	0.401
		log()	$Soil_{goethite}$	-0.024	0.029	-0.847	-0.01	0.717	48	0.401
		log()	$Soil_{illite}$	-0.018	0.026	-0.690	-0.01	0.476	47	0.494
BG	LUI	log()	Goethite	0.205	0.170	1.202	0.01	1.445	48	0.235
		log()	Illite	0.334	0.130	2.571	0.10	6.609	48	0.013
		log()	$Soil_{goethite}$	0.436	0.102	4.283	0.26	18.350	48	< 0.001
		log()	$Soil_{illite}$	0.643	0.098	6.563	0.47	43.070	47	< 0.001
XYL	LUI	log()	Goethite	0.248	0.233	1.065	0.00	1.133	48	0.292
		log()	Illite	0.179	0.208	0.857	-0.01	0.735	48	0.396
		log()	$Soil_{goethite}$	0.446	0.107	4.158	0.25	17.290	48	< 0.001
		log()	$Soil_{illite}$	0.701	0.125	5.631	0.39	31.710	47	< 0.001
NAG	LUI	log()	Goethite	0.192	0.184	1.042	0.00	1.086	48	0.303
		log()	Illite	0.059	0.184	0.323	-0.02	0.105	48	0.748
		log()	$Soil_{goethite}$	0.054	0.091	0.597	-0.01	0.356	48	0.554
		log()	$Soil_{illite}$	0.235	0.092	2.552	0.10	6.512	47	0.014
AP	LUI	log()	Goethite	0.139	0.100	1.398	0.02	1.953	48	0.169
		log()	Illite	-0.047	0.118	-0.396	-0.02	0.157	48	0.694
		log()	$Soil_{goethite}$	0.131	0.116	1.127	0.01	1.269	48	0.266
		log()	$Soil_{illite}$	0.329	0.116	2.833	0.13	8.028	47	0.007

Table S7-4. Linear model outputs (R function lm).

Response	Predictor	Transformation	class	estimate	STD.Error	t value	Adjusted R2	F	df	p-value
BG / OC	LUI	log()	Goethite	0.104	0.142	0.728	-0.01	0.530	48	0.470
		log()	Illite	0.269	0.113	2.374	0.09	5.634	48	0.022
		log()	$Soil_{goethite}$	0.428	0.086	4.977	0.33	24.770	48	< 0.001
		log()	$Soil_{illite}$	0.661	0.107	6.188	0.44	38.290	47	< 0.001
XYL / OC	LUI	log()	Goethite	0.147	0.200	0.733	-0.01	0.537	48	0.467
		log()	Illite	0.114	0.203	0.560	-0.01	0.313	48	0.578
		log()	$Soil_{goethite}$	0.438	0.111	3.960	0.23	15.680	48	< 0.001
		log()	$Soil_{illite}$	0.719	0.134	5.352	0.37	28.640	47	< 0.001
NAG / OC	LUI	log()	Goethite	0.090	0.165	0.549	-0.01	0.302	48	0.586
		log()	Illite	-0.006	0.170	-0.033	-0.02	0.001	48	0.974
		log()	$Soil_{goethite}$	0.047	0.081	0.575	-0.01	0.331	48	0.568
		log()	$Soil_{illite}$	0.253	0.100	2.517	0.10	6.334	47	0.015
AP / OC	LUI	log()	Goethite	0.038	0.085	0.451	-0.02	0.203	48	0.654
		log()	Illite	-0.112	0.113	-0.994	0.00	0.988	48	0.325
		log()	$Soil_{goethite}$	0.123	0.143	0.863	-0.01	0.744	48	0.393
		log()	$Soil_{illite}$	0.347	0.153	2.272	0.08	5.164	47	0.028
BG / total PLFA	LUI	log()	Goethite	-0.059	0.153	-0.386	-0.02	0.149	48	0.701
		log()	Illite	0.203	0.111	1.832	0.05	3.355	48	0.073
		log()	$Soil_{goethite}$	0.329	0.085	3.861	0.22	14.910	48	< 0.001
		log()	$Soil_{illite}$	0.561	0.081	6.895	0.49	47.540	47	< 0.001
XYL / total PLFA	LUI	log()	Goethite	-0.016	0.211	-0.076	-0.02	0.006	48	0.939
		log()	Illite	0.048	0.219	0.219	-0.02	0.048	48	0.827
		log()	$Soil_{goethite}$	0.339	0.097	3.484	0.19	12.140	48	0.001
		log()	$Soil_{illite}$	0.619	0.104	5.947	0.42	35.370	47	< 0.001
NAG / total PLFA	LUI	log()	Goethite	-0.072	0.177	-0.408	-0.02	0.166	48	0.685
		log()	Illite	-0.071	0.164	-0.436	-0.02	0.190	48	0.665
		log()	$Soil_{goethite}$	-0.053	0.084	-0.631	-0.01	0.398	48	0.531
		log()	$Soil_{illite}$	0.153	0.091	1.675	0.04	2.807	47	0.101
AP / total PLFA	LUI	log()	Goethite	-0.124	0.119	-1.045	0.00	1.092	48	0.301
		log()	Illite	-0.178	0.132	-1.350	0.02	1.823	48	0.183
		log()	$Soil_{goethite}$	0.024	0.131	0.179	-0.02	0.032	48	0.858
		log()	$Soil_{illite}$	0.247	0.130	1.901	0.05	3.613	47	0.063
BG / NAG	LUI	log()	Goethite	0.013	0.111	0.120	-0.02	0.014	48	0.905
		log()	Illite	0.275	0.207	1.325	0.02	1.756	48	0.191
		log()	$Soil_{goethite}$	0.381	0.097	3.920	0.23	15.370	48	< 0.001
		log()	$Soil_{illite}$	0.409	0.097	4.232	0.26	17.910	47	< 0.001
OC	LUI	log()	Goethite	0.101	0.071	1.428	0.02	2.038	48	0.160
		log()	Illite	0.065	0.063	1.030	0.00	1.061	48	0.308
		log()	$Soil_{goethite}$	0.008	0.064	0.120	-0.02	0.014	48	0.905
		log()	$Soil_{illite}$	-0.014	0.066	-0.209	-0.02	0.044	48	0.836
TN	LUI	log()	Goethite	0.181	0.060	3.022	0.14	9.131	48	0.004
		log()	Illite	0.062	0.040	1.557	0.03	2.426	48	0.126
		log()	$Soil_{goethite}$	0.087	0.068	1.270	0.01	1.614	48	0.210
		log()	$Soil_{illite}$	0.083	0.067	1.241	0.01	1.540	48	0.221
OP	LUI	log()	Goethite	0.562	0.148	3.792	0.21	14.380	48	< 0.001
		log()	Illite	0.396	0.174	2.272	0.08	5.161	48	0.028
		log()	Soil	0.675	0.190	3.548	0.19	12.590	48	< 0.001

Table S7-4. Linear model outputs (R function lm).

Response	Predictor	Transformation	class	estimate	STD.Error	t value	Adjusted R2	F	df	p-value
C/N	LUI	log()	Goethite	-0.080	0.038	-2.090	0.06	4.368	48	0.042
		log()	Illite	0.003	0.042	0.077	-0.02	0.006	48	0.939
		log()	$Soil_{goethite}$	-0.079	0.018	-4.493	0.28	20.190	48	< 0.001
		log()	$Soil_{illite}$	-0.068	0.024	-2.804	0.13	7.863	47	0.007
WEOC/WEON	LUI	log()	Soil	-2.311	0.831	-2.779	0.12	75.600	48	0.008
total PLFA	OC	log()	Goethite	0.579	0.075	7.665	0.54	58.760	48	< 0.001
		log()	Illite	1.376	0.175	7.843	0.55	61.520	48	< 0.001
		log()	$Soil_{goethite}$	0.011	0.002	6.307	0.44	39.780	48	< 0.001
		log()	$Soil_{illite}$	0.008	0.002	4.619	0.30	21.340	47	< 0.001
total PLFA / OC	CN	log()	Goethite	-0.050	0.024	-2.126	0.07	4.521	48	0.039
		log()	Illite	0.019	0.037	0.511	-0.02	0.261	48	0.612
		log()	$Soil_{goethite}$	-0.077	0.031	-2.446	0.09	5.981	48	0.018
		log()	$Soil_{illite}$	-0.079	0.024	-3.295	0.17	10.860	46	0.002

Table S7-5. Linear model outputs (R function lm) with backward model selection (R function stepAIC)

Goethite										
			lm()					Anova()		
Response	Transf.	Predictors	estimate	STD.Error	t value	Adjusted R2	df	Sum Sq.	F	p-value
Total PLFA	log()	OC	0.700	0.075	9.310	0.63	47	5.744	86.683	< 0.001
		C/N ratio	-0.088	0.024	-3.640			0.878	13.247	0.001
F:B	log()	PLFA_total	-0.164	0.068	-2.437	0.29	47	1.379	5.940	0.019
		organic P	-0.063	0.022	-2.886			1.934	8.330	0.006
G+ / G-	log()	PLFA_total	0.526	0.140	3.754	0.28	45	12.354	14.090	0.000
		pH	0.631	0.246	2.568			5.782	6.594	0.014
		soil type Leptosol	-0.730	0.304	-2.401			5.055	5.765	0.021
		DOP	-4.160	1.212	-3.432			10.328	11.779	0.001
BG activity	-	OC	36.969	8.587	4.305	0.26	48	19949	18.533	< 0.001
XYL activity	-	OC	26.053	3.644	7.149	0.53	45	9020	51.109	< 0.001
		DOC	-0.208	0.084	-2.479			1084	6.144	0.017
NAG activity	-	OC	26.769	7.616	3.515	0.19	47	10453	12.354	0.001
AP activity	-	AP activity soil	0.067	0.028	2.385	0.35	46	95023	5.686	0.021
		OC	104.860	41.235	2.543			108070	6.467	0.014
		DOC	-2.191	0.931	-2.355			92680	5.546	0.023
PLFA/OC	log()	G+ G-	0.079	0.032	2.484	0.27	45	0.363	6.171	0.017
		P_total	0.030	0.011	2.847			0.477	8.108	0.007
		C:N	-0.044	0.021	-2.089			0.257	4.363	0.042
		soil type	0.159	0.074	2.144			0.271	4.599	0.037
OC	-	pH	-0.573	0.102	-5.613	0.38	48	5.784	31.504	< 0.001
TN	-	LUI	0.026	0.010	2.659	0.34	47	0.009	7.071	0.011
		pH	-0.034	0.009	-3.863			0.019	14.925	< 0.001
Olsen P organic	log()	LUI	0.425	0.131	3.255	0.44	46	2.373	10.595	0.002
		total PLFA	0.179	0.065	2.748			1.692	7.554	0.009
		DOP	1.783	0.570	3.126			2.188	9.772	0.003
C/N ratio	-	C/N ratio soil	1.109	0.219	5.065	0.42	44	42.970	25.650	< 0.001
		% clay	0.003	0.001	2.216			8.227	4.911	0.032
		soil type	-1.215	0.436	-2.785			12.997	7.758	0.008
		precipitation	0.003	0.001	2.695			12.170	7.265	0.010
		DOC	0.023	0.008	2.812			13.251	7.910	0.007

Table S7-5. Linear model outputs (R function lm) with backward model selection (R function stepAIC)

Illite

			lm()					Anova()		
Response	**Transf.**	**Predictors**	**estimate**	**STD.Error**	**t value**	**Adjusted R2**	**df**	**Sum Sq.**	**F**	**p-value**
Total PLFA	-	pH	0.171	0.059	2.920	0.61	47	0.470	8.528	0.005
		OC	1.526	0.171	8.923			4.392	79.628	< 0.001
F:B	log()	total PLFA	-0.173	0.067	-2.566	0.47	45	1.191	6.585	0.014
		F:B ratio soil	3.951	1.471	2.686			1.306	7.217	0.010
		organic P	-0.092	0.031	-2.940			1.563	8.642	0.005
G+ / G-	log()	total PLFA	0.290	0.079	3.658	0.34	42	1.748	13.380	0.001
		G/G ratio soil	0.189	0.088	2.137			0.597	4.568	0.038
		OC	-1.249	0.403	-3.102			1.257	9.625	0.003
		soil type Leptosol	-0.302	0.123	-2.466			0.794	6.080	0.018
		DOP	-1.720	0.475	-3.620			1.712	13.102	0.001
BG activity	-	BG activity soil	0.003	0.002	2.095	0.42	47	213.210	4.389	0.042
		total PLFA	5.299	0.957	5.540			1491.160	30.693	< 0.001
XYL activity					no remaining parameter with p<0.05					
NAG activity	-	total PLFA	2.944	1.026	2.869	0.13	48	462.920	8.233	0.006
AP activity	-	total PLFA	0.118	0.053	2.201	0.25	45	0.707	4.846	0.033
		AP activity soil	0.000	0.000	2.363			0.814	5.582	0.023
		precipitation	0.001	0.000	2.245			0.736	5.041	0.030
		soil type Leptosol	-0.283	0.182	-2.389			0.833	5.709	0.021
PLFA/OC	-	pH	0.534	0.166	3.214	0.23	47	4.818	10.329	0.002
		organic P	0.137	0.043	3.166			4.676	10.025	0.003
OC	-	total PLFA	0.151	0.016	9.178	0.66	47	1.211	84.244	< 0.001
		pH	-0.108	0.029	-3.800			0.208	14.437	< 0.001
TN	-	G+ / G-	-0.007	0.003	-2.545	0.48	46	0.001	6.476	0.014
		total PLFA	0.014	0.002	6.672			0.010	44.513	< 0.001
organic P	log()	organic P soil	0.034	0.009	3.898	0.52	45	3.452	15.193	< 0.001
		total PLFA	0.259	0.069	3.745			3.186	14.025	< 0.001
		DOP	2.022	0.605	3.345			2.543	11.192	0.002
C/N ratio	-	C/N ratio soil	0.231	0.073	3.162	0.36	46	5.384	9.999	0.003
		total PLFA	0.469	0.101	4.644			11.610	21.563	< 0.001
		pH	-0.521	0.188	-2.779			4.158	7.722	0.008

Table S7-6. Structural equation model ouputs (R package lavaan).

Multigroup SEM C-cyle

Estimator	ML	Test statistic	10.966
Optimization method	NLMINB	Degrees of freedom	10
Number of model parameters	56	P-value (Chi-square)	0.36
Number of observations Group 1 (Goethite)	50	Test statistic Group 1 (Goethite)	4.841
Number of observations Group 2 (Illite)	49	Test statistic Group 2 (Illite)	6.125

	lhs	op	rhs	est.std	se	z	p-value	ci.lower	ci.upper
Group 1 (Goethite)	OC_soil	~	LUI	-0.005	0.141	-0.038	0.970	-0.283	0.272
	PLFA_soil	~	LUI	0.212	0.100	2.127	0.033	0.017	0.407
	Enzymes_soil	~	LUI	0.445	0.093	4.804	0.000	0.263	0.626
	Enzymes_soil	~	OC_soil	0.215	0.133	1.614	0.106	-0.046	0.476
	Enzymes_soil	~	PLFA_soil	0.336	0.134	2.501	0.012	0.073	0.599
	PLFA_soil	~	OC_soil	0.661	0.079	8.370	0.000	0.506	0.816
	OC_mineral	~	OC_soil	-0.123	0.138	-0.894	0.371	-0.394	0.147
	PLFA_mineral	~	PLFA_soil	-0.153	0.124	-1.239	0.215	-0.396	0.089
	Enzymes_mineral	~	OC_mineral	0.562	0.161	3.493	0.000	0.247	0.877
	Enzymes_mineral	~	PLFA_mineral	-0.029	0.178	-0.161	0.872	-0.378	0.320
	Enzymes_mineral	~	Enzymes_soil	0.164	0.138	1.188	0.235	-0.107	0.435
	PLFA_mineral	~	OC_mineral	0.727	0.069	10.536	0.000	0.592	0.862
	PLFA_mineral	~	OC_soil	0.301	0.123	2.457	0.014	0.061	0.541
	OC_mineral	~	LUI	0.138	0.137	1.004	0.315	-0.131	0.406
	PLFA_mineral	~	LUI	0.197	0.092	2.141	0.032	0.017	0.378
	Enzymes_mineral	~	LUI	-0.124	0.140	-0.883	0.377	-0.399	0.151
	OC_soil	~~	OC_soil	1.000	0.002	662.019	0.000	0.997	1.003
	PLFA_soil	~~	PLFA_soil	0.520	0.102	5.107	0.000	0.320	0.719
	Enzymes_soil	~~	Enzymes_soil	0.487	0.095	5.112	0.000	0.300	0.674
	OC_mineral	~~	OC_mineral	0.966	0.050	19.130	0.000	0.867	1.065
	PLFA_mineral	~~	PLFA_mineral	0.395	0.086	4.579	0.000	0.226	0.564
	Enzymes_mineral	~~	Enzymes_mineral	0.701	0.108	6.514	0.000	0.490	0.912
	LUI	~~	LUI	1.000	0.000	NA	NA	1.000	1.000
	OC_soil	~1		-0.070	0.142	-0.497	0.619	-0.348	0.207
	PLFA_soil	~1		0.086	0.102	0.847	0.397	-0.114	0.287
	Enzymes_soil	~1		-0.120	0.100	-1.198	0.231	-0.317	0.076
	OC_mineral	~1		1.214	0.186	6.531	0.000	0.849	1.578
	PLFA_mineral	~1		-0.822	0.125	-6.593	0.000	-1.067	-0.578
	Enzymes_mineral	~1		0.044	0.239	0.186	0.853	-0.425	0.514
	LUI	~1		0.000	0.000	NA	NA	0.000	0.000
Group 2 (Illite)	OC_soil	~	LUI	-0.086	0.142	-0.611	0.541	-0.364	0.191
	PLFA_soil	~	LUI	0.220	0.111	1.976	0.048	0.002	0.439
	Enzymes_soil	~	LUI	0.586	0.074	7.915	0.000	0.441	0.731
	Enzymes_soil	~	OC_soil	-0.128	0.103	-1.238	0.216	-0.330	0.074
	Enzymes_soil	~	PLFA_soil	0.508	0.102	4.966	0.000	0.308	0.709
	PLFA_soil	~	OC_soil	0.576	0.096	6.012	0.000	0.388	0.764
	OC_mineral	~	OC_soil	-0.216	0.135	-1.599	0.110	-0.481	0.049
	PLFA_mineral	~	PLFA_soil	-0.071	0.106	-0.667	0.505	-0.279	0.137
	Enzymes_mineral	~	OC_mineral	0.182	0.180	1.015	0.310	-0.170	0.535
	Enzymes_mineral	~	PLFA_mineral	0.346	0.177	1.948	0.051	-0.002	0.693
	Enzymes_mineral	~	Enzymes_soil	0.234	0.161	1.457	0.145	-0.081	0.548
	PLFA_mineral	~	OC_mineral	0.803	0.064	12.598	0.000	0.678	0.928
	PLFA_mineral	~	OC_soil	0.308	0.109	2.824	0.005	0.094	0.522
	OC_mineral	~	LUI	0.129	0.137	0.942	0.346	-0.139	0.397
	PLFA_mineral	~	LUI	0.105	0.089	1.181	0.238	-0.069	0.279
	Enzymes_mineral	~	LUI	-0.026	0.164	-0.159	0.873	-0.347	0.295
	OC_soil	~~	OC_soil	0.993	0.024	40.563	0.000	0.945	1.040
	PLFA_soil	~~	PLFA_soil	0.642	0.110	5.851	0.000	0.427	0.857
	Enzymes_soil	~~	Enzymes_soil	0.340	0.072	4.715	0.000	0.199	0.481
	OC_mineral	~~	OC_mineral	0.932	0.069	13.428	0.000	0.796	1.068
	PLFA_mineral	~~	PLFA_mineral	0.353	0.081	4.360	0.000	0.194	0.512
	Enzymes_mineral	~~	Enzymes_mineral	0.685	0.109	6.306	0.000	0.472	0.898
	LUI	~~	LUI	1.000	0.000	NA	NA	1.000	1.000
	OC_soil	~1		0.095	0.143	0.664	0.506	-0.185	0.374
	PLFA_soil	~1		-0.100	0.115	-0.868	0.385	-0.325	0.125
	Enzymes_soil	~1		0.142	0.085	1.676	0.094	-0.024	0.309
	OC_mineral	~1		-3.192	0.354	-9.011	0.000	-3.886	-2.497
	PLFA_mineral	~1		2.528	0.241	10.472	0.000	2.055	3.001
	Enzymes_mineral	~1		-2.768	0.684	-4.045	0.000	-4.110	-1.427
	LUI	~1		0.006	0.000	NA	NA	0.006	0.006

).

Table S7-6. Structural equation model ouputs (R package lavaan).

Multigroup SEM N-cyle

Estimator	ML	Test statistic	20.362
Optimization method	NLMINB	Degrees of freedom	12
Number of model parameters	54	P-value (Chi-square)	0.061
Number of observations Group 1 (Goethite)	50	Test statistic Group 1 (Goethite)	14.758
Number of observations Group 2 (Illite)	49	Test statistic Group 2 (Illite)	5.604

	lhs	op	rhs	est.std	se	z	p-value	ci.lower	ci.upper
Group 1 (Goethite)	ON_soil	~	LUI	0.146	0.138	1.059	0.290	-0.124	0.416
	PLFA_soil	~	LUI	0.107	0.099	1.081	0.280	-0.087	0.301
	N_Enzymes_soil	~	LUI	-0.075	0.116	-0.646	0.518	-0.302	0.152
	N_Enzymes_soil	~	ON_soil	0.560	0.148	3.770	0.000	0.269	0.850
	N_Enzymes_soil	~	PLFA_soil	0.059	0.163	0.360	0.719	-0.261	0.378
	PLFA_soil	~	ON_soil	0.694	0.073	9.507	0.000	0.551	0.838
	ON_mineral	~	ON_soil	-0.021	0.131	-0.161	0.872	-0.277	0.235
	PLFA_mineral	~	PLFA_soil	-0.027	0.097	-0.274	0.784	-0.217	0.164
	N_Enzymes_mineral	~	ON_mineral	0.495	0.198	2.503	0.012	0.107	0.883
	N_Enzymes_mineral	~	PLFA_mineral	-0.246	0.196	-1.256	0.209	-0.629	0.138
	N_Enzymes_mineral	~	N_Enzymes_soil	0.071	0.133	0.536	0.592	-0.189	0.331
	PLFA_mineral	~	ON_mineral	0.754	0.075	10.089	0.000	0.608	0.901
	ON_mineral	~	LUI	0.405	0.115	3.521	0.000	0.180	0.630
	PLFA_mineral	~	LUI	-0.030	0.106	-0.285	0.776	-0.237	0.177
	N_Enzymes_mineral	~	LUI	-0.070	0.145	-0.486	0.627	-0.354	0.214
	ON_soil	~~	ON_soil	0.979	0.040	24.388	0.000	0.900	1.057
	PLFA_soil	~~	PLFA_soil	0.485	0.098	4.930	0.000	0.292	0.677
	N_Enzymes_soil	~~	N_Enzymes_soil	0.645	0.109	5.936	0.000	0.432	0.858
	ON_mineral	~~	ON_mineral	0.838	0.091	9.163	0.000	0.659	1.017
	PLFA_mineral	~~	PLFA_mineral	0.450	0.094	4.780	0.000	0.266	0.635
	N_Enzymes_mineral	~~	N_Enzymes_mineral	0.883	0.085	10.364	0.000	0.716	1.050
	LUI	~~	LUI	1.000	0.000	NA	NA	1.000	1.000
	ON_soil	~1		-0.010	0.140	-0.072	0.942	-0.284	0.264
	PLFA_soil	~1		0.047	0.099	0.477	0.634	-0.146	0.240
	N_Enzymes_soil	~1		-0.215	0.116	-1.853	0.064	-0.442	0.012
	ON_mineral	~1		0.742	0.149	4.986	0.000	0.450	1.033
	PLFA_mineral	~1		-0.519	0.111	-4.661	0.000	-0.737	-0.301
	N_Enzymes_mineral	~1		0.133	0.206	0.643	0.520	-0.271	0.537
	LUI	~1		0.000	0.000	NA	NA	0.000	0.000
Group 2 (Illite)	ON_soil	~	LUI	0.121	0.140	0.865	0.387	-0.153	0.396
	PLFA_soil	~	LUI	0.084	0.099	0.853	0.394	-0.109	0.277
	N_Enzymes_soil	~	LUI	0.280	0.118	2.383	0.017	0.050	0.511
	N_Enzymes_soil	~	ON_soil	0.471	0.168	2.808	0.005	0.142	0.800
	N_Enzymes_soil	~	PLFA_soil	-0.095	0.177	-0.534	0.593	-0.443	0.253
	PLFA_soil	~	ON_soil	0.711	0.071	10.067	0.000	0.573	0.849
	ON_mineral	~	ON_soil	-0.001	0.140	-0.004	0.997	-0.275	0.274
	PLFA_mineral	~	PLFA_soil	-0.010	0.110	-0.088	0.930	-0.226	0.206
	N_Enzymes_mineral	~	ON_mineral	-0.028	0.172	-0.165	0.869	-0.366	0.309
	N_Enzymes_mineral	~	PLFA_mineral	0.426	0.162	2.631	0.009	0.109	0.743
	N_Enzymes_mineral	~	N_Enzymes_soil	0.121	0.136	0.885	0.376	-0.147	0.388
	PLFA_mineral	~	ON_mineral	0.640	0.087	7.345	0.000	0.469	0.811
	ON_mineral	~	LUI	0.227	0.135	1.683	0.092	-0.037	0.491
	PLFA_mineral	~	LUI	0.041	0.113	0.361	0.718	-0.181	0.262
	N_Enzymes_mineral	~	LUI	-0.136	0.139	-0.982	0.326	-0.409	0.136
	ON_soil	~~	ON_soil	0.985	0.034	28.947	0.000	0.919	1.052
	PLFA_soil	~~	PLFA_soil	0.473	0.098	4.823	0.000	0.281	0.665
	N_Enzymes_soil	~~	N_Enzymes_soil	0.732	0.107	6.828	0.000	0.522	0.942
	ON_mineral	~~	ON_mineral	0.949	0.061	15.633	0.000	0.830	1.067
	PLFA_mineral	~~	PLFA_mineral	0.577	0.107	5.386	0.000	0.367	0.787
	N_Enzymes_mineral	~~	N_Enzymes_mineral	0.825	0.098	8.419	0.000	0.633	1.017
	LUI	~~	LUI	1.000	0.000	NA	NA	1.000	1.000
	ON_soil	~1		0.039	0.142	0.278	0.781	-0.239	0.317
	PLFA_soil	~1		-0.073	0.098	-0.743	0.457	-0.266	0.120
	N_Enzymes_soil	~1		0.152	0.124	1.223	0.221	-0.092	0.396
	ON_mineral	~1		-1.570	0.211	-7.452	0.000	-1.983	-1.157
	PLFA_mineral	~1		0.986	0.170	5.790	0.000	0.652	1.320
	N_Enzymes_mineral	~1		-2.974	0.417	-7.134	0.000	-3.791	-2.157
	LUI	~1		0.006	0.000	NA	NA	0.006	0.006

Table S7-6. Structural equation model ouputs (R package lavaan).

	lhs	op	rhs	est.std	se	z	p-value	ci.lower	ci.upper
Group 1 (Goethite)	OP_soil	~	LUI	0.381	0.118	3.242	0.001	0.151	0.612
	PLFA_soil	~	LUI	0.183	0.148	1.236	0.216	-0.107	0.474
	P_Enzymes_soil	~	LUI	-0.030	0.138	-0.217	0.828	-0.301	0.241
	P_Enzymes_soil	~	OP_soil	0.477	0.122	3.903	0.000	0.237	0.717
	P_Enzymes_soil	~	PLFA_soil	0.043	0.128	0.331	0.740	-0.209	0.294
	PLFA_soil	~	OP_soil	0.035	0.151	0.230	0.818	-0.262	0.331
	OP_mineral	~	OP_soil	0.145	0.135	1.075	0.282	-0.119	0.409
	PLFA_mineral	~	PLFA_soil	-0.043	0.133	-0.321	0.748	-0.304	0.219
	P_Enzymes_mineral	~	OP_mineral	0.180	0.134	1.346	0.178	-0.082	0.443
	P_Enzymes_mineral	~	PLFA_mineral	0.183	0.138	1.330	0.183	-0.087	0.454
	P_Enzymes_mineral	~	P_Enzymes_soil	0.382	0.121	3.159	0.002	0.145	0.620
	PLFA_mineral	~	OP_mineral	0.340	0.133	2.552	0.011	0.079	0.601
	PLFA_mineral	~	P_Enzymes_soil	0.294	0.121	2.433	0.015	0.057	0.530
	OP_mineral	~	PLFA_soil	0.324	0.122	2.652	0.008	0.085	0.563
	OP_mineral	~	LUI	0.209	0.134	1.559	0.119	-0.054	0.472
	PLFA_mineral	~	LUI	0.104	0.131	0.797	0.426	-0.152	0.361
	P_Enzymes_mineral	~	LUI	-0.040	0.129	-0.310	0.756	-0.292	0.212
	OP_soil	~~	OP_soil	0.855	0.090	9.535	0.000	0.679	1.030
	PLFA_soil	~~	PLFA_soil	0.960	0.054	17.746	0.000	0.854	1.066
	P_Enzymes_soil	~~	P_Enzymes_soil	0.777	0.105	7.416	0.000	0.572	0.982
	OP_mineral	~~	OP_mineral	0.771	0.104	7.405	0.000	0.567	0.975
	PLFA_mineral	~~	PLFA_mineral	0.741	0.106	6.993	0.000	0.534	0.949
	P_Enzymes_mineral	~~	P_Enzymes_mineral	0.706	0.108	6.531	0.000	0.494	0.918
	LUI	~~	LUI	1.000	0.000	NA	NA	1.000	1.000
	OP_soil	~1		0.008	0.132	0.060	0.952	-0.251	0.267
	PLFA_soil	~1		0.029	0.140	0.208	0.835	-0.245	0.304
	P_Enzymes_soil	~1		-0.089	0.126	-0.703	0.482	-0.336	0.159
	OP_mineral	~1		-0.015	0.126	-0.121	0.903	-0.261	0.231
	PLFA_mineral	~1		0.058	0.123	0.473	0.636	-0.184	0.300
	P_Enzymes_mineral	~1		1.206	0.168	7.185	0.000	0.877	1.535
	LUI	~1		-0.021	0.000	NA	NA	-0.021	-0.021
Group 2 (Illite)	OP_soil	~	LUI	0.379	0.119	3.188	0.001	0.146	0.613
	PLFA_soil	~	LUI	0.133	0.152	0.876	0.381	-0.165	0.432
	P_Enzymes_soil	~	LUI	0.173	0.123	1.410	0.158	-0.068	0.414
	P_Enzymes_soil	~	OP_soil	0.522	0.109	4.773	0.000	0.308	0.736
	P_Enzymes_soil	~	PLFA_soil	-0.013	0.116	-0.112	0.911	-0.241	0.215
	PLFA_soil	~	OP_soil	0.050	0.154	0.324	0.746	-0.252	0.351
	OP_mineral	~	OP_soil	0.203	0.142	1.426	0.154	-0.076	0.482
	PLFA_mineral	~	PLFA_soil	-0.158	0.127	-1.246	0.213	-0.406	0.090
	P_Enzymes_mineral	~	OP_mineral	-0.054	0.140	-0.384	0.701	-0.328	0.221
	P_Enzymes_mineral	~	PLFA_mineral	0.515	0.129	3.985	0.000	0.262	0.768
	P_Enzymes_mineral	~	P_Enzymes_soil	0.395	0.129	3.058	0.002	0.142	0.648
	PLFA_mineral	~	OP_mineral	0.508	0.115	4.404	0.000	0.282	0.734
	PLFA_mineral	~	P_Enzymes_soil	-0.244	0.129	-1.888	0.059	-0.498	0.009
	OP_mineral	~	PLFA_soil	0.251	0.132	1.906	0.057	-0.007	0.508
	OP_mineral	~	LUI	0.088	0.145	0.606	0.544	-0.196	0.372
	PLFA_mineral	~	LUI	0.188	0.130	1.445	0.148	-0.067	0.444
	P_Enzymes_mineral	~	LUI	-0.278	0.128	-2.168	0.030	-0.528	-0.027
	OP_soil	~~	OP_soil	0.856	0.090	9.476	0.000	0.679	1.033
	PLFA_soil	~~	PLFA_soil	0.975	0.045	21.872	0.000	0.887	1.062
	P_Enzymes_soil	~~	P_Enzymes_soil	0.631	0.109	5.775	0.000	0.417	0.845
	OP_mineral	~~	OP_mineral	0.858	0.093	9.214	0.000	0.675	1.040
	PLFA_mineral	~~	PLFA_mineral	0.709	0.109	6.516	0.000	0.495	0.922
	P_Enzymes_mineral	~~	P_Enzymes_mineral	0.698	0.110	6.318	0.000	0.481	0.914
	LUI	~~	LUI	1.000	0.000	NA	NA	1.000	1.000
	OP_soil	~1		0.017	0.134	0.129	0.898	-0.245	0.279
	PLFA_soil	~1		-0.064	0.143	-0.448	0.654	-0.344	0.216
	P_Enzymes_soil	~1		0.078	0.115	0.677	0.498	-0.148	0.304
	OP_mineral	~1		0.060	0.134	0.451	0.652	-0.202	0.323
	PLFA_mineral	~1		-0.042	0.123	-0.340	0.734	-0.282	0.198
	P_Enzymes_mineral	~1		-9.095	0.932	-9.758	0.000	-10.922	-7.268
	LUI	~1		-0.015	0.000	NA	NA	-0.015	-0.015

Table S7-7. Mean, standard deviation, range (minimum and maximum values), and sample size for investigated parameters in goethite, illite and surrounding soil samples.

		Goethite					Illite				
Parameter	**unit**	**mean**	**sd**	**min**	**max**	**n**	**mean**	**sd**	**min**	**max**	**n**
OM accumulation											
Total carbon	g kg^{-1} mineral-sand	2.2	0.5	1.0	3.4	50	0.9	0.2	0.5	1.5	50
organic C	g kg^{-1} mineral-sand	2.2	0.5	1.0	3.4	50	0.9	0.2	0.5	1.5	50
inorganic C	g kg^{-1} mineral-sand	0.0	0.0	0.0	0.1	50	0.0	0.0	0.0	0.2	50
Total nitrogen	g kg^{-1} mineral-sand	0.2	0.0	0.1	0.3	50	0.1	0.0	0.1	0.2	50
Olsen-P total	mg kg^{-1} mineral-sand	2.8	3.4	0.6	23.1	50	3.1	3.0	0.7	14.2	50
Olsen-P inorganic	mg kg^{-1} mineral-sand	0.3	0.7	0.0	4.7	50	0.5	0.7	0.0	2.9	50
Olsen-P organic	mg kg^{-1} mineral-sand	2.5	2.7	0.6	18.4	50	2.6	2.3	0.7	11.3	50
Total carbon	g kg^{-1} mineral	4.4	1.1	2.0	6.8	50	3.2	0.7	1.9	5.5	50
organic C	g kg^{-1} mineral	4.4	1.1	2.0	6.8	50	3.2	0.8	1.8	5.5	50
inorganic C	g kg^{-1} mineral	0.0	0.0	0.0	0.2	50	0.0	0.1	0.0	0.7	50
Total nitrogen	g kg^{-1} mineral	0.4	0.1	0.2	0.6	50	0.5	0.1	0.4	0.8	50
Olsen-P total	mg kg^{-1} mineral	5.6	6.7	1.2	46.2	50	11.6	11.1	2.6	53.2	50
Olsen-P inorganic	mg kg^{-1} mineral	0.6	1.4	0.0	9.4	50	1.8	2.5	0.0	10.9	50
Olsen-P organic	mg kg^{-1} mineral	5.0	5.4	1.2	36.8	50	9.8	8.7	2.6	42.3	50
Total carbon	mg m^{-2} mineral	213.6	53.2	98.0	331.4	50	79.5	18.2	47.0	135.4	50
organic C	mg m^{-2} mineral	213.5	53.5	98.0	331.4	50	78.9	19.0	45.1	135.4	50
inorganic C	mg m^{-2} mineral	0.2	1.2	0.0	8.8	50	0.6	3.2	0.0	16.6	50
Total nitrogen	mg m^{-2} mineral	19.2	4.3	8.8	31.4	50	12.1	1.9	9.2	18.4	50
Olsen-P total	ng m^{-2} mineral	274.3	330.3	57.2	2266.5	50	286.0	273.0	64.5	1308.3	50
Olsen-P inorganic	ng m^{-2} mineral	27.4	67.8	0.0	460.2	50	44.9	60.5	0.0	268.3	50
Olsen-P organic	ng m^{-2} mineral	246.9	265.8	57.2	1806.3	50	241.2	212.9	63.4	1040.1	50
organic C:total N	-	11.1	1.7	7.9	14.8	50	6.5	1.0	4.4	8.9	50
Main microbial groups											
grampositive PLFAs	nmol g^{-1} mineral-sand	1.18	0.61	0.33	3.03	50	1.05	0.56	0.32	3.11	50
gramnegative PLFAs	nmol g^{-1} mineral-sand	0.45	0.26	0.08	1.41	50	0.48	0.27	0.18	1.41	50
bacterial PLFAs	nmol g^{-1} mineral-sand	2.32	1.04	0.70	5.18	50	2.20	1.03	0.81	6.01	50
fungal PLFAs	nmol g^{-1} mineral-sand	0.35	0.17	0.09	0.78	50	0.39	0.16	0.11	0.83	50
total PLFAs	nmol g^{-1} mineral-sand	2.67	1.09	0.79	5.70	50	2.59	1.04	1.08	6.43	50
Gram+:Gram-	-	2.91	1.11	0.51	5.09	50	2.36	0.80	0.58	3.83	50
F:B	-	0.17	0.08	0.02	0.43	50	0.21	0.13	0.04	0.62	50
Total PLFA:OC	nmol g^{-1} mineral-sand	1.21	0.34	0.65	2.19	50	2.99	0.78	1.82	4.79	50
Enzyme activities											
BG	nmol g^{-1} h^{-1} mineral-sand	65.30	38.23	11.16	196.26	50	16.29	9.13	5.41	45.25	50
NAG	nmol g^{-1} h^{-1} mineral-sand	60.36	49.71	9.09	323.87	50	13.42	8.03	1.64	43.60	50
XYL	nmol g^{-1} h^{-1} mineral-sand	34.84	22.91	2.64	113.13	50	4.73	4.80	0.81	21.05	50
AP	nmol g^{-1} h^{-1} mineral-sand	434.82	159.75	185.77	952.88	50	49.76	20.88	11.99	106.15	50
BG/total PLFA	h^{-1} mineral-sand	26.52	19.22	8.22	100.96	50	6.48	3.07	2.32	18.80	50
XYL/total PLFA	h^{-1} mineral-sand	25.26	27.16	3.76	187.23	50	5.36	2.87	0.67	15.53	50
NAG/total PLFA	h^{-1} mineral-sand	14.40	13.67	2.01	74.27	50	2.09	2.43	0.34	10.11	50
AP/total PLFA	h^{-1} mineral-sand	184.09	96.77	79.00	568.74	50	21.17	10.70	3.23	63.97	50
BG/OC	nmol kg^{-1} h^{-1} mineral-sand	29.62	16.14	8.61	82.65	50	18.95	9.52	7.51	49.27	50
XYL/OC	nmol kg^{-1} h^{-1} mineral-sand	27.61	22.59	3.87	155.71	50	15.73	8.88	2.19	40.00	50
NAG/OC	nmol kg^{-1} h^{-1} mineral-sand	16.00	12.93	1.82	79.11	50	5.67	5.84	1.12	23.37	50
AP/OC	nmol kg^{-1} h^{-1} mineral-sand	203.07	70.26	86.82	465.60	50	59.54	26.27	15.18	167.70	50
vector length	-	0.55	0.09	0.27	0.78	50	0.61	0.18	0.28	0.95	50
vector angle	°	76.47	5.74	50.47	86.27	50	65.21	8.83	32.21	77.25	50

* data is based one soil sample per site, without separation into soil goethite and soil illite

n.a. = not analyzed

Tabelle S7-8. OM and microbial properties of the pristine mineral-sand mixtures.

	Goethite-sand-mixture	Illite-sand-mixture
Total carbon (g kg^{-1})	0.2	0.1
Inorganic carbon (g kg^{-1})	n.d.	n.d.
Total nitrogen (g kg^{-1})	0.2	0.1
Inorganic nitrogen (g kg^{-1})	n.d.	n.d.
Total PLFAs (nmol g^{-1})	n.d.	n.d.
beta-glucosidase activity (nmol g^{-1} h^{-1})	32.8	n.d.
beta-xylosidase activity (nmol g^{-1} h^{-1})	n.d.	n.d.
N-acetylglucosaminidase activity (nmol g^{-1} h^{-1})	n.d.	n.d.
Acid phosphatase activity (nmol g^{-1} h^{-1})	454.1	n.d.

n.d.= not detectable

Declaration on the use of generative artificial intelligence

In the preparation of my work, I utilized systems based on generative artificial intelligence. Troubleshooting of R programming code was supported by OpenAI´s ChatGPT 3.5, GPT-4o, and o4-mini-high. Linguistic refinement of the introduction (Chapter I) and synthesis (Chapter VIII) was performed using OpenAI´s o3 and o4-mini models, as well as DeepL Write Pro.

Eidesstaatliche Erklärung

Ich erkläre: Ich habe die vorgelegte Dissertation selbständig und ohne unerlaubte fremde Hilfe und nur mit den Hilfen angefertigt, die ich in der Dissertation angegeben habe. Alle Textstellen, die wörtlich oder sinngemäß aus veröffentlichten Schriften entnommen sind, und alle Angaben, die auf mündlichen Auskünften beruhen, sind als solche kenntlich gemacht. Bei den von mir durchgeführten und in der Dissertation erwähnten Untersuchungen habe ich die Grundsätze guter wissenschaftlicher Praxis, wie sie in der „Satzung der Justus-Liebig-Universität Gießen zur Sicherung guter wissenschaftlicher Praxis“ niedergelegt sind, eingehalten.

Gießen, den _____, _____
[Datum] *[Unterschrift]*

Danksagung

Eine erfolgreiche Promotion lebt von den Menschen, die mich auf diesem Weg begleitet haben – von Mentorinnen und Lehrenden, Studierenden und Technikerinnen, Freundinnen und Freunden und Kolleginnen und Kollegen. Vielen Dank an alle, die mich unterstützt, inspiriert und motiviert haben.

Zuerst möchte ich Jan Siemens danken. Er hat mich fachlich exzellent ausgebildet und meine Forschung stets gefördert. Ich bin sehr dankbar dafür, dass ich in gleich drei Schwerpunktprogrammen arbeiten und dabei immer eigenverantwortlich vorgehen durfte. Auch Ines Mulder möchte ich danken, deren ansteckende Begeisterung und unermüdlicher Tatendrang mich immer wieder motiviert haben, auch die schwierigsten Probleme mit Optimismus anzugehen. Kenton Stutz danke ich für die tiefgründigen und oft philosophischen Telefonate sowie die vielen anregenden Gespräche auf Konferenzen. Für ihre freundliche Unterstützung und die immer konstruktiven, kritischen Rückmeldungen möchte ich Fritzi Lang meinen Dank aussprechen. Ein ganz besonderer Dank gilt Diana Hofmann, ohne deren fachkundige Hilfe die Radioaktivitätsarbeiten nicht so erfolgreich verlaufen wären. Ich habe es sehr geschätzt, in Jülich nicht nur einen Platz im Kontrollbereich zu bekommen, sondern dort gemeinsam viele, immer sehr angenehme Überstunden zu leisten.

Mein Dank richtet sich außerdem an all die Technikerinnen und Techniker, die mich in der Bodenkunde und anderen Fachbereichen mit Rat, Tat und unzähligen Stunden im Feld und Labor unterstützt haben. Besonders Elke Schneidenwind und Elke Müller möchte ich für die herzlichen Gespräche – gerne auch auf Hessisch – und die gelegentlichen Schokoladenpausen danken. Melanie Ketels danke ich für die Hilfe bei allen administrativen Fragen, Rita Geißler-Plaum und Belinda Schneider für ihre Expertise bei mikrobiologischen Fragestellungen sowie Andrea Ecker, Simon Horn, Stefan Köppchen, Elena Evguenieva-Hackenberg und Andreas Jäger für ihre tatkräftige Unterstützung in den Kontrollbereichen in Gießen und Jülich. Dem Reinigungsteam im iFZ danke ich sehr dafür, dass es den Putzplan so angepasst hat, dass meine Kalorimeterversuche ungestört laufen konnten, und dem Team der Elektro- und Feinmechanikwerkstatt dafür, dass für jede technische Herausforderung eine Lösung gefunden wurde.

Ebenso danke ich meinen Bürokollegen Kai und Katrin ganz herzlich für die WG-Atmosphäre in unserem Alkaka-Büro, die gemeinsamen Feierabendbiere, tiefsinnigen Gespräche und Sinnkrisen. Benjamin Heyde und Johannes Junck danke ich für jede Kaffeepause, das dumme Geschwätz und die gemeinsamen Momente. Auch die Studierenden, die mich als HiWis unterstützt oder im Rahmen ihrer Abschlussarbeiten begleitet haben, haben mit ihrer Neugier und ihrem Engagement meine Arbeit entscheidend bereichert.

Meinen Eltern, Großeltern, Tanten und Onkeln danke ich von Herzen für ihre beständige Unterstützung und ihr Verständnis während der gesamten Promotionszeit. Ganz am Ende möchte ich Annabel danken, die mich durch jede Krise getragen, mir Auszeiten und Urlaub ermöglicht und mit ihrer Liebe und Geduld dafür gesorgt hat, dass dieser Weg nicht nur erfolgreich, sondern auch erfüllt war. Vielen Dank an alle, die mich begleitet haben.